frontiers | Research Topics

Plant cell endomembrane dynamics and specialization

Edited by
Emily R. Larson, Lorena Norambuena and Cecilia Rodriguez-Furlan

Published in
Frontiers in Plant Science

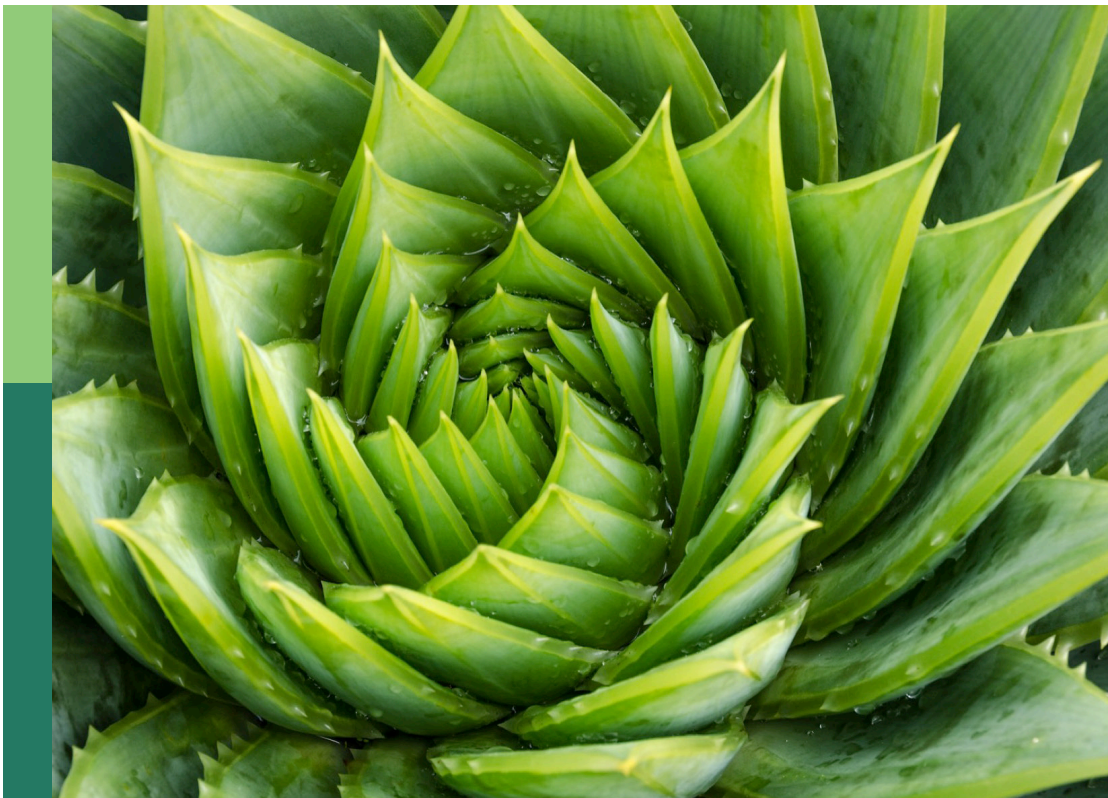

ISSN 1664-8714
ISBN 978-2-8325-3862-3
DOI 10.3389/978-2-8325-3862-3

About Frontiers

Frontiers is more than just an open access publisher of scholarly articles: it is a pioneering approach to the world of academia, radically improving the way scholarly research is managed. The grand vision of Frontiers is a world where all people have an equal opportunity to seek, share and generate knowledge. Frontiers provides immediate and permanent online open access to all its publications, but this alone is not enough to realize our grand goals.

Frontiers journal series

The Frontiers journal series is a multi-tier and interdisciplinary set of open-access, online journals, promising a paradigm shift from the current review, selection and dissemination processes in academic publishing. All Frontiers journals are driven by researchers for researchers; therefore, they constitute a service to the scholarly community. At the same time, the *Frontiers journal series* operates on a revolutionary invention, the tiered publishing system, initially addressing specific communities of scholars, and gradually climbing up to broader public understanding, thus serving the interests of the lay society, too.

Dedication to quality

Each Frontiers article is a landmark of the highest quality, thanks to genuinely collaborative interactions between authors and review editors, who include some of the world's best academicians. Research must be certified by peers before entering a stream of knowledge that may eventually reach the public - and shape society; therefore, Frontiers only applies the most rigorous and unbiased reviews. Frontiers revolutionizes research publishing by freely delivering the most outstanding research, evaluated with no bias from both the academic and social point of view. By applying the most advanced information technologies, Frontiers is catapulting scholarly publishing into a new generation.

What are Frontiers Research Topics?

Frontiers Research Topics are very popular trademarks of the *Frontiers journals series*: they are collections of at least ten articles, all centered on a particular subject. With their unique mix of varied contributions from Original Research to Review Articles, Frontiers Research Topics unify the most influential researchers, the latest key findings and historical advances in a hot research area.

Find out more on how to host your own Frontiers Research Topic or contribute to one as an author by contacting the Frontiers editorial office: frontiersin.org/about/contact

Plant cell endomembrane dynamics and specialization

Topic editors

Emily R. Larson — University of Bristol, United Kingdom

Lorena Norambuena — University of Chile, Chile

Cecilia Rodriguez-Furlan — Washington State University, United States

Citation

Larson, E. R., Norambuena, L., Rodriguez-Furlan, C., eds. (2023). *Plant cell endomembrane dynamics and specialization*. Lausanne: Frontiers Media SA.

doi: 10.3389/978-2-8325-3862-3

Table of contents

frontiers | Frontiers in Plant Science

TYPE Editorial
PUBLISHED 20 October 2023
DOI 10.3389/fpls.2023.1305963

OPEN ACCESS

EDITED AND REVIEWED BY
Simon Gilroy,
University of Wisconsin-Madison,
United States

*CORRESPONDENCE
Cecilia Rodriguez-Furlan
c.rodriguezfurlan@wsu.edu

RECEIVED 02 October 2023
ACCEPTED 10 October 2023
PUBLISHED 20 October 2023

CITATION
Rodriguez-Furlan C, Norambuena L and Larson ER (2023) Editorial: Plant cell endomembrane dynamics and specialization.
Front. Plant Sci. 14:1305963.
doi: 10.3389/fpls.2023.1305963

Editorial: Plant cell endomembrane dynamics and specialization

Cecilia Rodriguez-Furlan [1]*, Lorena Norambuena [2] and Emily R. Larson [3]

[1]School of Biological Sciences, Washington State University, Pullman, WA, United States, [2]Plant Molecular Biology Centre, Department of Biology, Facultad de Ciencias, Universidad de Chile, Santiago, Chile, [3]School of Biological Sciences, University of Bristol, Bristol, United Kingdom

KEYWORDS

endomembrane, trafficking, autophagy, Rab7, retromer, cell-plate, SNARE, viruses

Editorial on the Research Topic
Plant cell endomembrane dynamics and specialization

This special Research Topic highlights current research on the unique characteristics and specialization of the plant endomembrane system. These four reviews and five research articles emphasize the diversity of the molecular and regulatory mechanisms that control endomembrane compartment function, vesicle trafficking, and the dynamics and interactions among the molecules that assist plant cell function, development, and environmental responses.

During plant cell division, the cell plate forms dynamically, involving cytoskeletal reorganization and targeted vesicle trafficking. This process aggregates new cell wall material and membrane components that ultimately fuse with the existing cell walls. In this Research Topic, Shi et al. review the key molecular players involved in this process, like Rab GTPases, tethering complexes, and SNARE proteins that regulate this process. It also explores how these complexes have aided our study of how vesicles and cargo that form cell plates vary from those that traffic to other membranes. Additionally, Allsman et al. introduce a set of maize-specific markers and chemical resources designed for investigating cell plate positioning. Using these tools, the authors show that the delivery of material to the growing cell plate in maize occurs through mechanisms and molecular players divergent from those in Arabidopsis. This discovery is at the forefront of innovative research directions and offers invaluable tools to the scientific community that facilitate further exploration in this field.

While endomembrane protein trafficking pathways have received extensive attention, the specific cargo proteins remain largely uncharted. Li et al. use chemical genomics and proteomics to identify plasma membrane cargoes associated with EXO70A1-mediated secretion in Arabidopsis. EXO70 is one of eight subunits (Sec3, Sec5, Sec6, Sec8, Sec10, Sec15, Exo70, and Exo84) that form the exocyst complex to coordinate the fusion of vesicles with the plasma membrane. Unraveling the molecular components of this process is vital for understanding how plant cells regulate plasma membrane protein delivery, which is crucial for growth, development, and environmental responses.

Another critical aspect of endomembrane traffic involves material delivery to the vacuole. In this Research Topic, Rodriguez-Furlan et al. explore the regulatory function of RAB7 in vacuole traffic during development, biotic interactions, and abiotic stress. The authors provide insight into promising avenues for future research that will elucidate the central role of this endomembrane trafficking regulator. In the path to the vacuole, the retromer complex rescues proteins from degradation. The mini-review by Jha and Larson on the retromer subunit VPS26C, one of three VPS26 proteins in plants but whose function is less defined than other family members. VPS26A and VPS26B participate in canonical retromer pathways that send protein cargo from the trans-Golgi network to late endosomes and the Golgi, while VPS26C may form a complex that sends cargo back toward the plasma membrane, similar to the VPS26C "retriever" complex characterized in animal cells. The authors discuss the potential of a VPS26C-specific retriever complex in plants and highlight unanswered questions like how retromer/retriever complexes are recruited to cell membranes, if these complexes are cell-type dependent, and how VPS26C may function to specialize retromer/retriever pathways in plants.

Within the scope of vacuole-directed trafficking pathways, autophagy is a degradative pathway activated during specific developmental stages and stress responses. Kim et al. report that the FYVE3 proteins interact with the ATG8 isoforms in a phosphatidylinositol-3-phosphate-dependent manner. Although the mode of action of FYVE3 is unknown, the genetic data suggest that it regulates the later stages of autophagosome biogenesis, causing defects in vacuole delivery. This research represents a significant step towards unraveling the intricate processes underlying autophagosome biogenesis and subsequent transport to the vacuole.

The cellular importance of autophagy is largely documented, with its role on plant development and cell differentiation described in Arabidopsis. In this Research Topic, Norizuki et al. demonstrates the role of autophagy during spermatogenesis in the liverwort *Marchantia polimorpha*. The reorganization of plastids is particularly important during spermatogenesis and the authors show that the abolishment of autophagy results in plastid morphology and organization defects. More importantly, Merchantia plastids are degraded in the vacuole via autophagy. These findings demonstrate the importance of autophagy as a key regulator of cell function, with an impact on the development and physiology in liverworts.

The endomembrane system plays a crucial role during stress responses. In their review, Jovanović et al. explore the intricate molecular interactions between virus infection and plant endomembrane-associated pathways. The authors deliver a detailed overview of the numerous viruses that exploit elements of endomembrane pathways for infection, replication, and propagation. The review also explores the multiple endomembrane-related pathways plants use to establish defense pathways in response to infection. This innovative review systematically examines the remarkable progress made in elucidating these molecular interactions.

Endomembrane trafficking is modulated in response to environmental cues, with many SNARE proteins acting as key molecular regulators of vesicle fusion. Salinas-Cornejo et al. describe the molecular function of a SNARE-like protein in *Solanum lycopersicum*, SlSLSP6, whose gene expression is sensitive to salt stress, suggesting a particular function during related environmental stresses in the field. The overexpression of *SlSLSP6* in tomatoes increases salt tolerance, demonstrating endocytosis pathway regulation is related to salt stress responses.

This Research Topic encapsulates the intricacies of the plant endomembrane system and its profound influence on fundamental cellular processes. Together, these contributions enhance our comprehension of plant cell biology, laying the groundwork for future research endeavors and innovations to deepen our understanding of the intricate plant endomembrane trafficking networks.

Author contributions

CR-F: Writing – original draft, Writing – review & editing. LN: Writing – original draft, Writing – review & editing. ERL: Writing – original draft, Writing – review & editing.

Funding

The author(s) declare that no financial support was received for the research, authorship, and/or publication of this article.

Acknowledgments

We thank all the contributors to this special issue, reviewers, and external editors.

Conflict of interest

The authors declare that the research was conducted in the absence of any commercial or financial relationships that could be construed as a potential conflict of interest.

Publisher's note

frontiers | Frontiers in Plant Science

TYPE Original Research
PUBLISHED 09 February 2023
DOI 10.3389/fpls.2023.1101983

OPEN ACCESS

EDITED BY
Lorena Norambuena,
University of Chile, Chile

REVIEWED BY
Jeffrey Graham Duckett,
Natural History Museum, United Kingdom
Ayelen Mariana Distéfano,
Universidad Nacional de Mar del Plata, Argentina
Omar Pantoja,
National Autonomous University of Mexico, Mexico

*CORRESPONDENCE
Takashi Ueda
tueda@nibb.ac.jp

SPECIALTY SECTION
This article was submitted to Plant Cell Biology, a section of the journal Frontiers in Plant Science

RECEIVED 18 November 2022
ACCEPTED 23 January 2023
PUBLISHED 09 February 2023

CITATION
Norizuki T, Minamino N, Sato M and Ueda T (2023) Autophagy regulates plastid reorganization during spermatogenesis in the liverwort *Marchantia polymorpha*. *Front. Plant Sci.* 14:1101983. doi: 10.3389/fpls.2023.1101983

Autophagy regulates plastid reorganization during spermatogenesis in the liverwort *Marchantia polymorpha*

Takuya Norizuki[1,2], Naoki Minamino[1], Miyuki Sato[2] and Takashi Ueda[1,3]*

[1]Division of Cellular Dynamics, National Institute for Basic Biology, Okazaki, Japan, [2]Laboratory of Molecular Membrane Biology, Institute for Molecular and Cellular Regulation, Gunma University, Maebashi, Japan, [3]Department of Basic Biology, SOKENDAI (The Graduate University for Advanced Studies), Okazaki, Japan

Autophagy is a highly conserved system that delivers cytoplasmic components to lysosomes/vacuoles. Plastids are also degraded through autophagy for nutrient recycling and quality control; however, the involvement of autophagic degradation of plastids in plant cellular differentiation remains unclear. Here, we investigated whether spermiogenesis, the differentiation of spermatids into spermatozoids, in the liverwort *Marchantia polymorpha* involves autophagic degradation of plastids. Spermatozoids of *M. polymorpha* possess one cylindrical plastid at the posterior end of the cell body. By fluorescently labeling and visualizing plastids, we detected dynamic morphological changes during spermiogenesis. We found that a portion of the plastid was degraded in the vacuole in an autophagy-dependent manner during spermiogenesis, and impaired autophagy resulted in defective morphological transformation and starch accumulation in the plastid. Furthermore, we found that autophagy was dispensable for the reduction in plastid number and plastid DNA elimination. These results demonstrate a critical but selective role of autophagy in plastid reorganization during spermiogenesis in *M. polymorpha*.

KEYWORDS

autophagy, plastid, plastid DNA, spermiogenesis, spermatid, spermatozoid, *Marchantia polymorpha*

Introduction

Autophagy is a highly conserved mechanism that degrades cytoplasmic components in vacuoles/lysosomes for various cellular functions including nutrient recycling, homeostasis, and reorganization (Morishita and Mizushima, 2019). In plant cells, autophagy participates in various physiological processes such as development and abiotic and biotic stress responses (Marshall and Vierstra, 2018; Norizuki et al., 2020; Su et al., 2020). In addition

to bulk degradation for metabolic recycling, a wide range of cytoplasmic material is selectively degraded by autophagy in the vacuole/lysosome. The plastid (chloroplast) is a well-known target of selective autophagy in plant cells, which is important for responses to nutrition-limited conditions, senescence, and chloroplast damage (Izumi and Nakamura, 2018; Zhuang and Jiang, 2019; Wan and Ling, 2022). However, the role of autophagic degradation of plastids in cellular differentiation during plant development remains unknown.

Plastids exhibit a highly pleiomorphic nature during cellular differentiation and environmental changes, especially in non-green plastids (Osteryoung and Pyke, 2014). A striking morphological change in the plastid has also been observed during male gametogenesis in bryophytes. During sexual reproduction, bryophytes produce motile flagellated male gametes, termed spermatozoids. Most bryophyte spermatozoids consist of a cell body containing a cylindrical plastid filled with starch granules, a thin and helically elongated nucleus, two mitochondria, and two flagella protruding from the anterior edge of the cell body (Figure 1A; Renzaglia and Garbary, 2001). Transmission electron microscopy (TEM) has shown that plastids change their shape from spherical to cylindrical during spermiogenesis. Drastic reorganization also occurs inside the plastids. In the majority of plant species producing spermatozoids, as spermiogenesis proceeds, starch deposition increases and the thylakoidal structure is diminished, resulting in plastids mostly filled with starch granules (Carothers, 1975; Renzaglia and Garbary, 2001). However, the mechanism by which plastid reorganization occurs remains largely unknown.

Recently, autophagy has been shown to be required for organelle reorganization during spermiogenesis in bryophytes, including the moss *Physcomitrium patens* and the liverwort *Marchantia polymorpha* (Sanchez-Vera et al., 2017; Norizuki et al., 2022). In *P. patens*, impairment of autophagy results in an increased number of plastids without a change in the total area of the plastid (Sanchez-Vera et al., 2017), implying that autophagy suppresses plastid division through an unknown mechanism. However, it remains unclear whether bryophyte spermiogenesis involves autophagic degradation of the plastid and whether morphological transformation of the plastid is somehow mediated through autophagic activity.

In this study, we investigated whether autophagy is required for plastid reorganization during bryophyte spermiogenesis in *M. polymorpha*. Using confocal microscopy, we found that plastids dynamically changed their shape during spermatozoid formation.

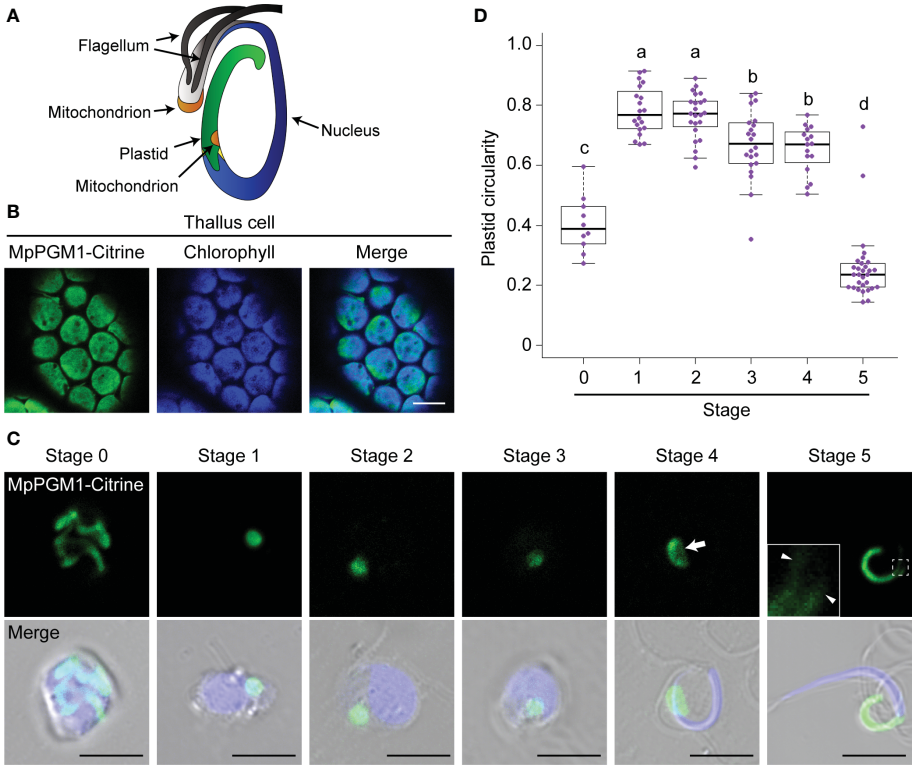

FIGURE 1
Morphological changes of the plastid during spermiogenesis in *M. polymorpha*. **(A)** Schematic illustration of a spermatozoid of *M. polymorpha*, depicted based on Carothers (1975). **(B)** Confocal images of thallus cells expressing MpPGM1-Citrine (green). The autofluorescence from chlorophyll is shown in blue. Eighteen cells were observed, and a representative result is presented. Scale bar = 10 µm. **(C)** Maximum-intensity projection images of cell-wall-digested antheridial cells and a spermatozoid at each developmental stage expressing MpPGM1-Citrine (green). A total of 20 stage-0, 29 stage-1, 32 stage-2, 31 stage-3, 22 stage-4, and 32 stage-5 cells were observed; representative images are presented. The nuclei were stained with Hoechst 33342 (blue). The arrow and arrowhead indicate the region of the weak signal from MpPGM1-Citrine and tubular extension from the plastid body, respectively. Scale bars = 5 µm. **(D)** The circularity of the plastid was calculated using the same set of samples analyzed in **(C)**. The boxes and solid lines in the boxes indicate the first and third quartiles and the median, respectively. The upper and lower whiskers are drawn at the greatest value smaller than 1.5× the interquartile range (IQR) above the third quartile and the smallest value greater than 1.5× the IQR below the first quartile, respectively. Different letters denote significant differences based on the Steel–Dwass test ($p < 0.05$).

We also found that a portion of the plastid was degraded in the vacuole *via* autophagy and impairment of autophagy resulted in defective morphological transformation and starch accumulation in the plastid during spermiogenesis. Furthermore, we discovered that plastid DNA was removed independently of autophagy. These results demonstrate that autophagy plays a critical and selective role in plastid reorganization during spermiogenesis in *M. polymorpha*.

Materials and methods

Plant materials and growth conditions

M. polymorpha accession Takaragaike-1 (Tak-1; Ishizaki et al., 2008) was grown asexually on 1/2× Gamborg's B5 medium containing 1.4% (w/v) agar at 22 °C under continuous white light. To induce antheridiophores, approximately two-week-old thalli were further cultivated on vermiculite soaked in 1:1000 Hyponex (HYPONeX JAPAN) at 22 °C under continuous white light for two weeks and then cultivated at 22 °C under continuous white light supplemented with far-red light. The transgenic plants used in this study are listed in Supplementary Table 1.

Vector construction and transformation

For nomenclature of genes, proteins, and mutants of *M. polymorpha*, we followed Bowman et al. (2016). Gene IDs were obtained from MarpolBase (http://marchantia.info/), genome version 5.1 (Montgomery et al., 2020). The primer sequences used in this study are listed in Supplementary Table 2.

To construct pENTR Mp*PGM1*, CDS for MpPGM1 (Mp4g13750) was amplified using PCR from cDNA prepared from Tak-1 thalli and subcloned into pENTR/D-TOPO (Thermo Fisher Scientific). To construct pENTR Mp*PGM1-mTurquoise2* (*monomeric Turquoise2*), the CDS for mTurquoise2, amplified by PCR, was inserted into the *Asc*I site of the pENTR Mp*PGM1* vector using the In-Fusion HD Cloning System (Clontech). To construct pENTR *TP-sGFP*, the sequence for the transit peptide (TP) of MpSIG2 (Mp4g13380; Kanazawa et al., 2013) was amplified *via* PCR from cDNA prepared from the Tak-1 thalli. The amplified fragments of TP_Mp*SIG2* and cDNA for sGFP were conjugated using PCR *via* homologous double crossover, and the amplified product was subcloned into pENTR/D-TOPO. The sequences flanked by the *att*L1 and *att*L2 sites in pENTR Mp*PGM1*, pENTR Mp*PGM1-mTurquoise2*, or pENTR *TP-sGFP* were introduced into pMpGWB308, pMpGWB103, or pMpGWB303 (Ishizaki et al., 2015), respectively, using the Gateway LR Clonase™ II Enzyme Mix (Thermo Fisher Scientific) according to the manufacturer's instructions.

Transformation of *M. polymorpha* was performed as previously described (Norizuki et al., 2022). Transformants were selected on plates containing 10 mg/L hygromycin B and 250 mg/L cefotaxime for the pMpGWB103 Mp*PGM1-mTurquoise2* vector, and 0.5 μM chlorsulfuron and 250 mg/L cefotaxime for the pMpGWB308 Mp*PGM1-Citrine* and pMpGWB303 *TP-sGFP* vectors.

Confocal microscopic and TEM observation

To observe thallus cells expressing MpPGM1-Citrine, five-day-old thalli were used.

To observe stage 0–4 spermatids, antheridia were fixed with 4% (w/v) paraformaldehyde and their cell walls were digested with 1% (w/v) Cellulase Onozuka RS (SERVA) and 0.25% (w/v) Pectolyase Y-23 (Kyowa Chemical Products), as previously described (Norizuki et al., 2022). The samples were incubated in PME buffer (50 mM PIPES, 5 mM EGTA, and 1 mM $MgSO_4$, adjusted to pH 6.8 using NaOH) containing 1 μg/mL Hoechst 33342 (Dojindo).

Spermatozoids (stage 5) were obtained by placing a mature antheridiophore upside-down on a drop of 20–30 μL water for 1 min and fixing in 4% (w/v) paraformaldehyde in PBS buffer (150 mM NaCl, 80 mM Na_2HPO_4, and 40 mM NaH_2PO_4, adjusted to pH 6.8, using NaOH) for 5 min. Fixed spermatozoids were centrifuged at 9,100 × *g* for 1 min, and the pellet was suspended in PBS buffer containing 1 μg/mL Hoechst 33342.

For simultaneous observation of plastid and vacuole markers in spermatids, antheridiophores were manually sectioned using a razor blade.

For immunostaining, fixed and cell-wall-digested antheridial cells were used, as previously described (Norizuki et al., 2022). As a primary antibody, the anti-double-stranded DNA (dsDNA) antibody (HYB331-01; Santa Cruz Biotechnology) was used at a 200× dilution. As a secondary antibody, Alexa Fluor™ 546 goat anti-mouse IgG (H+L) (Thermo Fisher Scientific), or goat anti-mouse IgG (H+L) Alexa Fluor™ Plus 488 (Thermo Fisher Scientific) were used at a 1000× dilution. The samples were mounted using ProLong™ Diamond Antifade Mountant (Thermo Fisher Scientific) and incubated for at least 24 h at room temperature in the dark.

For confocal microscopic observations, an LSM780 confocal microscope (Carl Zeiss) equipped with an oil immersion lens (×63, numerical aperture = 1.4) was used.

For TEM observation, wild-type and Mp*atg5-1*^{ge} antheridia were subjected to electron microscopy, as described previously (Norizuki et al., 2022).

Quantification and statistical analyses

Maximum-intensity projection images created from z-stacked images using ImageJ (version 1.50i; National Institute of Health) were used to calculate plastid circularity. To calculate the occupancy of starch granules in the area of the plastid, the total area of starch granules, which were observed as electron-dense structures, and the area of the plastid were calculated using ImageJ. The number of the large spherical vacuole and the plastid were counted using single-sectioned 22.49 μm × 22.49 μm images. To test the normality of the data, the Shapiro–Wilk test was performed using R (version 3.6.0; The R project), and samples were considered nonparametric when the *p* value was less than 0.05. For comparison between two groups, the Wilcoxon rank-sum test (for nonparametric samples) or Welch's *t* test (for parametric samples) was performed using R software. For statistical analyses among three or more groups, the Steel–Dwass test

was performed using R. Details of the statistical methods are indicated in each figure legend.

Results

The plastid changes its shape during spermiogenesis

To observe how the plastid changes its shape during spermiogenesis, we generated transgenic *M. polymorpha* expressing fluorescently tagged MpPGM1. *PGM* genes encode phosphoglucomutase (PGM), and plastidal PGM (AtPGM1) is required for starch synthesis in plastids of *Arabidopsis thaliana* (Caspar et al., 1985; Periappuram et al., 2000). In *M. polymorpha* thallus cells, MpPGM1-Citrine was localized in chloroplasts, overlapping with autofluorescence from chlorophyll, confirming that MpPGM1-Citrine can be used as a plastid marker in *M. polymorpha* (Figure 1B). Using this marker, we observed plastid reorganization during spermiogenesis, which can be divided into 1 + 5 stages (stages 0–5) based on flagellar formation and nuclear shape (Minamino et al., 2022). In cells at stage 0, which included spermatogenous cells, spermatid mother cells, and spermatids before the appearance of flagella, tentaculate plastids were observed. At stages 1–4, one plastid with a spherical or lens-like shape was observed in each cell. Notably, at stage 4, an area with a weaker fluorescent signal from MpPGM1-Citrine was detected around the center of the plastid (the arrow in Figure 1C), which could be the region where the posterior mitochondrion is embedded, as reported in a previous TEM observation (Carothers, 1975). In stage-5 cells, which are mature spermatozoids, the plastid exhibited a cylindrical shape with thin tubular extensions associated with the posterior end of the nucleus (arrowheads in Figure 1C), as described previously (Carothers, 1975). Consistent with this observation, the circularity of the plastid increased between stages 0 and 1 and drastically decreased before stage 5 (Figure 1D). Similar results were obtained using another plastid marker, TP-sGFP, sGFP fused with the transit peptide (TP) of MpSIG2, which is a nucleus-encoded subunit of plastid-encoded plastid RNA polymerase (Kanazawa et al., 2013) (Figure S1). These results indicate that dynamic morphological changes occur in the plastid during spermiogenesis in *M. polymorpha*.

Autophagy is involved in the plastid reorganization during spermiogenesis

We previously demonstrated that autophagy is required for reorganization of various organelles during spermiogenesis in *M. polymorpha* (Norizuki et al., 2022). To investigate whether autophagy is also involved in plastid reorganization during spermiogenesis, we observed plastids in spermatozoids of the Mp*atg5-1*^{ge} mutant, which is defective in autophagy (Norizuki et al., 2019; 2022). Whereas wild-type spermatozoids possessed one cylindrical plastid, more than 90% of Mp*atg5-1*^{ge} spermatozoids possessed one spherical plastid, and three out of the 54 Mp*atg5-1*^{ge} spermatozoids possessed two spherical plastids (Figures 2A, B). This result suggests that morphological changes in plastids involve autophagy. To gain further insight into the role of autophagy in plastid reorganization during spermiogenesis, we observed morphological changes in plastids during spermiogenesis in Mp*atg5-1*^{ge} spermatids. Compared with wild-type spermatids, striking differences were detected at stages 1 and 2; the plastids in Mp*atg5-1*^{ge} were complex in shape than the spherical wild-type plastids (Figures 3A–E). These results suggest that autophagy is involved in drastic morphological changes in the plastids during early spermiogenesis.

It has been reported that thylakoids are lost and starch deposition occurs as spermiogenesis proceeds, resulting in plastids mostly filled with starch granules in the spermatozoids of many plant species (Renzaglia and Garbary, 2001). Consistent with previous observations, the wild-type plastid at around stage 1-2 contained many starch granules that were observed as electron-dense structures using TEM. However, the plastids in Mp*atg5-1*^{ge} spermatids contained significantly fewer starch granules than wild-type plastids, suggesting that autophagy may be involved in starch synthesis regulation during spermiogenesis (Figures 3F, G). These results suggest that autophagy also plays important roles in plastid

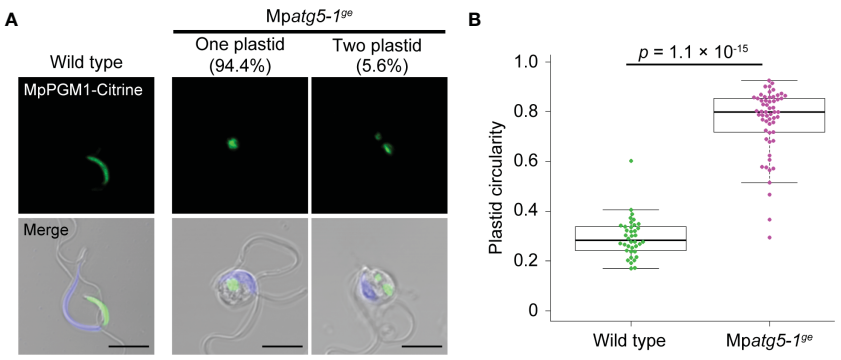

FIGURE 2
Impaired morphological changes of the plastid in the autophagy-defective mutant. **(A)** Confocal images of wild-type and Mp*atg5-1*^{ge} spermatozoids expressing MpPGM1-Citrine (green). The nuclei were stained with Hoechst 33342 (blue). Scale bars = 5 µm. A total of 38 wild-type and 54 Mp*atg5-1*^{ge} spermatozoids were observed and representative images are presented. **(B)** The circularity of the plastid was calculated using the same set of samples analyzed in **(A)**. The boxes and solid lines in the boxes indicate the first and third quartiles and the median, respectively. The upper and lower whiskers are drawn at the greatest value smaller than 1.5× the IQR above the third quartile and the smallest value greater than 1.5× the IQR below the first quartile, respectively. The *p* values obtained using the Wilcoxon rank-sum test are presented.

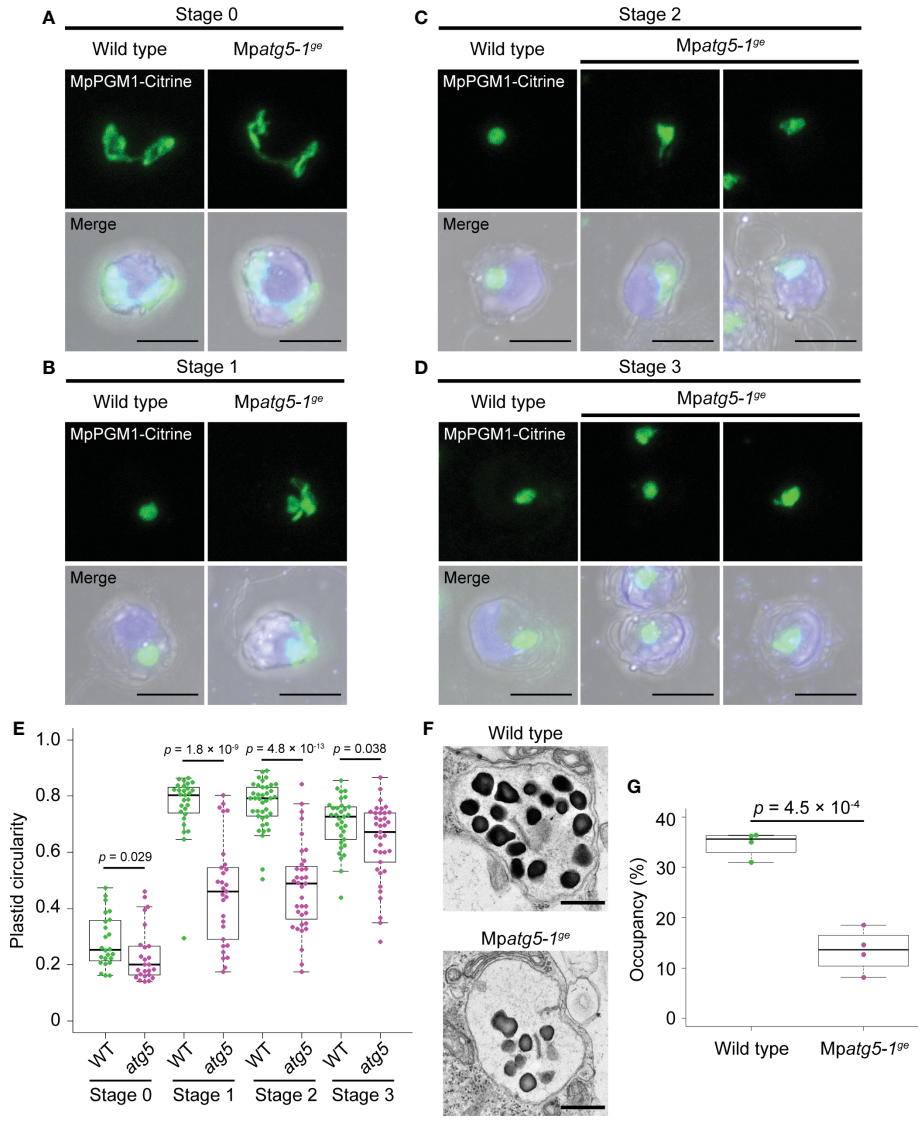

FIGURE 3
Defects in plastid reorganization during spermiogenesis in the autophagy-defective mutant. **(A–D)** Confocal images of the wild-type and Mp*atg5-1*^{ge} antheridial cells expressing MpPGM1-Citrine (green) at stage 0 **(A)**, 1 **(B)**, 2 **(C)**, and 3 **(D)**. Nuclei were stained with Hoechst 33342 (blue). Scale bars = 5 µm. A total of 24 stage-0, 28 stage-1, 39 stage-2, and 33 stage-3 cells were observed for wild-type antheridial cells, and 25 stage-0, 28 stage-1, 35 stage-2, and 37 stage-3 cells were observed for Mp*atg5-1*^{ge}. Representative images are presented. **(E)** Circularity of the plastid calculated in the same sets of wild-type (WT) and Mp*atg5-1*^{ge} (*atg5*) samples analyzed in **(A–D)**. **(F)** TEM observation of the plastids in wild-type and Mp*atg5-1*^{ge} spermatids around stage 1-2. Scale bars = 500 nm. Four plastids were observed for each genotype, and representative images are presented. **(G)** Occupancy of starch granules in plastids. Occupancy indicates the ratio of the total area of the starch granules within a plastid to the area of the plastid. Occupancy was calculated using the same sets of samples analyzed in **(F)**. For **(E)** and **(G)**, the boxes and solid lines in the boxes indicate the first and third quartiles and median, respectively. The upper and lower whiskers are drawn at the greatest value smaller than 1.5× the IQR above the third quartile and the smallest value greater than 1.5× the IQR below the first quartile, respectively. The *p* values obtained by the Wilcoxon rank-sum test **(E)** or Welch's *t* test **(G)** are shown.

reorganization, which is required for shaping plastid and starch synthesis during spermiogenesis, although its role in the regulation of the number of plastids is minor.

The plastid is degraded by autophagy during spermiogenesis

We previously demonstrated that multiple organelles including mitochondria are degraded in the vacuole through autophagy during spermiogenesis in *M. polymorpha* (Norizuki et al., 2022). The observation that the autophagy-defective mutant exhibited impaired morphological transformation of the plastid and starch accumulation prompted us to investigate whether autophagy-dependent degradation of the plastid occurs during spermiogenesis. For this purpose, we investigated a plastid marker in spermatids, in which the vacuolar membrane was also visualized using mCitrine-MpVAMP71 (Kanazawa et al., 2016; Minamino et al., 2017). In wild-type spermatids, fluorescence from MpPGM1-mTurquoise2 was detected in the vacuole lumen, indicating that some of the plastid stroma was transported into the vacuole for degradation (Figure 4A). However, in Mp*atg5-1*$^{ge/cf}$

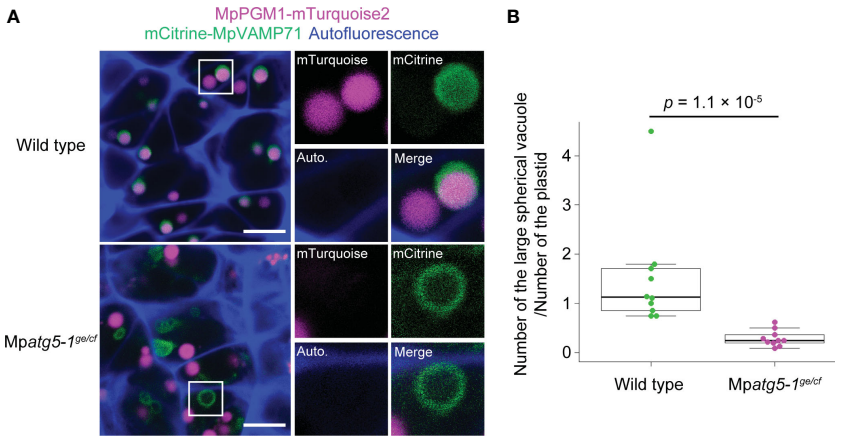

FIGURE 4
MpATG5-dependent vacuolar degradation of the plastid during spermiogenesis. **(A)** Confocal images of hand-sectioned antheridial cells of wild-type and Mp*atg5-1*$^{ge/cf}$ mutant plants co-expressing MpPGM1-mTurquoise2 (magenta) and mCitrine-MpVAMP71 (green). The autofluorescence probably from auronidin (Berland et al., 2019) is shown in blue. 10 images (22.49 µm × 22.49 µm) were obtained for each genotype, and representative images are presented. The right two panels show the enlarged images of the boxed regions. Scale bars = 5 µm. **(B)** The number of large spherical vacuoles observed in the confocal sections. The vacuole number was normalized by the plastid number, because most of wild-type and Mp*atg5* spermatozoids possess a single plastid (see Figures 2). Vacuoles and plastids in 10 images obtained in **(A)** were counted for each genotype. The boxes and solid lines in the boxes indicate the first and third quartiles and median, respectively. The upper and lower whiskers are drawn at the greatest value smaller than 1.5× the IQR above the third quartile and the smallest value greater than 1.5× the IQR below the first quartile, respectively. The *p* values obtained by the Wilcoxon rank-sum test is indicated.

spermatids (Norizuki et al., 2022), the fluorescent signal from MpPGM1-mTurquoise2 was not detected in the vacuole (Figure 4A). We also noted that the number of the large spherical vacuole detected in confocal images was significantly decreased in Mp*atg5-1*$^{ge/cf}$ spermatids (Figure 4B). The mistargeting of MpPGM1-mTurquoise2 should not be due to the reduced number of the functional vacuole, because vacuolar targeting and degradation of the plasma membrane protein MpSYP12A and Golgi proteins occur in Mp*atg5-1*$^{ge/cf}$ spermatids similar to wild-type spermatids (Norizuki et al., 2022). These results indicate that a portion of the plastid is degraded by autophagy during spermiogenesis in *M. polymorpha*.

Plastid DNA is eliminated from spermatids independent of autophagy

Unlike nuclear DNA, plastid and mitochondrial DNA are uniparentally inherited, with minor exceptions (Kuroiwa, 2010). In bryophytes, elimination of plastid DNA has been reported to occur during spermiogenesis in the liverwort *Dumortiera hirsuta* and the hornwort *Anthoceros punctatus* (Izumi and Ono, 1999; Shimamura et al., 1999). Based on our finding that a portion of the plastid is degraded *via* autophagy during spermiogenesis in *M. polymorpha* (Figure 4), we hypothesized that plastid DNA could be degraded through autophagy. To test this hypothesis, we detected organelle DNA using an dsDNA antibody. In addition to the strong signal in the nucleus representing nuclear DNA, we detected fluorescent signals in the cytoplasm of wild-type spermatids at stages 0–2. This signal overlapped with the plastid visualized using MpPGM1-Citrine, suggesting that this signal represents the plastid DNA (Figure 5A). Under our experimental conditions we did not detect mitochondrial DNA during spermiogenesis. In cells at stage 4, signal intensity from nuclear DNA was reduced compared with earlier stages, probably due to the restricted accessibility of the antibody to nuclear DNA resulting from chromatin compaction through the function of protamine (Figure 5B) (Kreitner, 1977; D'Ippolito et al., 2019). At this stage, the signal from plastid DNA was not detected, suggesting that elimination of plastid DNA occurs before stage 4 during spermiogenesis in *M. polymorpha* (Figure 5B). Contrary to our expectations, the removal of plastid DNA was also observed in Mp*atg5-1*^{ge} spermatids (Figure 5B). This result indicates that autophagy is dispensable for plastid DNA removal during spermiogenesis in *M. polymorpha*.

Discussion

In this study, we showed that autophagy is involved in the reorganization of plastids during spermiogenesis in *M. polymorpha*, especially during morphological transformation. Plastid degradation through autophagy has been intensively analyzed in *Arabidopsis thaliana*; it is divided into two types: a piecemeal type in which a portion of the plastid is degraded by autophagy (Ishida et al., 2008; Wang et al., 2013; Michaeli et al., 2014), and autophagic degradation of entire plastids (Wada et al., 2009; Izumi et al., 2017; Nakamura et al., 2018). These types of plastid degradation are both dependent on ATG5 activity (Ishida et al., 2008; Wang et al., 2013; Michaeli et al., 2014; Izumi et al., 2017; Nakamura et al., 2018) and responsible for normal stress responses (Izumi and Nakamura, 2018; Zhuang and Jiang, 2019; Wan and Ling, 2022); however, it remains unclear whether autophagy of plastids is involved in cellular differentiation.

10.3389/fpls.2023.1101983

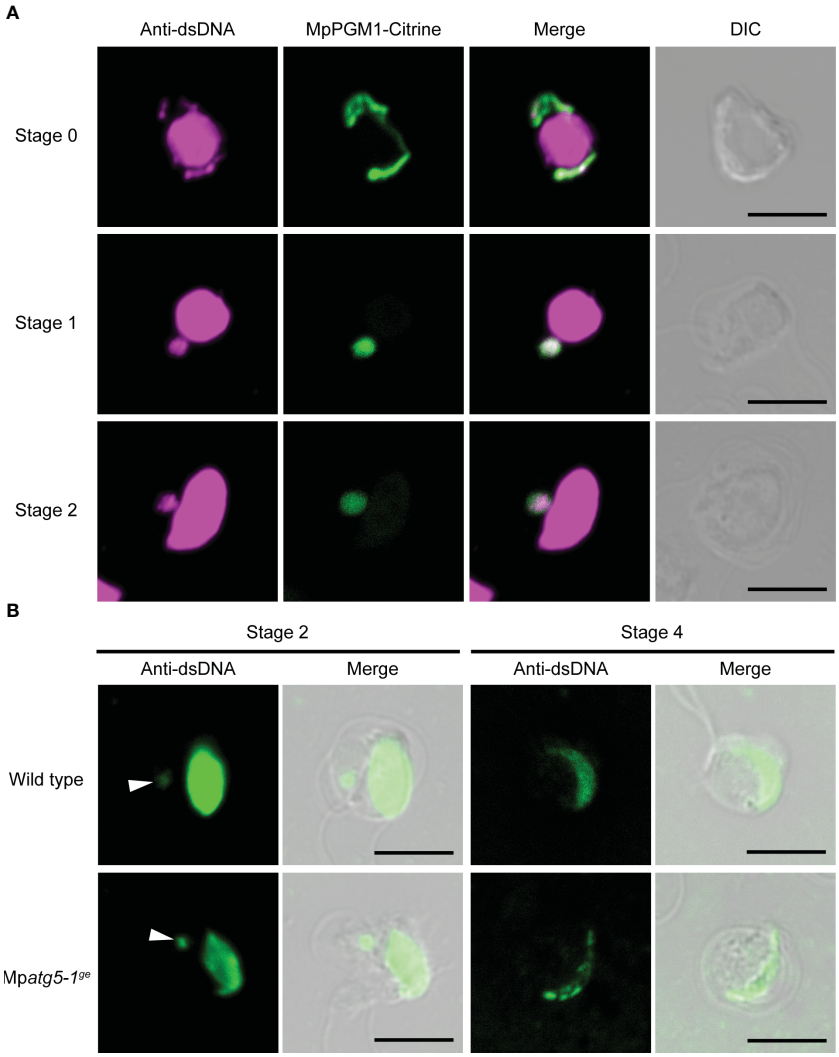

FIGURE 5
MpATG5-independent loss of plastid DNA during spermiogenesis. **(A)** Immunostaining of dsDNA (magenta) in wild-type antheridial cells expressing MpPGM1-Citrine (green). At least seven cells were observed at each stage and representative images are presented. Scale bars = 5 µm. DIC: differential interference contrast. **(B)** Immunostaining of dsDNA (green) in wild-type and Mp*atg5-1*^{ge} spermatids. Arrowheads indicate signals from plastid DNA. As a secondary antibody, Alexa Fluor 546 **(A)** or Alexa Fluor Plus 488 **(B)** was used. At least three cells were observed and representative images are presented. Scale bars = 5 µm.

In this study, we showed that in *M. polymorpha*, ATG5-dependent autophagic degradation of a portion of the plastid occurs during differentiation from the spermatid to the spermatozoid.

During spermiogenesis in *M. polymorpha*, the loss of function of Mp*ATG5* did not substantially affect the number of plastids (Figure 2A), suggesting that piecemeal plastid degradation occurs in spermatids undergoing spermiogenesis. Although several cargoes for the piecemeal-type autophagic degradation of plastids have been reported (Izumi and Nakamura, 2018; Zhuang and Jiang, 2019; Wan and Ling, 2022), it remains unknown which components of the plastid are degraded by autophagy during spermiogenesis in *M. polymorpha*. Although plastid DNA is eliminated during spermiogenesis in *M. polymorpha*, autophagy is unnecessary for this process, indicating that plastid DNA is not a direct target of autophagy (Figure 5). Several factors that affect plastid morphology in somatic plant cells have been reported, including sugar content and osmolarity (Haswell and Meyerowitz, 2006; Stettler et al., 2009; Veley et al., 2012). As starch accumulation is reduced in the Mp*atg5-1*^{ge} spermatid (Figures 3F, G), autophagy may regulate plastid morphology *via* degradation of the regulatory system for starch synthesis, which would affect sugar content and/or osmolarity in the plastid. However, a secondary effect due to the impaired reorganization of organelles other than the plastid cannot be ruled out, given the association of the plastid with other organelles, such as the nucleus and the posterior mitochondrion, during spermiogenesis (Carothers, 1975; Norizuki et al., 2022).

In addition to the plastid, our previous research has demonstrated that the endoplasmic reticulum, the Golgi apparatus, mitochondria, and peroxisomes are also degraded through autophagy during spermiogenesis in *M. polymorpha*. This autophagy-dependent reorganization is critical for spermatozoid function, such as motility and fertility. The degradation of mitochondria appears to occur before that of other organelles, indicating that the autophagic degradation of

each organelle may be regulated differently (Norizuki et al., 2022). The degradation of the plastid must also be distinctly regulated from that of other organelles; unlike endomembrane organelles such as the endoplasmic reticulum and Golgi apparatus, which are fully removed from spermatids during spermiogenesis, the plastid is retained in the mature spermatozoid (Figure 1A; Minamino et al., 2022; Norizuki et al., 2022). Further studies will be required to fully understand the molecular mechanisms underlying the degradation of each organelle. Intriguingly, organelle elimination occurs after spermiogenesis in some bryophyte species; the plastid and the posterior mitochondrion have been observed to be removed from spermatozoids during movement in water after release from the antheridia in certain bryophytes, such as the liverwort *Blasia pusilla* and the moss Sphagnum (Manton, 1957; Sears, 1980; Renzaglia and Duckett, 1987). Thus, the elimination of the plastid and mitochondria occurs at multiple stages in bryophytes.

Autophagy is also required for spermiogenesis in organisms other than *M. polymorpha*, but its roles seem to be differentiated among eukaryotic lineages (Norizuki et al., 2020). Even in bryophytes, distinct effects of defective autophagy on plastid reorganization have been reported. Although a larger number of plastids is observed in autophagy-defective mutants of the moss *P. patens* (Sanchez-Vera et al., 2017), the plastid number was not markedly altered by the Mp*atg5-1*^{ge} mutation in the liverwort *M. polymorpha* in our study (Figure 3A). The roles of autophagy in the reorganization of mitochondria and microtubule structures also differ between these species (Sanchez-Vera et al., 2017; Norizuki et al., 2022). These lines of evidence could reflect distinctly regulated organelle reorganization *via* autophagy among bryophytes, although bryophyte spermatozoids possess a shared organelle composition (Renzaglia and Garbary, 2001). Further analyses are needed to obtain insights into the shared and diversified mechanisms of organelle reorganization during spermiogenesis in bryophytes.

In conclusion, autophagy is important for morphological changes in plastids during spermiogenesis in *M. polymorpha*. Although plastids exhibit a pleiomorphic nature, it remains unclear how their complex morphology is controlled (Osteryoung and Pyke, 2014; Hanson and Conklin, 2020). Reorganization of the plastid during spermiogenesis in *M. polymorpha* should be a good model for analyzing the regulatory mechanisms of plastid morphology, with respect to not only the roles of autophagy but also to other cellular activities, given that the drastic morphological transformation occurs in a relatively short period in a synchronous manner in its antheridium.

Data availability statement

The original contributions presented in the study are included in the article/Supplementary Material. Further inquiries can be directed to the corresponding author.

Author contributions

TN performed the majority of the experiments. NM performed TEM experiments. TN and TU wrote the manuscript and MS and TU supervised the study. All authors contributed to the article and approved the submitted version.

Funding

This study was supported by Grants-in-Aid for Scientific Research from the Ministry of Education, Culture, Sports, Science, and Technology of Japan (20K15824 and 22K15149 to N.M., and 19H05675, 19H05670, and 21H02515 to T.U.), a Grant-in-Aid from the Japan Society for the Promotion of Science (JSPS) (19J13751 to TN), the Joint Research Program of the Institute for Molecular and Cellular Regulation, Gunma University (21014 to TU), and the NIBB Collaborative Research Program (22-NIBB329 to MS).

Acknowledgments

We thank Dr. Takayuki Kohchi (Kyoto University), Dr. Ryuichi Nishihama (Tokyo University of Science), and Dr. Takehiko Kanazawa (National Institute for Basic Biology) for sharing the vectors or plant materials. We thank Mr. Koji Hayashi (National Institute for Basic Biology) for his support with plant cultivation. We thank the Model Plant Section, Model Organisms Facility, and NIBB Trans-Scale Biology Center for providing plant cultivation facilities.

Conflict of interest

The authors declare that the research was conducted in the absence of any commercial or financial relationships that could be construed as a potential conflict of interest.

Publisher's note

Supplementary material

The Supplementary Material for this article can be found online at: https://www.frontiersin.org/articles/10.3389/fpls.2023.1101983/full#supplementary-material

References

Berland, H., Albert, N. W., Stavland, A., Jordheim, M., McGhie, T. K., Zhou, Y., et al. (2019). Auronidins are a previously unreported class of flavonoid pigments that challenges when anthocyanin biosynthesis evolved in plants. *Proc. Natl. Acad. Sci. U.S.A.* 116, 20232–20239. doi: 10.1073/pnas.1912741116

Bowman, J. L., Araki, T., Arteaga-Vazquez, M. A., Berger, F., Dolan, L., Haseloff, J., et al. (2016). The naming of names: guidelines for gene nomenclature in *Marchantia*. *Plant Cell Physiol.* 57, 257–261. doi: 10.1093/pcp/pcv193

Carothers, Z. B. (1975). "Comparative studies on spermatogenesis in bryophytes," in *The biology of the Male gamete*. Eds. J. G. Duckett and P. A. Racey (Cambridge, MA: Academic Press), 71–84.

Caspar, T., Huber, S. C., and Somerville, C. (1985). Alternations in growth, photosynthesis, and respiration in a starchless mutant of *Arabidopsis thaliana* (L.) deficient in chloroplast phosphoglucomutase activity. *Plant Physiol.* 79, 11–17. doi: 10.1104/pp.79.1.11

D'Ippolito, R. A., Minamino, N., Rivera-Casas, C., Cheema, M. S., Bai, D. L., Kasinsky, H. E., et al. (2019). Protamines from liverwort are produced by post-translational cleavage and C-terminal di-aminopropanelation of several male germ-specific H1 histones. *J. Biol. Chem.* 294, 16364–16373. doi: 10.1074/jbc.RA119.010316

Hanson, M. R., and Conklin, P. L. (2020). Stromules, functional extensions of plastids within the plant cell. *Curr. Opin. Plant Biol.* 58, 25–32. doi: 10.1016/j.pbi.2020.10.005

Haswell, E. S., and Meyerowitz, E. M. (2006). MscS-like proteins control plastid size and shape in *Arabidopsis thalina*. *Curr. Biol.* 16, 1–11. doi: 10.1016/j.cub.2005.11.044

Ishida, H., Yoshimoto, K., Izumi, M., Reisen, D., Yano, Y., Makino, A., et al. (2008). Mobilization of Rubisco and stroma-localized fluorescent proteins of chloroplasts to the vacuole by an *ATG* gene-dependent autophagic process. *Plant Physiol.* 148, 142–155. doi: 10.1104/pp.108.122770

Ishizaki, K., Chiyoda, S., Yamato, K. T., and Kohchi, T. (2008). *Agrobacterium*-mediated transformation of the haploid liverwort *Marchantia polymorpha* L., an emerging model for plant biology. *Plant Cell Physiol.* 49, 1084–1091. doi: 10.1093/pcp/pcn085

Ishizaki, K., Nishihama, R., Ueda, M., Inoue, K., Ishida, S., Nishimura, Y., et al. (2015). Development of gateway binary vector series with four different selection markers for the liverwort *Marchantia polymorpha*. *PLoS One* 10, e0138876. doi: 10.1371/journal.pone.0138876

Izumi, M., Ishida, H., Nakamura, S., and Hidema, J. (2017). Entire photodamaged chloroplasts are transported to the central vacuole by autophagy. *Plant Cell* 29, 377–394. doi: 10.1105/tpc.16.00637

Izumi, M., and Nakamura, S. (2018). Chloroplast protein turnover: the influence of extraplastidic processes, including autophagy. *Int. J. Mol. Sci.* 19, 828. doi: 10.3390/ijms19030828

Izumi, Y., and Ono, K. (1999). Changes in plastid DNA content during the life cycle of the hornwort *Anthoceros punctatus* L. *Cytologia* 64, 37–44. doi: 10.1508/cytologia.64.37

Kanazawa, T., Era, A., Minamino, N., Shikano, Y., Fujimoto, M., Uemura, T., et al. (2016). SNARE molecules in *Marchantia polymorpha*: Unique and conserved features of the membrane fusion machinery. *Plant Cell Physiol.* 57, 307–324. doi: 10.1093/pcp/pcv076

Kanazawa, T., Ishizaki, K., Kohchi, T., Hanaoka, M., and Tanaka, K. (2013). Characterization of four nuclear-encoded plastid RNA polymerase sigma factor genes in the liverwort *Marchantia polymorpha*: Blue-light- and multiple stress-responsive *SIG5* was acquired early in the emergence of terrestrial plants. *Plant Cell Physiol.* 54, 1736–1748. doi: 10.1093/pcp/pct119

Kreitner, G. L. (1977). Transformation of the nucleus in Marchantia spermatids: morphogenesis. *Am. J. Bot.* 64, 464–475. doi: 10.1002/j.1537-2197.1977.tb12370.x

Kuroiwa, T. (2010). Review of cytological studies on cellular and molecular mechanisms of uniparental (maternal or paternal) inheritance of plastid and mitochondrial genomes induced by active digestion of organelle nuclei (nucleoids). *J. Plant Res.* 123, 207–230. doi: 10.1007/s10265-009-0306-9

Manton, I. (1957). Observations with the electron microscope on the cell structure of the antheridium and spermatozoid of sphagnum. *J. Exp. Bot.* 8, 382–400. doi: 10.1093/jxb/8.3.382

Marshall, R. S., and Vierstra, R. D. (2018). Autophagy: The master of bulk and selective recycling. *Annu. Rev. Plant Biol.* 69, 173–208. doi: 10.1146/annurev-arplant-042817-040606

Michaeli, S., Honig, A., Levanony, H., Peled-Zehavi, H., and Galili, G. (2014). *Arabidopsis* ATG8-INTERACTING PROTEIN1 is involved in autophagy-dependent vesicular trafficking of plastid proteins to the vacuole. *Plant Cell* 26, 4084–4101. doi: 10.1105/tpc.114.129999

Minamino, N., Kanazawa, T., Nishihama, R., Yamato, K. T., Ishizaki, K., Kohchi, T., et al. (2017). Dynamic reorganization of the endomembrane system during spermatogenesis in *Marchantia polymorpha*. *J. Plant Res.* 130, 433–441. doi: 10.1007/s10265-017-0909-5

Minamino, N., Norizuki, T., Mano, S., Ebine, K., and Ueda, T. (2022). Remodeling of organelles and microtubules during spermiogenesis in the liverwort *Marchantia polymorpha*. *Development* 149, dev200951. doi: 10.1242/dev.200951

Montgomery, S. A., Tanizawa, Y., Galik, B., Wang, N., Ito, T., Mochizuki, T., et al. (2020). Chromatin organization in early land plants reveals an ancestral association between H3K27me3, transposons, and constitutive heterochromatin. *Curr. Biol.* 30, 573–588.e7. doi: 10.1016/j.cub.2019.12.015

Morishita, H., and Mizushima, N. (2019). Diverse cellular roles of autophagy. *Annu. Rev. Cell Dev. Biol.* 35, 453–475. doi: 10.1146/annurev-cellbio-100818-125300

Nakamura, S., Hidema, J., Sakamoto, W., Ishida, H., and Izumi, M. (2018). Selective elimination of membrane-damaged chloroplasts *via* microautophagy. *Plant Physiol.* 177, 1007–1026. doi: 10.1104/pp.18.00444

Norizuki, T., Kanazawa, T., Minamino, N., Tsukaya, H., and Ueda, T. (2019). *Marchantia polymorpha*, a new model plant for autophagy studies. *Front. Plant Sci.* 10. doi: 10.3389/fpls.2019.00935

Norizuki, T., Minamino, N., Sato, M., Tsukaya, H., and Ueda, T. (2022). Dynamic rearrangement and autophagic degradation of mitochondria during spermiogenesis in the liverwort *Marchantia polymorpha*. *Cell Rep.* 39, 110975. doi: 10.1016/j.celrep.2022.110975

Norizuki, T., Minamino, N., and Ueda, T. (2020). Role of autophagy in male reproductive processes in land plants. *Front. Plant Sci.* 11. doi: 10.3389/fpls.2020.00756

Osteryoung, K. W., and Pyke, K. A. (2014). Division and dynamic morphology of plastids. *Annu. Rev. Plant Biol.* 65, 443–472. doi: 10.1146/annurev-arplant-050213-035748

Periappuram, C., Steinhauer, L., Barton, D. L., Taylor, D. C., Chatson, B., and Zou, J. (2000). The plastidic phosphoglucomutase from Arabidopsis. A reversible enzyme reaction with an important role in metabolic control. *Plant Physiol.* 122, 1193–1199. doi: 10.1104/pp.122.4.1193

Renzaglia, K. S., and Duckett, J. G. (1987). Spermatogenesis in *Blasia pusilla*: from young antheridium through mature spermatozoid. *Bryologist* 90, 419–449. doi: 10.2307/3243109

Renzaglia, K. S., and Garbary, D. J. (2001). Motile gametes of land plants: diversity, development, and evolution. *Crit. Rev. Plant Sci.* 20, 107–213. doi: 10.1080/20013591099209

Sanchez-Vera, V., Kenchappa, C. S., Landberg, K., Bressendorff, S., Schwarzbach, S., Martin, T., et al. (2017). Autophagy is required for gamete differentiation in the moss *Physcomitrella patens*. *Autophagy* 13, 1939–1951. doi: 10.1080/15548627.2017.1366406

Sears, B. B. (1980). Elimination of plastids during spermatogenesis and fertilization in the plant kingdom. *Plasmid* 4, 233–255. doi: 10.1016/0147-619X(80)90063-3

Shimamura, M., Fukushima, H., Yamaguchi, T., and Deguchi, H. (1999). Behavior of plastid and plastid DNA during spermiogenesis in *Dumortiera hirsuta*. *Bryol. Res.* 7, 201–204. doi: 10.24474/bryologicalresearch.7.7_201

Stettler, M., Eicke, S., Mettler, T., Messerli, G., Hörtensteiner, S., and Zeeman, S. C. (2009). Blocking the metabolism of starch breakdown products in *Arabidopsis* leaves triggers chloroplast degradation. *Mol. Plant* 2, 1233–1246. doi: 10.1093/mp/ssp093

Su, T., Li, X., Yang, M., Shao, Q., Zhao, Y., Ma, C., et al. (2020). Autophagy: an intracellular degradation pathway regulating plant survival and stress response. *Front. Plant Sci.* 11. doi: 10.3389/fpls.2020.00164

Veley, K. M., Marshburn, S., Clure, C. E., and Haswell, E. S. (2012). Mechanosensitive channels protect plastids from hypoosomotic stress during normal plant growth. *Curr. Biol.* 22, 408–413. doi: 10.1016/j.cub.2012.01.027

Wada, S., Ishida, H., Izumi, M., Yoshimoto, K., Ohsumi, Y., Mae, T., et al. (2009). Autophagy plays a role in chloroplast degradation during senescence in individually darkened leaves. *Plant Physiol.* 149, 885–893. doi: 10.1104/pp.108.130013

Wang, Y., Yu, B., Zhao, J., Guo, J., Li, Y., Han, S., et al. (2013). Autophagy contributes to leaf starch degradation. *Plant Cell* 25, 1383–1399. doi: 10.1105/tpc.112.108993

Wan, C., and Ling, Q. (2022). Functions of autophagy in chloroplast protein degradation and homeostasis. *Front. Plant Sci.* 13. doi: 10.3389/fpls.2022.993215

Zhuang, X., and Jiang, L. (2019). Chloroplast degradation: Multiple routes into the vacuole. *Front. Plant Sci.* 10. doi: 10.3389/fpls.2019.00359

frontiers | Frontiers in Plant Science

TYPE Review
PUBLISHED 10 February 2023
DOI 10.3389/fpls.2023.1120841

OPEN ACCESS

EDITED BY
Emily R. Larson,
University of Bristol, United Kingdom

REVIEWED BY
Andrei Smertenko,
Washington State University, United States
Yohann Boutté,
UMR5200 Laboratoire de biogenèse membranaire (LBM), France

*CORRESPONDENCE
Dong Qian
qiand@lzu.edu.cn

SPECIALTY SECTION
This article was submitted to Plant Cell Biology, a section of the journal Frontiers in Plant Science

RECEIVED 10 December 2022
ACCEPTED 30 January 2023
PUBLISHED 10 February 2023

CITATION
Shi Y, Luo C, Xiang Y and Qian D (2023) Rab GTPases, tethers, and SNAREs work together to regulate *Arabidopsis* cell plate formation. *Front. Plant Sci.* 14:1120841. doi: 10.3389/fpls.2023.1120841

Rab GTPases, tethers, and SNAREs work together to regulate *Arabidopsis* cell plate formation

Yumei Shi, Changxin Luo, Yun Xiang and Dong Qian*

Ministry of Education (MOE) Key Laboratory of Cell Activities and Stress Adaptations, School of Life Sciences, Lanzhou University, Lanzhou, China

Cell plates are transient structures formed by the fusion of vesicles at the center of the dividing plane; furthermore, these are precursors to new cell walls and are essential for cytokinesis. Cell plate formation requires a highly coordinated process of cytoskeletal rearrangement, vesicle accumulation and fusion, and membrane maturation. Tethering factors have been shown to interact with the Ras superfamily of small GTP binding proteins (Rab GTPases) and soluble N-ethylmaleimide-sensitive factor attachment protein receptors (SNAREs), which are essential for cell plate formation during cytokinesis and are fundamental for maintaining normal plant growth and development. In *Arabidopsis thaliana*, members of the Rab GTPases, tethers, and SNAREs are localized in cell plates, and mutations in the genes encoding these proteins result in typical cytokinesis-defective phenotypes, such as the formation of abnormal cell plates, multinucleated cells, and incomplete cell walls. This review highlights recent findings on vesicle trafficking during cell plate formation mediated by Rab GTPases, tethers, and SNAREs.

KEYWORDS

***Arabidopsis*, vesicle trafficking, Rab GTPases, tethers, SNAREs, cytokinesis, cell plate**

1 Introduction

Cell division is fundamental to plant growth, development, and reproduction, including the processes of DNA replication, nuclear division, and cytokinesis (Tulin and Cross, 2014). Cytokinesis is the final step in cell division, which involves the process of separating a mother cell into two daughter cells by forming a new compartment between two newly formed daughter nuclei. This is a highly coordinated spatiotemporal event that involves specialized rearrangements of the cytoskeleton during cell division and a series of vesicle transport activities (Müller, 2019; Yi and Goshima, 2022). During cytokinesis, the aggregation and alignment of microtubules forms the phragmoplast, which promotes the orderly delivery of vesicles at the plane of cell division; furthermore, the fusion and fission of aggregated vesicles in the center of dividing cells promotes early cell plate formation (Euteneuer and McIntosh, 1980; Lee et al., 2001; Jürgens, 2005).

The formation of the cell plate goes through the following four distinct stages (Figure 1): (i) The Golgi-derived vesicles are guided to the cell division plane by the phragmoplast, and vesicles aggregate and fuse to form dumbbell structures. (ii) The initial collection of fused tubes at the center of the segmentation plane undergo a series of morphological changes, resulting in a tubulo-vesicular network, depolymerization of the microtubules underlying the tubulo-vesicle network, and stabilization of the microtubules adjacent to the edge of the fusion channel (Nishihama and Machida, 2001; Seguí-Simarro et al., 2004). (iii) Gradual merging into a tubular network form, which is a membrane morphology that subsequently forms into a smoother structure largely through network expansion. (iv) Formation of a fenestrated sheet that fuses with the parental plasma membrane (PM) (Samuels et al., 1995; Sinclair et al., 2022). This process involves various actions such as closing the plate fenestrae, adding pectin and xyloglucan, removing excess membranes, and replacing callose with cellulose. Eventually, the cell plate fuses with the mother cell wall, and the process ends with a transition to an entirely new lateral wall that separates the daughter cells (Samuels et al., 1995; Seguí-Simarro et al., 2004; Baluska et al., 2005).

During cell plate biogenesis, cytokinetic vesicles deliver cargo and contribute membrane material. Cytokinetic vesicles are primarily derived from the Golgi/*trans*-Golgi network (TGN) and are contributed by endosomal populations. ARF guanine exchange factors (ARF GEFs) BIG1-4 assist in the transport of newly synthesized proteins and endocytic products to the formed cell plate (Seguí-Simarro et al., 2004; Richter et al., 2014). Intracellular membrane fusion generally depends on Rab GTPases, tethering factors, and SNARE proteins (Jahn et al., 2003; Jahn and Scheller, 2006; Stenmark, 2009; Hong and Lev, 2014). Rab GTPases are master regulators of membrane trafficking, regulating the transport of vesicles during cell plate formation (Davis et al., 2016; Minamino and Ueda, 2019). Activation of Rab GTPases by GEFs promotes recruitment of tethering factors to the membranes (Stenmark, 2009). Tethering proteins provide specificity for targeting, and vesicle tethering initiates SNARE-dependent fusion of membrane vesicles to form cell plates (Yu and Hughson, 2010) (Figure 2). Some Rab GTPases, tethers, and SNAREs are localized to the cell plate during cytokinesis, and some of these mutations lead to typical cytokinesis-defective phenotypes, such as the formation of abnormal cell plates, binucleated or multinucleated cells, and cell wall stubs (Chow et al., 2008; Jaber et al., 2010; Qi et al., 2011; Zhang et al., 2011) (Figure 3).

2 The Rab family of small GTPase proteins are involved in plant cell plate formation

Rab GTPases are members of the Ras-like small GTP-binding protein superfamily, which are guanine nucleotide-binding proteins that act as molecular switches that can alternate between the following two conformations: the inactive form (GDP-bound) and the active form (GTP-bound). The conversion of Rab GTPases from a GDP-bound to a GTP-bound form requires a GEF (Cui et al., 2014; Rosquete et al., 2019). The Rab GTPase plays an important role in various forms of membrane transport, by activating and/or recruiting various membrane traffic regulators (also known as Rab effector proteins) (Prekeris, 2003; Sohn et al., 2003; Hutagalung and Novick, 2011). Rab GTPases are involved in the regulation of multiple cellular processes, including endosome organization, PM recycling, phagocytosis, cytokinesis and so on (Pereira-Leal and Seabra, 2001;

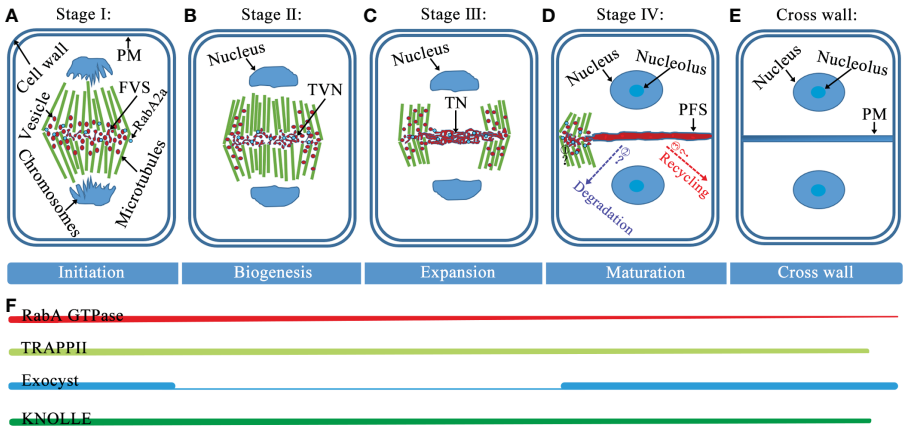

FIGURE 1
Model of cell plate formation stages and spatiotemporal distribution of Rab GTPases, tethers, and SNAREs. **(A)** Stage I, at this fusion of vesicles stage (FVS), during the initial fusion and fission of the bladder, the dumbbell structure forms. **(B)** Stage II, vesicles undergo fusion, fission, and conformational changes to form a tubulo-vesicular network (TVN). **(C)** Stage III, the TVN gradually merges into a tubular network (TN). **(D)** Stage IV, as the cell plate continues to smoothen and expand, the formation of a planar fenestrated sheet (PFS). The cell plate extends fusion tube connecting to the cell plate fusion site with PM and fuses with PM (Step1), and the black question mark indicates an unknown mechanism. After the cell plate is anchored to PM, the proteins diffused from the cell plate would be recycled and/or degraded (Step2 and 3), and dashed arrows with question marks indicate where these proteins are likely to go. **(E)** At the end of cytokinesis, the cell plate enters maturation when the new primary cross wall and daughter cells separate. **(F)** The association of RabA GTPase with the membrane provides cargo for cell plate formation and remains present throughout cell plate formation. Both TRAPPII and exocyst complexes are present at the onset of cytokinesis. Thereafter, the TRAPPII complex consistently marks the cell plate from cytoplasmic division and it is required for its biogenesis, while the outer capsule is primarily required for the maturation of the cell plate. Throughout the cell plate formation phase, SNARE-dependent membrane vesicles fuse to form the cell plate. Abbreviations: PM, plasma membrane; FVS, fusion of vesicles stage; TVN, tubulo-vesicular network; TN, tubular network; and PFS, planar fenestrated sheet.

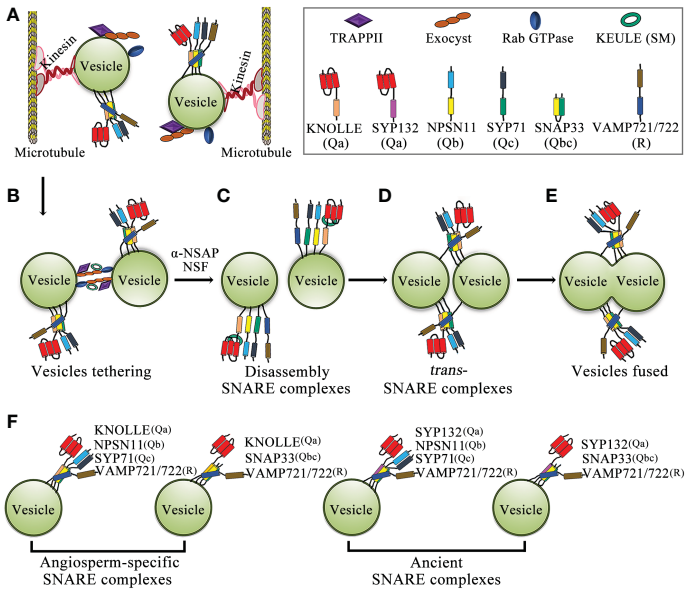

FIGURE 2
Schematic model of membrane-vesicle fusion during cytokinesis. **(A)** Vesicles carry Rab GTPase, two types of tethering complexes, TRAPPII and exocyst, and the KNOLLE-containing *cis*-SNARE complex through kinesin transport along microtubules to the plane of cell division. **(B)** Rab GTPases promote the tethering of two adjacent vesicles by tethering complexes (TRAPPII and exocyst). **(C)** The *cis*-SNARE complex is disassembled by NSF-ATPase and α-SNAP, and the Qa-SNARE KNOLLE interacts with the Sec/Munc18 protein KEULE to keep the KNOLLE in an open conformation. **(D)** KNOLLE interacts with SNARE partners of adjacent vesicles to form *trans*-SNARE complexes. **(E)** Two adjacent vesicles fused together. **(F)** Model of the SNARE complex in cytokinesis. The cytokinesis-specific Qa-SNARE KNOLLE forms two types of SNARE complexes. In addition, the evolutionarily ancient Qa-SNARE SYP132 forms two types of SNARE complexes. Abbreviations: SM, Sec1p/Munc18; α-SNAP, α-soluble NSF attachment protein; and NSF, n-ethylmaleimide-sensitive factor.

Woollard and Moore, 2008). Cytokinesis requires the activity of Rab GTPase to regulate vesicle-mediated material contributions to the developing cell plate (Chow et al., 2008). The *Arabidopsis* genome encodes at least 57 members of the Rab GTPases, which are grouped into eight subfamilies (RabA GTPase to RabH GTPase) (Vernoud et al., 2003; Woollard and Moore, 2008). Four subfamilies of Rab GTPases (RabA, RabE, RabF and RabH) are involved in the formation of the cell plate during cytokinesis (Table 1).

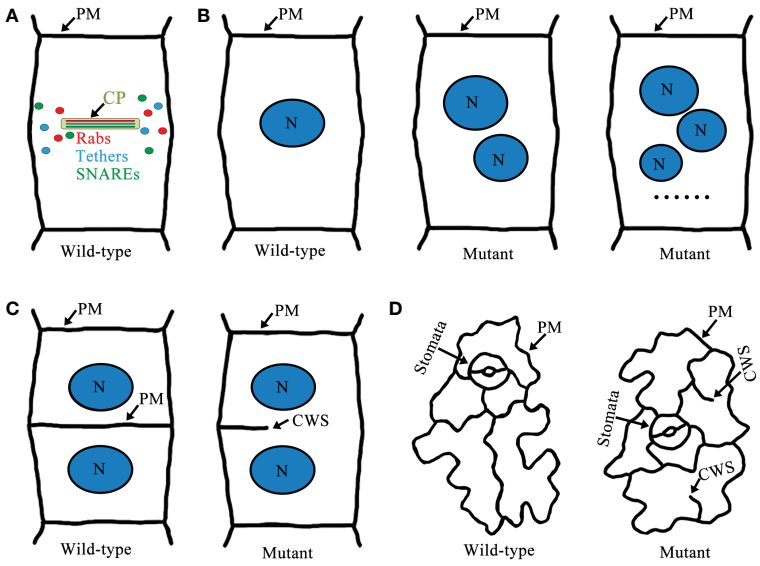

FIGURE 3
A schematic model of Rab GTPases, tethers, SNAREs cell plate localization and cytokinesis-defective mutants in *Arabidopsis*. **(A)** Localization of Rab GTPases, tethers, and SNAREs in the cell plate. **(B)** Wild-type root epidermal cells of *Arabidopsis* have normal cytokinesis and only one nucleus per cell. In cytokinesis-defective mutants there are two or more nuclei per cell. **(C)** Wild-type root epidermal cells have intact cell walls, but defects in cell plate formation in cytokinesis-defective mutants lead to the formation of cell wall stubs. **(D)** Wild-type cotyledon epidermal cells are intact cells with clear outlines. However, cytokinesis-defective mutants often have cell wall stubs. Abbreviations: CP, cell plate; N, nucleus; PM, plasma membrane; and CWS, cell wall stubs.

Ten RabA GTPases (RabA1b, RabA1c, RabA1d, RabA1e, RabA2a, RabA2b, RabA2c, RabA2d, RabA3, and RabA5c) are localized to the cell plate (Table 1). The gene BEX5 encodes RabA1b, which localizes to the TGN/EE, PM, and cell plates, and it functions in protein trafficking in *Arabidopsis* roots, presumably by regulating vesicle formation, budding, and trafficking from the TGN/EE to the PM/cell wall (Geldner et al., 2009; Feraru et al., 2012; Asaoka et al., 2013). *Bex5* mutants display the following defects: increased protein accumulation in abnormal trafficking inhibitor brefeldin A (BFA) compartments, abnormal endosomes, and defects in both exocytosis and transcytosis of PM proteins (Feraru et al., 2012). During cell division, RabA1c is relocated to the cell plate, and this process can be interrupted by the chemical compound endosidin 1 (ES1). In addition, RabA1c defines a group of TGNs that are related to VHA-a1-tagged TGN but only partially overlap with them (Qi and Zheng, 2013). RabA1c (S27N) and RabA1c (Q72L), which are dominant inhibitory mutants, are impaired in root growth and show severe cytokinesis defects (Qi and Zheng, 2013). In addition, root growth and cytokinesis in root cells of *raba1a/b/c* triple mutant seedlings are sensitive to low levels of ES1 (Kotzer et al., 2004; Lee et al., 2004; Qi and Zheng, 2013). RabA1d is localized at the TGN/EE and cell plates and is involved in vesicle trafficking and cell plate formation. The accumulation pattern of RabA1d is consistent with regions of active vesicle fusion during cell plate formation and cell growth, which suggests that it plays an important role in cell plate formation and membrane/cargo trafficking for membrane recycling (Takáč et al., 2012; Berson et al., 2014). RabA1e appears on the cell plate in cytokinesis and it may mediate vesicle transport during cytokinesis. In early-stage cell plates, YFP-RabA1e and YFP-RabA2a were consistently localized to a disk-shaped structure at the center of the dividing cell. In late-stage cell plates, the localization patterns of the two proteins were different, in which YFP-RabA2a were mainly localized to ring-shaped structures across the cell division plane, whereas YFP-RabA1e were mainly localized to both ring-shaped structures and disk-shaped structures. In addition, in late-stage cell plates, differences between YFP-RabA2a and YFP-RabA1e were more pronounced after treatment of cytokinesis inhibitor endosidin 7. RabA1e and RabA2a exhibit different

TABLE 1 Characteristics of Rab GTPases located in cell plates.

Type	Gene	AGI Gene	Localization	Function	Reference
RabA	RabA1b/BET5	AT1g16920	TGN/EE, PM, CP	Secretory pathway from TGN to PM; exocytic trafficking; recycling pathways.	Feraru et al., 2012 ; Asaoka et al., 2013
	RabA1c	At5g45750	TGN/EE, CP	Involved in cytokinesis; the polar secretion and circulation of PM proteins.	Qi et al., 2011; Qi and Zheng, 2013
	RabA1d	At4g18800	TGN/EE, CP	Cell plate formation and polarized cell expansion of root hairs; regulates vesicular trafficking at TGN.	Takáč et al., 2012; Berson et al., 2014
	RabA1e	At4g18430	E, RE, CP	Vesicle-mediated cargo delivery during cytokinesis and root hair elongation.	Geldner et al., 2009; Berson et al., 2014; Davis et al., 2016
	RabA2a	At1g09630	TGN/EE, CP	Involved in cytokinesis; vesicle secretion regulates vesicle trafficking from the TGN to the PM; regulation of K^+ homeostasis.	Chow et al., 2008; Park et al., 2014; Davis et al., 2016; Pang et al., 2022
	RabA2b	At1g07410	TGN/EE, PM, CP	Mediated PM trafficking to improve drought tolerance.	Chow et al., 2008; Ambastha et al., 2021
	RabA2c	At3g46830	TGN/EE, CP	Vesicle secretion and vesicle trafficking.	Chow et al., 2008
	RabA2d	At5g59150	TGN/EE, CP	Vesicle secretion and vesicle trafficking.	Chow et al., 2008
	RabA3	At1g01200	TGN/EE, CP	Vesicle secretion and vesicle trafficking.	Chow et al., 2008
	RabA5c	At2g43130	TGN/EE, CP	Involved in cytokinesis; regulates the specification of geometric edges in directional cell growth lateral roots; specifies a secretory pathway from the TGN/EE to the PM.	Rahni and Birnbaum, 2016; Kirchhelle et al., 2016; Kirchhelle et al., 2019; Elliott et al., 2020
RabE	RabE1c	At3g46060	Golgi, PM, CP	Post-Golgi trafficking to the PM; involved in the degradation of the peroxisomal protein receptor peroxin 7.	Speth et al., 2009; Ahn et al., 2013; Cui et al., 2013; Mayers et al., 2017
	RabE1d	At5g03520	Golgi, PM, CP	Response to pathogen; secretory pathways from the Golgi to the PM.	Zheng et al., 2005; Chow et al., 2008; Speth et al., 2009
RabF	RabF1/ARA6	At3g54840	PM, MVEs, RE, CP	Trafficking pathway from endosomes to the PM; may be involved in recycling and degradation.	Dhonukshe et al., 2006; Bottanelli et al., 2011; Ebine et al., 2011; Ebine et al., 2012; Inada et al., 2017
	RabF2b/ARA7	At4g19640	LE, PVC, TGN/EE, CP	Involved in cytokinesis; endocytosis; vesicle transport between the PVC and the vacuole.	Dhonukshe et al., 2006; Jia et al., 2013; Ito et al., 2016
RabH	RabH1b	At2g44610	Golgi, TGN/EE, CP	Influences cell elongation/growth and cellulose biosynthesis in hypocotyl growth; regulating the transport of cellulose synthase proteins between the Golgi apparatus and PM.	Chow et al., 2008; Johansen et al., 2009; He et al., 2018; Jia et al., 2018

E, endosome; TGN, trans-Golgi network; EE, early endosome; LE, late endosome; RE, recycling endosome; PVC, pre-vacuolar compartment; PM, plasma membrane; MVEs, multivesicular endosomes; and CP, cell plate.

subcellular behaviors, which implies that their localization and transport functions may involve different cellular components (Chow et al., 2008; Berson et al., 2014; Davis et al., 2016). In *Arabidopsis*, the small GTPases RabA2 (RabA2a, RabA2b, RabA2c, and RabA2d) and RabA3 are preferentially localized to the leading edge of the cell plate, implying that RabA2 and RabA3 play a role in the delivery and incorporation of novel substances into the assembled cell plate (Chow et al., 2008; Park et al., 2014; Mayers et al., 2017). Inducible expression of dominant inhibitory mutants of RabA2a (S26N), RabA2a (Q71L), and RabA2a (N125I) results in severely disrupted cell division patterns, binucleate and multinucleate cells, and significant inhibition of cytokinesis (Söllner et al., 2002; Chow et al., 2008). These results demonstrate that RabA2a is required for cytokinesis and transport to the cell plate *via* the Golgi and TGN, possibly by regulating secretion or endocytosis associated with cell plate development. RabA5c accumulates in unique vesicles and sometimes in the TGN, resides at the cell plate, and promotes cytokinesis (Kirchhelle et al., 2016; Kirchhelle et al., 2019; Elliott et al., 2020). Inducible expression of RabA5c (N25I) resulted in severe restriction of root growth, grossly abnormal cell geometries, and incomplete and misaligned cytokinesis in lateral roots (Kirchhelle et al., 2016).

In addition to RabA GTPases, there are five other subfamilies of Rab GTPases located in the cell plate of dividing cells, including two RabE GTPases (RabE1c and RabE1d), two RabF GTPases (RabF1 and RabF2b), and one RabH GTPase (RabH1b) (Table 1). Five members of the RabE subfamily (RabE1a to RabE1e) are believed to regulate post-Golgi trafficking to the PM, and live cell imaging shows that RabE1d and RabE1c localize to the Golgi apparatus, PM, and cell plate of dividing cells (Vernoud et al., 2003; Zheng et al., 2005; Chow et al., 2008; Speth et al., 2009). RabE1 interacts with the stomatal cytokinesis defect (SCD) complex, a multiprotein complex that in turn interacts with exocyst components to jointly promote secretion and endocytosis during cytokinesis; furthermore, overexpression of RabE1c rescues the growth and guard cell cytokinesis phenotypes of the temperature-sensitive mutant *scd1-1* (Mayers et al., 2017). In fixed *Arabidopsis* roots, RabF1 (Ara6) and RabF2b (Ara7) are localized to the cell plate and they are involved in the formation of cell plates during cytokinesis. *Arabidopsis* seedlings expressing dominant-negative RabF2b (Ara7 S24N) show stunted growth, root tip structure disorder, abnormal cytokinesis with multinucleated cells and incomplete cell walls (Dhonukshe et al., 2006). Interestingly, weak fluorescence is generally observed for YFP: RabH1b on the cell plate in addition to the Golgi localization signal, but the intensity of YFP: RabH1b signaling on the cell plate never exceeds the intensity in the same Golgi stack cells (Chow et al., 2008; He et al., 2018; Renna et al., 2018). These findings show that Rab GTPase plays an important role in vesicle trafficking during cell plate formation.

3 Tethering complexes involved in cell plate formation

Tethers refer to the initial contact between the donor and acceptor membranes, which is a highly selective transport process that facilitates vesicle docking and fusion. The initial connection between the carrier vesicle and its target membrane requires tethers, but not all putative tethers can bind the vesicle (Cai et al., 2007). Tethering factors fall into the following two main categories: long putative coiled-coil proteins and multisubunit tethering complexes (Cai et al., 2007; Koumandou et al., 2007; Ravikumar et al., 2017). Tethering complexes act by capturing vesicles and holding them in the vicinity of the target membrane, thereby they play an important role in cell plate assembly (Vukašinović and Žárský, 2016). Of these tethering factors, two important classes of tethering complexes, TRAPPII and exocysts, are required for plant cytokinesis (Rybak et al., 2014). In *Arabidopsis*, the TRAPPII complex consists of ten subunits, including the previously discovered TRAPPII subunits (Bet3, Bet5, Trs20, Trs23, Trs31, Trs33, Tca17, Trs120, and Trs130) and the recently reported plant-specific component TRAPP-interacting plant protein (TRIPP) (Zhang et al., 2018; Garcia et al., 2020). The *Arabidopsis* TRAPPII complex was discovered by screening cytokinesis-defective mutants and it is required for cell plate biogenesis (Jaber et al., 2010; Rybak et al., 2014). The exocyst is an evolutionarily conserved tethered complex consisting of eight subunits (Sec3, Sec5, Sec6, Sec8, Sec10, Sec15, Exo70, and Exo84). The exocyst and other regulatory proteins tether secretory vesicles to the cell membrane prior to membrane fusion, and the exocyst is necessary for the maturation of the cell plate during cytokinesis (He and Guo, 2009; Heider and Munson, 2012; Rybak et al., 2014). Two tethering complexes, TRAPPII and the exocyst, physically interact with each other and coordinate the spatiotemporal regulation of cell plate initiation (Rybak et al., 2014; Müller and Jürgens, 2016). During the initiation and maturation of the cell plate, TRAPPII colocalizes with exocysts and persists there during cell plate assembly. Switching between these tethering complexes is associated with changes in the membrane properties and mediates the biogenesis of the cell plate through distinct stages (Figure 1) (Rybak et al., 2014).

Four TRAPPII subunits (TRS120/VAN4, TRS130/CLUB, TPIPP and TRS33) are essential for cell plate formation (Table 2). TRS120 and TRS130 are localized in the TGN/EE and cell plate, and they are required for cell plate biogenesis (Ravikumar et al., 2017, 2018). Mutations in TRS120 or TRS130 result in a lethal and typical cytoplasmic defect in seedlings, including cell wall stubs, multinucleate cells, and incomplete connective walls. In addition, in both mutants, vesicles aggregate at the division plane but fail to assemble into the cell plate (Jaber et al., 2010; Thellmann et al., 2010; Qi et al., 2011; Ravikumar et al., 2017; Ravikumar et al., 2018). Interestingly, organization and trafficking of the endoplasmic reticulum (ER)-Golgi interface are normal in *trs120* and *trs130* mutants; however, trafficking from the post-Golgi to the cell plate and cell wall, but not to the vacuole, is impaired (Qi et al., 2011). Recently, TRIPP was found to be a plant-specific member of the highly conserved TRAPPII complex, which is localized to TGN/EE in interphase cells, and localized to the cell plate during both early and late cytokinesis; furthermore, the TRAPPII complex is involved in the formation of the cell plate in cytokinesis (Smertenko et al., 2017; Garcia et al., 2020). Loss-of-function *tripp* mutants exhibit infertility, dwarfism, and partial photomorphogenesis in the dark, and the *tripp* mutant has reduced polarity of the auxin transporter PIN2, incomplete transverse cell wall formation, and disordered localization of TRAPPII-specific component formation (Garcia et al., 2020; Hughes, 2020). In addition, TRS33 is required for the

TABLE 2 Characteristics of tethers located in cell plates.

Type	Gene	AGI Gene	Localization	Function	Reference
TRAPPII	TRS120/ VAN4	AT5g11040	TGN/EE, CP	Required for cell plate biogenesis during cytokinesis; polar localization of PIN2; mediated exocytosis at the TGN; regulated the post-Golgi trafficking.	Qi et al., 2011; Naramoto et al., 2014; Rybak et al., 2014; Ravikumar et al., 2018; Kalde et al., 2019
	TRS130/ CLUB	AT5g54440	TGN/EE, CP	Required for cell plate biogenesis during cytokinesis; regulating intracellular trafficking; polar localization of PIN2; regulates the post-Golgi trafficking.	Jaber et al., 2010; Qi et al., 2011; Rybak et al., 2014; Ravikumar et al., 2017; Kalde et al., 2019
	TRIPP	AT3g17900	TGN/EE, CP	Involved in cytokinesis; polar localization of PIN2; plant specific component of TRAPPII vesicle transport complex.	Garcia et al., 2020
	TRS33	AT3g05000	TGN/EE, Golgi	Involved in cytokinesis; auxin distribution; polar localization of both PIN1 and PIN2.	Kalde et al., 2019; Garcia et al., 2020; Zhang et al., 2020
Exocyst	SEC3A	AT1g47550	PM, CP, Cytoplasm	As a polarity determinant that links between polarized exocytosis and cell morphogenesis; tethers secretory vesicles to specific domains of the PM.	Zhang et al., 2013; Bloch et al., 2016; Li et al., 2017
	SEC6	AT1g71820	PM, CP, Cytoplasm	Involved in vesicle tethering during cell plate formation; regulate membrane fusion; help to tether the vesicles before fusion; polar auxin transport and PIN protein recycling.	Fendrych et al., 2010; Wu et al., 2013; Tan et al., 2016; Tan et al., 2022
	SEC8	AT3g10380	CP, PM, Cytoplasm	Involved in cytokinesis; involved in recycling of PIN1, PIN2 and the brassinosteroid receptor BRI1 to the PM; involved in the localized deposition of seed coat pectin.	Kulich et al., 2010; Drdová et al., 2013; Janková Drdová et al., 2019
	SEC10	AT5g12370	PM, CP, Cytoplasm	Involved in exocytotic vesicle fusion; PIN protein recycling and polar auxin transport.	Drdová et al., 2013; Zmienko et al., 2020
	SEC15B	At4g02350	PM, CP, Cytoplasm	Involved in cytokinesis; involved in tethering vesicles to the PM.	Rybak et al., 2014; Mayers et al., 2017
	EXO70 A1	AT5g03540	PM, CP, Cytoplasm	Involved in cytokinesis; auxin efflux carrier recycling and polar auxin transport; involved in cell and organ morphogenesis; required for exocyst recruitment to the PM; secretion; EXO70A1 is required for the location of CASP1 at the Casparian Strip Domain (CSD).	Synek et al., 2006; Fendrych et al., 2010; Drdová et al., 2013; Kalmbach et al., 2017; Larson et al., 2020; Synek et al., 2021; Hématy et al., 2022
	EXO84B	At5g49830	PM, CP	Required for Cell plate maturation and cell plate to PM fusion in the final stages of cytokinesis; affects CASP1 localization in CSD and secretion of many integral membrane proteins.	Fendrych et al., 2010 Kulich et al., 2010; Cole et al., 2014; Synek et al., 2021; Hématy et al., 2022

TGN, trans-Golgi network; EE, early endosome; PM, plasma membrane; and CP, cell plate.

membrane association of TRS120 and for its localization during cytokinesis (Garcia et al., 2020). The *trs33-1* mutant exhibited shorter roots, stunted growth, and sterility, due to impaired cytokinesis, similar to *trappii* mutants (Thellmann et al., 2010; Garcia et al., 2020). Furthermore, TRAPPII is functionally upstream of several RabA GTPases in *Arabidopsis*, indicating that it can also function as a Rab GEF (Qi et al., 2011; Kalde et al., 2019). These studies indicate that TRAPPII regulates vesicle trafficking and the assembly of cell plates, and it is essential for plant growth and development.

Seven exocyst subunits (SEC3A, SEC6, SEC8, SEC10, SEC15, EXO70A1, and EXO84B) are localized to the cell plate (Table 2). SEC3A is preferentially expressed in tissues containing dividing and expanding cells (Zhang et al., 2013; Bloch et al., 2016; Li et al., 2017). Moreover, SEC3A-GFP is temporarily located in the early cell plate, disappears during cell plate elongation and reappears in the division wall. In interphase cells, SEC3A-GFP is localized in the cytoplasm and PM, where it forms solid punctate structures (Zhang et al., 2013; Li et al., 2017). At the start of cytokinesis, SEC6-GFP, GFP-SEC8, GFP-SEC15b, and EXO70A1-GFP were tightly associated with the cell plate at the moment of its emergence and were localized to the cell plate as determined by fluorescence; then, during the formation of the cell plate, the signal diminished until it reappeared at the time of cell plate insertion (Fendrych et al., 2010; Rybak et al., 2014; Gu and Rasmussen, 2022). SEC6 localizes to the cell plate, cytoplasm, post-cytokinetic wall, and somewhat to PM as determined by labeling (Fendrych et al., 2010; Tan et al., 2022). Moreover, SEC6 interacts with the SM (Sec1p/Munc18) protein KEULE and may act as a novel molecular link between vesicles and the machinery for membrane fusion; alternatively, it may directly regulate membrane fusion during the formation of plant cell plates (Wu et al., 2013). In addition, pollen-rescued *sec6* mutants (*PRsec6*) form numerous binucleate cells and cell wall stubs in embryonic cells and abnormally dividing guard cells and cell wall stubs in leaf epidermal cells (Wu et al., 2013). Furthermore, the *sec6-1-/+* and *sec6-2-/+* mutants show approximately 15% of pollen grains broken in cytokinesis during pollen mitosis I (PMI) and impaired cell plate formation (Fendrych et al., 2010; Tan et al., 2022). SEC8 localizes to the nascent cell plate and later to the extension region of the cell plate, and it is involved in cytokinesis (Fendrych et al., 2010). *Sec8* mutants show severe dwarfism and male-specific transmission defects, and root cortical cells elongate at a slower rate in shorter elongation zones (Cole et al., 2005; Kulich et al., 2010; Cole et al., 2014). SEC10 is uniformly localized in the PM, cytoplasm, and cell plates; however, the T-DNA

insertion mutant of *sec10* shows no obvious phenotypic defects, possibly due to functional redundancy (Fendrych et al., 2010; Drdová et al., 2013; Vukašinović et al., 2014). RFP-SEC15B is primarily localized to the cell plate and punctate structures at or near the PM (Fendrych et al., 2010; Rybak et al., 2014; Mayers et al., 2017). EXO70A1 is involved in cell plate initiation, and the *exo70a1* mutant shows impaired initial cell plate morphology during cell plate assembly (Synek et al., 2006; Fendrych et al., 2010; Synek et al., 2021). EXO84B is required for the maturation of the cell plate, and changes in membrane properties drive the observed changes in polysaccharide composition, because tethering complexes bind distinct populations of vesicles with different cargos to the cell plate or cross wall (Fendrych et al., 2010; Cole et al., 2014). The *exo84b* mutant shows sterile dwarfs, slow growth, infrequent cell divisions, major defects with cell dynamics at the cellular level, leaf-like epidermis with cell wall stubs, highly asymmetric stomata, and incomplete division of stomatal guard cells (Fendrych et al., 2010; Hématy et al., 2022). These results show that the exocyst complex is mainly involved in the initiation and maturation of the cell plate and formation of the new primary cell wall during *Arabidopsis* cytokinesis.

4 SNAREs mediate membrane fusion during cell plate formation

SNAREs are responsible for mediating vesicle-to-target membrane fusion, and the *Arabidopsis* genome encodes at least 64 SNAREs (Sanderfoot, 2007; Luo et al., 2022). SNARE proteins are classified as Q-SNARE or R-SNARE according to the core SNARE complex residues (glutamine and arginine, respectively) that contribute to structural assembly. Q-SNAREs are further divided into Qa-, Qb-, Qc-, and Qbc-SNAREs (Fasshauer et al., 1998; Bock et al., 2001; Lipka et al., 2007; Luo et al., 2022). SNAREs are involved in a variety of biological processes such as auxin polar transport, vesicle trafficking, autophagy, gravitropism, and biotic and abiotic stress responses (Saito and Ueda, 2009; Larson et al., 2014; Won and Kim, 2020). In addition, SNARE protein-mediated membrane fusion promotes cell plate formation in dividing cells (Lukowitz et al., 1996; El Kasmi et al., 2013; Park et al., 2018). SNAREs are the core machinery mediating membrane fusion, and an important step in membrane fusion is the formation of *trans*-SNARE complexes, which connect cell membranes so that they can fuse together (Jahn and Scheller, 2006; Saito and Ueda, 2009). Each functional SNARE complex requires two or three Q-SNAREs and one R-SNARE to generate fusion complexes based on homology to synaptic SNAREs; furthermore, cell plate formation requires vesicle fusion mediated by SNAREs and their regulators (Südhof and Rothman, 2009; Luo et al., 2022). Initially, inactive cis-SNARE complexes assemble on the ER and traffic along the secretory pathway through the Golgi and TGN to the cell division plane (Karnahl et al., 2017). In the cell division plane, the *cis*-SNARE complex is broken by NSF ATPase, and Qa-SNARE KNOLLE interacts with the Sec1p/Munc18 (SM) protein KEULE to keep KNOLLE in an open conformation, thereby promoting the formation of *trans*-SNARE complexes on adjacent vesicles by KNOLLE and its SNARE partners (Waizenegger et al., 2000; Assaad et al., 2001; Südhof and Rothman, 2009; Carr and Rizo, 2010; Park et al., 2012). KEULE also interacts with the exocyst and it provides a direct link between tethering and the formation of *trans*-SNARE complexes (Wu et al., 2013). To date, four complete SNARE complexes have been found to mediate membrane fusion during *Arabidopsis* cytokinesis (Figure 2) (El Kasmi et al., 2013; Park et al., 2018).

Five Qa-SNAREs (KNOLLE, SYP132, SYP121, SYP122, and SYP31) are involved in vesicle fusion during cell plate formation (Table 3). The Qa-SNARE KNOLLE is a cytokinesis-specific Syntaxin that accumulates in the TGN during early mitosis, then localizes to the cell plate during cytokinesis, and degrades *via* multivesicular bodies (MVBs) after completion of the newly formed PM (Lauber et al., 1997; Stierhof and El Kasmi, 2010; Reichardt et al., 2011). KNOLLE is expressed in a cell cycle-dependent manner and it mediates cell plate formation through vesicle fusion in the cell division plane (Lukowitz et al., 1996; Lauber et al., 1997). Moreover, KNOLLE is required for both somatic cytokinesis and endosperm cellularization (Park et al., 2018). *Knolle* mutant embryos develop abnormally and exhibit severe cytokinesis defects, such as incomplete cell walls and two or more nuclei, leading to seedlings lacking functional meristems, forming plaques of necrotic tissue, and eventually dying (Lukowitz et al., 1996). Evolutionarily ancient and originating from the algal ancestor Qa-SNARE, SYP132 localizes to the PM and cell plate. Moreover, SYP132 is essential for secretion and it plays an important role in membrane fusion during cytokinesis. In addition, the *syp132* mutant can have cytokinesis defects, such as multinucleated cells, cell wall stubs, cell wall debris, and nonfused vesicle bands on the cell division plane (Park et al., 2018). The Qa-SNARE SYP121 is localized to the PM and TGN, accumulates strongly on the cell plate during cytokinesis, and constitutively cycles between the PM and endosomes; however, the accumulation of the Qa-SNARE SYP122 in cell plates is relatively weak compared with that of SYP121 (Reichardt et al., 2011; Karnik et al., 2015; Liu et al., 2022). The Qa-SNARE SYP31 localizes to cell plates in *Arabidopsis* suspension cells, indicating that it is involved in cell plate formation during somatic cytokinesis. Furthermore, AtCDC48 interacts specifically with SYP31 in an ATP-dependent manner, but not with KNOLLE, which may be necessary for the fusion of "other" secretory membranes in the cell division plane (Rancour et al., 2002). In addition, Qa-SNAREs SYP31 and SYP32 regulate membrane trafficking and Golgi morphology during pollen development, and *syp31*/+ *syp32*/+ double mutants show developmental defects in pollen with abnormal cell plate formation during PMI (Rancour et al., 2002; Rui et al., 2021).

The other three SNAREs, Qb-SNARE (NPSN11), Qc-SNARE (SYP71), and Qbc-SNARE (SNAP33), are involved in vesicle fusion during cell plate formation (Table 3). NPSN11 is a novel plant-specific Qb-SNARE that is highly expressed in tissues with active cell division and localized to the cell plate during cytokinesis. SYP71 of Qc-SNARE located at the PM, endosome, endoplasmic reticulum, and cell plate (El Kasmi et al., 2013). SNAP33 of Qbc-SNARE is a widely expressed membrane-associated protein localized to the PM, endosome, and cell plates (Heese et al., 2001; El Kasmi et al., 2013). Furthermore, SNAP33 is involved in membrane fusion during cell plate formation and plays a role in cytokinesis. In addition, *snap33*

TABLE 3 Characteristics of SNAREs located in cell plates.

Type	Gene	AGI Gene	Localization	Function	Reference
Qa	KNOLLE /SYP111	AT1g08560	TGN/EE, MVB, CP	Membrane fusion during cell plate formation; secretory vesicles trafficking on PM.	Lauber et al., 1997; Völker et al., 2001; El Kasmi et al., 2013; Park et al., 2018
	SYP132	AT5g08080	PM, CP	Membrane fusion in cytokinesis; involved in secretory pathways; vesicular trafficking at the PM; promotes PM H^+-ATPase trafficking; response to bacterial pathogens.	Ichikawa et al., 2014; Park et al., 2018; Xia et al., 2019; Baena et al., 2022
	SYP121 /PEN1	AT3g11820	TGN/EE, PM, CP	As a negative regulator in innate immunity; affect K^+ channel and promote K^+ absorption; vesicular trafficking at the PM.	Honsbein et al., 2009 Reichardt et al., 2011; Liu et al., 2022; Cui et al., 2022; Rubiato et al., 2022
	SYP122	AT3g52400	PM, CP	Vesicular trafficking at the PM; involved in secretion; negative regulation of programmed cell death.	Zhang et al., 2007; Liu et al., 2022; Rubiato et al., 2022
	SYP31	At5g05760	Golgi, CP	Involved in cell division and secretion pathways; Regulation of Golgi morphology; involved in ER-Golgi trafficking.	Rancour et al., 2002; Bubeck et al., 2008; Rui et al., 2021
Qb	NPSN11	AT2g35190	CP, PM, E	Membrane fusion during cell division; involved in cell secretion.	Zheng et al., 2002; El Kasmi et al., 2013; Park et al., 2018
Qc	SYP71	At3g09740	CP, PM, E, ER	Membrane fusion during cell plate formation; involved in vesicular trafficking to ER.	Suwastika et al., 2008; El Kasmi et al., 2013; Park et al., 2018
Qbc	SNAP33	AT5g61210	Cytoplasm, E, PM, CP	Membrane fusion during cell plate formation; innate immune and abiotic stress responses; involved in the secretion process.	Heese et al., 2001; El Kasmi et al., 2013; Park et al., 2018; Won and Kim, 2020
R	VAMP721	AT1g04750	TGN/EE, E, PM, CP	Involved in cell plate formation; regulating auxin transport and auxin distribution; regulation of K^+ uptake; involved in exocytosis and response to ER stress; Regulates the cell secretory pathway.	Yun et al., 2013; Zhang et al., 2011; Zhang et al., 2020; Zhang et al., 2021; Kim et al., 2019; Larson et al., 2020
	VAMP722	AT2g33120	TGN/EE, E, PM, CP		
	SEC22	At1g11890	Nuclear envelope, ER, CP	Cytoskeleton organization and stability; works in the early secretory pathway; ER-Golgi trafficking.	Chatre et al., 2005; El-Kasmi et al., 2011; Guan et al., 2021

E, endosome; TGN, trans-Golgi network; EE, early endosome; ER, endoplasmic reticulum; MVBs, multivesicular bodies; PM, plasma membrane; and CP, cell plate.

mutant seedlings show minor cytokinesis defects, and only later cotyledon lesions lead to lethality (Heese et al., 2001). S*nap33 npsn11* double mutant embryos show severe defects in cytokinesis and impaired cell plate formation, and the *snap33 syp71* double mutant has severe cytokinesis-related phenotypes (El Kasmi et al., 2013).

Three R-SNAREs (VAMP721, VAMP722, and SEC22) are involved in vesicle fusion during cell plate formation (Table 3). VAMP721 and VAMP722 are localized to the PM, the TGN/EE, and preferentially to expanding cell plates during cytokinesis. Moreover, VAMP721 and VAMP722 mediate PM secretion and vesicle fusion on the cell plate (Zhang et al., 2011). Furthermore, the *vamp721 vamp722* mutant shows cell wall stub and delayed expansion of the cell plate, and the seedlings of the double mutant are underdeveloped and eventually show lethal dwarfing phenotypes (Zhang et al., 2011; Zhang et al., 2021). The third R-SNARE, SEC22 is visible at the plane of cell division during cytokinesis, where it colocalizes with KNOLLE and works in the early secretory pathway, which is essential for the integrity of the ER network and the Golgi complex (Chatre et al., 2005; El-Kasmi et al., 2011; Guan et al., 2021). In addition, *sec22-4* mutants have delayed germination, short primary roots, dwarfing and partial abortion, and changes in the shape of their trichomes, pavement cells, and stomatal morphology (El-Kasmi et al., 2011). Taken together, these results show that multiple types of SNAREs are required to mediate the fusion of vesicles during cell plate formation.

5 Perspective

Endomembrane trafficking undergoes various transitions during cell plate formation. During the early stages of cell plate formation, late secretory vesicles derived from the TGN migrate along the phragmoplast toward the cell equator. Dynamic reorganization of the cytoplasm drives lateral expansion of the cell plate, resulting in the shedding of vesicles at the edges of the growing cell plate. Then, the constant flow of vesicles toward the edge of the newly formed cell plate causes the cell plate to swell and eventually fuse with the original PM (Mayer and Jürgens, 2004). During cell plate formation, Rab GTPases, tethers, and SNAREs are localized to certain membranes and function in particular vesicle trafficking events; furthermore, they are crucial regulators of membrane targeting, identity, and fusion (Chow et al., 2008; Martinière and Moreau, 2020; Risselada and Mayer, 2020). Rab GTPases are master regulators of membrane trafficking, regulating the transport of vesicles during cell plate formation (Davis et al., 2016; Minamino and Ueda, 2019). The two tethering complexes (TRAPPII and exocyst) physically interact to coordinate the formation of cell plates during cytokinesis. The TRAPPII complex marks the cell plate throughout cytokinesis and is required for cell plate biogenesis; however, the exocyst is required for maturation of the cell plate (Rybak et al., 2014; Boruc and Van Damme, 2015). Tethering proteins provide specificity for targeting, and vesicle tethering initiates SNARE-dependent fusion of membrane vesicles to form cell plates (Yu and Hughson, 2010). Rab GTPases,

tethers, and SNAREs function synergistically to promote vesicle fusion, which increases the specificity and efficiency of membrane fusion (Ebine et al., 2008; Ohya et al., 2009; Boutté et al., 2010; Ebine et al., 2011).

Rab GTPases and SNARE complexes are functionally linked by tethering complexes, which mediate the tethering of these two membranes components prior to membrane fusion (Wickner and Schekman, 2008; Takemoto et al., 2018). RabF1 localizes to the PM, where it plays a regulatory role in the formation of a SNARE complex containing endosome associated VAMP727 and PM-localized SYP121 (Ebine et al., 2011). In addition, RabA, B, D, and E GTPases are identified in the TRAPPII interactome, and TRAPPII functions as the upstream of RabA2a, which is likely to behave as a GEF for the RabA2a GTPase (Kalde et al., 2019). Furthermore, tethers mediating the physical contact between vesicles and target membranes, together with Rab GTPases, play a key role in determining the specificity of vesicle targeting and fusion events (Cai et al., 2007). Therefore, Rab GTPases, tethers, and SNAREs may coordinate the regulation of the cell plate formation (Tables 1, 2, 3; Figure 3A). However, the spatialization of the three on the cell plate is not completely clear, future research should focus on determining their precise spatiotemporal location on the cell plate and the interaction network between them. Besides, cell plate formation stage IV peripheral microtubules come in contact with the cell cortex and then cell plate extends fusion tubes connecting to the cell plate fusion site at the PM, and fuses with the PM (Boruc and Van Damme, 2015; Smertenko et al., 2017; Rodriguez-Furlan et al., 2019). Thus, to reveal the fine coordination between Rab GTPases, tethers, and SNAREs, the mechanism required for fusion of the cell plate with the PM remains to be identified, and how proteins diffused from the cell plate are recovered or degraded at this stage remains to be studied (Figure 1).

The process of cell plate localization and formation is highly complicated, and some molecular mechanisms are well understood, but many questions remain to be answered. How are vesicles transported along the phragmoplast to the cell division plane for delicate tethering and fusion? Many Rab GTPases, tethers, and SNAREs members are located to the cell plate, and how do they each coordinate the regulation of cell plate formation? Is there a difference in the molecular composition and cargo of the vesicles that are involved in the assembly of cell plates? It is not clear whether vesicles carrying different cargoes destined for the cell plate are regulated by different Rab GTPases. The identification of more proteins and mechanisms involved in cell plate formation remains a goal. A better understanding of the molecular mechanism of cell plate formation will be gained over time with further research.

Author contributions

YS, CL, YX, and DQ wrote the manuscript. All authors contributed to the article and approved the submitted version.

Funding

This work was supported by the National Natural Science Foundation of China (31970195, 32170331 and 32170330).

Acknowledgments

We thank members of the Xiang laboratory for helpful discussion.

Conflict of interest

The authors declare that the research was conducted in the absence of any commercial or financial relationships that could be construed as a potential conflict of interest.

Publisher's note

References

Ahn, C. S., Han, J. A., and Pai, H. S. (2013). Characterization of *in vivo* functions of *Nicotiana benthamiana* RabE1. *Planta* 237, 161–172. doi: 10.1007/s00425-012-1760-5

Ambastha, V., Matityahu, I., Tidhar, D., and Leshem, Y. (2021). RabA2b overexpression alters the plasma-membrane proteome and improves drought tolerance in *Arabidopsis*. *Front. Plant Sci.* 12, 738694. doi: 10.3389/fpls.2021.738694

Asaoka, R., Uemura, T., Ito, J., Fujimoto, M., Ito, E., Ueda, T., et al. (2013). *Arabidopsis* RABA1 GTPases are involved in transport between the *trans*-golgi network and the plasma membrane, and are required for salinity stress tolerance. *Plant J.* 73, 240–249. doi: 10.1111/tpj.12023

Assaad, F. F., Huet, Y., Mayer, U., and Jurgens, G. (2001). The cytokinesis gene KEULE encodes a Sec1 protein that binds the syntaxin KNOLLE. *J. Cell Biol.* 152, 531–543. doi: 10.1083/jcb.152.3.531

Baena, G., Xia, L., Waghmare, S., and Karnik, R. (2022). SNARE SYP132 mediates divergent traffic of plasma membrane h^+-ATPase AHA1 and antimicrobial PR1 during bacterial pathogenesis. *Plant Physiol.* 189, 1639–1661. doi: 10.1093/plphys/kiac149

Baluska, F., Liners, F., Hlavacka, A., Schlicht, M., Van Cutsem, P., McCurdy, D. W., et al. (2005). Cell wall pectins and xyloglucans are internalized into dividing root cells and accumulate within cell plates during cytokinesis. *Protoplasma* 225, 141–155. doi: 10.1007/s00709-005-0095-5

Berson, T., von Wangenheim, D., Takáč, T., Šamajová, O., Rosero, A., Ovečka, M., et al. (2014). *Trans*-golgi network localized small GTPase RabA1d is involved in cell plate formation and oscillatory root hair growth. *BMC Plant Biol.* 14, 252. doi: 10.1186/s12870-014-0252-0

Bloch, D., Pleskot, R., Pejchar, P., Potocky, M., Trpkosova, P., Cwiklik, L., et al. (2016). Exocyst SEC3 and phosphoinositides define sites of exocytosis in pollen tube initiation and growth. *Plant Physiol.* 172, 980–1002. doi: 10.1104/pp.16.00690

Bock, J. B., Matern, H. T., Peden, A. A., and Scheller, R. H. (2001). A genomic perspective on membrane compartment organization. *Nature* 409, 839–841. doi: 10.1038/35057024

Boruc, J., and Van Damme, D. (2015). Endomembrane trafficking overarching cell plate formation. *Curr. Opin. Plant Biol.* 28, 92–98. doi: 10.1094/MPMI.2001.14.6.695

Bottanelli, F., Foresti, O., Hanton, S., and Denecke, J. (2011). Vacuolar transport in *tobacco* leaf epidermis cells involves a single route for soluble cargo and multiple routes for membrane cargo. *Plant Cell* 23, 3007–3025. doi: 10.1105/tpc.111.085480

Boutté, Y., Frescatada-Rosa, M., Men, S., Chow, C. M., Ebine, K., Gustavsson, A., et al. (2010). Endocytosis restricts *Arabidopsis* KNOLLE syntaxin to the cell division plane during late cytokinesis. *EMBO J.* 29, 546–558. doi: 10.1038/emboj.2009.363

Bubeck, J., Scheuring, D., Hummel, E., Langhans, M., Viotti, C., Foresti, O., et al. (2008). The syntaxins SYP31 and SYP81 control ER-golgi trafficking in the plant secretory pathway. *Traffic* 9, 1629–1652. doi: 10.1111/j.1600-0854.2008.00803.x

Cai, H., Reinisch, K., and Ferro-Novick, S. (2007). Coats, tethers, rabs, and SNAREs work together to mediate the intracellular destination of a transport vesicle. *Dev. Cell* 12, 671–682. doi: 10.1016/j.devcel.2007.04.005

Carr, C. M., and Rizo, J. (2010). At The junction of SNARE and SM protein function. *Curr. Opin. Plant Biol.* 22, 488–495. doi: 10.1016/j.ceb.2010.04.006

Chatre, L., Brandizzi, F., Hocquellet, A., Hawes, C., and Moreau, P. (2005). Sec22 and Memb11 are v-SNAREs of the anterograde endoplasmic reticulum-golgi pathway in *tobacco* leaf epidermal cells. *Plant Physiol.* 139, 1244–1254. doi: 10.1104/pp.105.067447

Chow, C. M., Neto, H., Foucart, C., and Moore, I. (2008). Rab-A2 and rab-A3 GTPases define a *trans*-golgi endosomal membrane domain in *Arabidopsis* that contributes substantially to the cell plate. *Plant Cell* 20, 101–123. doi: 10.1105/tpc.107.052001

Cole, R. A., McInally, S. A., and Fowler, J. E. (2014). Developmentally distinct activities of the exocyst enable rapid cell elongation and determine meristem size during primary root growth in *Arabidopsis*. *BMC Plant Biol.* 14, 386. doi: 10.1186/s12870-014-0386-0

Cole, R. A., Synek, L., Zarsky, V., and Fowler, J. E. (2005). SEC8, a subunit of the putative *Arabidopsis* exocyst complex, facilitates pollen germination and competitive pollen tube growth. *Plant Physiol.* 138, 2005–2018. doi: 10.1104/pp.105.062273

Cui, S., Fukao, Y., Mano, S., Yamada, K., Hayashi, M., and Nishimura, M. (2013). Proteomic analysis reveals that the rab GTPase RabE1c is involved in the degradation of the peroxisomal protein receptor PEX7 (peroxin 7). *J. Biol. Chem.* 288, 6014–6023. doi: 10.1074/jbc.M112.438143

Cui, X., Wang, S., Huang, Y., Ding, X., Wang, Z., Zheng, L., et al. (2022). *Arabidopsis* SYP121 acts as an ROP2 effector in the regulation of root hair tip growth. *Mol. Plant* 15, 1008–1023. doi: 10.1016/j.molp.2022.04.008

Cui, Y., Zhao, Q., Gao, C., Ding, Y., Zeng, Y., Ueda, T., et al. (2014). Activation of the Rab7 GTPase by the MON1-CCZ1 complex is essential for PVC-to-vacuole trafficking and plant growth in *Arabidopsis*. *Plant Cell* 26, 2080–2097. doi: 10.1105/tpc.114.123141

Davis, D. J., McDowell, S. C., Park, E., Hicks, G., Wilkop, T. E., and Drakakaki, G. (2016). The RAB GTPase RABA1e localizes to the cell plate and shows distinct subcellular behavior from RABA2a under endosidin 7 treatment. *Plant Signal. Behav.* 11, e984520. doi: 10.4161/15592324.2014.984520

Dhonukshe, P., Baluska, F., Schlicht, M., Hlavacka, A., Samaj, J., Friml, J., et al. (2006). Endocytosis of cell surface material mediates cell plate formation during plant cytokinesis. *Dev. Cell* 10, 137–150. doi: 10.1016/j.devcel.2005

Drdová, E. J., Synek, L., Pečenková, T., Hála, M., Kulich, I., Fowler, J. E., et al. (2013). The exocyst complex contributes to PIN auxin efflux carrier recycling and polar auxin transport in *Arabidopsis*. *Plant J.* 73, 709–719. doi: 10.1111/tpj.12074

Ebine, K., Fujimoto, M., Okatani, Y., Nishiyama, T., Goh, T., Ito, E., et al. (2011). A membrane trafficking pathway regulated by the plant-specific RAB GTPase ARA6. *Nat. Cell Biol.* 13, 853–859. doi: 10.1038/ncb2270

Ebine, K., Miyakawa, N., Fujimoto, M., Uemura, T., Nakano, A., and Ueda, T. (2012). Endosomal trafficking pathway regulated by ARA6, a RAB5 GTPase unique to plants. *Small GTPases* 3, 23–27. doi: 10.4161/sgtp.18299

Ebine, K., Okatani, Y., Uemura, T., Goh, T., Shoda, K., Niihama, M., et al. (2008). A SNARE complex unique to seed plants is required for protein storage vacuole biogenesis and seed development of *Arabidopsis thaliana*. *Plant Cell* 20, 3006–3021. doi: 10.1105/tpc.107.057711

El Kasmi, F., Krause, C., Hiller, U., Stierhof, Y. D., Mayer, U., Conner, L., et al. (2013). SNARE complexes of different composition jointly mediate membrane fusion in *Arabidopsis* cytokinesis. *Mol. Biol. Cell* 24, 1593–1601. doi: 10.1091/mbc.E13-02-0074

El-Kasmi, F., Pacher, T., Strompen, G., Stierhof, Y. D., Muller, L. M., Koncz, C., et al. (2011). *Arabidopsis* SNARE protein SEC22 is essential for gametophyte development and maintenance of golgi-stack integrity. *Plant J.* 66, 268–279. doi: 10.1111/j.1365-313X.2011.04487.x

Elliott, L., Moore, I., and Kirchhelle, C. (2020). Spatio-temporal control of post-golgi exocytic trafficking in plants. *J. Cell Sci.* 133, jcs237065. doi: 10.1242/jcs.237065

Euteneuer, U., and McIntosh, J. R. (1980). Polarity of midbody and phragmoplast microtubules. *J. Cell Biol.* 87, 509–515. doi: 10.1083/jcb.87.2.509

Fasshauer, D., Sutton, R. B., Brunger, A. T., and Jahn, R. (1998). Conserved structural features of the synaptic fusion complex: SNARE proteins reclassified as q-and r-SNAREs. *Proc. Natl. Acad. U. S. A.* 95, 15781–15786. doi: 10.1073/pnas.95.26.15781

Fendrych, M., Synek, L., Pecenkova, T., Toupalova, H., Cole, R., Drdova, E., et al. (2010). The *Arabidopsis* exocyst complex is involved in cytokinesis and cell plate maturation. *Plant Cell* 22, 3053–3065. doi: 10.1105/tpc.110.074351

Feraru, E., Feraru, M. I., Asaoka, R., Paciorek, T., De Rycke, R., Tanaka, H., et al. (2012). BEX5/RabA1b regulates *trans*-golgi network-to-plasma membrane protein trafficking in *Arabidopsis*. *Plant Cell* 24, 3074–3086. doi: 10.1105/tpc.112.098152

Garcia, V. J., Xu, S. L., Ravikumar, R., Wang, W., Elliott, L., Gonzalez, E., et al. (2020). TRIPP is a plant-specific component of the *Arabidopsis* TRAPPII membrane trafficking complex with important roles in plant development. *Plant Cell* 32, 2424–2443. doi: 10.1105/tpc.20.00044

Geldner, N., Denervaud-Tendon, V., Hyman, D. L., Mayer, U., Stierhof, Y. D., and Chory, J. (2009). Rapid, combinatorial analysis of membrane compartments in intact plants with a multicolor marker set. *Plant J.* 59, 169–178. doi: 10.1111/j.1365-313X.2009.03851.x

Gu, Y., and Rasmussen, C. G. (2022). Cell biology of primary cell wall synthesis in plants. *Plant Cell* 34, 103–128. doi: 10.1093/plcell/koab249

Guan, L., Yang, S., Li, S., Liu, Y., Liu, Y., Yang, Y., et al. (2021). AtSEC22 regulates cell morphogenesis *via* affecting cytoskeleton organization and stabilities. *Front. Plant Sci.* 12, 635732. doi: 10.3389/fpls.2021.635732

He, B., and Guo, W. (2009). The exocyst complex in polarized exocytosis. *Curr. Opin. Cell Biol.* 21, 537–542. doi: 10.1016/j.ceb.2009.04.007

He, M., Lan, M., Zhang, B., Zhou, Y., Wang, Y., Zhu, L., et al. (2018). Rab-H1b is essential for trafficking of cellulose synthase and for hypocotyl growth in *Arabidopsis thaliana*. *J. Integr. Plant Biol.* 60, 1051–1069. doi: 10.1111/jipb.12694

Heese, M., Gansel, X., Sticher, L., Wick, P., Grebe, M., Granier, F., et al. (2001). Functional characterization of the KNOLLE-interacting t-SNARE AtSNAP33 and its role in plant cytokinesis. *J. Cell Biol.* 155, 239–249. doi: 10.1083/jcb.200107126

Heider, M. R., and Munson, M. (2012). Exorcising the exocyst complex. *Traffic* 13, 898–907. doi: 10.1111/j.1600-0854.2012.01353.x

Hématy, K., De Bellis, D., Wang, X., Mähönen, A. P., and Geldner, N. (2022). Analysis of exocyst function in endodermis reveals its widespread contribution and specificity of action. *Plant Physiol.* 189, 557–566. doi: 10.1093/plphys/kiac019

Hong, W., and Lev, S. (2014). Tethering the assembly of SNARE complexes. *Trends Cell Biol.* 24, 35–43. doi: 10.1016/j.tcb.2013.09.006

Honsbein, A., Sokolovski, S., Grefen, C., Campanoni, P., Pratelli, R., Paneque, M., et al. (2009). A tripartite SNARE-k^+ channel complex mediates in channel-dependent k^+ nutrition in *Arabidopsis*. *Plant Cell* 21, 2859–2877. doi: 10.1105/tpc.109.066118

Hughes, P. W. (2020). It's a TRAPP! *Arabidopsis* transport protein particle (TRAPP) complexes contain a novel plant-specific subunit. *Plant Cell* 32, 2081–2082. doi: 10.1105/tpc.20.00375

Hutagalung, A. H., and Novick, P. J. (2011). Role of rab GTPases in membrane traffic and cell physiology. *Physiol. Rev.* 91, 119–149. doi: 10.1152/physrev.00059.2009

Ichikawa, M., Hirano, T., Enami, K., Fuselier, T., Kato, N., Kwon, C., et al. (2014). Syntaxin of plant proteins SYP123 and SYP132 mediate root hair tip growth in *Arabidopsis thaliana*. *Plant Cell Physiol.* 55, 790–800. doi: 10.1093/pcp/pcu048

Inada, N., Ebine, K., Ito, E., Nakano, A., and Ueda, T. (2017). Constitutive activation of plant-specific RAB5 GTPase confers increased resistance against adapted powdery mildew fungus. *Plant Biotechnol. (Tokyo)* 34, 89–95. doi: 10.5511/plantbotechnology.17.0501a

Ito, E., Uemura, T., Ueda, T., and Nakano, A. (2016). Distribution of RAB5-positive multivesicular endosomes and the *trans*-golgi network in root meristematic cells of *Arabidopsis thaliana*. *Plant Biotechnol. (Tokyo)* 33, 281–286. doi: 10.5511/plantbiotechnology.16.0218a

Jaber, E., Thiele, K., Kindzierski, V., Loderer, C., Rybak, K., Jurgens, G., et al. (2010). A putative TRAPPII tethering factor is required for cell plate assembly during cytokinesis in *Arabidopsis*. *New Phytol.* 187, 751–763. doi: 10.1111/j.1469-8137.2010.03331.x

Jahn, R., Lang, T., and Südhof, T. C. (2003). Membrane fusion. *Cell* 112, 519–533. doi: 10.1016/s0092-8674(03)00112-0

Jahn, R., and Scheller, R. H. (2006). SNAREs-engines for membrane fusion. *Nat. Rev. Mol. Cell Biol.* 7, 631–643. doi: 10.1038/nrm2002

Janková Drdová, E., Klejchová, M., Janko, K., Hála, M., Soukupová, H., Cvrčková, F., et al. (2019). Developmental plasticity of *Arabidopsis* hypocotyl is dependent on exocyst complex function. *J. Exp. Bot.* 70, 1255–1265. doi: 10.1093/jxb/erz005

Jia, T., Gao, C., Cui, Y., Wang, J., Ding, Y., Cai, Y., et al. (2013). ARA7(Q69L) expression in transgenic *Arabidopsis* cells induces the formation of enlarged multivesicular bodies. *J. Exp. Bot.* 64, 2817–2829. doi: 10.1093/jxb/ert125

Jia, P. F., Xue, Y., Li, H. J., and Yang, W. C. (2018). Golgi-localized LOT regulates *trans*-golgi network biogenesis and pollen tube growth. *Proc. Natl. Acad. Sci. U. S. A.* 115, 12307–12312. doi: 10.1073/pnas.1809206115

Johansen, J. N., Chow, C. M., Moore, I., and Hawes, C. (2009). AtRAB-H1b and AtRAB-H1c GTPases, homologues of the yeast Ypt6, target reporter proteins to the golgi when expressed in nicotiana tabacum and *Arabidopsis thaliana*. *J. Exp. Bot.* 60, 3179–3193. doi: 10.1093/jxb/erp153

Jürgens, G. (2005). Cytokinesis in higher plants. *Annu. Rev. Plant Biol.* 56, 281–299. doi: 10.1146/annurev.arplant.55.031903.141636

Kalde, M., Elliott, L., Ravikumar, R., Rybak, K., Altmann, M., Klaeger, S., et al. (2019). Interactions between transport protein particle (TRAPP) complexes and rab GTPases in *Arabidopsis*. *Plant J.* 100, 279–297. doi: 10.1111/tpj.14442

Kalmbach, L., Hematy, K., De Bellis, D., Barberon, M., Fujita, S., Ursache, R., et al. (2017). Transient cell-specific EXO70A1 activity in the CASP domain and casparian strip localization. *Nat. Plants* 3, 17058. doi: 10.1038/nplants.2017.58

Karnahl, M., Park, M., Mayer, U., Hiller, U., and Jurgens, G. (2017). ER assembly of SNARE complexes mediating formation of partitioning membrane in *Arabidopsis* cytokinesis. *Elife* 6, e25327. doi: 10.7554/eLife.25327

Karnik, R., Zhang, B., Waghmare, S., Aderhold, C., Grefen, C., and Blatt, M. R. (2015). Binding of SEC11 indicates its role in SNARE recycling after vesicle fusion and identifies

two pathways for vesicular traffic to the plasma membrane. *Plant Cell* 27, 675–694. doi: 10.1105/tpc.114.134429

Kim, S., Choi, Y., Kwon, C., and Yun, H. S. (2019). Endoplasmic reticulum stress-induced accumulation of VAMP721/722 requires CALRETICULIN 1 and CALRETICULIN 2 in *Arabidopsis*. *J. Integr. Plant Biol.* 61, 974–980. doi: 10.1111/jipb.12728

Kirchhelle, C., Chow, C. M., Foucart, C., Neto, H., Stierhof, Y. D., Kalde, M., et al. (2016). The specification of geometric edges by a plant rab GTPase is an essential cell-patterning principle during organogenesis in *Arabidopsis*. *Dev. Cell* 36, 386–400. doi: 10.1016/j.devcel.2016.01.020

Kirchhelle, C., Garcia-Gonzalez, D., Irani, N. G., Jerusalem, A., and Moore, I. (2019). Two mechanisms regulate directional cell growth in *Arabidopsis* lateral roots. *Elife* 8, e47988. doi: 10.7554/eLife.47988

Kotzer, A. M., Brandizzi, F., Neumann, U., Paris, N., Moore, I., and Hawes, C. (2004). AtRabF2b (Ara7) acts on the vacuolar trafficking pathway in *tobacco* leaf epidermal cells. *J. Cell Sci.* 117, 6377–6389. doi: 10.1242/jcs.01564

Koumandou, V. L., Dacks, J. B., Coulson, R. M., and Field, M. C. (2007). Control systems for membrane fusion in the ancestral eukaryote; evolution of tethering complexes and SM proteins. *BMC Evol. Biol.* 7, 29. doi: 10.1186/1471-2148-7-29

Kulich, I., Cole, R., Drdova, E., Cvrckova, F., Soukup, A., Fowler, J., et al. (2010). *Arabidopsis* exocyst subunits SEC8 and EXO70A1 and exocyst interactor ROH1 are involved in the localized deposition of seed coat pectin. *New Phytol.* 188, 615–625. doi: 10.1111/j.1469-8137.2010.03372.x

Larson, E. R., Domozych, D. S., and Tierney, M. L. (2014). SNARE VTI13 plays a unique role in endosomal trafficking pathways associated with the vacuole and is essential for cell wall organization and root hair growth in. *Arabidopsis. Ann. Bot.* 114, 1147–1159. doi: 10.1093/aob/mcu041

Larson, E. R., Ortmannová, J., Donald, N. A., Alvim, J., Blatt, M. R., and Žárský, V. (2020). Synergy among exocyst and SNARE interactions identifies a functional hierarchy in secretion during vegetative growth. *Plant Cell* 32, 2951–2963. doi: 10.1105/tpc.20.00280

Lauber, M. H., Waizenegger, I., Steinmann, T., Schwarz, H., Mayer, U., Hwang, I., et al. (1997). The *Arabidopsis* KNOLLE protein is a cytokinesis-specific syntaxin. *J. Cell Biol.* 139, 1485–1493. doi: 10.1083/jcb.139.6.1485

Lee, Y. R., Giang, H. M., and Liu, B. (2001). A novel plant kinesin-related protein specifically associates with the phragmoplast organelles. *Plant Cell* 13, 2427–2439. doi: 10.1105/tpc.010225

Lee, G. J., Sohn, E. J., Lee, M. H., and Hwang, I. (2004). The *Arabidopsis* rab5 homologs rha1 and ara7 localize to the prevacuolar compartment. *Plant Cell Physiol.* 45, 1211–1220. doi: 10.1093/pcp/pch142

Li, Y., Tan, X., Wang, M., Li, B., Zhao, Y., Wu, C., et al. (2017). Exocyst subunit SEC3A marks the germination site and is essential for pollen germination in *Arabidopsis thaliana*. *Sci. Rep.* 7, 40279. doi: 10.1038/srep40279

Lipka, V., Kwon, C., and Panstruga, R. (2007). SNARE-ware: the role of SNARE-domain proteins in plant biology. *Annu. Rev. Cell Dev. Biol.* 23, 147–174. doi: 10.1146/annurev.cellbio.23.090506.123529

Liu, M., Rubiato, H. M., and Nielsen, M. E. (2022). Mobility of the syntaxin PEN1 in *Arabidopsis* reflects functional specialization of the conserved SYP12 clade. *Plant Signal. Behav.* 17, 2084–2278. doi: 10.1080/15592324.2022.2084278

Lukowitz, W., Mayer, U., and Jürgens, G. (1996). Cytokinesis in the *Arabidopsis* embryo involves the syntaxin-related KNOLLE gene product. *Cell* 84, 61–71. doi: 10.1016/s0092-8674(00)80993-9

Luo, C., Shi, Y., and Xiang, Y. (2022). SNAREs regulate vesicle trafficking during root growth and development. *Front. Plant Sci.* 13, 853251. doi: 10.3389/fpls.2022.85325

Martinière, A., and Moreau, P. (2020). Complex roles of rabs and SNAREs in the secretory pathway and plant development: a never-ending story. *J. Microsc.* 280, 140–157. doi: 10.1111/jmi.12952

Mayer, U., and Jürgens, G. (2004). Cytokinesis: lines of division taking shape. *Curr. Opin. Plant Biol.* 7, 599–604. doi: 10.1016/j.pbi.2004.07.008

Mayers, J. R., Hu, T., Wang, C., Cardenas, J. J., Tan, Y., Pan, J., et al. (2017). SCD1 and SCD2 form a complex that functions with the exocyst and RabE1 in exocytosis and cytokinesis. *Plant Cell* 29, 2610–2625. doi: 10.1105/tpc.17.00409

Minamino, N., and Ueda, T. (2019). RAB GTPases and their effectors in plant endosomal transport. *Curr. Opin. Plant Biol.* 52, 61–68. doi: 10.1016/j.pbi.2019.07.007

Müller, S. (2019). Plant cell division - defining and finding the sweet spot for cell plate insertion. *Curr. Opin. Cell Biol.* 60, 9–18. doi: 10.1016/j.ceb.2019.03.006

Müller, S., and Jürgens, G. (2016). Plant cytokinesis-no ring, no constriction but centrifugal construction of the partitioning membrane. *Semin. Cell Dev. Biol.* 53, 10–18. doi: 10.1016/j.semcdb.2015.10.037

Naramoto, S., Nodzyłski, T., Dainobu, T., Takatsuka, H., Okada, T., Friml, J., et al. (2014). VAN4 encodes a putative TRS120 that is required for normal cell growth and vein development in *Arabidopsis*. *Plant Cell Physiol.* 55, 750–763. doi: 10.1093/pcp/pcu012

Nishihama, R., and Machida, Y. (2001). Expansion of the phragmoplast during plant cytokinesis: a MAPK pathway may MAP it out. *Curr. Opin. Plant Biol.* 4, 507–512. doi: 10.1016/s1369-5266(00)00208-9

Ohya, T., Miaczynska, M., Coskun, U., Lommer, B., Runge, A., Drechsel, D., et al. (2009). Reconstitution of rab-and SNARE-dependent membrane fusion by synthetic endosomes. *Nature* 459, 1091–1097. doi: 10.1038/nature08107

Pang, L., Ma, Z., Zhang, X., Huang, Y., Li, R., Miao, Y., et al. (2022). The small GTPase RABA2a recruits SNARE proteins to regulate the secretory pathway in parallel with the exocyst complex in *Arabidopsis*. *Mol. Plant* 15, 398–418. doi: 10.1016/j.molp.2021.11.008

Park, E., Diaz-Moreno, S. M., Davis, D. J., Wilkop, T. E., Bulone, V., and Drakakaki, G. (2014). Endosidin 7 specifically arrests late cytokinesis and inhibits callose biosynthesis, revealing distinct trafficking events during cell plate maturation. *Plant Physiol.* 165, 1019–1034. doi: 10.1104/pp.114.241497

Park, M., Krause, C., Karnahl, M., Reichardt, I., El Kasmi, F., Mayer, U., et al. (2018). Concerted action of evolutionarily ancient and novel SNARE complexes in flowering-plant cytokinesis. *Dev. Cell* 44, 500–511.e504. doi: 10.1016/j.devcel.2017.12.027

Park, M., Touihri, S., Muller, I., Mayer, U., and Jurgens, G. (2012). Sec1/Munc18 protein stabilizes fusion-competent syntaxin for membrane fusion in *Arabidopsis* cytokinesis. *Dev. Cell* 22, 989–1000. doi: 10.1016/j.devcel.2012.03.002

Pereira-Leal, J. B., and Seabra, M. C. (2001). Evolution of the rab family of small GTP-binding proteins. *J. Mol. Biol.* 313, 889–901. doi: 10.1006/jmbi.2001.5072

Prekeris, R. (2003). Rabs, rips, FIPs, and endocytic membrane traffic. *ScientificWorldJournal.* 3, 870–880. doi: 10.1100/tsw.2003.69

Qi, X., Kaneda, M., Chen, J., Geitmann, A., and Zheng, H. (2011). A specific role for *Arabidopsis* TRAPPII in post-golgi trafficking that is crucial for cytokinesis and cell polarity. *Plant J.* 68, 234–248. doi: 10.1111/j.1365-313X.2011.04681.x

Qi, X., and Zheng, H. (2013). Rab-A1c GTPase defines a population of the *trans*-golgi network that is sensitive to endosidin1 during cytokinesis in *Arabidopsis*. *Mol. Plant* 6, 847–859. doi: 10.1093/mp/sss116

Rahni, R., and Birnbaum, K. D. (2016). Plant cell shape: trafficking gets edgy. *Dev. Cell* 36, 353–354. doi: 10.1016/j.devcel.2016.02.005

Rancour, D. M., Dickey, C. E., Park, S., and Bednarek, S. Y. (2002). Characterization of AtCDC48. evidence for multiple membrane fusion mechanisms at the plane of cell division in plants. *Plant Physiol.* 130, 1241–1253. doi: 10.1104/pp.011742

Ravikumar, R., Kalbfuss, N., Gendre, D., Steiner, A., Altmann, M., Altmann, S., et al. (2018). Independent yet overlapping pathways ensure the robustness and responsiveness of *trans*-golgi network functions in *Arabidopsis*. *Development* 145, dev169201. doi: 10.1242/dev.169201

Ravikumar, R., Steiner, A., and Assaad, F. F. (2017). Multisubunit tethering complexes in higher plants. *Curr. Opin. Plant Biol.* 40, 97–105. doi: 10.1016/j.pbi.2017.08.009

Reichardt, I., Slane, D., El Kasmi, F., Knoll, C., Fuchs, R., Mayer, U., et al. (2011). Mechanisms of functional specificity among plasma-membrane syntaxins in *Arabidopsis*. *Traffic* 12, 1269–1280. doi: 10.1111/j.1600-0854.2011.01222.x

Renna, L., Stefano, G., Slabaugh, E., Wormsbaecher, C., Sulpizio, A., Zienkiewicz, K., et al. (2018). TGNap1 is required for microtubule-dependent homeostasis of a subpopulation of the plant *trans*-golgi network. *Nat. Commun.* 9, 5313. doi: 10.1038/s41467-018-07662-4

Richter, S., Kientz, M., Brumm, S., Nielsen, M. E., Park, M., Gavidia, R., et al. (2014). Delivery of endocytosed proteins to the cell-division plane requires change of pathway from recycling to secretion. *Elife* 3, e02131. doi: 10.7554/eLife.02131

Risselada, H. J., and Mayer, A. (2020). SNAREs, tethers and SM proteins: how to overcome the final barriers to membrane fusion? *Biochem. J.* 477, 243–258. doi: 10.1042/BCJ20190050

Rodriguez-Furlan, C., Minina, E. A., and Hicks, G. R. (2019). Remove, recycle, degrade: regulating plasma membrane protein accumulation. *Plant Cell* 31, 2833–2854. doi: 10.1105/tpc.19.00433

Rosquete, M. R., Worden, N., Ren, G., Sinclair, R. M., Pfleger, S., Salemi, M., et al. (2019). AtTRAPPC11/ROG2: a role for TRAPPs in maintenance of the plant *trans*-golgi network/early endosome organization and function. *Plant Cell* 31, 1879–1898. doi: 10.1105/tpc.19.00110

Rubiato, H. M., Liu, M., O'Connell, R. J., and Nielsen, M. E. (2022). Plant SYP12 syntaxins mediate an evolutionarily conserved general immunity to filamentous pathogens. *ELife* 11, e73487. doi: 10.7554/eLife.73487

Rui, Q., Tan, X., Liu, F., Li, Y., Liu, X., Li, B., et al. (2021). Syntaxin of plants31 (SYP31) and SYP32 is essential for golgi morphology maintenance and pollen development. *Plant Physiol.* 186, 330–343. doi: 10.1093/plphys/kiab049

Rybak, K., Steiner, A., Synek, L., Klaeger, S., Kulich, I., Facher, E., et al. (2014). Plant cytokinesis is orchestrated by the sequential action of the TRAPPII and exocyst tethering complexes. *Dev. Cell* 29, 607–620. doi: 10.1016/j.devcel.2014.04.029

Saito, C., and Ueda, T. (2009). Chapter 4: functions of RAB and SNARE proteins in plant life. *Int. Rev. Cell Mol. Biol.* 274, 183–233. doi: 10.1016/s1937-6448(08)02004-2

Samuels, A. L., Giddings, T. H.Jr., and Staehelin, L. A. (1995). Cytokinesis in *tobacco* BY-2 and root tip cells: a new model of cell plate formation in higher plants. *J. Cell Biol.* 130, 1345–1357. doi: 10.1105/tpc.106.040923

Sanderfoot, A. (2007). Increases in the number of SNARE genes parallels the rise of multicellularity among the green plants. *Plant Physiol.* 144, 6–17. doi: 10.1104/pp.106.092973

Seguí-Simarro, J. M., Austin, J. R., White, E. A., and Staehelin, L. A. (2004). Electron tomographic analysis of somatic cell plate formation in meristematic cells of *Arabidopsis* preserved by high-pressure freezing. *Plant Cell* 16, 836–856. doi: 10.1105/tpc.017749

Sinclair, R., Hsu, G., Davis, D., Chang, M., Rosquete, M., Iwasa, J. H., et al. (2022). Plant cytokinesis and the construction of new cell wall. *FEBS Lett.* 596, 2243–2255. doi: 10.1002/18733468.14426

Smertenko, A., Assaad, F., Baluska, F., Bezanilla, M., Buschmann, H., Drakakaki, G., et al. (2017). Plant cytokinesis: terminology for structures and processes. *Trends Cell Biol.* 27, 885–894. doi: 10.1016/j.tcb.2017.08.008

Sohn, E. J., Kim, E. S., Zhao, M., Kim, S. J., Kim, H., Kim, Y. W., et al. (2003). Rha1, an *Arabidopsis* Rab5 homolog, plays a critical role in the vacuolar trafficking of soluble cargo proteins. *Plant Cell* 15, 1057–1070. doi: 10.1105/tpc.009779

Söllner, R., Glässer, G., Wanner, G., Somerville, C. R., Jürgens, G., and Assaad, F. F. (2002). Cytokinesis-defective mutants of *Arabidopsis*. *Plant Physiol.* 129, 678–690. doi: 10.1104/pp.004184

Speth, E. B., Imboden, L., Hauck, P., and He, S. Y. (2009). Subcellular localization and functional analysis of the *Arabidopsis* GTPase RabE. *Plant Physiol.* 149, 1824–1837. doi: 10.1104/pp.108.132092

Stenmark, H. (2009). Rab GTPases as coordinators of vesicle traffic. *Nat. Rev. Mol. Cell Biol.* 10, 513–525. doi: 10.1038/nrm2728

Stierhof, Y. D., and El Kasmi, F. (2010). Strategies to improve the antigenicity, ultrastructure preservation and visibility of trafficking compartments in *Arabidopsis* tissue. *Eur. J. Cell Biol.* 89, 285–297. doi: 10.1016/j.ejcb.2009.12.003

Südhof, T. C., and Rothman, J. E. (2009). Membrane fusion: grappling with SNARE and SM proteins. *Science* 323, 474–477. doi: 10.1126/science.1161748

Suwastika, I. N., Uemura, T., Shiina, T., Sato, M. H., and Takeyasu, K. (2008). SYP71, a plant-specific qc-SNARE protein, reveals dual localization to the plasma membrane and the endoplasmic reticulum in *Arabidopsis*. *Cell Struct. Funct.* 33, 185–192. doi: 10.1247/csf.08024

Synek, L., Pleskot, R., Sekeres, J., Serrano, N., Vukasinovic, N., Ortmannova, J., et al. (2021). Plasma membrane phospholipid signature recruits the plant exocyst complex *via* the EXO70A1 subunit. *Proc. Natl. Acad. Sci. U. S. A.* 118, e2105287118. doi: 10.1073/pnas.2105287118

Synek, L., Schlager, N., Elias, M., Quentin, M., Hauser, M. T., and Zarsky, V. (2006). AtEXO70A1, a member of a family of putative exocyst subunits specifically expanded in land plants, is important for polar growth and plant development. *Plant J.* 48, 54–72. doi: 10.1111/j.1365-313X.2006.02854.x

Takáč, T., Pechan, T., Samajová, O., Ovečka, M., Richter, H., Eck, C., et al. (2012). Wortmannin treatment induces changes in *Arabidopsis* root proteome and post-golgi compartments. *J. Proteome. Res.* 11, 3127–3142. doi: 10.1021/pr201111n

Takemoto, K., Ebine, K., Askani, J. C., Kruger, F., Gonzalez, Z. A., Ito, E., et al. (2018). Distinct sets of tethering complexes, SNARE complexes, and rab GTPases mediate membrane fusion at the vacuole in *Arabidopsis*. *Proc. Natl. Acad. Sci. U.S.A.* 115, E2457–E2466. doi: 10.1073/pnas.1717839115

Tan, X., Feng, Y., Liu, Y., and Bao, Y. (2016). Mutations in exocyst complex subunit SEC6 gene impaired polar auxin transport and PIN protein recycling in *Arabidopsis* primary root. *Plant Sci.* 250, 97–104. doi: 10.1016/j.plantsci.2016.06.001

Tan, X., Xu, H., Ye, J., Wang, J., Liu, W., Liu, F., et al. (2022). *Arabidopsis* exocyst subunit SEC6 is involved in cell plate formation during microgametogenesis. *Biochem. Biophys. Res. Commun.* 598, 100–106. doi: 10.1016/j.bbrc.2022.01.092

Thellmann, M., Rybak, K., Thiele, K., Wanner, G., and Assaad, F. F. (2010). Tethering factors required for cytokinesis in *Arabidopsis*. *Plant Physiol.* 154, 720–732. doi: 10.1104/pp.110.154286

Tulin, F., and Cross, F. R. (2014). A microbial avenue to cell cycle control in the plant superkingdom. *Plant Cell* 26, 4019–4038. doi: 10.1105/tpc.114.129312

Vernoud, V., Horton, A. C., Yang, Z., and Nielsen, E. (2003). Analysis of the small GTPase gene superfamily of *Arabidopsis*. *Plant Physiol.* 131, 1191–1208. doi: 10.1104/pp.013052

Völker, A., Stierhof, Y. D., and Jürgens, G. (2001). Cell cycle-independent expression of the *Arabidopsis* cytokinesis-specific syntaxin KNOLLE results in mistargeting to the plasma membrane and is not sufficient for cytokinesis. *J. Cell Sci.* 114, 3001–3012. doi: 10.1242/jcs.114.16.3001

Vukašinović, N., Cvrčková, F., Eliáš, M., Cole, R., Fowler, J. E., Žárský, V., et al. (2014). Dissecting a hidden gene duplication: the *Arabidopsis thaliana* SEC10 locus. *PloS One* 9, e94077. doi: 10.1371/journal.pone.0094077

Vukašinović, N., and Žárský, V. (2016). Tethering complexes in the arabidopsis endomembrane system. *Front. Cell. Dev. Biol.* 4, 46. doi: 10.3389/fcell.2016.00046

Waizenegger, I., Lukowitz, W., Assaad, F., Schwarz, H., Jürgens, G., and Mayer, U. (2000). The *Arabidopsis* KNOLLE and KEULE genes interact to promote vesicle fusion during cytokinesis. *Curr. Biol.* 10, 1371–1374. doi: 10.1016/s0960-9822(00)00775-2

Wickner, W., and Schekman, R. (2008). Membrane fusion. *Nat. Struct. Mol. Biol.* 15, 658–664. doi: 10.1038/nsmb.145

Won, K. H., and Kim, H. (2020). Functions of the plant qbc SNARE SNAP25 in cytokinesis and biotic and abiotic stress responses. *Mol. Cells* 43, 313–322. doi: 10.14348/molcells.2020.2245

Woollard, A. A., and Moore, I. (2008). The functions of rab GTPases in plant membrane traffic. *Curr. Opin. Plant Biol.* 11, 610–619. doi: 10.1016/j.pbi.2008.09.010

Wu, J., Tan, X., Wu, C., Cao, K., Li, Y., and Bao, Y. (2013). Regulation of cytokinesis by exocyst subunit SEC6 and KEULE in *Arabidopsis thaliana*. *Mol. Plant* 6, 1863–1876. doi: 10.1093/mp/sst082

Xia, L., Mar Marques-Bueno, M., Bruce, C. G., and Karnik, R. (2019). Unusual roles of secretory SNARE SYP132 in plasma membrane h^+-ATPase traffic and vegetative plant growth. *Plant Physiol.* 180, 837–858. doi: 10.1104/pp.19.00266

Yi, P., and Goshima, G. (2022). Division site determination during asymmetric cell division in plants. *Plant Cell* 34, 2120–2139. doi: 10.1093/plcell/koac069

Yu, I. M., and Hughson, F. M. (2010). Tethering factors as organizers of intracellular vesicular traffic. *Annu. Rev. Cell Dev. Biol.* 26, 137–156. doi: 10.1146/annurev.cellbio.042308.113327

Yun, H. S., Kwaaitaal, M., Kato, N., Yi, C., Park, S., Sato, M. H., et al. (2013). Requirement of vesicle-associated membrane protein 721 and 722 for sustained growth during immune responses in *Arabidopsis*. *Mol. Cells* 35, 481–488. doi: 10.1007/s10059-013-2130-2

Zhang, J., Chen, J., Wang, L., Zhao, S., Li, J., Liu, B., et al. (2018). AtBET5 is essential for exine pattern formation and apical meristem organization in *Arabidopsis*. *Plant Sci.* 274, 231–241. doi: 10.1016/j.plantsci.2018.05.033

Zhang, Z., Feechan, A., Pedersen, C., Newman, M. A., Qiu, J. L., Olesen, K. L., et al. (2007). A SNARE-protein has opposing functions in penetration resistance and defence signalling pathways. *Plant J.* 49, 302–312. doi: 10.1111/j.1365-313X.2006.02961.x

Zhang, Y., Immink, R., Liu, C. M., Emons, A. M., and Ketelaar, T. (2013). The *Arabidopsis* exocyst subunit SEC3A is essential for embryo development and accumulates in transient puncta at the plasma membrane. *New Phytol.* 199, 74–88. doi: 10.1111/nph.12236

Zhang, L., Ma, J., Liu, H., Yi, Q., Wang, Y., Xing, J., et al. (2021). SNARE proteins VAMP721 and VAMP722 mediate the post-golgi trafficking required for auxin-mediated development in *Arabidopsis*. *Plant J.* 108, 426–440. doi: 10.1111/tpj.15450

Zhang, B., Wang, H., and Zhang, Y. (2020). SNARE proteins and their role in plant ion channel regulation. *Plant Growth Regul.* 92, 443–453. doi: 10.1007/s10725-020-00656-7

Zhang, L., Zhang, H., Liu, P., Hao, H., Jin, J. B., and Lin, J. (2011). *Arabidopsis* r-SNARE proteins VAMP721 and VAMP722 are required for cell plate formation. *PloS One* 6, e26129. doi: 10.1371/journal.pone.0026129

Zheng, H., Bednarek, S. Y., Sanderfoot, A. A., Alonso, J., Ecker, J. R., and Raikhel, N. V. (2002). NPSN11 is a cell plate-associated SNARE protein that interacts with the syntaxin KNOLLE. *Plant Physiol.* 129, 530–539. doi: 10.1104/pp.003970

Zheng, H., Camacho, L., Wee, E., Batoko, H., Legen, J., Leaver, C. J., et al. (2005). A rab-e GTPase mutant acts downstream of the rab-d subclass in biosynthetic membrane traffic to the plasma membrane in *tobacco* leaf epidermis. *Plant Cell* 17, 2020–2036. doi: 10.1105/tpc.105.031112

Zmienko, A., Marszalek-Zenczak, M., Wojciechowski, P., Samelak-Czajka, A., Luczak, M., Kozlowski, P., et al. (2020). AthCNV: a map of DNA copy number variations in the *Arabidopsis* genome. *Plant Cell* 32, 1797–1819. doi: 10.1105/tpc.19.00640

frontiers | Frontiers in Plant Science

TYPE Original Research
PUBLISHED 15 March 2023
DOI 10.3389/fpls.2023.1160162

OPEN ACCESS

EDITED BY
Cecilia Rodriguez-Furlan,
Washington State University, United States

REVIEWED BY
Takuya Norizuki,
Gunma University, Japan
Ariadna Gonzalez Solis,
University of Wisconsin-Madison,
United States
Laura Lucia Saavedra,
Unidad Ejecutora de Doble Dependecia
INTA-CONICET, Argentina

*CORRESPONDENCE
Taijoon Chung
taijoon@pusan.ac.kr

SPECIALTY SECTION
This article was submitted to
Plant Cell Biology,
a section of the journal
Frontiers in Plant Science

RECEIVED 06 February 2023
ACCEPTED 28 February 2023
PUBLISHED 15 March 2023

CITATION
Kim JH, Jung H, Song K, Lee HN and
Chung T (2023) The phosphatidylinositol
3-phosphate effector FYVE3 regulates
FYVE2-dependent autophagy in
Arabidopsis thaliana.
Front. Plant Sci. 14:1160162.
doi: 10.3389/fpls.2023.1160162

The phosphatidylinositol 3-phosphate effector FYVE3 regulates FYVE2-dependent autophagy in *Arabidopsis thaliana*

Jeong Hun Kim, Hyera Jung, Kyoungjun Song, Han Nim Lee and Taijoon Chung*

Department of Biological Sciences, Pusan National University, Busan, Republic of Korea

Phosphatidylinositol 3-phosphate (PI3P) is a signaling phospholipid that play a key role in endomembrane trafficking, specifically autophagy and endosomal trafficking. However, the mechanisms underlying the contribution of PI3P downstream effectors to plant autophagy remain unknown. Known PI3P effectors for autophagy in *Arabidopsis thaliana* include ATG18A (Autophagy-related 18A) and FYVE2 (Fab1p, YOTB, Vac1p, and EEA1 2), which are implicated in autophagosome biogenesis. Here, we report that FYVE3, a paralog of plant-specific FYVE2, plays a role in FYVE2-dependent autophagy. Using yeast two-hybrid and bimolecular fluorescence complementation assays, we determined that the FYVE3 protein was associated with autophagic machinery containing ATG18A and FYVE2, by interacting with ATG8 isoforms. The FYVE3 protein was transported to the vacuole, and the vacuolar delivery of FYVE3 relies on PI3P biosynthesis and the canonical autophagic machinery. Whereas the *fyve3* mutation alone barely affects autophagic flux, it suppresses defective autophagy in *fyve2* mutants. Based on the molecular genetics and cell biological data, we propose that FYVE3 specifically regulates FYVE2-dependent autophagy.

KEYWORDS

ATG8, autophagosome, autophagy, phosphatidylinositol 3-phosphate, phosphoinositide, vacuolar trafficking

Introduction

Endomembrane trafficking comprises dynamic membrane flow where various membrane lipids and cargo proteins are sorted and transported to their appropriate destinations. Newly synthesized proteins are targeted to various endomembrane compartments *via* multiple routes, including secretory and vacuolar trafficking. Proteins

endocytosed from the cell surface are sorted at the endosomal compartments and either recycled to the plasma membrane or targeted to the vacuole (or lysosome in animals) for degradation. Cytoplasmic proteins may be sequestered by the autophagic membrane and delivered to the vacuole/lysosome for degradation.

The best-characterized type of autophagy is macroautophagy (hereafter referred to as autophagy), in which a membrane sac called the phagophore is expanded and sealed to form the autophagosome sequestering a small portion of the cytoplasm (Marshall and Vierstra, 2018). The autophagosome fuses with the vacuole, releasing its cargo into the vacuolar lumen as an autophagic body. Finally, the autophagic body is rapidly degraded by acid hydrolases in the vacuole. The formation of phagophores and autophagosomes is facilitated by autophagy-related (ATG) proteins, which are conserved in nearly all eukaryotes. ATG8 is a ubiquitin-fold protein conjugated to the membrane lipid phosphatidylethanolamine on the phagophore. As ATG8 resides on the autophagic membrane even after autophagosome fusion, lipidated ATG8 is a useful marker for phagophores, autophagosomes, and autophagic bodies. ATG5 and ATG7 are among the ATG proteins essential for the ATG8 conjugation and general autophagy, whereas ATG2 and ATG18A form a protein complex that transfers membrane lipids to the phagophore and contributes to phagophore growth (Kim et al., 2020).

Phosphatidylinositol 3-phosphate (PI3P) is a signaling phospholipid that plays regulatory roles in endomembrane trafficking (Schink et al., 2013). In eukaryotic cells, PI3P is enriched at the cytosolic leaflet of endosomal, autophagosomal, and vacuolar (or lysosomal) membranes. In budding yeast and plants, PI3P is produced from phosphatidylinositol by the phosphatidylinositol 3-kinase (PI3K) complex containing the catalytic subunit VPS34 (Vacuolar Protein Sorting 34). There are two distinct PI3K complexes which have 3 common and 1 specific subunits. The PI3K complex I, consisting of VPS34, VPS15, VPS30/ATG6, and ATG14, is responsible for PI3P production at the autophagic membrane, while the PI3K complex II, having VPS38 instead of ATG14, generates PI3P on the endosomal membrane (Schink et al., 2013).

Despite its low abundance in biological membranes, PI3P on endosomal and vacuolar membranes is essential for plant development. Null mutations of *vps34* and *atg6* in *Arabidopsis thaliana* cause lethality (Fujiki et al., 2007; Lee et al., 2008), and *vps38* mutants show pleiotropic phenotypes resulting from defective endosomal sorting and vacuolar trafficking (Lee et al., 2018; Liu et al., 2018; Yuan et al., 2018). Less obvious developmental phenotypes are observed in *Arabidopsis atg14a atg14b* double mutants, although they are defective in autophagy (Liu et al., 2020). Generally, plants with compromised functions of vacuoles and endosomes display lethality or severe developmental abnormality (González Solís et al., 2022), whereas autophagy-deficient plants do not. Instead, the autophagy mutants are hypersensitive to different types of abiotic and biotic stress (Qi et al., 2021).

The mechanism underlying the contribution of PI3P to autophagy and endosome trafficking remains poorly understood in plant cells (Chung, 2019). The regulatory roles of PI3P in endomembrane trafficking are primarily mediated by PI3P effectors, which bind to PI3P and, directly or indirectly *via* protein interactions, serve different downstream functions such as cargo selection, membrane bending, vesicle transport, tethering, scaffolding, and signaling (Schink et al., 2013). In *Arabidopsis*, PI3P-binding proteins have been shown to localize at endosomal and/or autophagic membranes. For example, SNX1 (Pourcher et al., 2010) and SNX2b (Phan et al., 2008) localize to endosomes, and FYVE4 (Liu et al., 2021) is primarily cytosolic but can be recruited to endosomal membranes. FYVE1/FREE1 (Gao et al., 2014; Gao et al., 2015), ATG18A (Zhuang et al., 2017; Kang et al., 2018; Kim et al., 2022) and FYVE2/CFS1 (Cell death-related endosomal FYVE/SYLF protein 1) (Sutipatanasomboon et al., 2017; Kim et al., 2022; Zhao et al., 2022) localize at both endosomes and autophagosomes. Genetic analyses of mutants defective in the PI3P-binding proteins indicated that these proteins are involved in endosomal sorting (e.g., SNX1, SNX2b, FYVE4), autophagic degradation (e.g., ATG18A, FYVE2/CFS1), or both (e.g., FYVE1/FREE1). However, molecular mechanisms for these putative PI3P effectors are not fully defined, and how PI3P binding impacts their functions is unknown.

PI3P effectors typically bind to PI3P *via* their FYVE, PX, or PH domains (de Jong and Munnik, 2021). In *Arabidopsis*, the FYVE domain is shared by FYVE1/FREE1, FYVE2/CFS1, FYVE3/CFS2, and FYVE4. Both FYVE2/CFS1 and FYVE3/CFS2 proteins harbor the PI3P-binding FYVE domain and C-terminal SYLF domain, which assists yeast SYLF-containing proteins to bind actin filaments and phosphoinositides (Robertson et al., 2009; Urbanek et al., 2015; Sutipatanasomboon et al., 2017) (Figure S1A). FYVE2/CFS1 facilitates the efficient progression of autophagy and interacts with a variety of proteins such as ATG18A, SAR1B, and VPS23A, which are important for autophagosome biogenesis, COPII vesicle trafficking, and membrane scission, respectively (Sutipatanasomboon et al., 2017; Kim et al., 2022; Zhao et al., 2022). By contrast, no apparent defect in autophagic flux was observed in its paralogous *fyve3/cfs2* single mutants (Kim et al., 2022; Zhao et al., 2022). Thus, currently no evidence supports the involvement of FYVE3/CFS2 in autophagy and other membrane trafficking routes.

Here, we aimed to assess genetic and cell biology data to ascertain the role of *Arabidopsis* FYVE3/CFS2 in autophagy. We showed that FYVE3 was incorporated into the autophagic machinery *via* interaction with ATG8. An autophagy pathway consisting of core ATG proteins and PI3P effectors was proposed, based on our genetic data indicating a specific involvement of FYVE3 in FYVE2-dependent autophagy.

Materials and methods

Plant materials

The *Arabidopsis thaliana* T-DNA insertional mutants of *atg2-1* (Inoue et al., 2006), *atg5-1* (Thompson et al., 2005), *atg7-2* (Chung et al., 2010), *fyve2-2*, and *fyve3-1* (Kim et al., 2022) and transgenic plants expressing *ProUBQ10:GFP-ATG8A* (Kim et al., 2013) and *ProVHA-a1:VHAa1-GFP* (Dettmer et al., 2006) were previously

described, and their progenies were used. *ProUBQ10:YFP-ARA7, ProUBQ10:YFP-SYP32* (Geldner et al., 2009), and *ProUBQ10:Citrine-2xFYVE* (Simon et al., 2014) were obtained from the Arabidopsis Biological Resource Center (ABRC).

Clones and DNA constructs

cDNA and expression clones were obtained from the ABRC with the following identifiers: *Arabidopsis ATG6* (G19464), *FYVE2* (G18828), *FYVE3* (GC105091), SA*R1B* (G19464), *SAR1C* (G11541), pIX-Halo-ATG8F (HALO_SFI_23-A01), pIX-Halo-ATG8I (HALO_SFI_71-H06), PSAT4-DEST-n(1-174)EYFP-C1 (CD3-1089), PSAT5-DEST-c(175-END)EYFP-C1(B) (CD3-1097). To make entry clones containing FYVE3 cDNA lacking the stop codon and TRAF1A, *FYVE3* and *TRAF1A* cDNA were amplified using primers listed in Supplementary Table 1. The *FYVE3* and *TRAF1A* PCR products were inserted into the pENTR/TOPO and pDONR221 vectors (Thermo Fisher Scientific), respectively. cDNA entry clones containing ATG8E, ATG8F, ATG8I, and ATG18A was generated as described previously (Kim et al., 2022).

Preparation of transgenic plants

To obtain binary vectors for transgenic plants expressing *ProUBQ10:GFP-FYVE3* or *ProUBQ10:mCherry-FYVE3*, recombination of the entry clone containing *FYVE3* cDNA with *pMDC99-AtUBQ10p-GFP* and *pMDC99-AtUBQ10p-mCherry* (Suttangkakul et al., 2011) was performed *via* the LR Clonase II reaction (Thermo Fisher Scientific). The binary vectors were introduced into *Agrobacterium tumefaciens* strain GV3101. To obtain stable transformants, Agrobacterium transformants were used to infect *Arabidopsis* using the floral dip method (Clough and Bent, 1998).

Plant growth conditions

Seeds were surface-sterilized with 50%(v/v) bleach and then washed using sterile water. The seeds were germinated on 1× Murashige & Skoog (MS) solid medium [1× MS salt including vitamins (Duchefa, Haarlem, the Netherlands) with 1% (w/v) sucrose, 0.25% (w/v) phytagel (Sigma, St Louis, MO, USA)] or liquid medium with gentle shaking (100 rpm). Plants were incubated under long-day conditions (16 h light and 8 h dark) at 21-23°C.

To induce autophagy, the seedlings incubated in the liquid medium for 7 d were transferred to nitrogen-deficient medium (1 × MS micronutrient solution, 3 mM $CaCl_2$, 1.5 mM $MgSO_4$, 1.25 mM KH_2PO_4, 5 mM KCl and 1% sucrose, pH 5.7) and further incubated for indicated duration. For drug treatment, seedlings were treated with 0.5 μM AZD 8055 (LC Laboratories), 30 μM wortmannin (Sigma), and 0.5 μM Concanamycin A (Cayman).

Phenotypic analysis of the fixed carbon starvation response was performed as described (Chung et al., 2010). Briefly, after incubating seedlings on 1× MS-suc solid medium (1× MS salt including vitamins, 29 mM mannitol, and 0.25% phytagel) for 14 d, the seedlings were then deprived of light for 10 d. Seedlings resuming growth were counted after 18 d of recovery.

Immunoblot analysis

Seedlings frozen in liquid nitrogen were homogenized using a TNPI lysis buffer [50 mM Tris-Cl, 150 mM NaCl, 0.5% (w/v) sodium dodecyl sulfate (SDS), 0.5% (v/v) Triton-X 100, 5% (v/v) glycerol, 2 mM dithiothreitol, 1 mM phenylmethyl sulfonyl fluoride, and 10 mM iodoacetamide, pH 8.0]. Lysates were clarified by centrifugation at 16,000 × *g* at 4°C for 10 min, and the supernatant was mixed with 5 × SDS- polyacrylamide gel electrophoresis (PAGE) sample buffer [200 mM Tris-HCl (pH 6.8), 25% (v/v) glycerol, 10% (w/v) SDS, 10% (v/v) 2-mercaptoethanol]. The samples were boiled at 95°C for 10 min to ensure denaturation of protein samples and loaded into SDS-PAGE. The separated proteins were then transferred onto the Immobilon-P polyvinylidene fluoride membranes (Millipore, St Louis, MO, USA).

To prepare membrane proteins, seedlings expressing *GFP-FYVE3* were homogenized with ice-chilled pestle and mortar in TNPI buffer [50 mM Tris-Cl, 150 mM NaCl, 1 mM phenylmethyl sulfonyl fluoride, 10 mM iodoacetamide, pH 8.0]. After centrifugation at 500 × *g* at 4°C for 5 min, 5% of the supernatant was set aside as total extract, and 95% of the supernatant was further separated into soluble and pellet fractions by centrifugation at 20,000 × *g* at 4°C for 15 min.

Western blot analysis was performed as previously described (Kim et al., 2022). Anti-GFP (Sigma-Aldrich 11814460001), Anti-H3 (Abcam ab1791), Anti-BiP (Agrisera AS09481), and Anti-UDP-glucose pyrophosphorylase (UGPase; Agrisera AS05 086) antibodies were used. The protein band intensity of the immunoblots was quantified by ImageJ (National Institute of Health).

Quantitative real-time PCR analysis

To evaluate RNA abundance, seedlings were grown on 1 x MS medium for 10 d, frozen with liquid nitrogen, and homogenized in TRIsure agent (Bioline, London, UK). The RNA extract was treated with DNase I (New England Biolabs), and cDNA was synthesized using RevertAid H Minus reverse transcriptase (Thermo Fisher Scientific) with oligo$(dT)_{20}$ primers. Quantitative real-time PCR (qRT-PCR) was performed using Step One Plus Real-Time PCR System (Applied Biosystems) and EvaGreen (SolGent, Daejeon, Korea). The relative transcript abundance of target genes was calculated by the ΔΔCT method using the *UBC9* cDNA as an internal control. All primer sequences are provided in Table S1.

Yeast two-hybrid analysis

The entry clone containing FYVE3 cDNA was recombined with the destination vector pDEST22 (Thermo Fisher Scientific) *via* the

LR Clonase II reaction. The resulting pDEST22-FYVE3 and pDEST32 expression vectors for bait proteins fused to SAR1B, SAR1C, ATG8A, ATG8E, ATG8F, ATG8I, ATG18A and FYVE2 (Kim et al., 2022) were used for transformation of the AH109 strain and Y187 strain through the Yeastmaker Yeast Transformation System 2 (Clontech, Mountain View, CA, USA). To determine protein interaction, yeast colonies isolated from Trp- and Leu-deficient medium were transferred to Trp-, Leu-, and His- deficient medium containing 0 and 1 mM 3-amino-1,2,4-triazole.

Bimolecular fluorescence complementation

The expression vectors PSAT5-c(175-END)EYFP-C1(B)-SAR1B/ATG8A/ATG18A/ATG6 were described previously (Kim et al., 2022). To generate the expression vectors PSAT4-n(1-174) EYFP-C1-FYVE3 and PSAT5-c(175-END)EYFP-C1(B)-FYVE2/TRAF1A, entry clones containing FYVE3, FYVE2, and TRAF1A cDNA were recombined with the destination vectors PSAT4-n(1-174)EYFP-C1 and PSAT5-c(175-END)EYFP-C1(B), respectively, *via* the LR Clonase II reaction. The BiFC assay using *Arabidopsis* leaf protoplasts was performed as previously described (Kim et al., 2022).

Confocal microscopy, image processing, and quantification

To observe fluorescence signals from *Arabidopsis* plants or leaf protoplasts, either an LSM 510 or AxioObserver LSM 800 confocal microscope (Carl Zeiss) was used. For LSM 510, a 488 nm laser and BP500-530IR emission filter were used to detect GFP signals. For LSM 800, a 488 nm laser was used for excitation and fluorescence was detected at the 410-546 nm range to acquire GFP, citrine, and YFP signals. To detect mRFP and mCherry, a 587 nm laser was used for excitation, and fluorescence was detected at the 595-700 nm range.

Quantitative analysis of the confocal microscopy images was conducted ImageJ (NIH) as previously described (Kim et al., 2022). Data were presented as mean ± standard error. Student's *t*-test was used to measure significance *via* VassarStats (http://www.vassarstats.net/).

Accession numbers

ATG2 (At3g19190), ATG5 (At5g17290), ATG6 (At3g61710), ATG7 (At5g45900), ATG8A (At4g21980), ATG8E (At2g45170), ATG8F (At4g16520), ATG8I (At3g15580), ATG18A (At3g62770), RABF2b/ARA7 (At4g19640), FYVE2/CFS1 (At3g43230), FYVE3 (At1g29800), SAR1B (At1g56330), SAR1C (At4g02080), SYP32 (At3g24350), TRAF1A (At5g43560), UBC9 (At4g27960), and VHA-a1 (At2g28520).

Results

FYVE3 interacts with specific ATG8 isoforms

To gain insight into the FYVE3 protein, we studied its physical interaction with other proteins. An *Arabidopsis* interactome study identified yeast two-hybrid (Y2H) interactions of FYVE3 with ATG8D (Arabidopsis Interactome Mapping Consortium, 2011). To identify additional interactors, we performed Y2H assay using FYVE3 as a prey and select ATG proteins, FYVE2, and SAR1 isoforms as baits. Our Y2H assay demonstrated interaction of FYVE3 with select ATG8 isoforms such as ATG8A and ATG8F but not with ATG8E and ATG8I (Figure 1A).

The positive Y2H interactions were further tested using *in planta* interaction assays using bimolecular fluorescence complementation (BiFC) in *Arabidopsis* leaf protoplasts. The BiFC interaction of NYFP-FYVE3 with CYFP-ATG8A was verified (Figure 1B), whereas no considerable fluorescence was reconstituted from negative controls of NYFP-FYVE3 paired with

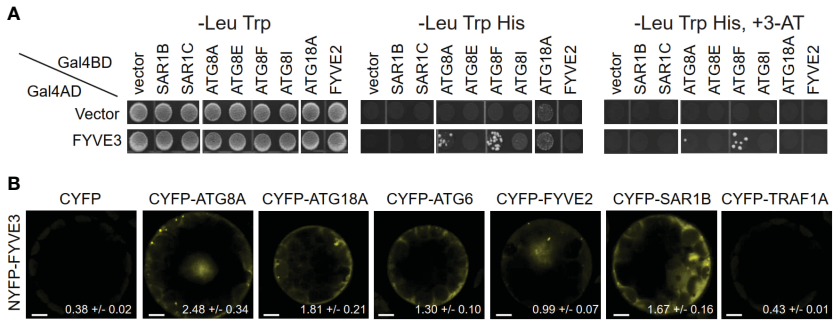

FIGURE 1
FYVE3 interacts with ATG8 and associates with FYVE2-related autophagic machinery. **(A)** Yeast two-hybrid (Y2H) interactions of FYVE3 with select ATG8 isoforms. Gal4BD, Gal4 binding domain; Gal4AD, Gal4 activation domain; 3-AT, 3-amino-1,2,4-triazole. **(B)** Bimolecular fluorescence complementation (BiFC) interactions of FYVE3 in *Arabidopsis* protoplasts. Quantification of overall reconstituted fluorescence is shown at the bottom of each image (mean ± S.E.; n = 30 to 37 images). Scale bars = 5 μm.

either CYFP or CYFP-TRAF1A (Qi et al., 2017) (Figure 1B). In addition, interactions of FYVE3 with SAR1B, ATG18A, ATG6, and FYVE2 were detected in BiFC experiments (Figure 1B), although these interactions were not apparent in Y2H (Figure 1A). We previously showed that FYVE2 interacts with SAR1B and ATG18A (Kim et al., 2022). Thus, FYVE3 may be brought into proximity of SAR1B, FYVE2, and ATG18A, for example, by their simultaneous binding to a scaffold protein. These data suggested that FYVE3 associates with ATG8A, FYVE2, SAR1B, ATG18A, and ATG6 in plant cells.

FYVE3 is recruited from the cytosol to autophagic and endosomal membranes

To investigate the subcellular distribution and trafficking of FYVE3 proteins, we prepared *Arabidopsis* transgenic plants expressing FYVE3 fused to either GFP or mCherry. The membrane fractionation experiment indicated that GFP-FYVE3 was primarily observed in the soluble fraction (Figure S2). We then determined the subcellular distribution of mCherry-FYVE3 by co-localizing it with various organelle markers (Figure 2). Root cells expressing mCherry-FYVE3 had diffuse fluorescence with relatively scarce punctate signals. The mCherry-FYVE3 puncta often overlapped with the puncta of the PI3P biosensor citrine-2xFYVE (Figures 2A, G), the late endosome marker YFP-ARA7 (Figures 2B, G), and the autophagic marker GFP-ATG8A (Figures 2C, G). However, relatively few mCherry-FYVE3 puncta overlapped with markers for the TGN (Figures 2D, G) and Golgi stacks (Figure 2E, G).

We also located mCherry-FYVE3 puncta relative to GFP-FYVE2 (Figure 2F). GFP-FYVE2 were mostly localized at cytoplasmic puncta, some of which were also decorated with mCherry-FYVE3. Although mCherry-FYVE3 puncta were fewer than GFP-FYVE2 puncta, the former mostly overlapped with the latter (Figures 2F, G). As FYVE2 was shown to localize on the autophagic membrane and, to a lesser extent, on the endosomal membrane (Kim et al., 2022), these data indicated that mCherry-FYVE3 puncta mainly represent either autophagic or endosomal compartments that are abundant in PI3P, whereas the diffuse signal corresponds to a cytosolic pool of mCherry-FYVE3.

Association of FYVE3 with autophagic membranes requires ATG8 lipidation and PI3P

The subcellular distribution of FYVE3 is consistent with their protein interaction with select ATG8 isoforms, suggesting that FYVE3 binds to ATG8 on phagophores during autophagosome biogenesis. As fluorescent fusions of FYVE3 are largely co-localized with autophagic puncta, we then examined whether these proteins are delivered together to the vacuole for degradation and detected as autophagic bodies. Observation of the autophagic bodies requires

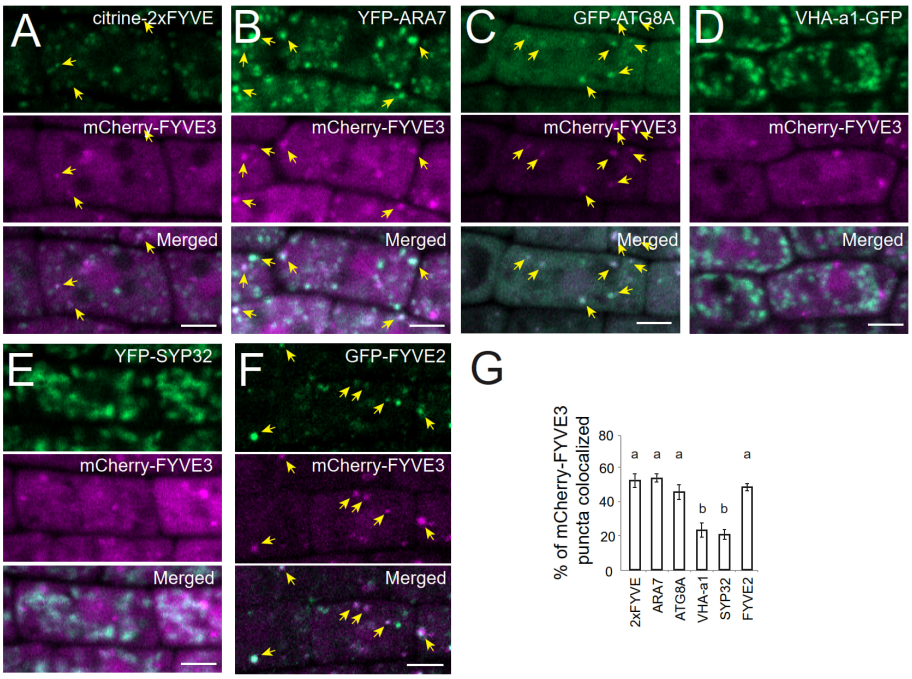

FIGURE 2
At the subcellular level, mCherry-FYVE3 is mainly cytosolic but can be found at the PI3P-enriched membrane of autophagic and endosomal organelles. **(A-F)**, Representative images of root tip cells co-expressing mCherry-FYVE3 with a variety of organelle markers, such as PI3P biosensor **(A)**, late endosome marker **(B)**, phagophore and autophagosome marker **(C)**, trans-Golgi network marker **(D)**, Golgi stack marker **(E)**, and GFP-FYVE2 **(F)**, which associates with autophagic and endosomal membranes. Scale bars = 5 μm. Arrows indicate mCherry-FYVE3 puncta that overlap with co-expressed markers, whose quantification is shown in **(G)**. Columns marked with different letters represent significantly different means according to the *t*-test (mean ± S.E.; n = 11–12 images; $p < 0.01$).

10.3389/fpls.2023.1160162

the treatment of GFP-ATG8 transgenic plants with concanamycin A (ConA), an inhibitor of vacuolar proton pumps. Transgenic plants expressing both GFP-ATG8A and mCherry-FYVE3 were treated with ConA, and their root cell images were compared with DMSO-treated controls (Figure 3A). In ConA-treated roots, 81% of the intravacuolar mCherry-FYVE3 bodies emitted a GFP-ATG8A signal (Figure 3A). ConA-treated roots expressing GFP-FYVE2 and mCherry-FYVE3 also showed a moderate level of co-localization in the vacuole (Figure 3B). Similarly, ConA-treated root cells expressing mCherry-FYVE3 alone showed intravacuolar puncta resembling autophagic bodies (Figure S3A). These data indicated that fluorescent fusions of FYVE3 are degraded in the vacuolar lumen, together with ATG8A and FYVE2.

To define the molecular mechanism underlying the vacuolar trafficking of FYVE3 fluorescent fusions, we tested the effect of ConA and the PI3K inhibitor wortmannin (Wm) treatment on the

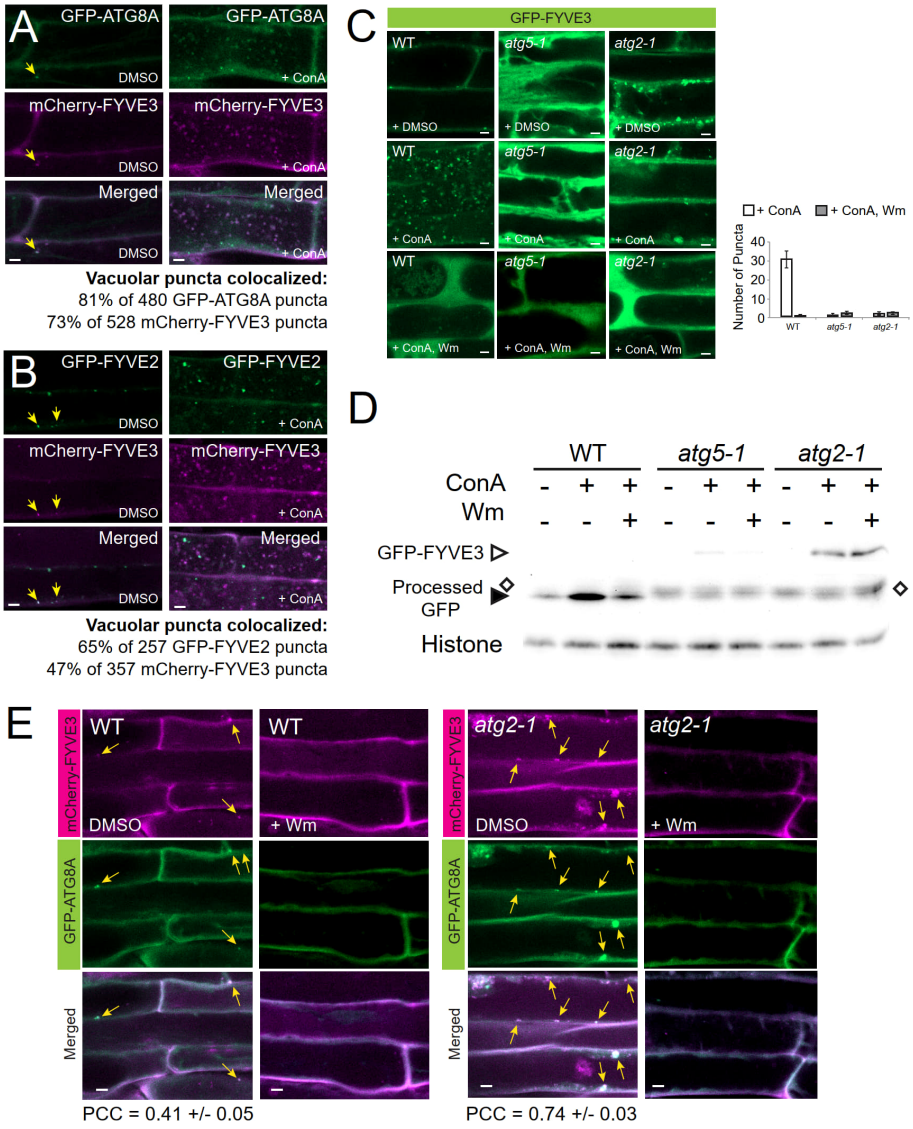

FIGURE 3
Fluorescent fusions of FYVE3 are delivered to the vacuole in a manner dependent on canonical autophagy machinery and PI 3-kinase activity. **(A)** and **(B)**, Confocal images of mature root cells co-expressing mCherry-FYVE3 with either GFP-ATG8A **(A)** or GFP-FYVE2 **(B)**. Seedlings grown in a nitrogen-rich medium were treated with DMSO or 0.5 μM ConA for 16 h prior to confocal microscopy. In the images of DMSO-treated cells, arrows indicate cytoplasmic puncta showing both GFP and mCherry signal. Percentages of vacuolar bodies showing both GFP and mCherry signal were calculated from ConA-treated cells. **(C)**, Confocal images of mature root cells expressing GFP-FYVE3 in the genetic background of WT, *atg5-1*, and *atg2-1*. Transgenic seedlings were incubated in nitrogen-rich liquid medium and treated with DMSO, 0.5 μM ConA, or 0.5 μM ConA plus 30 μM Wm for 16 h. The graph on the right shows the number of vacuolar puncta (mean ± S.E.; n = 12–13 images) per 1,000 μm^2 area of the central vacuole. **(D)**, GFP-FYVE3 cleavage assay. WT, *atg5-1*, or *atg2-1* seedlings expressing GFP-FYVE3 were incubated as described in **(C)**, and protein extract was prepared for immunoblot analysis using anti-GFP (upper) and anti-histone H3 (lower; for loading control) antibodies. Open diamonds indicate the position of protein bands that are not stabilized by ConA and migrates slightly slower than free GFP bands (indicated by a solid arrowhead). Representative images selected from 3 repeat experiments are shown. **(E)**, Confocal images of mature root cells expressing GFP-ATG8A and mCherry-FYVE3 in WT (left images) and *atg2-1* (right images) background. Seedlings were incubated in a nitrogen-lacking liquid medium for 48 h and treated with DMSO or 30 μM Wm for 1 h prior to microscopic observation. Arrows indicate GFP-ATG8A puncta overlapping with mCherry-FYVE3 signal. The Pearson correlation coefficients (PCCs) were calculated from 10 (WT) and 13 (*atg2-1*) images (mean ± S.E.). Scale bars = 5 μm.

subcellular localization of GFP-FYVE3 (Figure 3C). As expected, autophagic body-like puncta were observed in the vacuole of ConA-treated wild-type (WT) seedlings expressing GFP-FYVE3 (Figure 3C, WT, + ConA). Accumulation of the GFP-FYVE3 bodies was suppressed by Wm treatment (Figure 3C, WT, + ConA, Wm), suggesting that GFP-FYVE3 is also targeted to the vacuole *via* PI3K-dependent trafficking. To test whether core *ATG* genes are involved in this trafficking, we introgressed the *GFP-FYVE3* transgene into *atg2-1* and *atg5-1* background by a genetic cross. *atg5-1* is defective in ATG8 lipidation (Chung et al., 2010), whereas *atg2-1* accumulates a high level of lipidated ATG8 (Kang et al., 2018). When we observed their progenies by confocal microscopy, no autophagic body-like GFP-FYVE3 puncta were observed in ConA-treated *atg5-1* and *atg2-1* vacuoles (Figure 3C), demonstrating that canonical autophagy mediates the vacuolar targeting of GFP-FYVE3.

The vacuolar targeting of GFP-FYVE3 was validated by the immunoblot analysis using anti-GFP antibodies, similar to the GFP-ATG8 and GFP-FYVE2 cleavage assays (Kim et al., 2022). In WT, a very faint band corresponding to GFP-FYVE3 was detected, whereas free GFP released from GFP-FYVE3 was readily observed and its intensity increased by ConA (Figure 3D) and dark (Figure S3B) treatments, indicating that the free GFP band is a partial degradation product in the vacuole. In *atg5-1* and *atg2-1*, the GFP-FYVE3 band intensity was increased, whereas ConA and dark treatments did not affect the intensity of protein bands (indicated by open diamonds in Figures 3D and S3B) that migrated slightly slower than free GFP bands (solid arrowheads in Figures 3D and S3B). Combined with confocal microscopy data (Figure 3C), these immunoblot results indicated that GFP-FYVE3 is delivered to the vacuole for degradation *via* canonical, ATG2- and ATG5-dependent autophagy pathway. Consistently, nitrogen starvation increased the ratio of free GFP to GFP-FYVE3 in WT but not in an *atg7-2* background (Figure S3C). The intensity of the slower-migrating protein band appeared to increase by nitrogen starvation (Figure S3C). Although we do not know the nature of this protein band, the same phenomenon was observed in *atg7-2* mutants expressing the autophagy marker GFP-ATG8 (Spitzer et al., 2015). These data indicated that the vacuolar trafficking of GFP-FYVE3 showed a typical pattern of the autophagy marker.

To define the molecular requirement for the formation of GFP-FYVE3 puncta, we examined the effect of *atg5* and *atg2* mutations and Wm treatment. The abundance of GFP-FYVE3 puncta decreases and increases in *atg5* and *atg2*, respectively (Figure S3D). Again, Wm effectively diminished the accumulation of GFP-FYVE3 puncta in *atg2* (Figure S3D). The PI3P-dependent accumulation of GFP-FYVE3 puncta in *atg2* cytoplasm is very similar to that of GFP-ATG8A (Kang et al., 2018), and may result from arrested elongation/maturation of phagophores in *atg2*.

To investigate the effect of *atg2* mutation on mCherry-FYVE3 to the autophagic membrane, we co-localized mCherry-FYVE3 with GFP-ATG8A in WT and *atg2* background. *atg2* root cells over-accumulated cytoplasmic mCherry-FYVE3 puncta, which extensively overlapped with GFP-ATG8A puncta (Figure 3E). Thus, *ATG2* is essential for the targeting of mCherry-FYVE3 to the vacuole, but is dispensable for mCherry-FYVE3 recruitment to the phagophore.

FYVE3 is required for the over-accumulation of autophagic structures in *fyve2* background

To test the potential functions of *FYVE3* in autophagy, we employed *fyve3-1*, a T-DNA insertional allele (Kim et al., 2022). RT-PCR analysis indicated that *fyve3-1* is a knock-out allele, and there is no apparent transcriptional feedback between *FYVE2* and *FYVE3* genes (Figure S1B). Because of the FYVE and SYLF domains shared by FYVE2 and FYVE3, we initially postulated a genetic redundancy of *FYVE2* and *FYVE3*. In *fyve2* mutant background, phagophores are over-accumulated and autophagic flux is partially compromised (Kim et al., 2022). However, no significant change in autophagic flux was measured in *fyve3* single mutants, and *fyve2 fyve3* double mutants did not show further reduction in autophagic flux, when compared with *fyve2* single mutants (Kim et al., 2022; Figure S4). These data were inconsistent with a simple model that *FYVE2* and *FYVE3* are duplicates. To further investigate the genetic relationship between these two genes, we quantified the abundance of autophagic organelles in N-starved WT, *fyve2, fyve3*, and *fyve2 fyve3* double mutant cells expressing the autophagic marker GFP-ATG8A. Confocal microscopy analysis confirmed previous observation that *fyve2* root cells over-accumulated GFP-ATG8A puncta in the cytoplasm, compared with WT (Figure 4A; Kim et al., 2022). As previously reported (Kim et al., 2022), Wm effectively blocked the formation of GFP-ATG8A puncta in *fyve2* (Figure 4A). In contrast, *fyve3* single mutants did not accumulate GFP-ATG8A puncta (Figure 4A). Notably, less than 10% of GFP-ATG8A puncta were detected in *fyve2 fyve3* double mutants, relative to *fyve2* mutants (Figure 4A). Complementation experiments revealed that the expression of *mCherry-FYVE3* transgene in *fyve2 fyve3* mutants restored the accumulation of GFP-ATG8A puncta (Figure S5). These results indicate that *FYVE3* is responsible for the over-accumulation of immature autophagic structures in *fyve2*.

Based on autophagy reporter analysis using *fyve3* single and *fyve2 fyve3* double mutants, we hypothesized that FYVE3 might serve a specific function during autophagosome formation. This hypothesis was tested using a different mutant combination of *atg2* and *fyve3* (Figure 4B). Compared with *fyve2, atg2* mutants accumulate even more autophagic puncta, and autophagic flux is compromised almost completely (Kang et al., 2018; Kim et al., 2022). Unlike *fyve2 fyve3* double mutants, *atg2 fyve3* double mutant cells showed over-accumulation of GFP-ATG8A puncta as *atg2* single mutants did (compare Figure 4B with Figure 4A). As *fyve3* did not suppress the over-accumulation of GFP-ATG8A puncta in *atg2*, *FYVE3* appears to play a specific role in the formation of GFP-ATG8A puncta in *fyve2*. Of note, treatment with Wm only partially suppressed the GFP-ATG8A puncta in *atg2 fyve3* double mutants (Figure 4B).

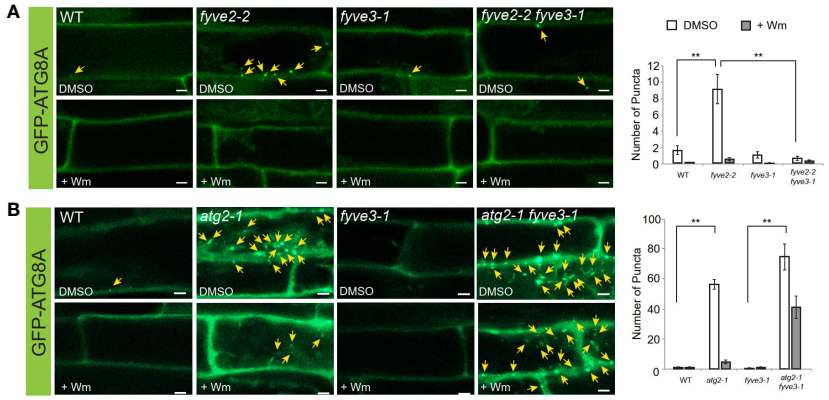

FIGURE 4
fyve3 suppresses the accumulation of autophagic puncta in *fyve2* but not those in *atg2*. **(A, B)** Representative confocal microscopy images (left) and quantification (right) of GFP-ATG8A puncta (arrows at the images) acquired from mature root cells with indicated genetic background. Transgenic *Arabidopsis* seedlings expressing GFP-ATG8A were incubated in a nitrogen-lacking liquid media for 48 h and treated with either wortmannin (Wm) or solvent control (DMSO) for 1 h prior to image acquisition. Scale bars = 5 μm. Columns marked with asterisks represent means that significantly differ from each other, according to the *t*-test. Mean ± S.E.; n = 12 to 26 images; **p < 0.01.

Further genetic analysis, including *atg2 fyve2 fyve3* triple mutants, also confirmed that *FYVE3* is specifically required for the accumulation of GFP-ATG8A puncta in *fyve2* (Figure 5). Under N starvation, *atg2 fyve2 fyve3* triple mutants accumulated as many GFP-ATG8A puncta as *atg2*, *atg2 fyve2*, and *atg2 fyve3* mutants (Figure 5A), masking the suppressive effects of *fyve3* on *fyve2* mutation. A similar trend was observed when seedlings were treated with AZD8055 (AZD; Figure 5B), which induces autophagy by inhibiting Target Of Rapamycin kinase (Soto-Burgos and Bassham, 2017; Dauphinee et al., 2019).

Accumulation of autophagic puncta can result from either induction of autophagy or retarded biogenesis of autophagosomes. Autophagic flux analysis is necessary to distinguish these two possibilities. As *fyve3* alone did not significantly affect autophagic flux (Kim et al., 2022; Figure S4), we assessed the effect of *fyve3* on autophagic flux in *atg2* and *fyve2* mutant background. To quantify autophagic flux in different mutants, we used the GFP-ATG8A cleavage assay (Chung et al., 2010; Shin et al., 2014), where anti-GFP immunoblot analysis of seedlings expressing GFP-ATG8A is performed, and autophagic flux is determined from the protein band intensity of free GFP moiety, relative to that of GFP-ATG8A. GFP-ATG8A transgenic seedlings in WT, *atg2*, *fyve2*, and *fyve3*, or their double/triple mutant background were exposed to either N starvation (Figure 5C) or AZD (Figure 5D) and subjected to GFP-ATG8A cleavage assay. In both conditions, autophagic flux was fully inhibited in any genetic background containing *atg2* and also greatly interfered in *fyve2* (Figures 5C, D). In contrast, *fyve2 fyve3* double mutant was indistinguishable from WT and *fyve3*, confirming that *fyve3* suppresses *fyve2* (Figures 5C, D).

Finally, the physiological function of *FYVE3* gene expression was tested by phenotypic analysis of *fyve3* single and *fyve2 fyve3* double mutants. Autophagy-deficient mutants are hypersensitive to carbon starvation (Hanaoka et al., 2002; Chung et al., 2010). Our fixed-carbon starvation experiments showed that *fyve2-2* seedlings showed hypersensitivity to light deprivation, whereas *fyve3-1* did not (Figure 5E). Importantly, *fyve2-2 fyve3-1* double mutants showed a WT-like sensitivity, demonstrating that the suppression effect of *fyve3* on *fyve2* is physiologically significant.

Discussion

FYVE3 is a putative PI3P effector involved in autophagy (Chung, 2019), but its function remains unelucidated. In this study, we investigated the role of FYVE3 in plant autophagy. We demonstrated that FYVE3 interacts with ATG8 isoforms (Figure 1), associates with ATG8-positive autophagic membranes (Figure 2), and is degraded in the vacuole in a manner dependent on core *ATG* genes and PI3K (Figure 3). As autophagic flux is not significantly altered by *fyve3* single mutation under N starvation (Figures 4, 5), FYVE3 could be considered an autophagic cargo that does not play a critical role in autophagosome biogenesis. However, this scenario is unlikely, because genetic analysis of *fyve2 fyve3* double mutants indicated that *fyve3* suppressed *fyve2* phenotypes, such as over-accumulation of autophagic puncta, reduction in autophagic flux, and starvation response (Figures 4, 5). This suppression by *fyve3* is in contrast with the hyperaccumulation of autophagic markers in *atg2 fyve3* double mutants, where no suppression was observed. Based on these genetic interactions, we propose that *FYVE3* acts upstream of *FYVE2* but downstream of *ATG2* during autophagosome formation (Figure 5F).

The phenotypic consequence of *fyve3* mutation is not evident unless it is combined with *fyve2* mutation, which prevented us and others from identifying its involvement in autophagy (Kim et al., 2022; Zhao et al., 2022). In our previous work (Kim et al., 2022), we employed 48-h nitrogen starvation for autophagic flux assay, whereas 24-h starvation was used for the assay in this study. Nevertheless, we observed a similar suppression in the autophagic flux analysis in which 21-d-old leaves of *fyve2 fyve3* mutants were used (Kim et al., 2022). Zhao et al. (2022) reported that the steady-state level of the autophagic cargo receptor NBR1 was comparable between *fyve2* and *fyve2 fyve3*, but did not directly assess the

10.3389/fpls.2023.1160162

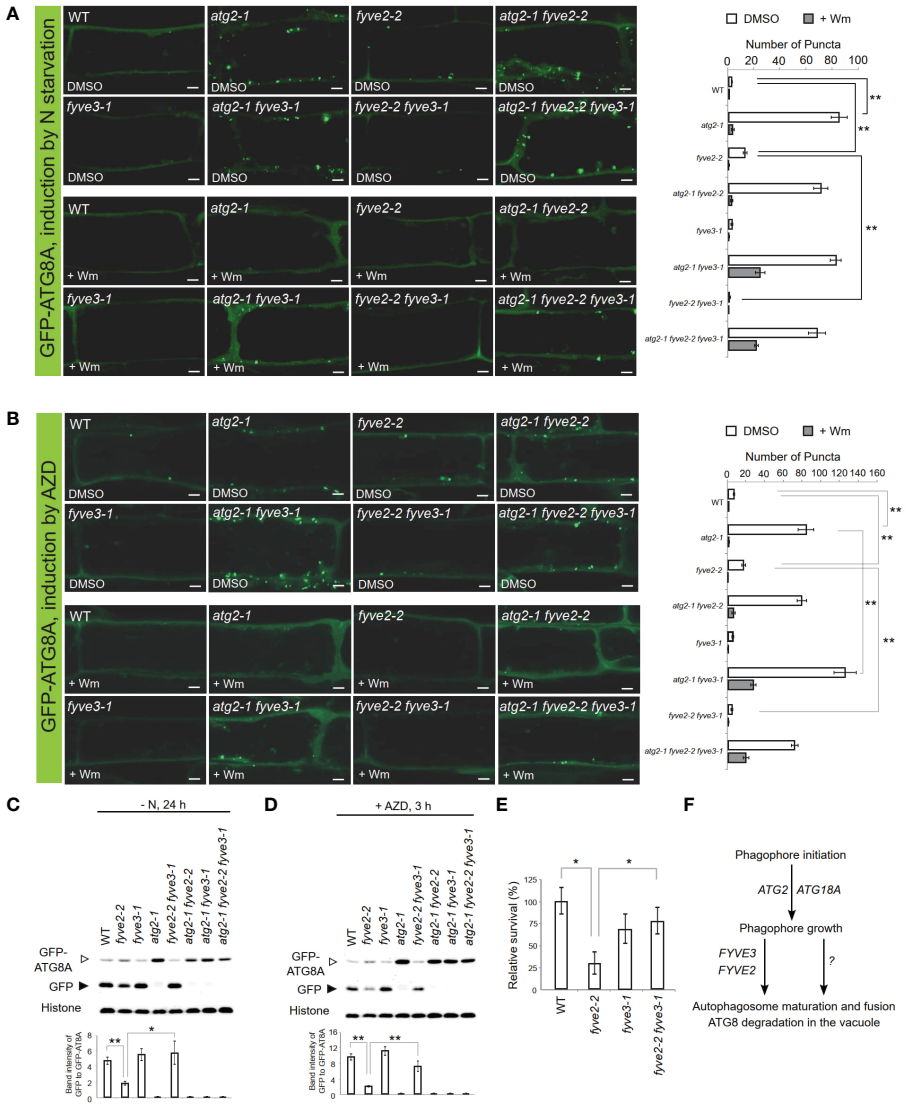

FIGURE 5
FYVE3 acts upstream of *FYVE2* and downstream of *ATG2* in a genetic pathway defined by the autophagy marker GFP-ATG8A. **(A, B)** Representative confocal microscopy images (left) and quantification (right) of GFP-ATG8A puncta (arrows at the images) acquired from mature root cells with indicated genetic background. *Arabidopsis* transgenic seedlings expressing GFP-ATG8A were incubated in either nitrogen-lacking liquid media for 12 h **(A)** or nitrogen-sufficient liquid media containing AZD8055 for 1 h **(B)**, and treated with either wortmannin (Wm) or solvent control (DMSO) for 1 h prior to image acquisition. Scale bars = 5 μm. **(C, D)**, GFP-ATG8A cleavage immunoblot assays. *Arabidopsis* transgenic seedlings expressing GFP-ATG8A with various genetic backgroundsa were incubated in either nitrogen-lacking liquid media for 24 h **(C)** or nitrogen-sufficient liquid media containing AZD8055 for 3 h **(D)** prior to protein extraction. Quantification of relative protein band intensities is shown below. **(E)** Phenotypic analysis for fixed-carbon starvation response. **(F)** A model for FYVE2 and FYVE3 functions in autophagosome dynamics. Columns marked with asterisks represent means that significantly differ from each other, according to the *t*-test. Mean ± S.E.; n = 14 to 16 images **(A, B)**, or 4 seedling populations **(C, D, E)**; *0.01 < p < 0.05; **p < 0.01.

autophagic flux of *fyve2 fyve3* (i.e., *cfs1 cfs2*) double mutants. As *NBR1* is transcriptionally regulated in an autophagy-independent manner (Jung et al., 2020), further work is needed to investigate how NBR1 is regulated in *fyve2* and *fyve3* mutants.

The biochemical function of FYVE3 on the autophagic membrane is not clear. As autophagic flux is almost completely inhibited by *atg2* but only partially by *fyve2* (Kang et al., 2018; Kim et al., 2022), we postulate two separate autophagic routes, FYVE2-dependent and FYVE2-independent routes (Figure 5F). FYVE3 may specifically participate in FYVE2-dependent autophagy. Considering the suppression effect indicating the involvement of FYVE3 in FYVE2-dependent autophagy, the absence of *fyve3* single mutant phenocopying *fyve2* is noteworthy. This can be explained if FYVE3 is a negative regulator of FYVE2-mediated autophagy. For example, FYVE3 may compete with autophagosome biogenesis factors for ATG8 binding. Alternatively, it is possible that FYVE3 both positively mediates the FYVE2-dependent autophagy and negatively regulates the FYVE2-independent route. In the absence of FYVE3, vacuolar delivery of ATG8 through the FYVE2-independent pathway may increase and compensate for a reduced

autophagic flux of ATG8 through the FYVE2-dependent autophagy. In the latter model, the interaction of FYVE3 with ATG8 may be responsible for recruiting FYVE2 on expanding phagophores (Kim et al., 2022). Further investigation is needed to reveal the nature of FYVE2-dependent autophagy and a specific role for FYVE3 in this pathway.

In summary, our study uncovers a regulatory module of FYVE2 and FYVE3 and its potential role in autophagosome biogenesis (Figure 5F). Our study suggests that FYVE3 participates in FYVE2-dependent autophagy *via* its interaction with PI3P and ATG8 isoforms. Thus, future investigation should ask what regions of FYVE3 are responsible for these interactions, whether FYVE3 is a positive or negative regulator of FYVE2-dependent autophagy, and how core ATG proteins and PI3P collaborate with FYVE2 and FYVE3.

Data availability statement

The raw data supporting the conclusions of this article will be made available by the authors, without undue reservation.

Author contributions

JK performed most experiments. JK, HJ, KS, HL and TC developed genetic materials. TC wrote the manuscript with support from JK, HJ and HL. All authors contributed to the article and approved the submitted version.

Funding

This work was supported by the National Research Foundation of Korea (NRF) grants funded by the Korea government (MSIT) (NRF-2019R1A2C1084203 and NRF-2022R1A2C1003658) to TC.

Conflict of interest

The authors declare that the research was conducted in the absence of any commercial or financial relationships that could be construed as a potential conflict of interest.

Publisher's note

Supplementary material

The Supplementary Material for this article can be found online at: https://www.frontiersin.org/articles/10.3389/fpls.2023.1160162/full#supplementary-material

References

Arabidopsis Interactome Mapping Consortium. (2011). Evidence for network evolution in an arabidopsis interactome map. *Science* 333, 601–607. doi: 10.1126/science.1203877

Chung, T. (2019). How phosphoinositides shape autophagy in plant cells. *Plant Sci.* 281, 146–158. doi: 10.1016/j.plantsci.2019.01.017

Chung, T., Phillips, A. R., and Vierstra, R. D. (2010). ATG8 lipidation and ATG8-mediated autophagy in arabidopsis require ATG12 expressed from the differentially controlled ATG12A and ATG12B loci. *Plant J.* 62, 483–493. doi: 10.1111/j.1365-313X.2010.04166.x

Clough, S. J., and Bent, A. F. (1998). Floral dip: A simplified method for agrobacterium-mediated transformation of arabidopsis thaliana. *Plant J.* 16, 735–743. doi: 10.1046/j.1365-313x.1998.00343.x

Dauphinee, A. N., Cardoso, C., Dalman, K., Ohlsson, J. A., Fick, S. B., Robert, S., et al. (2019). Chemical screening pipeline for identification of specific plant autophagy modulators. *Plant Physiol.* 181, 855–866. doi: 10.1104/pp.19.00647

de Jong, F., and Munnik, T. (2021). Attracted to membranes: lipid-binding domains in plants. *Plant Physiol.* 185, 707–723. doi: 10.1093/plphys/kiaa100

Dettmer, J., Hong-Hermesdorf, A., Stierhof, Y. D., and Schumacher, K. (2006). Vacuolar h+-ATPase activity is required for endocytic and secretory trafficking in arabidopsis. *Plant Cell* 18, 715–730. doi: 10.1105/tpc.105.037978

Fujiki, Y., Yoshimoto, K., and Ohsumi, Y. (2007). An arabidopsis homolog of yeast ATG6/VPS30 is essential for pollen germination. *Plant Physiol.* 143, 1132–1139. doi: 10.1104/pp.106.093864

Gao, C., Luo, M., Zhao, Q., Yang, R., Cui, Y., Zeng, Y., et al. (2014). A unique plant ESCRT component, FREE1, regulates multivesicular body protein sorting and plant growth. *Curr. Biol.* 24, 2556–2563. doi: 10.1016/j.cub.2014.09.014

Gao, C., Zhuang, X., Cui, Y., Fu, X., He, Y., Zhao, Q., et al. (2015). Dual roles of an arabidopsis ESCRT component FREE1 in regulating vacuolar protein transport and autophagic degradation. *Proc. Natl. Acad. Sci. U. S. A.* 112, 1886–1891. doi: 10.1073/pnas.1421271112

Geldner, N., Denervaud-Tendon, V., Hyman, D. L., Mayer, U., Stierhof, Y. D., and Chory, J. (2009). Rapid, combinatorial analysis of membrane compartments in intact plants with a multicolor marker set. *Plant J.* 59, 169–178. doi: 10.1111/j.1365-313X.2009.03851.x

González Solís, A., Berryman, E., and Otegui, M. S. (2022). Plant endosomes as protein sorting hubs. *FEBS Lett.* 596, 2288–2304. doi: 10.1002/1873-3468.14425

Hanaoka, H., Noda, T., Shirano, Y., Kato, T., Hayashi, H., Shibata, D., et al. (2002). Leaf senescence and starvation-induced chlorosis are accelerated by the disruption of an arabidopsis autophagy gene. *Plant Physiol.* 129, 1181–1193. doi: 10.1104/pp.011024

Inoue, Y., Suzuki, T., Hattori, M., Yoshimoto, K., Ohsumi, Y., and Moriyasu, Y. (2006). AtATG genes, homologs of yeast autophagy genes, are involved in constitutive autophagy in arabidopsis root tip cells. *Plant Cell Physiol.* 47, 1641–1652. doi: 10.1093/pcp/pcl031

Jung, H., Lee, H. N., Marshall, R. S., Lomax, A. W., Yoon, M. J., Kim, J., et al. (2020). Arabidopsis cargo receptor NBR1 mediates selective autophagy of defective proteins. *J. Exp. Bot.* 71, 73–89. doi: 10.1093/jxb/erz404

Kang, S., Shin, K. D., Kim, J. H., and Chung, T. (2018). Autophagy-related (ATG) 11, ATG9 and the phosphatidylinositol 3-kinase control ATG2-mediated formation of autophagosomes in arabidopsis. *Plant Cell Rep.* 37, 653–664. doi: 10.1007/s00299-018-2258-9

Kim, J. H., Jung, H., and Chung, T. (2020). Birth, growth, maturation, and demise of plant autophagic vesicles. *J. Plant Biol.* 63, 155–164. doi: 10.1007/s12374-020-09252-8

Kim, J. H., Lee, H. N., Huang, X., Jung, H., Otegui, M. S., Li, F., et al. (2022). FYVE2, a phosphatidylinositol 3-phosphate effector, interacts with the COPII machinery to control autophagosome formation in arabidopsis. *Plant Cell* 34, 351–373. doi: 10.1093/plcell/koab263

Kim, J., Lee, H., Lee, H. N., Kim, S. H., Shin, K. D., and Chung, T. (2013). Autophagy-related proteins are required for degradation of peroxisomes in arabidopsis hypocotyls during seedling growth. *Plant Cell* 25, 4956–4966. doi: 10.1105/tpc.113.117960

Lee, Y., Kim, E. S., Choi, Y., Hwang, I., Staiger, C. J., Chung, Y. Y., et al. (2008). The arabidopsis phosphatidylinositol 3-kinase is important for pollen development. *Plant Physiol.* 147, 1886–1897. doi: 10.1104/pp.108.121590

Lee, H. N., Zarza, X., Kim, J. H., Yoon, M. J., Kim, S. H., Lee, J. H., et al. (2018). Vacuolar trafficking protein VPS38 is dispensable for autophagy. *Plant Physiol.* 176, 1559–1572. doi: 10.1104/pp.17.01297

Liu, F., Hu, W., Li, F., Marshall, R. S., Zarza, X., Munnik, T., et al. (2020). AUTOPHAGY-RELATED14 and its associated phosphatidylinositol 3-kinase complex promotes autophagy in arabidopsis. *Plant Cell* 32, 3939–3960. doi: 10.1105/tpc.20.00285

Liu, F., Hu, W., and Vierstra, R. D. (2018). The vacuolar protein sorting-38 subunit of the arabidopsis phosphatidylinositol-3-Kinase complex plays critical roles in autophagy, endosome sorting, and gravitropism. *Front. Plant Sci.* 9. doi: 10.3389/fpls.2018.00781

Liu, C., Zeng, Y., Li, H., Yang, C., Shen, W., Xu, M., et al. (2021). A plant-unique ESCRT component, FYVE4, regulates multivesicular endosome biogenesis and plant growth. *New Phytol.* 231, 193–209. doi: 10.1111/nph.17358

Marshall, R. S., and Vierstra, R. D. (2018). Autophagy: The master of bulk and selective recycling. *Annu. Rev. Plant Biol.* 69, 173–208. doi: 10.1146/annurev-arplant-042817-040606

Phan, N. Q., Kim, S. J., and Bassham, D. C. (2008). Overexpression of arabidopsis sorting nexin AtSNX2b inhibits endocytic trafficking to the vacuole. *Mol. Plant* 1, 961–976. doi: 10.1093/mp/ssn057

Pourcher, M., Santambrogio, M., Thazar, N., Thierry, A. M., Fobis-Loisy, I., Miege, C., et al. (2010). Analyses of sorting nexins reveal distinct retromer-subcomplex functions in development and protein sorting in arabidopsis thaliana. *Plant Cell* 22, 3980–3991. doi: 10.1105/tpc.110.078451

Qi, H., Xia, F., and Xiao, S. (2021). Autophagy in plants: Physiological roles and post-translational regulation. *J. Integr. Plant Biol.* 63, 161–179. doi: 10.1111/jipb.12941

Qi, H., Xia, F. N., Xie, L. J., Yu, L. J., Chen, Q. F., Zhuang, X. H., et al. (2017). TRAF family proteins regulate autophagy dynamics by modulating AUTOPHAGY PROTEIN6 stability in arabidopsis. *Plant Cell* 29, 890–911. doi: 10.1105/tpc.17.00056

Robertson, A. S., Allwood, E. G., Smith, A. P., Gardiner, F. C., Costa, R., Winder, S. J., et al. (2009). The WASP homologue Las17 activates the novel actin-regulatory activity of Ysc84 to promote endocytosis in yeast. *Mol. Biol. Cell* 20, 1618–1628. doi: 10.1091/mbc.E08-09-0982

Schink, K. O., Raiborg, C., and Stenmark, H. (2013). Phosphatidylinositol 3-phosphate, a lipid that regulates membrane dynamics, protein sorting and cell signalling. *Bioessays* 35, 900–912. doi: 10.1002/bies.201300064

Shin, K. D., Lee, H. N., and Chung, T. (2014). A revised assay for monitoring autophagic flux in arabidopsis thaliana reveals involvement of AUTOPHAGY-RELATED9 in autophagy. *Mol. Cells* 37, 399–405. doi: 10.14348/molcells.2014.0042

Simon, M. L., Platre, M. P., Assil, S., van Wijk, R., Chen, W. Y., Chory, J., et al. (2014). A multi-colour/multi-affinity marker set to visualize phosphoinositide dynamics in arabidopsis. *Plant J.* 77, 322–337. doi: 10.1111/tpj.12358

Soto-Burgos, J., and Bassham, D. C. (2017). SnRK1 activates autophagy *via* the TOR signaling pathway in arabidopsis thaliana. *PloS One* 12, e0182591. doi: 10.1371/journal.pone.0182591

Spitzer, C., Li, F., Buono, R., Roschzttardtz, H., Chung, T., Zhang, M., et al. (2015). The endosomal protein CHARGED MULTIVESICULAR BODY PROTEIN1 regulates the autophagic turnover of plastids in arabidopsis. *Plant Cell* 27, 391–402. doi: 10.1105/tpc.114.135939

Sutipatanasomboon, A., Herberth, S., Alwood, E. G., Haweker, H., Muller, B., Shahriari, M., et al. (2017). Disruption of the plant-specific CFS1 gene impairs autophagosome turnover and triggers EDS1-dependent cell death. *Sci. Rep.* 7, 8677–017-08577-8. doi: 10.1038/s41598-017-08577-8

Suttangkakul, A., Li, F., Chung, T., and Vierstra, R. D. (2011). The ATG1/ATG13 protein kinase complex is both a regulator and a target of autophagic recycling in arabidopsis. *Plant Cell* 23, 3761–3779. doi: 10.1105/tpc.111.090993

Thompson, A. R., Doelling, J. H., Suttangkakul, A., and Vierstra, R. D. (2005). Autophagic nutrient recycling in arabidopsis directed by the ATG8 and ATG12 conjugation pathways. *Plant Physiol.* 138, 2097–2110. doi: 10.1104/pp.105.060673

Urbanek, A. N., Allwood, E. G., Smith, A. P., Booth, W. I., and Ayscough, K. R. (2015). Distinct actin and lipid binding sites in Ysc84 are required during early stages of yeast endocytosis. *PloS One* 10, e0136732. doi: 10.1371/journal.pone.0136732[doi

Yuan, R., Lan, J., Fang, Y., Yu, H., Zhang, J., Huang, J., et al. (2018). The arabidopsis USL1 controls multiple aspects of development by affecting late endosome morphology. *New Phytol.* 219, 1388–1405. doi: 10.1111/nph.15249

Zhao, J., Bui, M. T., Ma, J., Künzl, F., Picchianti, L., de la Concepcion, ,.J. C., et al. (2022). Plant autophagosomes mature into amphisomes prior to their delivery to the central vacuole. *J. Cell Biol.* 221, e202203139. doi: 10.1083/jcb.202203139

Zhuang, X., Chung, K. P., Cui, Y., Lin, W., Gao, C., Kang, B. H., et al. (2017). ATG9 regulates autophagosome progression from the endoplasmic reticulum in arabidopsis. *Proc. Natl. Acad. Sci. USA* 114, E426–E435. doi: 10.1073/pnas.1616299114

frontiers | Frontiers in Plant Science

TYPE Original Research
PUBLISHED 31 May 2023
DOI 10.3389/fpls.2023.1171957

OPEN ACCESS

EDITED BY
Emily R. Larson,
University of Bristol, United Kingdom

REVIEWED BY
Fatima Cvrckova,
Charles University, Czechia
Jitka Ortmannová,
(ASCR), Czechia
Jinbo Shen,
Zhejiang Agriculture and Forestry University, China

*CORRESPONDENCE
Christopher J. Staiger
staiger@purdue.edu

RECEIVED 22 February 2023
ACCEPTED 15 May 2023
PUBLISHED 31 May 2023

CITATION
Li X, Zhu P, Chen Y-J, Huang L, Wang D, Newton DT, Hsu C-C, Lin G, Tao WA, Staiger CJ and Zhang C (2023) The EXO70 inhibitor Endosidin2 alters plasma membrane protein composition in Arabidopsis roots.
Front. Plant Sci. 14:1171957.
doi: 10.3389/fpls.2023.1171957

The EXO70 inhibitor Endosidin2 alters plasma membrane protein composition in Arabidopsis roots

Xiaohui Li[1,2], Peipei Zhu[3,4], Yen-Ju Chen[1,2], Lei Huang[1,2], Diwen Wang[1,2], David T. Newton[5], Chuan-Chih Hsu[3], Guang Lin[6,7], W. Andy Tao[3,4], Christopher J. Staiger[1,2,8]* and Chunhua Zhang[1,2]

[1]Department of Botany and Plant Pathology, Purdue University, West Lafayette, IN, United States, [2]Center for Plant Biology, Purdue University, West Lafayette, IN, United States, [3]Department of Biochemistry, Purdue University, West Lafayette, IN, United States, [4]Department of Chemistry, Purdue University, West Lafayette, IN, United States, [5]Department of Statistics, Purdue University, West Lafayette, IN, United States, [6]Department of Mathematics, Purdue University, West Lafayette, IN, United States, [7]School of Mechanical Engineering, Purdue University, West Lafayette, IN, United States, [8]Department of Biological Sciences, Purdue University, West Lafayette, IN, United States

To sustain normal growth and allow rapid responses to environmental cues, plants alter the plasma membrane protein composition under different conditions presumably by regulation of delivery, stability, and internalization. Exocytosis is a conserved cellular process that delivers proteins and lipids to the plasma membrane or extracellular space in eukaryotes. The octameric exocyst complex contributes to exocytosis by tethering secretory vesicles to the correct site for membrane fusion; however, whether the exocyst complex acts universally for all secretory vesicle cargo or just for specialized subsets used during polarized growth and trafficking is currently unknown. In addition to its role in exocytosis, the exocyst complex is also known to participate in membrane recycling and autophagy. Using a previously identified small molecule inhibitor of the plant exocyst complex subunit EXO70A1, Endosidin2 (ES2), combined with a plasma membrane enrichment method and quantitative proteomic analysis, we examined the composition of plasma membrane proteins in the root of Arabidopsis seedlings, after inhibition of the ES2-targetted exocyst complex, and verified our findings by live imaging of GFP-tagged plasma membrane proteins in root epidermal cells. The abundance of 145 plasma membrane proteins was significantly reduced following short-term ES2 treatments and these likely represent candidate cargo proteins of exocyst-mediated trafficking. Gene Ontology analysis showed that these proteins play diverse functions in cell growth, cell wall biosynthesis, hormone signaling, stress response, membrane transport, and nutrient uptake. Additionally, we quantified the effect of ES2 on the spatial distribution of EXO70A1 with live-cell imaging. Our results indicate that the plant exocyst complex mediates constitutive dynamic transport of subsets of plasma membrane proteins during normal root growth.

KEYWORDS

plasma membrane protein enrichment, exocytosis, proteomics, small molecule inhibitors, exocyst

Highlights

- The proteomics profile of Arabidopsis plasma membrane proteins changes following 2-h treatment with the EXO70A1 inhibitor, ES2.

Introduction

The plant plasma membrane serves as a selective physical barrier between intracellular contents and the environment as well as a signaling platform for transmitting information from the exterior to induce cellular responses. Plasma membrane proteins can be classified as integral, lipid-anchored, and peripheral, based on the mode of association with the plasma membrane (Stillwell, 2016). Integral membrane proteins possess one to several transmembrane domains; lipid-anchored proteins associate with the plasma membrane through covalently attached fatty acids; peripheral membrane proteins associate with the plasma membrane through interactions with other membrane proteins, polar head groups of the lipid bilayer, or both. Several well-characterized plasma membrane-localized nutrient transporters, hormone receptors and transporters, and cell wall biosynthetic enzymes are known to undergo constitutive delivery and turnover (Li et al., 2002; Friml, 2010; Takano et al., 2010; Kleine-Vehn et al., 2011; Irani et al., 2012; Bashline et al., 2013; Chen et al., 2015; Wang et al., 2015; Zhu et al., 2018; Vellosillo et al., 2021). Proteomic analyses of plasma membrane proteins reveal that the composition is altered in response to biotic and abiotic stresses (Nohzadeh Malakshah et al., 2007; Nouri and Komatsu, 2010; Elmore et al., 2012; Takahashi et al., 2013; Nie et al., 2015; Cao et al., 2016; Chen et al., 2016; Voothuluru et al., 2016); however, the mechanisms for delivery of most of these plasma membrane proteins are not well characterized. Investigating how plants maintain the variety, abundance, and dynamics of plasma membrane proteins is essential for understanding cell growth, development, and response to stresses.

The conventional plant secretory pathway involves trafficking through the endoplasmic reticulum, Golgi and post-Golgi vesicles to deliver lipids and proteins to the plasma membrane or extracellular space (Denecke et al., 2012; Drakakaki and Dandekar, 2013; Zhu et al., 2020; Aniento et al., 2022). The exocyst complex is a conserved octameric protein complex that primarily functions to mediate the tethering of secretory vesicles to the site of membrane fusion during the last step of exocytic trafficking (Elias et al., 2003; Zhang et al., 2010; Žárský et al., 2013; Wu and Guo, 2015; Synek et al., 2021; Žárský, 2022). In addition, the exocyst complex also associates with the endocytic and autophagy machinery to modulate membrane recycling and autophagy (Prigent et al., 2003; Kulich et al., 2013; Žárský et al., 2013; Ortega et al., 2022; Žárský, 2022). One plant exocyst subunit, EXO70A1, was recently characterized as a landmark for exocyst complex recruitment to the plasma membrane, through its interactions with anionic phospholipids (Synek et al., 2021). Loss of EXO70A1 function disrupts the recruitment of other exocyst subunits to the plasma membrane in Arabidopsis root epidermal cells (Synek et al., 2021). Some known cargo proteins for plant exocyst complex-mediated trafficking include PIN auxin transporters (Drdová et al., 2013), brassinosteroid receptor (Zhang et al., 2016), and cellulose synthase complexes (Zhu et al., 2018; Zhang et al., 2021). However, it is not known what other plasma membrane proteins are delivered to the plasma membrane through the exocyst complex. Whereas the half-life for turnover of plasma membrane proteins in mammalian cells varies from a few hours to a few days (Tweto and Doyle, 1976; Doyle and Baumann, 1979; Chu and Doyle, 1985), we know much less about the mechanisms and dynamics of protein delivery to the plasma membrane in plants.

Previously, the small molecule Endosidin2 (ES2) was shown to target the EXO70A1 subunit of Arabidopsis exocyst complex and to inhibit exocytosis in plant and mammalian cells (Zhang et al., 2016; Huang et al., 2019). Short-term ES2 treatment inhibits the transport of PIN-FORMED (PIN) family auxin transporter, PIN2, and the brassinosteroid receptor BRI1, to the plasma membrane (Zhang et al., 2016), and also impairs the recycling of PIN2 (Lešková et al., 2020). In mammalian cells, ES2 treatment reduces the cell surface abundance of a membrane-anchored metalloproteinase MT2-MMP (Gómez-Escudero et al., 2017). In addition, given the role of the exocyst complex in autophagy, a recent study examined the consequences of ES2 treatment in autophagy events in mammalian cells, and found that a 24-h ES2 treatment resulted in decreased autophagy (Ortega et al., 2022). To characterize changes in plasma membrane protein composition after short-term inhibition of the exocyst complex, and to identify additional proteins that are transported through the exocyst complex, we used ES2 to inhibit the exocyst complex. We enriched plasma membrane from roots of Arabidopsis seedlings treated with ES2 and DMSO solvent control and identified proteins using mass spectrometry analysis. We then performed quantitative and comparative proteomic analyses to identify plasma membrane proteins with altered abundance in ES2-treated samples and considered proteins with reduced abundance as candidate cargo proteins of exocyst-mediated trafficking in plants. We identified a subset of proteins with significantly reduced abundance at the plasma membrane after two hours of 40 μM ES2 treatment. Gene Ontology analysis of proteins with reduced abundance demonstrated enrichment for functions in cell growth, cell wall biosynthesis, membrane transport, hormone signaling, and stress responses. The abundance of many protein kinases and several uncharacterized proteins was reduced by ES2 treatment as well. Our results show that the exocyst complex mediates dynamic transport of a diverse set of proteins essential for plant growth and environmental adaptation.

Materials and methods

Plasma membrane enrichment

Arabidopsis PIP2A-GFP seeds (Cutler et al., 2000) were sterilized and sowed on half-strength Murashige and Skoog (½ MS) media with vitamins (Caisson Labs, Smithfield, UT, USA), 1% (w/v) sucrose, and 0.8% (w/v) agar (Fisher Scientific, Waltham, MA,

USA). The seeds were well separated from each other in both horizontal and vertical orientations on 10 cm x 10 cm square petri plates. Plates were placed in vertical orientation so that the seedings grew on the surface of the agar media. The plants were grown in a growth chamber (Percival Scientific, Perry, IA, USA) under continuous light of 130 µmol $m^{-2}s^{-1}$ at 23°C. Six-day-old seedlings were removed from the agar plates and transferred to liquid ½ MS media with 1% (w/v) sucrose and 40 µM ES2 or 0.5% DMSO (mock). After two hours of treatment under light, the roots of the seedlings were quickly excised and transferred to the plasma membrane enrichment buffer. The process of plasma membrane enrichment followed exactly the published protocol (Collins et al., 2017). To evaluate the enrichment of plasma membrane proteins by Western blot assay, 12 µg of protein from each fraction was loaded onto SDS-PAGE gels and the presence of PIP2A-GFP, Sec12, and SYP41 was detected after transfer to PVDF membrane. The anti-GFP antibody was used at 1:1000 dilution (Takara Bio USA, catalog # 632381, San Jose, CA, USA); anti-Sec12 antibody (Bar-Peled and Raikhel, 1997) was used at 1:5000 dilution; and anti-SYP41 antibody (Bassham et al., 2000) was used at 1:500 dilution. HRP-conjugated goat anti-mouse and goat anti-rabbit antibodies were used at 1:10,000 dilution. The plasma membrane enrichment experiments were repeated four times under identical conditions.

Methanol-chloroform precipitation

The mass spectrometry sample preparation procedure was based on previous literature (Hsu et al., 2018). Protein concentrations from enriched plasma membrane fractions were quantified using the bicinchoninic acid method. For each sample, 250 µg of enriched plasma membrane protein was processed for mass spectrometry analysis. Proteins from each sample were reduced and alkylated with 10 mM tris-(2-carboxyethyl) phosphine (TECP) and 40 mM chloroacetamide (CAA) at 95°C for 5 min. Methanol, chloroform, and ddH_2O were added to each 100 µl sample in a volume ratio of 4:1:3, respectively (Wessel and Flügge, 1984). The solution was mixed and centrifuged at 16,000x g for 3 min to obtain aqueous and organic phases. Four volumes of methanol were added to the sample after removing the upper aqueous layer carefully without disturbing the intermediate protein disk. The solution was mixed and centrifuged again at the same settings. The supernatant was removed, the precipitated protein pellet was washed with 400 µL methanol, and the sample was air-dried.

Protein digestion

The precipitated protein pellet was dissolved with 100 µl of 12 mM sodium deoxycholate (SDC) and 12 mM sodium lauroyl sarcosinate (SLS) in 100 mM Tris-HCl (pH 8.5). Protein amount was quantified by BCA assay (Thermo Fisher Scientific). Dissolved protein extract was diluted 5-fold with 50 mM triethylammonium hydrogen carbonate buffer (TEAB) and digested with Lys-C (Wako Chemicals USA Inc., Richmond, VA, USA) in a ratio of 1:100 (w/w) enzyme-to-protein ratio for 3 h at 37°C, and trypsin (Sigma-Aldrich, St. Louis, MO, USA) in a ratio of 1:50 (w/w) enzyme-to-protein ratio for overnight at 37°C. SDC and SLS were removed by adding 100% acetyl acetate in a ratio of 1:1 (vol/vol) sample to acetyl acetate volume ratio. The digests were desalted by homemade stage tip with styrene divinyl benzene (SDB-XC) membrane (3M) after the digests were acidified with 10% trifluoroacetic acid (TFA) to a pH ~3.

Dimethyl labeling

Every 50–100 µg of tryptic peptides was dissolved in 100 µl of 100 mM TEAB and mixed with 4 µl of 4% $^{13}CD_2O$ or $^{12}CH_2O$, and then 4 µl of freshly prepared 0.6 M sodium cyanoborohydride was immediately added (Boersema et al., 2009). The mixture was agitated for 1 h at room temperature. The reaction was quenched by adding 16 µl of ice-cold 1% ammonium hydroxide and agitated for 1 min. Heavy and light dimethyl-labeled peptides were mixed after the labeled peptides were acidified with 20 µl of 10% formic acid and then fractionated by basic pH reverse-phase stage tips.

Basic pH reverse-phase fractionation

Two mg of the Magic C18-AQ beads (5 µm particles) were suspended in 200 µL of methanol and loaded into a 200 µL StageTip with a 20 µm polypropylene frit (Agilent, Santa Clara, CA, USA) (Dimayacyac-Esleta et al., 2015). The C18 StageTip was activated with 50 µL of 100% acetonitrile (ACN) and washed with 50 µL of 200 mM ammonium formate, pH 10. After the StageTip was activated and washed, 25–50 µg of dimethyl-labeled peptides were fractionated from the StageTip with 50 µL of 6 different ACN concentrations: 5, 10, 15, 20, 25% and 80% of ACN in 200 mM ammonium formate, pH 10. The eluted peptides were dried and stored at -20°C.

LC-MS/MS analysis

Twenty-five µg of dimethyl-labeled peptides used in fractionations were dissolved in 5 µL of 0.3% formic acid (FA) with 3% ACN and 4 µL of each fraction injected into an EasynLC 1000 (Thermo Fisher Scientific). Peptides were separated on a 45 cm in-house packed column (360 µm OD × 75 µm ID) containing C18 resin (2.2 µm, 100Å, Michrom Bioresources, Auburn, CA, USA) with a 30 cm column heater (Analytical Sales and Services, Flanders, NJ, USA) set at 60°C. The mobile phase buffer for 25 µg peptide fractions consisted of 0.1% FA in ultrapure water (buffer A) with an eluting buffer of 0.1% FA in 80% ACN (buffer B) run with a 150 min gradient of 5–30% buffer B at a flow rate of 250 nL/min. The Easy-nLC 1000 was coupled online with a Velos Pro LTQ-Orbitrap mass spectrometer (Thermo Fisher Scientific). The mass spectrometer was operated in the data-dependent mode in which a full MS scan (from m/z 350–1500 with a resolution of 30,000 at m/z 400) was followed by MS/MS of the 10 most intense ions being

subjected to collision-induced dissociation (CID) fragmentation (normalized collision energy–30%, automatic gain control–3E4, max injection time–100 ms).

Proteomics data analyses

The raw files were searched directly against the *Arabidopsis thaliana* protein database (TAIR10) with no redundant entries using MaxQuant software (version 1.6.1.0) (Tyanova et al., 2016a) with 1% false-discovery rate (FDR) cutoff for protein and peptide. The first peptide precursor mass tolerance was set at 20 ppm, and MS/MS tolerance was set at 0.6 Da. Search criteria included a static carbamidomethylation of cysteines and variable modifications of oxidation on methionine residues and acetylation at N-terminus of proteins. The search was performed with full tryptic digestion and allowed a maximum of two missed cleavages on the peptides analyzed from the sequence database. Dimethyl-labeling quantitation was performed by setting the multiplicity as 2 (DimethLys0 and DimethNter0; DimethLys6 and DimethNter6). Re-quantify and match between runs function were enabled.

After database searches, the Perseus software platform (Version 1.6.1.3) (Tyanova et al., 2016b) was used to further analyze the MaxQuant-derived protein groups file. First, the rows marked to be "only identified by site", "reverse" and "potential contaminants" were filtered out. The Heavy/Light ratio was transformed to Light/Heavy (L/H) ratio for convenience, and then to $\log_2$L/H ratio. Normalization was performed by median subtraction. Proteins with less than 3 valid values among the 4 replicates were filtered out. One sample t-test was performed with both side and p-value threshold of 0.05. Proteins that passed t-test and with a mean $\log_2$L/H ratio ≤ -0.32193 were considered to be 20% reduction candidates. Histogram and multi-scatter plots were generated by Perseus software. The reduced abundance candidate list was uploaded to PANTHER platform for Gene Ontology (GO) analysis, including functional classification and statistical overrepresentation (Mi et al., 2013; Mi et al., 2017).

The Venn diagram was generated using the online tool provided by Van de Peer Lab at the Bioinformatics and Evolutionary Genomics Core of Ghent University, Belgium (http://bioinformatics.psb.ugent.be/webtools/Venn/). The presence of signal peptide and transmembrane domains in candidate proteins was predicted using the DeepTMHMM package (v1.0.24) provided by Department of Bio and Health Informatics, Technical University of Denmark (https://dtu.biolib.com/DeepTMHMM) (Hallgren et al., 2022).

Confocal microscopy

For imaging of fluorescence-tagged protein marker lines, 6-d-old light-grown seedlings expressing PIN2-GFP (Xu and Scheres, 2005), BRI1-GFP (Wang et al., 2001), FER-GFP (Escobar-Restrepo et al., 2007), PIP2A-GFP (Cutler et al., 2000), or GFP-EXO70A1 (Fendrych et al., 2010) were treated in liquid ½ MS medium containing 0.5% DMSO (mock) or 40 µM ES2 for 2 h. Live imaging was performed with a Zeiss LSM 710 Axio Imager laser-scanning confocal microscope operated with Zeiss ZEN software (Carl Zeiss Microscopy LLC, White Plains, NY, USA). The PIN2-GFP, BRI1-GFP, FER-GFP and PIP2A-GFP lines were imaged with a Zeiss Plan-Apochromat 100x/NA1.40 DIC Oil immersion objective at 2048×2048 pixel scanning resolution. The GFP-EXO70A1 line was imaged with a Zeiss Plan-Apochromat 63x/NA1.40 Oil immersion objective at 4096×4096 pixel scanning resolution. The GFP-EXO70A1 seedlings were stained with 10 µg/mL Propidium Iodide (PI) (Biotium Inc., Fremont, CA, USA; Cat # 40016) in ½ liquid MS medium containing DMSO or ES2 in the dark for 10 min, and quickly rinsed in PI-free medium before imaging. GFP was excited with a 488-nm laser line, and PI was excited with a 543-nm laser line. Images were collected from root epidermal cells at the transition zone.

Quantitative image analysis of GFP fluorescence intensity was performed using the FIJI distribution of ImageJ (Ver 1.54b). The regions of interest (ROI) were selected for plasma membrane, cytoplasmic background in the compartment-free region, and the entire cytoplasmic region. The mean fluorescence intensity of the GFP signal for each ROI was measured. The average PM fluorescence intensity was normalized by subtracting the mean fluorescence intensity of the cytoplasmic background. The plasma membrane / cytoplasm ratio was calculated by first subtracting the mean fluorescence intensity of the region outside of the root and then dividing the PM mean fluorescence intensity by the mean fluorescence intensity of the entire cytoplasmic region. Values for individual cells from each seedling were averaged and considered as one data point. Normalization and averaging were performed in Microsoft Excel. Statistical analyses using a Student's *t*-test were conducted, and box plots were generated with GraphPad Prism software.

Results

Plasma membrane enrichment

We chose to use a transgenic line expressing PIP2A-GFP as the plant material for our experiments because PIP2A-GFP is localized predominantly at the plasma membrane by microscopy and its cellular localization is not affected by 2 h of 40 µM ES2 treatment (Cutler et al., 2000; Zhang et al., 2016). The GFP tag also allowed the use of anti-GFP antibody to examine the quality of enriched plasma membrane fractions. Six-day-old PIP2A-GFP seedlings were treated with either 40 µM ES2 or 0.5% DMSO for 2 h, a condition in which plant exocytosis is reduced but not completely inhibited (Zhang et al., 2016). After treatment, roots were excised and used for plasma membrane enrichment (Figure 1A). We adapted a protocol that allows quick enrichment of plasma membrane and does not require large amounts of plant tissue (Zhang and Peck, 2011; Collins et al., 2017).

Enrichment was evaluated by detecting the presence of proteins known to localize to the plasma membrane (PIP2A-GFP) (Cutler et al., 2000), endoplasmic reticulum (ER) (Sec12) (Bar-Peled and Raikhel, 1997), and Golgi/trans-Golgi network (TGN) (SYP41)

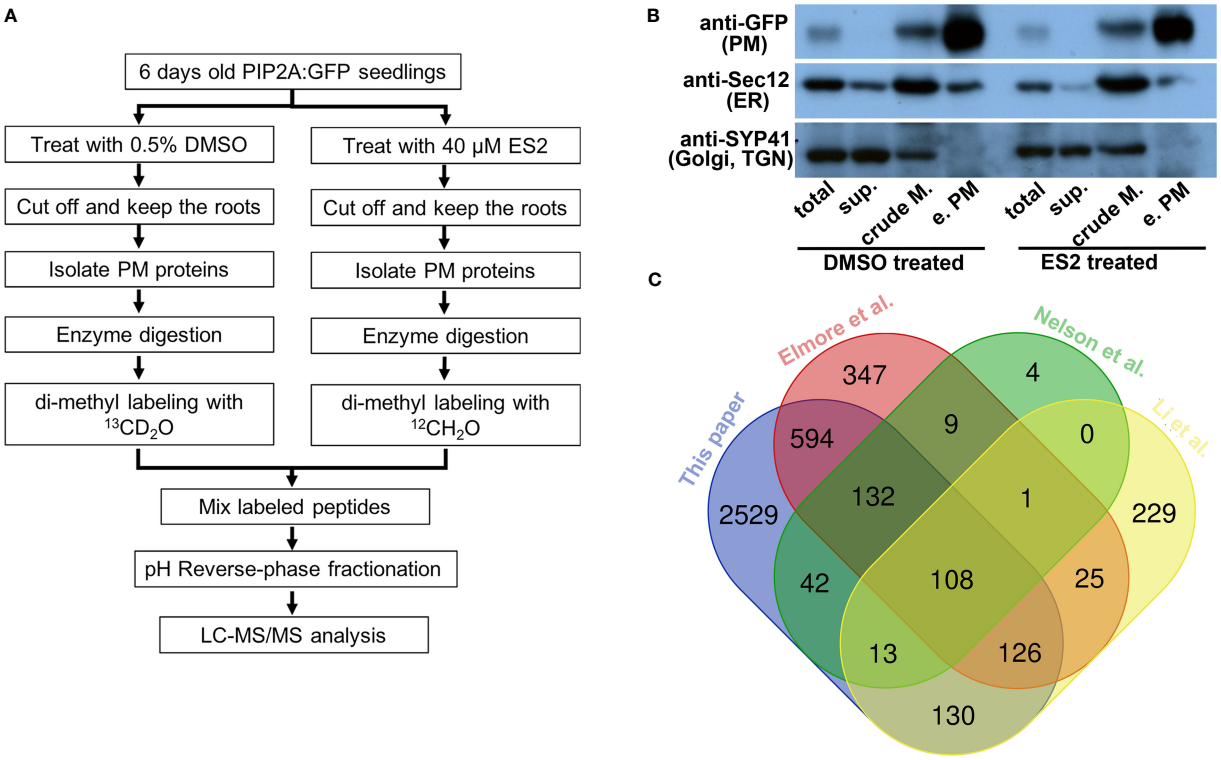

FIGURE 1
Characterization of enriched plasma membrane fractions shows the high quality of the sample preparation. **(A)** Flowchart of sample preparation for mass spectrometry analysis. **(B)** Western blot characterization of enriched plasma membrane fractions. Protein amount of 12.5 μg from total protein (total), soluble protein (sup.), crude membrane fraction (crude M.) and enriched plasma membrane fraction (e.PM) was separated in SDS-PAGE and transferred to PVDF membrane. The same membrane was blotted with anti-GFP, anti-Sec12 and anti-SYP41 antibodies. **(C)** The Venn diagram comparing the proteins that were identified from different proteomics experiments.

(Bassham et al., 2000) in different fractions using Western blots with anti-GFP, anti-Sec12, and anti-SYP41 antibodies, respectively (Figure 1B). PIP2A-GFP was enriched in the plasma membrane fraction when compared to the crude membrane fraction (Figure 1B, anti-GFP). The ER membrane protein, Sec12, was detected in both crude membrane and plasma membrane fractions; however, the abundance of Sec12 in the plasma membrane fraction was markedly lower than the crude membrane fraction (Figure 1B, anti-Sec12). The Golgi/TGN protein, SYP41, was detected in the crude membrane fraction but not in the enriched plasma membrane fraction (Figure 1B, anti-SYP41). Immunoblots demonstrated that although proteins from other organelles were present in the enriched plasma membrane fraction, their abundance was substantially reduced in comparison with plasma membrane proteins. We prepared four independent biological replicates of enriched plasma membrane fractions for the mass spectrometry proteomics analysis.

Mass spectrometry analyses of enriched plasma membrane proteins

From each enriched plasma membrane fraction, 25 μg of protein was digested with Lys-C and trypsin. Resulting peptides from ES2-treated plant samples were dimethyl labeled with $^{12}CH_2O$ (light, L) and peptides from DMSO-treated samples were dimethyl labeled with $^{13}CD_2O$ (heavy, H). Dimethyl-labeled peptides from ES2-treatment and control samples were combined and fractionated before LC-MS/MS analysis. The peptides that were detected by LC-MS/MS were assigned to proteins and the abundance of each protein was calculated through a MaxQuant database search. The ratio of each protein's abundance in differentially labeled samples was calculated using the same process. The data were processed further with the Perseus platform by filtering out rows with invalid values (potential contaminants, the reverse peptides, and peptides only identified by site) from the MaxQuant database search. We further filtered the data by removing proteins with less than three detected values in the four replicates. To compare the data from different replicates, the ratio of protein abundance between differentially labeled proteins was transformed to $\log_2$ phase and further normalized by median subtraction and then analyzed by histogram (Supplemental Figure S1). The normal distribution of $\log_2$ phase of ratios centered by zero between differentially labeled proteins indicates that the majority of proteins that we detected were not altered by ES2 treatment.

We detected 3675 proteins from four independent replicate experiments (Supplementary Table S1). To further evaluate the plasma membrane preparation, we compared our protein list with those published from different Arabidopsis tissues using another

plasma membrane preparation method (Figure 1C). First, we compared our plasma membrane protein list with one generated from two-week-old liquid cultured *Arabidopsis* seedlings using a two-phase partition of microsomes and Trypsin-catalyzed ^{18}O labeling (Nelson et al., 2006). We found 295 overlapping proteins, accounting for 95% of the proteins detected in Nelson et al.'s experiments (309 proteins in total) (Figure 1C). Elmore et al. used an aqueous two-phase partitioning approach for leaves of four-week-old Arabidopsis plants grown in soil condition and consistently identified more than 1300 proteins in replicate experiments (Elmore et al., 2012). We found 960 overlapping proteins, accounting for more than 70% of the proteins detected in Elmore et al.'s experiments (Figure 1C). Li et al. isolated plasma membrane fractions from Arabidopsis suspension-cultured cells using a two-phase partition method and identified over 600 proteins by proteomic analysis (Li et al., 2012). About 60% of the proteins that were detected from cultured cells were consistently identified in our experiments (Figure 1C). Substantial overlap between our plasma membrane protein list and others that use a different method or tissue indicates that our proteomic data can be used to compare the effects of ES2 on the abundance of plasma membrane proteins.

To examine whether the enriched plasma membrane fraction was free from contaminants from other large membrane-bound compartments, we checked our proteomics list for the presence of proteins residing in the nuclear envelope and vacuole. The nuclear envelope protein SAD1/UNC-84 DOMAIN PROTEIN 1 (SUN1, AT5G04990; Oda and Fukuda, 2011) was detected, but its abundance was unchanged following ES2 treatment, with a mean log2 fold-change of 0.00. Another nuclear envelope protein SAD1/UNC-84 DOMAIN PROTEIN 2 (SUN2, AT3G10730; Oda and Fukuda, 2011) was not detected. The vacuole membrane protein TONOPLAST INTRINSIC PROTEIN 1;1 (γ-TIP or TIP1;1, AT2G36830; Nelson et al., 2006) was not detected. These results indicate that the enriched plasma membrane fraction was relatively free from contamination of nuclear envelope or vacuolar membranes.

To investigate whether ES2 treatment altered the membrane identity of the plasma membrane fraction, we checked our proteomics list for the presence of several markers of membrane-bound organelles. The autophagosome markers ATG8e (AT2G45170) and ATG8f (AT4G16520) were not detected. The early endosome marker ARA6 (AT3G54840; Ebine et al., 2011), ER marker SEC12 (AT2G04170; Bar-Peled and Raikhel, 1997), and Golgi marker SYP32 (AT3G24350) and ALPHA-MANNOSIDASE 1 (ManI, AT1G51590; Kajiura et al., 2010) were all present but unchanged following ES2 treatment, with a mean log2 fold-change of 0.06 for ARA6, 0.05 for SEC12, 0.00 for SYP32, and -0.01 for ManI (Supplementary Table S1). These results indicate that the membrane identify of the plasma membrane was not altered following ES2 treatment.

To identify proteins with altered abundance after ES2 treatment, we performed a moderated t-test (Smyth, 2004) for each protein using the limma package in R. The moderated t-test uses a hierarchical empirical Bayesian model to shrink the sample standard deviation estimates for each protein towards a pooled value. This stabilizes the t-statistics and increases the power of the test to detect true differences in protein abundance. Since multiple significance tests were performed, we used the Benjamini-Hochberg procedure to bound the expected false-discovery rate at 10%. After the correction, 330 proteins had adjusted p-values less than 0.10. Thus, we can estimate that roughly 300 of the 330 proteins have $\log_2$ ratios significantly different from 0. Among these 330 proteins, 145 had reduced abundance (Supplementary Tables S2, S3) and 185 had increased abundance (Supplementary Table S4) in the plasma membrane fraction of ES2-treated samples. To highlight the proteins with the most dramatic changes, the top twenty proteins with decreased and increased abundance were listed in Tables 1, 2, respectively. Because ES2 binds to the EXO70A1 subunit of the exocyst complex and inhibits its function (Zhang et al., 2016), and because EXO70A1 serves as a landmark for exocyst complex recruitment to the plasma membrane (Synek et al., 2021), we expect that proteins with reduced abundance at the plasma membrane are candidate cargos of exocyst-mediated trafficking.

Confocal imaging of GFP-tagged plasma membrane proteins following ES2 treatment

To confirm the identification of proteins with reduced abundance after ES2 treatment, we performed live imaging of GFP-tagged plasma membrane proteins in Arabidopsis root epidermal cells using laser scanning confocal microscopy (Figure 2). We selected three protein candidates: the auxin efflux carrier protein PIN-FORMED 2 (PIN2), the leucine-rich-repeat receptor kinase of brassinosteroid signaling BRASSINOSTEROID INSENSITIVE 1 (BRI1), and the receptor kinase FERONIA (FER), each of which had reduced plasma membrane abundance after ES2 treatment in our proteomics analysis. PIN2 had a mean log2 fold-change of -0.27, BRI1 had a mean log2 fold-change of -0.31, and FER had a mean log2 fold-change of -0.38. (Supplementary Table S1). We quantified GFP-tagged protein fluorescence intensity on the plasma membrane and normalized by subtracting the mean background fluorescence intensity from a cytoplasmic compartment-free region (Figure 2C). The abundance of all three proteins at the plasma membrane region were significantly decreased after a 2-h ES2 treatment (Figure 2D). To further evaluate the change of abundance between the plasma membrane and entire cytoplasmic region, we also quantified the plasma membrane / cytoplasm intensity ratio as another indicator of plasma membrane protein abundance (Figure 2E). The plasma membrane / cytoplasm intensity ratios for all three proteins were significantly reduced after a 2-h ES2 treatment compared to mock treatment (Figure 2E). Our analysis showed for the first time that the plasma membrane abundance of FER was decreased following ES2 treatment. As a negative control, we measured the abundance of PLASMA MEMBRANE INTRINSIC PROTEIN 2A (PIP2A), which was shown to have unaltered plasma membrane abundance after ES2 treatment in the proteomics analyses, with a mean log2 fold-change of 0.05 (Supplementary Table S1). The plasma

TABLE 1 Top 20 proteins with reduced abundance in enriched plasma membrane fractions after a 2-h ES2 treatment and their Gene Ontology terms in biological processes category.

Protein ID	Protein Name	Protein Symbol	Mean L/H	Representative GO Terms (Biological Processes)	No. of TM Helices	Presence of signal peptide
AT1G66230	MYB DOMAIN PROTEIN 20	ATMYB20	0.02	regulation of secondary cell wall biogenesis (GO:2000652)	0	NO
AT3G16630	Kinesin-like protein KIN-13A	KIN13A	0.09	microtubule depolymerization (GO:0007019)	0	NO
AT3G61480	Quinoprotein amine dehydrogenase, beta chain-like RIC1-like guanyl-nucleotide exchange factor		0.10	intracellular protein transport (GO:0006886)	0	NO
AT3G22240	CYSTEINE-RICH TRANSMEMBRANE MODULE 9	ATHCYSTM9	0.26	indole-containing compound biosynthetic process (GO:0042435)	0	NO
AT3G08610	NADH dehydrogenase ubiquinone 1 alpha subcomplex subunit		0.30	catabolic process (GO:0009056)	1	NO
AT4G36670	POLYOL/MONOSACCHARIDE TRANSPORTER 6	ATPMT6	0.31	response to temperature stimulus (GO:0009266)	12	NO
AT3G45650	Protein NRT1/PTR FAMILY 2.7	NPF2.7	0.35	GO:0015698	12	NO
AT5G25820	Exostosin family protein		0.35	root morphogenesis (GO:0010015)	1	NO
AT1G65730	Probable metal-nicotianamine transporter YSL7	YSL7	0.37	catabolic process (GO:0009056)	17	NO
AT1G12950	Protein DETOXIFICATION 31	DTX31	0.38	root hair elongation (GO:0048767)	12	NO
AT2G25980	JACALIN-RELATED LECTIN 20	JAL20	0.38		0	NO
AT5G35940	Mannose-binding lectin superfamily protein		0.38	organic acid metabolic process (GO:0006082)	0	NO
AT5G40780	LYSINE HISTIDINE TRANSPORTER 1	LHT1	0.39	amino acid transmembrane transport (GO:0003333)	11	NO
AT1G17260	AUTOINHIBITED H(+)-ATPASE 10	AHA10	0.40	proton transmembrane transport (GO:1902600)	10	NO
AT2G01520	MLP-LIKE PROTEIN 328	MLP328	0.40	defense response (GO:0006952)	0	NO
AT2G39510	USUALLY MULTIPLE ACIDS MOVE IN AND OUT TRANSPORTERS 14	UMAMIT14	0.40	L-glutamate import across plasma membrane (GO:0098712)	10	NO
AT5G26260	TRAF-like family protein		0.40	plant epidermis development (GO:0090558)	0	YES
AT3G20380	TRAF-like family protein		0.41		0	YES
AT1G14160	CASP-LIKE PROTEIN 1A1	CASPL1A1	0.42	cell wall modification (GO:0042545)	4	NO
AT1G50630	Extracellular ligand-gated ion channel protein (DUF3537)		0.42	root development (GO:0048364)	7	NO

The L/H value is the ratio of the abundance in ES2-treated samples divided by the abundance in mock-treated samples. The number of TM helices and presence of signal peptide were predicted by the DeepTMHMM package.

TABLE 2 Top 20 proteins with increased abundance in enriched plasma membrane fractions after a 2-h ES2 treatment and their Gene Ontology terms in biological processes category.

Protein ID	Protein Name	Protein Symbol	Mean L/H	Representative GO Term (Biological Processes)	No. of TM Helices	Presence of signal peptide
AT4G14320	Zinc-binding ribosomal protein family protein	RPL36AB	13.84	translation (GO:0006412)	0	NO
AT1G15520	ATP-BINDING CASSETTE G40	ABCG40/ PDR12	10.93	abscisic acid transport (GO:0080168)	12	NO
AT1G80660	H(+)-ATPASE 9	AHA9	10.25	proton transmembrane transport (GO:1902600)	10	NO
AT3G56860	UBP1-ASSOCIATED PROTEIN 2A	UBA2A	8.33	abscisic acid-activated signaling pathway (GO:0009738)	0	NO
AT1G33680	KH domain-containing protein	ATKH3	7.77	regulation of gene expression (GO:0010468)	0	NO
AT5G42380	CALMODULIN LIKE 37	CML37	7.35	response to water deprivation (GO:0009414)	0	NO
AT1G20880	RNA-binding (RRM/RBD/RNP motifs) family protein		7.10	biological_process_unknown (GO:0008150)	0	NO
AT1G78260	RNA-binding (RRM/RBD/RNP motifs) family protein		7.07	plant epidermis development (GO:0090558)	0	NO
AT5G18150	Methyltransferase-related protein		7.00	regulation of defense response (GO:0031347)	0	NO
AT3G13060	EVOLUTIONARILY CONSERVED C-TERMINAL REGION 5	ECT5	6.96	mRNA destabilization (GO:0061157)	0	NO
AT4G03110	RNA-BINDING PROTEIN-DEFENSE RELATED 1	RBP-DR1	6.78	plant-type hypersensitive response (GO:0009626)	0	NO
AT3G07660	flocculation protein (DUF1296)		6.37	biological_process_unknown (GO:0008150)	0	NO
AT5G56670	Ribosomal protein S30 family protein	RPS30C	5.57	translation (GO:0006412)	0	NO
AT4G36960	RNA-binding (RRM/RBD/RNP motifs) family protein		5.46	organic cyclic compound catabolic process (GO:1901361)	0	NO
AT3G13222	GBF-INTERACTING PROTEIN 1	GIP1	5.31	positive regulation of DNA binding (GO:0043388)	0	NO
AT3G13460	EVOLUTIONARILY CONSERVED C-TERMINAL REGION 2	ECT2	5.27	mRNA destabilization (GO:0061157)	0	NO
AT1G29350	RNA polymerase II degradation factor-like protein (DUF1296)		5.11	regulation of nitrogen compound metabolic process (GO:0051171)	0	NO
AT2G38540	LIPID TRANSFER PROTEIN 1	ATLTP1	5.09	lipid transport (GO:0006869)	0	YES
AT4G22670	HSP70-INTERACTING PROTEIN 1	HIP1	4.98	chaperone cofactor-dependent protein refolding (GO:0051085)	0	NO
AT2G46780	RNA-binding (RRM/RBD/RNP motifs) family protein		4.93	plant epidermis development (GO:0090558)	0	NO

The L/H value is the ratio of the abundance in ES2-treated samples divided by the abundance in mock-treated samples. The number of TM helices and presence of signal peptide were predicted by the DeepTMHMM package.

10.3389/fpls.2023.1171957

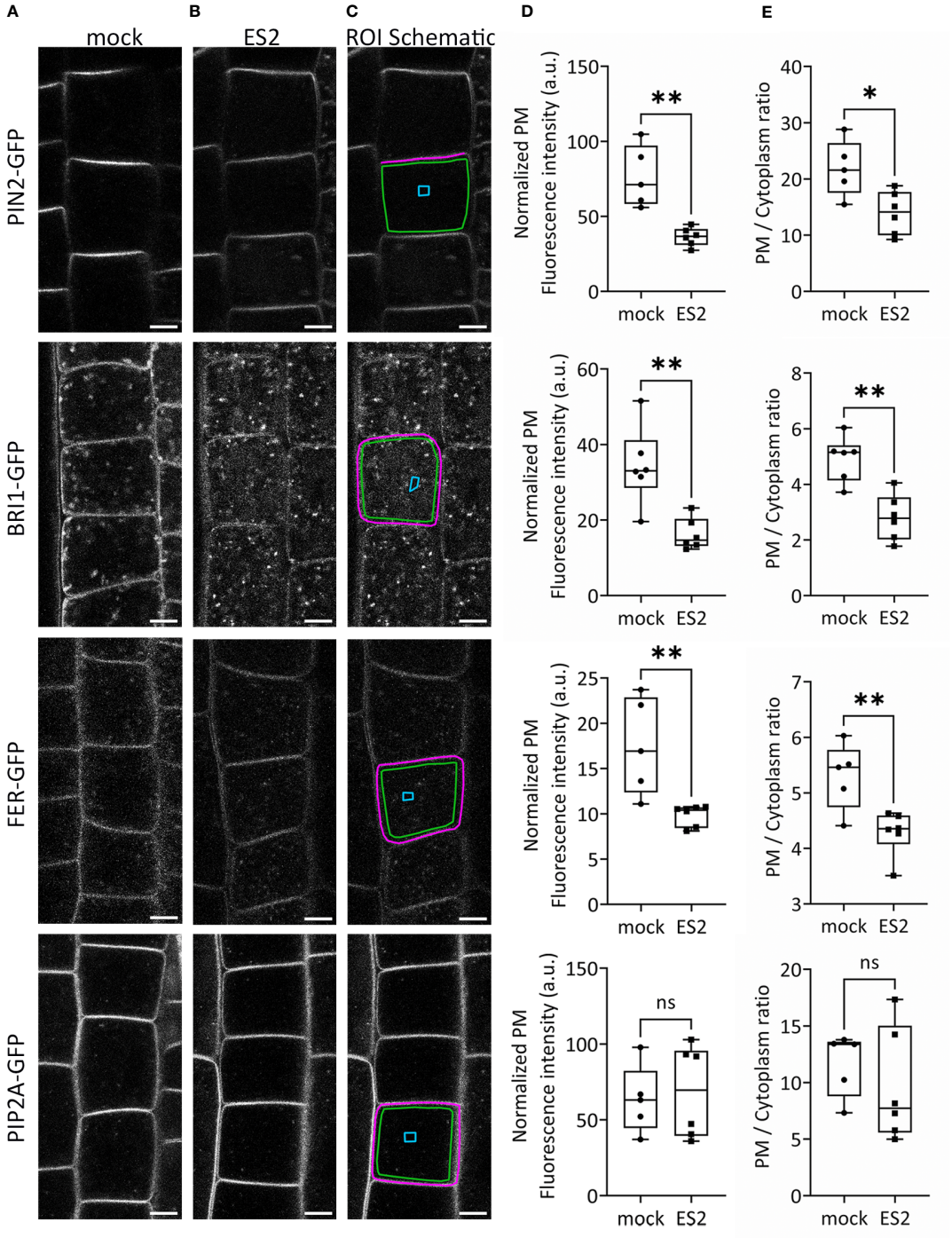

FIGURE 2
The abundance of several proteins at the plasma membrane is reduced following ES2 treatment. **(A, B)** Representative confocal microscope images of root epidermal cells from 6-d-old transgenic seedlings expressing PIN2-GFP, BRI1-GFP, FER-GFP or PIP2A-GFP following a 2-h mock treatment **(A)** or a 40 μM ES2 treatment **(B)**. **(C)** Schematic illustration of the region of interest (ROI) selection. The plasma membrane (PM) ROI is indicated by a magenta line; cytoplasmic background in the compartment-free subregion is indicated by a blue box (used as the background for normalization); the entire cytoplasmic region is indicated by a green box. Scale bar = 5 μm for all images. **(D)** Quantification of the normalized average PM fluorescence intensity from images similar to those shown in **(A**, **B)** The average PM fluorescence intensity was normalized by subtracting the mean fluorescence intensity of the cytoplasmic background. **(E)** Quantification of the average PM/cytoplasm fluorescence intensity ratio. The PM/cytoplasm mean fluorescence intensity ratio was calculated by first subtracting the mean fluorescence intensity of the region outside of the root as the imaging background, and then dividing the PM mean fluorescence intensity by the entire cytoplasm mean fluorescence intensity. (N = 21–75 cells from 5–7 seedlings). Statistical analysis was performed with an unpaired two-tailed Student's *t*-test, * denotes P value < 0.05, ** denotes P value < 0.01, ns denotes not significant. In the box plot, whiskers indicate the maximum and minimum values of the dataset, whereas individual data points represent the average value from each seedling.

membrane abundance and plasma membrane / cytoplasm intensity ratio of PIP2A-GFP were not altered by ES2 treatment (Figures 2D, E).

Gene Ontology enrichment analysis of candidate cargos for ES2-targeted trafficking

To better understand the biological functions of the candidate cargo proteins for ES2-targeted trafficking, we performed Gene Ontology (GO) enrichment analysis of the biological processes category on the 145 proteins with reduced abundance at the plasma membrane using the PANTHER classification system (Mi et al., 2013; Mi et al., 2017). We found that 49 proteins could be classified into protein families that were enriched in abundance on our list when compared to their abundance in the reference list of *Arabidopsis thaliana* genome (Figure 3). The fold enrichment for different biological processes ranged from 3.7 to 200. The 49 candidate exocytosis cargo proteins belong to gene families that function in plant cell growth, cell wall biosynthesis, hormone signaling, response to stresses and membrane transport (Figure 3; Supplementary Table S2). The proteins for the regulation of DNA-templated transcription (GO:0006355), nucleic acid metabolic process (GO:0090304) and gene expression (GO:0010467) were much lower than the numbers that were expected from the Arabidopsis genome (Figure 3), indicating the trafficking of these proteins was not mediated by the exocyst complex.

We further examined the annotated functions of proteins with significantly reduced abundance in ES2-treated samples. We found the abundance of three primary cell wall cellulose synthases (CESA1, CESA3, and CESA6), CELLULOSE SYNTHASE-INTERACTIVE PROTEIN 1 (CSI1), and KORRIGAN (KOR) was significantly reduced in ES2-treated samples (Supplementary Table S2). Proteins involved in lignin metabolism were also reduced, as were multiple proteins involved in brassinosteroid and auxin signaling. The abundance of some proteins that respond to cold and phosphate deficiency was significantly reduced in ES2-treated samples. Another group of proteins that was affected by ES2 treatment are transporters responsible for the movement of phosphate, sulphate, potassium, and oligopeptides across the plasma membrane. The abundance of two annexins involved in phloem sucrose unloading (Wang et al., 2018) was also significantly reduced (Supplementary Table S2).

In addition to the proteins mentioned above, there are other proteins with reduced abundance at the plasma membrane, but they were not enriched in functional groups in the GO enrichment analysis. These include multiple receptor-like protein kinases, transporters, enzymes for carbohydrate metabolism and protein glycosylation, as well as proteins with uncharacterized functions. Although these proteins were not enriched in our list, they may have diverse functions and cellular localization patterns among different members of the family. Collectively, our GO term enrichment analysis indicates that the exocyst complex mediates constitutive transport of numerous proteins that function in cell growth, cell wall biosynthesis, hormone signaling, stress response, and membrane transport.

Bioinformatic analysis of potential cargo proteins for plant exocyst complex

Plants use both conventional and unconventional trafficking pathways to deliver proteins to the plasma membrane and extracellular space (Drakakaki and Dandekar, 2013; Ding et al., 2014; Robinson et al., 2016; Aniento et al., 2022). In the conserved conventional trafficking pathway, proteins with a signal peptide are inserted into the endoplasmic reticulum during translation and are then transported to Golgi through vesicles and further secreted through post-Golgi vesicles (Novick et al., 1981; Rothman, 2002; Schekman, 2010). However, increasing evidence from proteomic

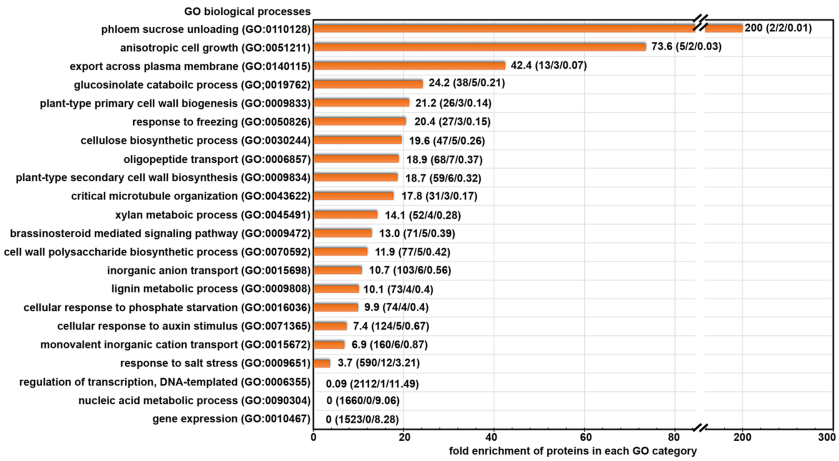

FIGURE 3
Gene Ontology terms of biological processes category that are enriched in our protein list with significantly reduced abundance after ES2 treatment. Numbers on each row represent: fold enrichment (total number of proteins in the category/number of proteins identified in the reduced protein list/number of proteins expected in reduced protein list). Fold enrichment represents the ratio of the number of proteins identified divided by the number of proteins expected in the list.

analysis shows that many proteins that are secreted out of the cell or targeted to the plasma membrane do not have signal peptides, indicating the existence of unconventional trafficking pathways for these proteins (Oh et al., 2005; Soares et al., 2007; Wen et al., 2007; Han et al., 2010; Chen et al., 2016). Plant exocyst complex has been shown to regulate cargo proteins through both conventional and unconventional pathways (Wang et al., 2010; Drdová et al., 2013; Lin et al., 2015; Mayers et al., 2017).

To test whether the candidate cargo proteins contain signal peptides that allow them to traffic through the conventional pathway, we analyzed the presence of signal peptides in proteins that had reduced abundance in ES2-treated samples using the DeepTMHMM package, a deep-learning method for signal peptide and transmembrane domain prediction (Hallgren et al., 2022). DeepTMHMM predicted that 36 of the 145 proteins with reduced abundance contained signal peptides (Supplementary Table S5). The existence of a signal peptide in a small percentage of proteins indicates that consistent with previous findings, plant exocyst complex mediates the transport of proteins in both conventional and unconventional trafficking pathways. To understand how these candidate cargo proteins are associated to the plasma membrane, we analyzed the presence of potential transmembrane domains in these 145 proteins using the DeepTMHMM package. We found 64 of the 145 proteins were predicted to have at least one transmembrane domain (Supplementary Table S5).

The behavior of the exocyst complex and its regulators is different than candidate cargo proteins

All eight subunits of the exocyst complex were detected in the enriched plasma membrane fractions (Supplementary Table S1). However, we did not find a statistically significant reduction in their abundance in ES2-treated samples (Supplementary Table S1). Among the eight exocyst subunits, only SEC3 showed a 13% reduction in the mean value after ES2 treatment but was not statistically different (Supplementary Table S1). STOMATAL CYTOKINESIS-DEFECTIVE 1 (SCD1), a component of the candidate activator of plant RabE GTPase that regulates the exocyst complex (Mayers et al., 2017), was detected in plasma membrane fractions but its abundance was not altered by ES2 treatment (Supplementary Table S1). We identified 12 Syntaxins of Plants (SYP), SYP111, SYP121, SYP122, SYP132, SYP21, SYP22, SYP32, SYP43, SYP51, SYP52, SYP61, and SYP71, but none of these were statistically significantly reduced (Supplementary Table S1). In summary, our proteomics results indicate that the abundance of candidate tSNARE proteins, together with the exocyst complex and the SCD complex, were not significantly affected by a 2-h, 40 μM ES2 treatment.

Confocal imaging of GFP-EXO70A1 following ES2 treatment

To investigate whether ES2 affects the spatial distribution or abundance at the plasma membrane of its target, EXO70A1, we performed live imaging of root epidermal cells from GFP-EXO70A1 seedlings using laser scanning confocal microscopy (Figure 4). Consistent with previous findings (Zhang et al., 2016; Larson et al., 2020; Synek et al., 2021), EXO70A1 in mock-treated epidermal cells showed a polarized distribution with highest abundance at the plasma membrane on the outer periclinal face, but was present at all six faces of the cell (Figure 4A). A 2-h, 40 μM ES2 treatment significantly reduced the abundance of EXO70A1 at the plasma membrane on the outer periclinal face (Figures 4B, D), and disrupted the polarized distribution of EXO70A1 at the outer periclinal face when fluorescence intensity was expressed as a ratio with the cytosolic region (Figure 4E) or as a ratio with the other faces of the same cell (Figure 4F). However, when EXO70A1 at the other three faces of the plasma membrane visible in medial optical sections, including the inner periclinal face and the two anticlinal faces (green line in Figure 4C), was examined, the apparent abundance expressed as a ratio with cytosol was not affected by ES2 treatment (Figure 4G). When all four faces of the plasma membrane were combined and averaged, there was a modest decrease in the abundance of EXO70A1, but this was not statistically significant (Figure 4H). In total, a 2-h ES2 treatment had greatest effect on the polarized distribution of EXO70A1 and its association with the plasma membrane at the outer periclinal face of root epidermal cells, but a rather modest reduction in overall abundance at the plasma membrane on all faces of the cell.

Gene Ontology enrichment analysis of proteins with increased abundance after ES2 treatment

Our statistical analysis identified 185 proteins with increased abundance in enriched plasma membrane fractions of ES2-treated samples (Supplementary Table S4). To better understand the function of these proteins, we performed Gene Ontology enrichment analysis of the biological function category. We found that this list of proteins is enriched in biological functions of COPII-coated vesicle cargo loading, mRNA catabolic process, negative regulation of translation, proton membrane transport, aerobic respiration, leaf senescence, ribonucleoprotein complex biogenesis, and amide biosynthesis process (Supplementary Figure S3). The functional relationship between exocyst complex and these proteins has not been well characterized. We speculate that some of these proteins might be involved in cellular responses to the inhibition of exocytosis.

Discussion

Exocyst complex mediates constitutive transport of proteins with diverse functions during plant growth and development

Using quantitative and comparative proteomics analysis, we identified 145 proteins with significantly reduced abundance at the plasma membrane of Arabidopsis roots following ES2 treatment.

10.3389/fpls.2023.1171957

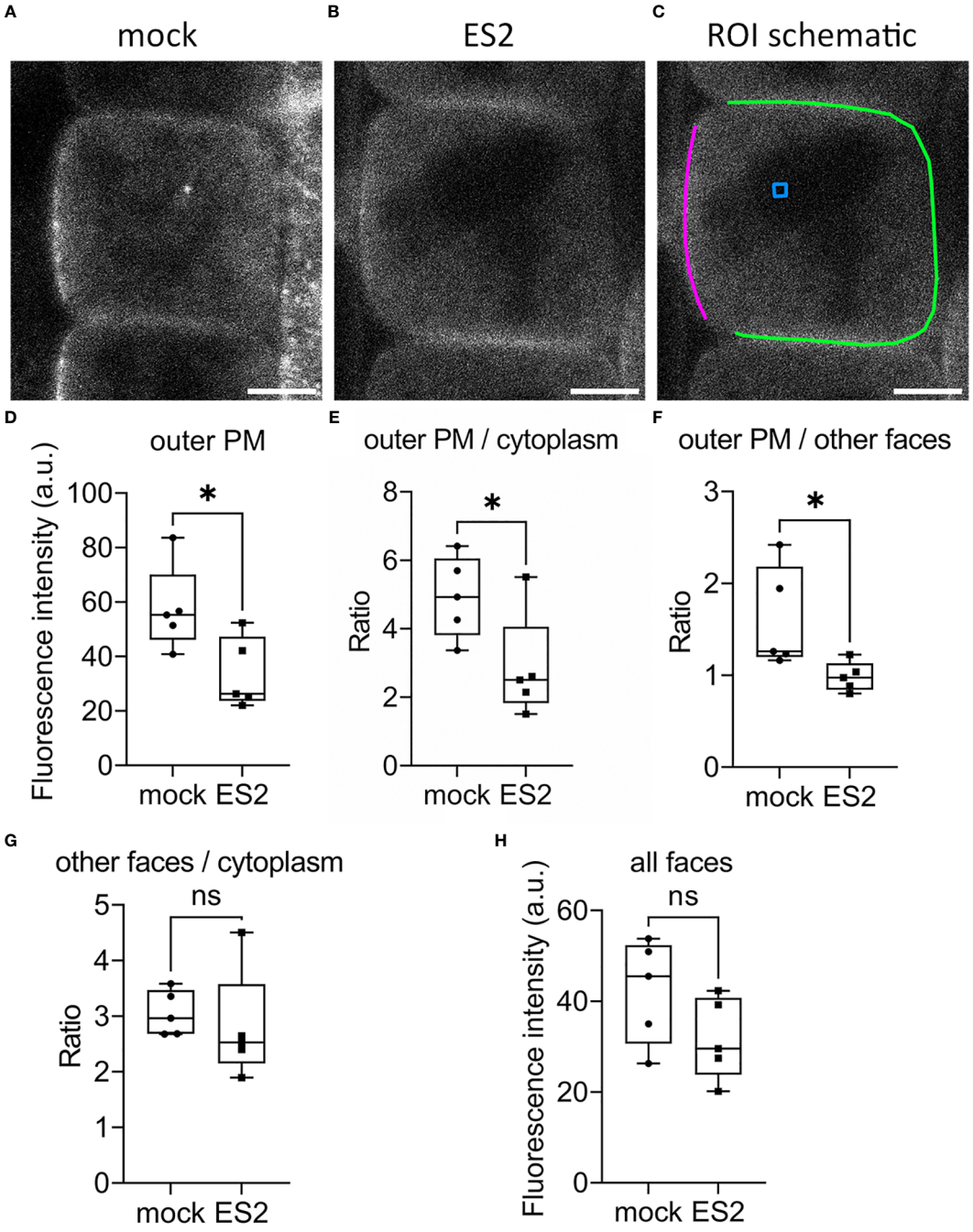

FIGURE 4
The abundance of EXO70A1 at the plasma membrane on the outer periclinal face is decreased following ES2 treatment. **(A, B)** Representative confocal microscopy images of root epidermal cells from 6-d-old transgenic seedlings expressing GFP-EXO70A1 following a 2-h mock treatment **(A)** or a 40 μM ES2 treatment **(B)**. Scale bar = 5 μm for all images. **(C)** Schematic illustration of the region of interest (ROI) selection. The plasma membrane on the outer periclinal face was marked with a magenta line, whereas the plasma membrane of the other three faces was marked with a green line. The cytoplasmic background in the vacuole or nucleus region (used for background subtraction) was indicated with a blue box. **(D)** Quantification of the average GFP-EXO70A1 fluorescence intensity at the plasma membrane on the outer periclinal face (as marked with a magenta line in **C**) from images similar to those shown in **(A, B, E)** Quantification of the ratio of fluorescence intensity of GFP-EXO70A1 at the plasma membrane on the outer periclinal face compared to the entire cytoplasmic region after normalization. **(F)** Quantification of the ratio of GFP-EXO70A1 fluorescence intensity at the plasma membrane on the outer periclinal face compared to the other three faces (marked with a green line in **C**). **(G)** Quantification of the ratio of fluorescence intensity of GFP-EXO70A1 at the plasma membrane on the other three faces compared to the entire cytoplasmic region after normalization. **(H)** Quantification of the average fluorescence intensity of GFP-EXO70A1 at the plasma membrane on all visible faces of the plasma membrane in medial views of the epidermal cell. Fluorescence intensities at the plasma membrane and entire cytoplasmic region were normalized by subtracting the cytoplasmic background as indicated with a blue box in **(C)** (N = 17–23 cells from 5 seedlings). Statistical analysis was performed with an unpaired two-tailed Student's *t*-test, * denotes P value < 0.05, ns denotes not significant. In the box plot, whiskers indicate the maximum and minimum values of the dataset, whereas individual data points represent the average value from each seedling.

Some of these proteins possess transmembrane domains and are likely integral membrane proteins delivered to the plasma membrane by secretion. The candidate proteins without a predicted transmembrane domain could be associated with the plasma membrane through lipid anchors, through interaction with other membrane proteins, or by association with polar head groups of the lipid bilayer. These candidates of exocyst-mediated trafficking perform functions in cell growth, cell wall biosynthesis, hormone signaling, stress responses, membrane transport, nutrient transport, and protein phosphorylation. The dynamics of many hormone-signaling proteins are well characterized; however, the role of exocyst complex in regulating their trafficking awaits further study. The functional diversity of proteins that are transported through the exocyst complex is consistent with the pleiotropic phenotypes observed in plants deficient for the exocyst complex (Cole et al., 2005; Synek et al., 2006; Hála et al., 2008; Fendrych et al., 2010; Kulich et al., 2010; Wang et al., 2010; Pečenková et al., 2011; Drdová et al., 2013; Zhang et al., 2013; Kulich et al., 2015; Drdová et al., 2019; Ogura et al., 2019; Synek et al., 2021; Hématy et al., 2022). Our results indicate that the plant exocyst complex plays essential roles for growth and adaptation by mediating constitutive transport of proteins with diverse functions to the plasma membrane.

Some other important plasma membrane proteins, such as Rho family small GTPases (ROPs), multidrug resistance-like ABC transporter family proteins, and aquaporin plasma membrane intrinsic proteins were not affected by ES2 treatment in this proteomics study (Supplementary Table S1), which is consistent with the previous live-cell imaging results (Zhang et al., 2016). Our current results indicate that these important plasma membrane proteins could have slow turnover rates or are not delivered to the plasma membrane through the ES2-targeted exocyst complex.

Cargo protein exocytosis and exocyst complex membrane association

Time-lapse imaging revealed that the plant exocyst complex colocalizes with its cargo protein (Cellulose Synthase Complex or CSC) during the tethering process and then separates from the cargo after successful fusion (Zhu et al., 2018; Zhang and Staiger, 2021; Zhang et al., 2021). In our proteomics study, we detected a significant reduction in the abundance of cargo proteins, such as cellulose synthases, but did not detect a statistically significant reduction in the abundance of the exocyst complex subunits. The abundance of SCD complex components and candidate tSNAREs on the plasma membrane was also not affected by ES2 treatment. Previous live-cell imaging data reveal that exocyst subunits are polarized to the outer periclinal face of root epidermal cells (Zhang et al., 2016; Larson et al., 2020; Synek et al., 2021) and are disrupted by ES2 treatment (Zhang et al., 2016) or genetic disruption of EXO70A1 (Synek et al., 2021), but not by genetic disruption of some SNARE proteins that physically interact with the exocyst complex (Larson et al., 2020). The plasma membrane enrichment reflects the overall abundance of each plasma membrane protein, but not their polarized distribution on a specific face of the plasma membrane. Results from live-cell imaging and our proteomics analyses indicated that ES2 treatment affected the polarized distribution of the exocyst complex in root epidermal cells but did not markedly affect its association with the plasma membrane. The lifetime of exocyst foci on the plasma membrane of root epidermal cells is around 10 s; however, inhibition of exocytosis by a 2-h Brefeldin A (BFA) treatment did not affect membrane localization of the exocyst complex (Fendrych et al., 2013). Thus, exocyst complex association with the plasma membrane may not depend on the other components of the exocytosis machinery.

Previous studies demonstrate that exocyst subunits physically interact and associate with the SCD1/2 complex (Mayers et al., 2017), and EXO70 physically interacts with several SNAREs (Larson et al., 2020). Although ES2 disrupts the polarized localization of EXO70A1, our current data do not directly reflect whether ES2 disrupts the physical interaction of exocyst subunits with SCD1/2 complex or SNARE proteins, and/or affects the localization pattern of SCD1/2 and SNAREs. One future direction would be to quantify the localization of fluorescent-tagged SCD1/2 and SNAREs following ES2 treatment. Further, it would be interesting to quantify the association of exocyst subunits with other components of the exocytosis machinery through high spatial-temporal resolution live-cell imaging of double marker lines.

Future directions in understanding plant plasma membrane protein dynamics

Due to the importance of plant plasma membrane proteins, multiple comparative proteomic studies have been conducted to investigate the profiles of plasma membrane proteins in response to environmental stresses and cell growth status. The composition of plasma membrane proteins changes upon salt stress, cold treatment, osmotic stress, immune signaling, nutrient deficiency and different growth stages of cultured cells (Nohzadeh Malakshah et al., 2007; Nouri and Komatsu, 2010; Elmore et al., 2012; Li et al., 2012; Cao et al., 2016; Chen et al., 2016; Li et al., 2018). These proteomic studies show that the plasma membrane serves as a hub for cells to respond to environmental and growth cues. These studies further indicate that the vesicle trafficking machinery that facilitates the transport of these proteins is essential for plants to respond to biotic and abiotic stresses. Previous findings on the essential functions of plant exocyst complex in plant growth and immune responses (Synek et al., 2006; Fendrych et al., 2010; Kulich et al., 2010; Kulich et al., 2015; Cole et al., 2018; Du et al., 2018; Guo et al., 2018; Žárský, 2022) support the hypothesis that the exocyst complex choreographs the dynamic change of specific proteins at the plasma membrane in response to different environmental stimuli and growth cues.

In comparison with yeast and mammalian cells, we understand less about the mechanisms of plasma membrane protein delivery and turnover in plants. In this study, using very stringent filtering and cutoff, we found 145 proteins that have significantly (at 10% FDR) reduced abundance at the plasma membrane after a 2-h, 40 μM ES2 treatment, a condition that inhibits but does not completely arrest exocytosis and plant growth. We found that the abundance of

some plant plasma membrane proteins was reduced by more than 50%, indicating that the half-time of turnover of these proteins is less than 2 h. We speculate that these proteins undergo fast delivery to the plasma membrane mediated by the exocyst complex and have a rapid turnover at the plasma membrane. There are other proteins that have lower abundance in ES2-treated samples but did not pass the statistical test. We believe these proteins have slower delivery and/or turnover rates at the plasma membrane. It is not well understood how plants control precise delivery of cargo proteins with different dynamics.

Conclusion

Using a 2-h treatment with the exocyst subunit EXO70A1 inhibitor ES2 in combination with plasma membrane enrichment, quantitative proteomic analyses, and live-cell imaging, we identified subsets of plasma membrane proteins that require the ES2-targeted exocyst complex for constitutive trafficking to the plasma membrane in Arabidopsis root cells. Our dataset provides new insights for the identification of novel cargo proteins of the exocyst complex.

Data availability statement

The datasets presented in this study can be found in online repositories. The names of the repository/repositories and accession number(s) can be found below: ProteomeXchange Consortium via the PRIDE database, with the identifier of PXD037455.

Author contributions

CZ and XL: conceptualization. XL, PZ, Y-JC, LH, and DW: investigation. XL and DN: formal analysis. XL, PZ, C-CH, GL, WAT, and CZ: methodology. CZ and WAT: resources. XL and CZ: data curation, visualization, and validation. CZ, XL, and CJS: writing - original draft. PZ, Y-JC, DN, LH, DW, C-CH, GL, and WAT: writing - review & editing. CZ, GL, WAT, and CJS: supervision. CZ and XL: funding acquisition. CJS: agrees to serve as the author responsible for contact and ensures communication. All authors contributed to the article and approved the submitted version.

Funding

GL gratefully acknowledges the support from National Science Foundation (DMS-1555072, DMS-1736364 and DMS-1821233). XL, LH, DW, and CZ were supported by Start-up funds from the Office of the Provost at Purdue University. XL was also partially supported by a research assistantship from the Purdue Center for Plant Biology.

Acknowledgments

We dedicate this work to the memory of CZ, who initiated and conceived the project, and unfortunately passed away on May 15, 2021. CZ was a brilliant scientist with a sharp mind, a dear friend to all, a supportive mentor, and a valued colleague. We thank Dr. Glenn R. Hicks (University of California Riverside and Swedish University of Agricultural Sciences) for critical comments and editing of the manuscript, and Dr. Sharon Kessler (Purdue University) for providing the FER-GFP marker line.

Conflict of interest

The authors declare that the research was conducted in the absence of any commercial or financial relationships that could be construed as a potential conflict of interest.

Publisher's note

Supplementary material

The Supplementary Material for this article can be found online at: https://www.frontiersin.org/articles/10.3389/fpls.2023.1171957/full#supplementary-material

References

Aniento, F., Sánchez de Medina Hernández, V., Dagdas, Y., Rojas-Pierce, M., and Russinova, E. (2022). Molecular mechanisms of endomembrane trafficking in plants. *Plant Cell* 34, 146–173. doi: 10.1093/plcell/koab235

Bar-Peled, M., and Raikhel, N. V. (1997). Characterization of AtSEC12 and AtSAR1 (proteins likely involved in endoplasmic reticulum and golgi transport). *Plant Physiol.* 114, 315–324. doi: 10.1104/pp.114.1.315

Bashline, L., Li, S., Anderson, C. T., Lei, L., and Gu, Y. (2013). The endocytosis of cellulose synthase in arabidopsis is dependent on μ2, a clathrin-mediated endocytosis adaptin. *Plant Physiol.* 163, 150–160. doi: 10.1104/pp.113.221234

Bassham, D. C., Sanderfoot, A. A., Kovaleva, V., Zheng, H., and Raikhel, N. V. (2000). AtVPS45 complex formation at the trans-golgi network. *Mol. Biol. Cell* 11, 2251–2265. doi: 10.1091/mbc.11.7.2251

Boersema, P. J., Raijmakers, R., Lemeer, S., Mohammed, S., and Heck, A. J. R. (2009). Multiplex peptide stable isotope dimethyl labeling for quantitative proteomics. *Nat. Protoc.* 4, 484–494. doi: 10.1038/nprot.2009.21

Cao, J., Yang, C., Li, L., Jiang, L., Wu, Y., Wu, C., et al. (2016). Rice plasma membrane proteomics reveals *Magnaporthe oryzae* promotes susceptibility by sequential activation of host hormone signaling pathways. *Mol. Plant-Microbe Interact.* 29, 902–913. doi: 10.1094/MPMI-08-16-0165-R

Chen, S., Luo, Y., Ding, G., and Xu, F. (2016). Comparative analysis of *Brassica napus* plasma membrane proteins under phosphorus deficiency using label-free and MaxQuant-based proteomics approaches. *J. Proteomics* 133, 144–152. doi: 10.1016/j.jprot.2015.12.020

Chen, J., Wang, Y., Wang, F., Yang, J., Gao, M., Li, C., et al. (2015). The rice CK2 kinase regulates trafficking of phosphate transporters in response to phosphate levels. *Plant Cell* 27, 711–723. doi: 10.1105/tpc.114.135335

Chu, F. F., and Doyle, D. (1985). Turnover of plasma membrane proteins in rat hepatoma cells and primary cultures of rat hepatocytes. *J. Biol. Chem.* 260, 3097–3107. doi: 10.1016/S0021-9258(18)89478-9

Cole, R. A., Peremyslov, V. V., Van Why, S., Moussaoui, I., Ketter, A., Cool, R., et al. (2018). A broadly conserved NERD genetically interacts with the exocyst to affect root growth and cell expansion. *J. Exp. Bot.* 69, 3625–3637. doi: 10.1093/jxb/ery162

Cole, R. A., Synek, L., Zarsky, V., and Fowler, J. E. (2005). SEC8, a subunit of the putative arabidopsis exocyst complex, facilitates pollen germination and competitive pollen tube growth. *Plant Physiol.* 138, 2005–2018. doi: 10.1104/pp.105.062273

Collins, C. A., Leslie, M. E., Peck, S. C., and Heese, A. (2017). "Simplified enrichment of plasma membrane proteins from arabidopsis thaliana seedlings using differential centrifugation and brij-58 treatment," in *Methods in molecular biology. brassinosteroids: methods and protocols*. Eds. E. Russinova and A. I. Caño-Delgado (New York, NY: Springer), 155–168.

Cutler, S. R., Ehrhardt, D. W., Griffitts, J. S., and Somerville, C. R. (2000). Random GFP::cDNA fusions enable visualization of subcellular structures in cells of *Arabidopsis* at a high frequency. *Proc. Natl. Acad. Sci.* 97, 3718–3723. doi: 10.1073/pnas.97.7.3718

Denecke, J., Aniento, F., Frigerio, L., Hawes, C., Hwang, I., Mathur, J., et al. (2012). Secretory pathway research: the more experimental systems the better. *Plant Cell* 24, 1316–1326. doi: 10.1105/tpc.112.096362

Dimayacyac-Esleta, B. R. T., Tsai, C.-F., Kitata, R. B., Lin, P.-Y., Choong, W.-K., Lin, T.-D., et al. (2015). Rapid high-pH reverse phase StageTip for sensitive small-scale membrane proteomic profiling. *Anal. Chem.* 87, 12016–12023. doi: 10.1021/acs.analchem.5b03639

Ding, Y., Robinson, D. G., and Jiang, L. (2014). Unconventional protein secretion (UPS) pathways in plants. *Curr. Opin. Cell Biol.* 29, 107–115. doi: 10.1016/j.ceb.2014.05.008

Doyle, D., and Baumann, H. (1979). Turnover of the plasma membrane of mammalian cells. *Life Sci.* 24, 951–966. doi: 10.1016/0024-3205(79)90313-8

Drakakaki, G., and Dandekar, A. (2013). Protein secretion: how many secretory routes does a plant cell have? *Plant Sci.* 203–204, 74–78. doi: 10.1016/j.plantsci.2012.12.017

Drdová, E. J., Klejchová, M., Janko, K., Hála, M., Soukupová, H., Cvrčková, F., et al. (2019). Developmental plasticity of arabidopsis hypocotyl is dependent on exocyst complex function. *J. Exp. Bot.* 70, 1255–1265. doi: 10.1093/jxb/erz005

Drdová, E. J., Synek, L., Pečenková, T., Hála, M., Kulich, I., Fowler, J. E., et al. (2013). The exocyst complex contributes to PIN auxin efflux carrier recycling and polar auxin transport in arabidopsis. *Plant J.* 73, 709–719. doi: 10.1111/tpj.12074

Du, Y., Overdijk, E. J. R., Berg, J. A., Govers, F., and Bouwmeester, K. (2018). Solanaceous exocyst subunits are involved in immunity to diverse plant pathogens. *J. Exp. Bot.* 69, 655–666. doi: 10.1093/jxb/erx442

Ebine, K., Fujimoto, M., Okatani, Y., Nishiyama, T., Goh, T., Ito, E., et al. (2011). A membrane trafficking pathway regulated by the plant-specific RAB GTPase ARA6. *Nat. Cell Biol.* 13, 853–859. doi: 10.1038/ncb2270

Elias, M., Drdova, E., Ziak, D., Bavlnka, B., Hala, M., Cvrckova, F., et al. (2003). The exocyst complex in plants. *Cell Biol. Int.* 27, 199–201. doi: 10.1016/S1065-6995(02)00349-9

Elmore, J. M., Liu, J., Smith, B., Phinney, B., and Coaker, G. (2012). Quantitative proteomics reveals dynamic changes in the plasma membrane during *Arabidopsis* immune signaling. *Mol. Cell. Proteomics* 11, M111.014555. doi: 10.1074/mcp.M111.014555

Escobar-Restrepo, J.-M., Huck, N., Kessler, S., Gagliardini, V., Gheyselinck, J., Yang, W.-C., et al. (2007). The FERONIA receptor-like kinase mediates male-female interactions during pollen tube reception. *Science* 317, 656–660. doi: 10.1126/science.1143562

Fendrych, M., Synek, L., Pečenková, T., Drdová, E. J., Sekereš, J., de Rycke, R., et al. (2013). Visualization of the exocyst complex dynamics at the plasma membrane of arabidopsis thaliana. *Mol. Biol. Cell* 24, 510–520. doi: 10.1091/mbc.e12-06-0492

Fendrych, M., Synek, L., Pečenková, T., Toupalová, H., Cole, R., Drdová, E., et al. (2010). The arabidopsis exocyst complex is involved in cytokinesis and cell plate maturation. *Plant Cell* 22, 3053–3065. doi: 10.1105/tpc.110.074351

Friml, J. (2010). Subcellular trafficking of PIN auxin efflux carriers in auxin transport. *Eur. J. Cell Biol.* 89, 231–235. doi: 10.1016/j.ejcb.2009.11.003

Gómez-Escudero, J., Moreno, V., Martín-Alonso, M., et al. (2017). E-cadherin cleavage by MT2-MMP regulates apical junctional signaling and epithelial homeostasis in the intestine. *J. Cell Sci.* 130, 4013–4027. doi: 10.1242/jcs.203687

Guo, J., Xu, C., Wu, D., Zhao, Y., Qiu, Y., Wang, X., et al. (2018). Bph6 encodes an exocyst-localized protein and confers broad resistance to planthoppers in rice. *Nat. Genet.* 50, 297–306. doi: 10.1038/s41588-018-0039-6

Hála, M., Cole, R., Synek, L., Drdová, E., Pečenková, T., Nordheim, A., et al. (2008). An exocyst complex functions in plant cell growth in *Arabidopsis* and tobacco. *Plant Cell* 20, 1330–1345. doi: 10.1105/tpc.108.059105

Hallgren, J., Tsirigos, K. D., Pedersen, M. D., Almagro Armenteros, J. J., Marcatili, P., Nielsen, H., et al. (2022). DeepTMHMM predicts alpha and beta transmembrane proteins using deep neural networks. *Bioinformatics*. 2022.04.08.487609. doi: 10.1101/2022.04.08.487609

Han, B., Chen, S., Dai, S., Yang, N., and Wang, T. (2010). Isobaric tags for relative and absolute quantification-based comparative proteomics reveals the features of plasma membrane-associated proteomes of pollen grains and pollen tubes from *Lilium davidii*. *J. Integr. Plant Biol.* 52, 1043–1058. doi: 10.1111/j.1744-7909.2010.00996.x

Hématy, K., De Bellis, D., Wang, X., Mähönen, A. P., and Geldner, N. (2022). Analysis of exocyst function in endodermis reveals its widespread contribution and specificity of action. *Plant Physiol.* 189, 557–566. doi: 10.1093/plphys/kiac019

Hsu, C.-C., Zhu, Y., Arrington, J. V., Paez, J. S., Wang, P., Zhu, P., et al. (2018). Universal plant phosphoproteomics workflow and its application to tomato signaling in response to cold stress. *Mol. Cell. Proteomics* 17, 2068–2080. doi: 10.1074/mcp.TIR118.000702

Huang, L., Li, X., Li, Y., Yin, X., Li, Y., Wu, B., et al. (2019). Endosidin2-14 targets the exocyst complex in plants and fungal pathogens to inhibit exocytosis. *Plant Physiol.* 180, 1756–1770. doi: 10.1104/pp.18.01457

Irani, N. G., Di Rubbo, S., Mylle, E., Van den Begin, J., Schneider-Pizoń, J., Hniliková, J., et al. (2012). Fluorescent castasterone reveals BRI1 signaling from the plasma membrane. *Nat. Chem. Biol.* 8, 583–589. doi: 10.1038/nchembio.958

Kajiura, H., Koiwa, H., Nakazawa, Y., Okazawa, A., Kobayashi, A., Seki, T., et al. (2010). Two Arabidopsis thaliana Golgi α-mannosidase I enzymes are responsible for plant N-glycan maturation. *Glycobiology* 20, 235–247. doi: 10.1093/glycob/cwp170

Kleine-Vehn, J., Wabnik, K., Martinière, A., Łangowski, Ł., Willig, K., Naramoto, S., et al. (2011). Recycling, clustering, and endocytosis jointly maintain PIN auxin carrier polarity at the plasma membrane. *Mol. Syst. Biol.* 7, 540. doi: 10.1038/msb.2011.72

Kulich, I., Cole, R., Drdová, E., Cvrčková, F., Soukup, A., Fowler, J., et al. (2010). Arabidopsis exocyst subunits SEC8 and EXO70A1 and exocyst interactor ROH1 are involved in the localized deposition of seed coat pectin. *New Phytol.* 188, 615–625. doi: 10.1111/j.1469-8137.2010.03372.x

Kulich, I., Pečenková, T., Sekereš, J., Smetana, O., Fendrych, M., Foissner, I., et al. (2013). Arabidopsis exocyst subcomplex containing subunit EXO70B1 is involved in autophagy-related transport to the vacuole. *Traffic* 14, 1155–1165. doi: 10.1111/tra.12101

Kulich, I., Vojtíková, Z., Glanc, M., Ortmannová, J., Rasmann, S., and Žárský, V. (2015). Cell wall maturation of arabidopsis trichomes is dependent on exocyst subunit EXO70H4 and involves callose deposition. *Plant Physiol.* 168, 120–131. doi: 10.1104/pp.15.00112

Larson, E. R., Ortmannová, J., Donald, N. A., Alvim, J., Blatt, M. R., and Žárský, V. (2020). Synergy among exocyst and SNARE interactions identifies a functional hierarchy in secretion during vegetative growth. *Plant Cell* 32, 2951–2963. doi: 10.1105/tpc.20.00280

Lešková, A., Labajová, M., Krausko, M., Zahradníková, A., Baluška, F., Mičieta, K., et al. (2020). Endosidin 2 accelerates PIN2 endocytosis and disturbs intracellular trafficking of PIN2, PIN3, and PIN4 but not of SYT1 (DC bassham, ed.). *PloS One* 15, e0237448. doi: 10.1371/journal.pone.0237448

Li, B., Takahashi, D., Kawamura, Y., and Uemura, M. (2012). Comparison of plasma membrane proteomic changes of arabidopsis suspension-cultured cells (T87 line) after cold and ABA treatment in association with freezing tolerance development. *Plant Cell Physiol.* 53, 543–554. doi: 10.1093/pcp/pcs010

Li, B., Takahashi, D., Kawamura, Y., and Uemura, M. (2018). "Plasma membrane proteomics of arabidopsis suspension-cultured cells associated with growth phase using nano-LC-MS/MS," in *Methods in molecular biology. plant membrane proteomics: methods and protocols*. Eds. H.-P. Mock, A. Matros and K. Witzel (New York, NY: Springer), 185–194.

Li, J., Wen, J., Lease, K. A., Doke, J. T., Tax, F. E., and Walker, J. C. (2002). BAK1, an *Arabidopsis* LRR receptor-like protein kinase, interacts with BRI1 and modulates brassinosteroid signaling. *Cell* 110, 213–222. doi: 10.1016/S0092-8674(02)00812-7

Lin, Y., Ding, Y., Wang, J., Shen, J., Kung, C. H., Zhuang, X., et al. (2015). Exocyst-positive organelles and autophagosomes are distinct organelles in plants. *Plant Physiol.* 169, 1917–1932. doi: 10.1104/pp.15.00953

Mayers, J. R., Hu, T., Wang, C., Cárdenas, J. J., Tan, Y., Pan, J., et al. (2017). SCD1 and SCD2 form a complex that functions with the exocyst and RabE1 in exocytosis and cytokinesis. *Plant Cell* 29, 2610–2625. doi: 10.1105/tpc.17.00409

Mi, H., Huang, X., Muruganujan, A., Tang, H., Mills, C., Kang, D., et al. (2017). PANTHER version 11: expanded annotation data from gene ontology and reactome pathways, and data analysis tool enhancements. *Nucleic Acids Res.* 45, D183–D189. doi: 10.1093/nar/gkw1138

Mi, H., Muruganujan, A., Casagrande, J. T., and Thomas, P. D. (2013). Large-Scale gene function analysis with the PANTHER classification system. *Nat. Protoc.* 8, 1551–1566. doi: 10.1038/nprot.2013.092

Nelson, C. J., Hegeman, A. D., Harms, A. C., and Sussman, M. R. (2006). A quantitative analysis of *Arabidopsis* plasma membrane using trypsin-catalyzed ^{18}O labeling. *Mol. Cell. Proteomics* 5, 1382–1395. doi: 10.1074/mcp.M500414-MCP200

Nie, L., Feng, J., Fan, P., Chen, X., Guo, J., Lv, S., et al. (2015). Comparative proteomics of root plasma membrane proteins reveals the involvement of calcium

signalling in NaCl-facilitated nitrate uptake in *Salicornia europaea*. *J. Exp. Bot.* 66, 4497–4510. doi: 10.1093/jxb/erv216

Nohzadeh Malakshah, S., Habibi Rezaei, M., Heidari, M., and Hosseini Salekdeh, G. (2007). Proteomics reveals new salt responsive proteins associated with rice plasma membrane. *Biosci. Biotechnol. Biochem.* 71, 2144–2154. doi: 10.1271/bbb.70027

Nouri, M.-Z., and Komatsu, S. (2010). Comparative analysis of soybean plasma membrane proteins under osmotic stress using gel-based and LC MS/MS-based proteomics approaches. *Proteomics* 10, 1930–1945. doi: 10.1002/pmic.200900632

Novick, P., Ferro, S., and Schekman, R. (1981). Order of events in the yeast secretory pathway. *Cell* 25, 461–469. doi: 10.1016/0092-8674(81)90064-7

Oda, Y., and Fukuda, H. (2011). Dynamics of arabidopsis SUN proteins during mitosis and their involvement in nuclear shaping: dynamics and functions of arabidopsis SUN proteins. *Plant J.* 66, 629–641. doi: 10.1111/j.1365-313X.2011.04523.x

Ogura, T., Goeschl, C., Filiault, D., Mirea, M., Slovak, R., Wolhrab, B., et al. (2019). Root system depth in arabidopsis is shaped by *EXOCYST70A3* via the dynamic modulation of auxin transport. *Cell* 178, 400–412.e16. doi: 10.1016/j.cell.2019.06.021

Oh, I. S., Park, A. R., Bae, M. S., Kwon, S. J., Kim, Y. S., Lee, J. E., et al. (2005). Secretome analysis reveals an *Arabidopsis* lipase involved in defense against *Alternaria brassicicola*. *Plant Cell* 17, 2832–2847. doi: 10.1105/tpc.105.034819

Ortega, M. A., Villiger, R. K., Harrison-Chau, M., Lieu, S., Tamashiro, K.-K., Lee, A. J., et al. (2022). Exocyst inactivation in urothelial cells disrupts autophagy and activates non-canonical NF-κB signaling. *Dis. Models Mech.* 15, dmm049785. doi: 10.1242/dmm.049785

Pečenková, T., Hála, M., Kulich, I., Kocourková, D., Drdová, E., Fendrych, M., et al. (2011). The role for the exocyst complex subunits Exo70B2 and Exo70H1 in the plant–pathogen interaction. *J. Exp. Bot.* 62, 2107–2116. doi: 10.1093/jxb/erq402

Prigent, M., Dubois, T., Raposo, G., Derrien, V., Tenza, D., Rossé, C., et al. (2003). ARF6 controls post-endocytic recycling through its downstream exocyst complex effector. *J. Cell Biol.* 163, 1111–1121. doi: 10.1083/jcb.200305029

Robinson, D. G., Ding, Y., and Jiang, L. (2016). Unconventional protein secretion in plants: a critical assessment. *Protoplasma* 253, 31–43. doi: 10.1007/s00709-015-0887-1

Rothman, J. E. (2002). The machinery and principles of vesicle transport in the cell. *Nat. Med.* 8, 1059–1062. doi: 10.1038/nm770

Schekman, R. (2010). Charting the secretory pathway in a simple eukaryote. *Mol. Biol. Cell* 21, 3781–3784. doi: 10.1091/mbc.e10-05-0416

Smyth, G. K. (2004). Linear models and empirical bayes methods for assessing differential expression in microarray experiments. *Stat. Appl. Genet. Mol. Biol.* 3, 1–25. doi: 10.2202/1544-6115.1027

Soares, N. C., Francisco, R., Ricardo, C. P., and Jackson, P. A. (2007). Proteomics of ionically bound and soluble extracellular proteins in *Medicago truncatula* leaves. *Proteomics* 7, 2070–2082. doi: 10.1002/pmic.200600953

Stillwell, W. (2016). "Membrane proteins," in *An introduction to biological membranes* (Elsevier), 89–110. doi: 10.1016/B978-0-444-63772-7.00006-3

Synek, L., Pleskot, R., Sekereš, J., Serrano, N., Vukašinović, N., Ortmannová, J., et al. (2021). Plasma membrane phospholipid signature recruits the plant exocyst complex via the EXO70A1 subunit. *Proc. Natl. Acad. Sci.* 118, e2105287118. doi: 10.1073/pnas.2105287118

Synek, L., Schlager, N., Eliáš, M., Quentin, M., Hauser, M.-T., and Žárský, V. (2006). AtEXO70A1, a member of a family of putative exocyst subunits specifically expanded in land plants, is important for polar growth and plant development. *Plant J.* 48, 54–72. doi: 10.1111/j.1365-313X.2006.02854.x

Takahashi, D., Li, B., Nakayama, T., Kawamura, Y., and Uemura, M. (2013). Plant plasma membrane proteomics for improving cold tolerance. *Front. Plant Sci.* 4, 90. doi: 10.3389/fpls.2013.00090

Takano, J., Tanaka, M., Toyoda, A., Miwa, K., Kasai, K., Fuji, K., et al. (2010). Polar localization and degradation of *Arabidopsis* boron transporters through distinct trafficking pathways. *Proc. Natl. Acad. Sci.* 107, 5220–5225. doi: 10.1073/pnas.0910744107

Tweto, J., and Doyle, D. (1976). Turnover of the plasma membrane proteins of hepatoma tissue culture cells. *J. Biol. Chem.* 251, 872–882. doi: 10.1016/S0021-9258(17)33865-6

Tyanova, S., Temu, T., and Cox, J. (2016a). The MaxQuant computational platform for mass spectrometry-based shotgun proteomics. *Nat. Protoc.* 11, 2301–2319. doi: 10.1038/nprot.2016.136

Tyanova, S., Temu, T., Sinitcyn, P., Carlson, A., Hein, M. Y., Geiger, T., et al. (2016b). The Perseus computational platform for comprehensive analysis of (prote)omics data. *Nat. Methods* 13, 731–740. doi: 10.1038/nmeth.3901

Vellosillo, T., Dinneny, J. R., Somerville, C. R., and Ehrhardt, D. W. (2021). TRANVIA (TVA) facilitates cellulose synthase trafficking and delivery to the plasma membrane. *Proc. Natl. Acad. Sci.* 118, e2021790118. doi: 10.1073/pnas.2021790118

Voothuluru, P., Anderson, J. C., Sharp, R. E., and Peck, S. C. (2016). Plasma membrane proteomics in the maize primary root growth zone: novel insights into root growth adaptation to water stress. *Plant Cell Environ.* 39, 2043–2054. doi: 10.1111/pce.12778

Wang, J., Ding, Y., Wang, J., Hillmer, S., Miao, Y., Lo, S. W., et al. (2010). EXPO, an exocyst-positive organelle distinct from multivesicular endosomes and autophagosomes, mediates cytosol to cell wall exocytosis in *Arabidopsis* and tobacco cells. *Plant Cell* 22, 4009–4030. doi: 10.1105/tpc.110.080697

Wang, L., Li, H., Lv, X., Chen, T., Li, R., Xue, Y., et al. (2015). Spatiotemporal dynamics of the BRI1 receptor and its regulation by membrane microdomains in living *Arabidopsis* cells. *Mol. Plant* 8, 1334–1349. doi: 10.1016/j.molp.2015.04.005

Wang, Z.-Y., Seto, H., Fujioka, S., Yoshida, S., and Chory, J. (2001). BRI1 is a critical component of a plasma-membrane receptor for plant steroids. *Nature* 410, 380–383. doi: 10.1038/35066597

Wang, J., Song, J., Clark, G., and Roux, S. J. (2018). ANN1 and ANN2 function in post-phloem sugar transport in root tips to affect primary root growth. *Plant Physiol.* 178, 390–401. doi: 10.1104/pp.18.00713

Wen, F., VanEtten, H. D., Tsaprailis, G., and Hawes, M. C. (2007). Extracellular proteins in pea root tip and border cell exudates. *Plant Physiol.* 143, 773–783. doi: 10.1104/pp.106.091637

Wessel, D., and Flügge, U. I. (1984). A method for the quantitative recovery of protein in dilute solution in the presence of detergents and lipids. *Anal. Biochem.* 138, 141–143. doi: 10.1016/0003-2697(84)90782-6

Wu, B., and Guo, W. (2015). The exocyst at a glance. *J. Cell Sci.* 128, 2957–2964. doi: 10.1242/jcs.156398

Xu, J., and Scheres, B. (2005). Dissection of arabidopsis ADP-RIBOSYLATION FACTOR 1 function in epidermal cell polarity. *Plant Cell* 17, 525–536. doi: 10.1105/tpc.104.028449

Žárský, V. (2022). Exocyst functions in plants – secretion and autophagy. *FEBS Lett.* 1873–3468. doi: 10.1002/1873-3468.14430

Žárský, V., Kulich, I., Fendrych, M., and Pečenková, T. (2013). Exocyst complexes multiple functions in plant cells secretory pathways. *Curr. Opin. Plant Biol.* 16, 726–733. doi: 10.1016/j.pbi.2013.10.013

Zhang, C., Brown, M. Q., van de Ven, W., Zhang, Z.-M., Wu, B., Young, M. C., et al. (2016). Endosidin2 targets conserved exocyst complex subunit EXO70 to inhibit exocytosis. *Proc. Natl. Acad. Sci.* 113, E41–E50. doi: 10.1073/pnas.1521248112

Zhang, W., Huang, L., Zhang, C., and Staiger, C. J. (2021). Arabidopsis myosin XIK interacts with the exocyst complex to facilitate vesicle tethering during exocytosis. *Plant Cell* 33, 2454–2478. doi: 10.1093/plcell/koab116

Zhang, Y., Immink, R., Liu, C.-M., Emons, A. M., and Ketelaar, T. (2013). The arabidopsis exocyst subunit SEC3A is essential for embryo development and accumulates in transient puncta at the plasma membrane. *New Phytol.* 199, 74–88. doi: 10.1111/nph.12236

Zhang, Y., Liu, C.-M., Emons, A.-M. C., and Ketelaar, T. (2010). The plant exocyst. *J. Integr. Plant Biol.* 52, 138–146. doi: 10.1111/j.1744-7909.2010.00929.x

Zhang, Z. J., and Peck, S. C. (2011). Simplified enrichment of plasma membrane proteins for proteomic analyses in *Arabidopsis thaliana*. *Proteomics* 11, 1780–1788. doi: 10.1002/pmic.201000648

Zhang, W., and Staiger, C. J. (2021). Revising the role of cortical cytoskeleton during secretion: actin and myosin XI function in vesicle tethering. *Int. J. Mol. Sci.* 23, 317. doi: 10.3390/ijms23010317

Zhu, X., Li, S., Pan, S., Xin, X., and Gu, Y. (2018). CSI1, PATROL1, and exocyst complex cooperate in delivery of cellulose synthase complexes to the plasma membrane. *Proc. Natl. Acad. Sci.* 115, E3578–E3587. doi: 10.1073/pnas.1800182115

Zhu, D., Shang, M., Gao, C., and Shen, J. (2020). Protein trafficking in plant cells: Tools and markers. *China Life Sci.* 63, 343–363. doi: 10.1007/s11427-019-9598-3

frontiers | Frontiers in Plant Science

TYPE Mini Review
PUBLISHED 20 June 2023
DOI 10.3389/fpls.2023.1184047

OPEN ACCESS

EDITED BY
Caiji Gao,
South China Normal University, China

REVIEWED BY
Li Hongbo,
South China Normal University, China
Jean-Marc Neuhaus,
Université de Neuchâtel, Switzerland

*CORRESPONDENCE
Suryatapa Ghosh Jha
sjha@keckscience.claremont.edu
Emily R. Larson
emily.larson@bristol.ac.uk

RECEIVED 10 March 2023
ACCEPTED 31 May 2023
PUBLISHED 20 June 2023

CITATION
Jha SG and Larson ER (2023) Diversity of retromer-mediated vesicular trafficking pathways in plants.
Front. Plant Sci. 14:1184047.
doi: 10.3389/fpls.2023.1184047

Diversity of retromer-mediated vesicular trafficking pathways in plants

Suryatapa Ghosh Jha[1*] and Emily R. Larson[2*]

[1]William Myron Keck Science Department - Biology, Claremont McKenna, Pitzer, and Scripps Colleges, Claremont, CA, United States, [2]School of Biological Sciences, University of Bristol, Bristol, United Kingdom

The plant endomembrane system is organized and regulated by large gene families that encode proteins responsible for the spatiotemporal delivery and retrieval of cargo throughout the cell and to and from the plasma membrane. Many of these regulatory molecules form functional complexes like the SNAREs, exocyst, and retromer, which are required for the delivery, recycling, and degradation pathways of cellular components. The functions of these complexes are well conserved in eukaryotes, but the extreme expansion of the protein subunit families in plants suggests that plant cells require more regulatory specialization when compared with other eukaryotes. The retromer is associated with retrograde sorting and trafficking of protein cargo back towards the TGN and vacuole in plants, while in animals, there is new evidence that the VPS26C ortholog is associated with recycling or 'retrieving' proteins back to the PM from the endosomes. The human VPS26C was shown to rescue *vps26c* mutant phenotypes in *Arabidopsis thaliana*, suggesting that the retriever function could be conserved in plants. This switch from retromer to retriever function may be associated with core complexes that include the VPS26C subunit in plants, similar to what has been suggested in other eukaryotic systems. We review what is known about retromer function in light of recent findings on functional diversity and specialization of the retromer complex in plants.

KEYWORDS

retromer, endomembrane system, retriever, vesicle traffic, protein recycling

1 Introduction

The endomembrane system is a highly coordinated network that controls cellular function and development in living organisms. This system is responsible for the synthesis, sorting, and distribution of proteins within cells in a manner that is often crucial for their growth and viability. The endosomal trafficking of cargo to the storage and lytic vacuoles in plants, or the lysosome in animal systems, involves the action of Soluble NSF Attachment Receptors (SNAREs) that control the fusion of vesicles carrying cargo to target membranes. A retrograde trafficking pathway that involves the retromer complex is necessary for transporting cargo and endosomal membrane proteins to the *trans*-Golgi network (TGN)

and coordinated with the trafficking of cargo to the vacuole. In animals, retromer defects can impair insulin signaling (Ma et al., 2014; Yang et al., 2016), while mutations in the core retromer subunits are linked to neurological disorders, including Parkinson's (Williams et al., 2017) and Alzheimer's diseases (Tammineni et al., 2017). In plants, a retromer defect can result in altered growth and development and impair the ability of the plant to adapt to stress. For example, in *Arabidopsis thaliana*, retromer loss of function is linked to defects in root hair growth and patterning, shoot gravitropism, increased sensitivity to drought stress, and immunity-associated cell death pathways (Munch et al., 2015; Jha et al., 2018; Liang et al., 2022). The coordination of endosomal trafficking pathways between the TGN and the vacuole was also underscored by reports that a genetic interaction between specific retromer-dependent endosomal trafficking pathways and a VTI-SNARE dependent pathway to the lytic vacuole are required for both shoot gravitropism (Hashiguchi et al., 2010) and root hair growth in Arabidopsis (Jha et al., 2018).

The trafficking of receptor proteins from late endosomes and Golgi/TGN to the vacuole is facilitated by the retromer complex. Retromers function by binding to specific receptors on transport vesicles and directing them back to the TGN for further sorting and distribution. However, the identity of the protein complexes involved in retrograde endosomal trafficking in eukaryotes has expanded to include a retromer-like "retriever" complex (McNally et al., 2017). This complex is formed by interactions between core retromer-like proteins that traffic cargo from the endosomes to the plasma membrane rather than the TGN (McNally et al., 2017). While it is clear that the retromer functions between plants and animals are not always directly comparable, studies in multiple systems have suggested that the core subunits of the retromer complex could be responsible for specializing its subcellular localization and function (McNally et al., 2017; Jha et al., 2018; Ivanov and Robinson, 2020; Zelazny et al., 2013b).

In this review, we summarize our understanding of the retromer complex in plants, focusing on a newly described, evolutionarily conserved Vacuolar Protein Sorting (VPS) 26 protein (VPS26C) that is required for root hair growth and has a putative retriever function similar to its human ortholog, DSCR3/VPS26C. We also discuss genetic studies that implicate interactions between trafficking pathways regulated by the retromer and the VTI family of SNAREs in controlling plant development in plants. Finally, we discuss the recent advances in retromer biology, the current gaps in knowledge, and the tools we need to further elucidate the functional scope of retromer/retriever-dependent endosomal recycling pathways in plant development.

2 The classic retromer complex

The retromer complex was initially characterized in yeast and shown to function in the endosome-to-Golgi trafficking of the transmembrane receptor for vacuolar carboxypeptidase Y, Vps10p (Seaman et al., 1998). Retromers were subsequently defined as a hetero-pentameric complex of large and small subunits. In yeast, the large retromer subunit consists of three highly conserved proteins, VPS35, VPS29, and VPS26 (Haft et al., 2000; Seaman, 2004), that is responsible for interacting with cargo proteins in a retrograde trafficking pathway from endosomes to the TGN (Seaman et al., 1998; Burda et al., 2002). The small subunit of the retromer in yeast is a dimer of two nexin proteins, VPS5p, and VPS17p that function in membrane binding, curvature, and tubulation (Horazdovsky et al., 1997; Carlton et al., 2005).

In mammalian systems, the large retromer subunit is composed of VPS35 and VPS29 proteins that complex with one of two VPS26 paralogs, VPS26A or VPS26B (Seaman et al., 1998). VPS26A and VPS26B in mice are not functionally redundant (Bugarcic et al., 2011), suggesting that different versions of the large retromer complex function in distinct endosomal trafficking pathways. The small subunit of the mammalian retromer is a heterodimer of two sorting nexins, either SNX1 or SNX2 and SNX5 or SNX6, which function in binding membranes and recruiting the large retromer subunit to the endosomal membrane (Bonifacino and Hurley, 2008; Collins, 2008). While the large and small retromer subunits form a stable complex in yeast, the interaction between these two subunits is much weaker and transient in other eukaryotes (Harbour and Seaman, 2011; Swarbrick et al., 2011). Along with the sorting nexins of the small retromer subunit, many animal genomes encode additional sorting nexins that function in retrograde trafficking pathways that involve the retromer complex. For example, SNX3 can interact with the large retromer subunit to control endosomal trafficking pathways involved in sorting the transcription factor Wnt (Harterink et al., 2011), while SNX27 is a cargo adapter for the large retromer subunit on endosomal membranes (Gallon et al., 2014). The Wiscott-Aldrich syndrome and SCAR Homolog (WASH) complex also associates with the retromer subunits and nexins to coordinate actin nucleation and control endosomal sorting of transmembrane receptors (Bartuzi et al., 2016).

The retromer in animal systems can retrieve and recycle transmembrane receptors from endosomal membranes to and from the plasma membrane and the TGN, respectively, and mediate transport between organelles (Table 1). The retromer-mediated retrieval of receptors includes Carboxypeptidase Y (Seaman et al., 1998), Bone Morphogenetic Protein (BMP) Type I receptor SMA-6 (Gleason et al., 2014), the phagocytic receptor CED-1 from phagosomes to the plasma membrane (Chen et al., 2010), and neurotransmitter receptor, GLR-1, from dendrites to the cell body (Zhang et al., 2012) in *Caenorhabditis elegans*. Retromer-mediated recycling of G-Protein Coupled Receptors (GPCRs) have also been reported in studies using human cell lines (Bugarcic et al., 2011; Temkin et al., 2011) and *Drosophila melanogaster* (Wang et al., 2014). In addition, retromer complexes have been implicated in the retrograde trafficking of transmembrane proteins from the plasma membrane to the TGN in *C. elegans* (Bai and Grant, 2015), and transport between peroxisomes and mitochondria in human cell lines (Braschi et al., 2010), all of which highlight the essential role of the retromer complex in regulating signaling pathways and organelle transport that are crucial for cell function and development.

TABLE 1 List of receptors trafficked by retromer-dependent pathways in non-plant systems.

Study system	Receptor	Trafficking Route	Reference
Caenorhabditis elegans	Carboxypeptidase Y	Endosomes to TGN	Seaman et al., 1998
Caenorhabditis elegans	BMP Type I receptor SMA-6	Endosomes to TGN	Gleason et al., 2014
Caenorhabditis elegans	Phagocytic receptor CED-1	Phagosomes to PM	Chen et al., 2010
Caenorhabditis elegans	Neurotransmitter receptor GLR-1	Dendrites to cell body	Zhang et al., 2012
Human cell lines	G-Protein-Coupled Receptors (GCPRs)	Endosomes to TGN	Bugarcic et al., 2011; Temkin et al., 2011
Drosophila melanogaster	G-Protein-Coupled Receptors (GPCRs)	Endosomes to TGN	Wang et al., 2014
Human cell lines	Mitochondria Anchored Protein Ligase (MAPL)	Mitochondria to Peroxisome	Braschi et al., 2010

A study using human cell lines demonstrated the formation of the retromer-like 'retriever' complex, involving the DSCR3/VPS26C protein (McNally et al., 2017). Using biochemical assays, this study demonstrated that DSCR3/VPS26C forms a complex with VPS29 and a VPS35-like (C16orf62) protein, leading to three major conclusions about the retriever complex in human cells. Firstly, the retriever complex localizes to endosomal membranes through its recruitment by the Copper Metabolism MURR1 Domain (COMMD)/Coiled-Coil Domain Containing CCDC22/CCDC93 (CCC) complex, which associates with the WASH complex to mediate transmembrane receptor sorting (Bartuzi et al., 2016). Secondly, DSCR3/VPS26C mediates the interaction between the retriever complex and the cargo adaptor Sorting Nexin (SNX) 17 to regulate the retrograde trafficking of a subset of plasma membrane proteins. Lastly, siRNA suppression of CCDC22 and CCDC93 interrupted the endosomal association of the retriever complex with SNX17, which led to the mis-sorting of the $\alpha_5\beta_1$ integrin, one of the VPS26C/SNX17 cargo proteins.

This working model was used to characterize the retromer-dependent trafficking that facilitates membrane curvature, tubulation, and retrograde transport of cargo in animal systems. However, this model was challenged by that of the retrograde transport of the CI-MPR receptor from late endosomal membranes to the TGN (Kvainickas et al., 2017; Simonetti et al., 2017). There is new evidence that SNX proteins within the small retromer subunit are required for retrograde trafficking of the CI-MPR receptor in humans, while downregulation of the VPS35 large retromer subunit had no effect on the recycling of this receptor from late endosomal membranes (Kvainickas et al., 2017; Simonetti et al., 2017). Hence, there is support for a new model for retromer trafficking in which the small subunit is essential for the retrograde trafficking of receptors from late endosomal membranes to the TGN (Figure 1A).

3 Retromer function in plants

The availability of several plant genomes and the strong conservation of retromer subunit sequences were used to identify retromer subunits in a variety of plant species. In Arabidopsis, VPS35 and VPS26 are both encoded by three gene family members, while VPS29 is a single copy gene. In contrast, the small retromer subunit is composed of a heterodimer containing SNX1 and either SNX2a or SNX2b, which are homologs of the yeast VPS5p sorting nexin (Niemes et al., 2010). In plants, genetic studies showed that the core retromer functions independently of its interaction with the sorting nexins (Pourcher et al., 2010), which is a diversion from mammalian systems where the retromer complex assembly involves sorting nexins (Wassmer et al., 2009; Zelazny et al., 2013a) (Figure 1B).

The large and small retromer subunits are required for endosomal trafficking pathways that control diverse aspects of plant development. Genetic analysis has shown that single *vps26a* and *vps26b* mutants have no developmental defects in Arabidopsis, but the *vps26a vps26b* double mutant displays severely stunted growth, indicating functional redundancy between the VPS26 paralogs (Zelazny et al., 2013b). A similar analysis of VPS35 family members showed that a *vps35b vps35c* double mutant exhibits a dwarfed growth phenotype, early senescence, and defects in trafficking proteins to the storage vacuole (Yamazaki et al., 2008). Mutations in *vps29* and *snx1* have similar developmental phenotypes and defects in organ initiation as that observed in *pin* mutants. These results suggest that VPS29 and SNX1 function in a common pathway to regulate PIN-FORMED (PIN) protein recycling and cell polarity (Jaillais et al., 2007; Kleine-Vehn et al., 2008). In Arabidopsis, retromer subunit mutants describe a role for VPS35A and VPS26A in shoot gravitropism (Hashiguchi et al., 2010), VPS35B and VPS26B in innate immunity (Munch et al., 2015), VPS29 in the transport of Sugar-Dependent-1 (SDP1) from peroxisomes to oil bodies during seedling development (Thazar-Poulot et al., 2015), and SNX1 in the trafficking of IRT1 and the efficiency of iron uptake machinery in roots (Ivanov et al., 2014). The retromer complex was also implicated in the delivery of lipid enzymes to viral replication organelles (VROs) in Tomato Bushy Stunt Virus (TBSV), which is a Tombusvirus in plants (Feng et al., 2021). These results highlight the diverse roles for both the large and small retromer subunits in endosomal trafficking pathways that control plant development.

Recent research on retromer biology has elucidated the mechanism of retromer recruitment processes in Arabidopsis. The plant specific endosomal regulator, BLISTER, was identified

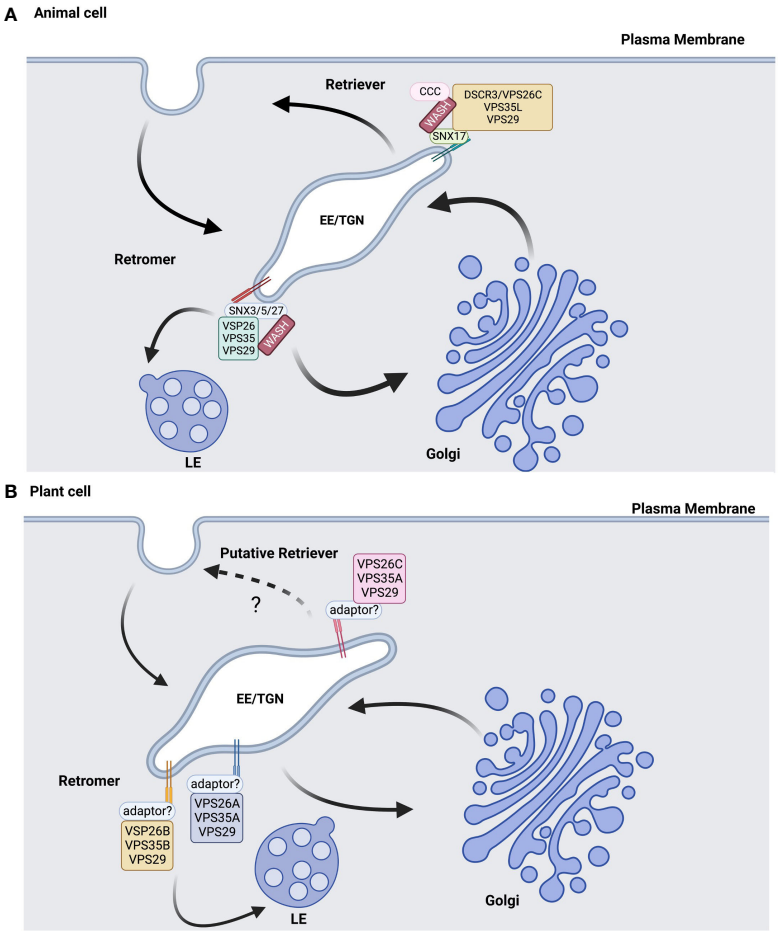

FIGURE 1
Retromer/retriever models in animal and plant cells are similar but not identical. **(A)** In animal cells, the retromer complex is composed of VPS25, VPS35, and VPS29 core subunits, syntaxin (SNX) small subunits, and the WASH complex in trans-Golgi Network (TGN)-derived early endosomes (EE). Different SNX small subunits and the CCC complex associate with WASH to recruit the retriever cargo back to the plasma membrane and differentiate this complex from the retromer, which sorts cargo for retrograde trafficking towards the Golgi and late endosomes (LE). **(B)** In plants, the core subunits may determine the retromer and retriever functions, with VPS26C potentially contributing to returning endomembrane cargo back to the PM as part of a retriever-like complex. Diagrams informed by the studies referenced in this review and were created with BioRender.com.

and characterized to function in membrane recruitment of the retromer core complex in the sorting and trafficking of soluble vacuolar proteins to the TGN and recycling of endocytosed plasma membrane proteins (Li et al., 2023). This report not only identified a mechanism of core retromer function but also retromer function in alternative trafficking pathways other than the conventional endosome to TGN pathways. Moreover, the ESCRT-associated protein ALIX is a conserved protein previously characterized to function in vacuolar degradation of abscisic acid receptors that also interacts with the retromer complex. In the absence of ALIX, the aberrant recruitment of VPS29 and VPS26 to the membrane results in defective localization and trafficking of Vacuolar Sorting Receptors (VSRs) (Hu et al., 2022). Additionally, retromer association with the gibberellic acid-signaling mediator DELLA mediates recycling pathways (Salanenka et al., 2018) and the interaction of the core retromer protein VPS35 with RabG3f to control late endosome-vacuole fusion (Rodriguez-Furlan et al., 2019; Zelazny et al., 2013b) reinforce the functional range of the retromer complex in regulating recycling pathways to the TGN and vacuole, as well as to the plasma membrane.

3.1 Evolutionary divergence of VPS26 function in plants and other eukaryotes

Phylogenetic analysis of genes encoding the VPS26 large retromer protein has shown that DSCR3/VPS26C represents a third VPS26 gene family member that is evolutionarily conserved and part of a smaller, monophyletic clade distinct from the *VPS26A* and *VPS26B* homologs across plant and animal species (Koumandou et al., 2011). Along with VPS26C, other subunits of the retriever complex are very well conserved and potentially co-evolved from the

last eukaryotic ancester, being lost only in fungi (McNally et al., 2017). This strong conservation of retromer/retriever genes in eukaryotes indicates the molecular functions are crucial for most all eukaryotic cell function. In Arabidopsis, VPS26C forms a complex with VPS35A and VPS29 that is required for the regulation of polarized growth in root hairs. VPS26C orthologs exhibit functional conservation, indicated by the complementation of the *vps26c* mutant phenotype in Arabidopsis by the human *DSCR3/VPS26C* (Jha et al., 2018). Like the Arabidopsis VPS26C subunit, the DSCR3/VPS26C human ortholog also associates with VPS29 and a VPS35-like protein (McNally et al., 2017). Moreover, consistent with Zelazny et al. (2013b), who suggested that the localization of the retromer complexes could be mediated by the VPS26 isoforms, VPS26C did not localize to wortmannin-sensitive compartments, which indicated that it does not require RabG3f for its recruitment (Jha et al., 2018).

Differences in retromer and retriever function are mediated in part by the cargo proteins that they traffic to the TGN or plasma membrane, as well as by the cargo adaptor used to recruit these complexes to the endosomal membrane. Proteomic and genetic analyses of the VPS26C complex in human cell culture reported that the VPS26C retriever complex participates in a trafficking pathway directed to plasma membrane (McNally et al., 2017), a deviation from that of the retromers that are conventionally involved in trafficking cargo to the Golgi/TGN. In addition, the functional conservation of VPS26C orthologs in different organisms could indicate that VPS26C evolved a new functionality in endosomal trafficking pathways that are distinct from the classic retromer complex in Arabidopsis. The membrane recruitment of VPS26C in mammalian cells involved the CCDC22/CCDC93/COMMD protein complex. Arabidopsis has homologs of CCDC22 and CCDC93 but not COMMD (Reviewed in Law et al., 2022). Therefore, further investigation will be needed to determine the cargo and proteins involved in the membrane recruitment of the VPS26C complex and the functional specificity of the VPS26C-dependent complexes in plants (Figure 1).

3.2 Genetic crosstalk between retromers and the VTI SNARE family

The VTI SNARE family participates in trafficking cargo to the lytic or storage vacuoles in Arabidopsis (Sanmartin et al., 2007; Larson et al., 2014). Null mutants for each of the VTI SNAREs exhibit unique phenotypes, suggesting that they have distinct functions in plants. The *vti11* mutant has defective leaf vasculature (Shirakawa et al., 2009), aberrant central lytic vacuole formation (Sanmartin et al., 2007), and a shoot agravitropic phenotype, while those of *VTI12* display no developmental phenotype when grown on a nutrient-rich medium but have accelerated senescence when grown on nutrient-deficient media, suggesting a role in plant autophagy (Surpin et al., 2003). Moreover, *vti12* plants also exhibit abnormal accumulation of 12S globulin precursors in siliques, indicating VTI12-mediated trafficking of vacuolar storage proteins (Sanmartin et al., 2007); while *vti13* is defective in root hair growth and cell wall organization in root epidermal and hair cells in Arabidopsis, suggesting these trafficking pathways are required for cell shape and growth (Larson et al., 2014).

Studies have linked VTI11 and VTI13-mediated anterograde trafficking pathways to the lytic vacuole with endosomal trafficking pathways mediated by the retromer. A suppressor screen of *vti11* found that mutations within genes encoding the core retromer proteins VPS35A and VPS26A were sufficient to suppress the *vti11* shoot agravitropic 'zigzag' phenotype in double mutants (Hashiguchi et al., 2010). Although the mechanism of this genetic interaction is not defined, the mis-sorting of membranes to vacuoles in *vti11 vps26a* or *vti11 vps35a* double mutants resulted in a recovery of the vacuolar dynamics necessary for amyloplast movement in endodermal cells that restored shoot gravitropism (Hashiguchi et al., 2010). A similar interaction between mutations in the VPS26C retromer subunit and the VTI13 SNARE was described by (Jha et al., 2018), where a loss-of-function mutation for *VPS26C* restored the root hair growth and wall organization phenotype of the *vti13* mutant. While the cellular mechanism responsible for this suppression is currently unknown, it is interesting that VPS35A physically interacts both with VPS26A and VPS26C in Arabidopsis (Jha et al., 2018; Zelazny et al., 2013b) and that VPS35B and VPS35C cannot substitute for VPS35A in endosomal trafficking pathways that control shoot gravitropism (Hashiguchi et al., 2010). VPS35A function is also required for cargo trafficking to the lytic vacuole (Nodzyński et al., 2013), indicating that retromer function may be required for multiple trafficking pathways between both the lytic vacuole and TGN. Understanding the coordination of the endosomal trafficking pathways that are required for trafficking of cargo between these organelles and the identity of the proteins involved in these pathways is required to determine the cellular mechanisms that mediate the diverse developmental processes in plants.

4 Conclusion

In plants, the current literature addresses the interactions of the core retromer subunits and the effects these proteins have on developmental pathways. These studies characterized retromer function using genetics-based approaches, including loss-of-function mutants to correlate retromer function with developmental defects. Although these studies are seminal in demonstrating the importance of retromer proteins, there is still a substantial gap in our knowledge about the cell biology of plant retromers, including the mechanism of their membrane recruitment, their potential interacting/adapter proteins, and the identification of their cargo. Studies have explored retromer mechanisms, but these studies are underrepresented in the existing literature. There are several key questions that need to be addressed to fill these gaps, some of which are outlined below:

1. VPS26C interacts with core retromer subunit VPS35A and VPS29. However, the human ortholog DSCR3/VPS26C is

part of a 'retriever' complex that recycles cargo to the plasma membrane. The functional conservation of VPS26C orthologs in humans and plants begs the question: Does the plant VPS26C function in retromer (endosome to TGN) or retriever (endosomes to plasma membrane) pathways?
2. Is the membrane recruitment process of retromers and retrievers the same in plants and animals?
3. Given that VPS26C interacts with core retromer subunits that function in the classical retromer pathway, is the retromer/retriever distinction in plants cell type-dependent?
4. If there are diverse recycling routes, there must be diverse types of cargo. How could we identify these cargoes?

Using and developing new tools in immunochemistry, proximity-based labeling and proteomics, and high-resolution imaging could help address these gaps in retromer cell biology by enabling the investigation of subcellular phenotypes and interactomes of retromers, identifying cargo and define the diverse pathways they function in to maintain optimal plant development.

Author contributions

SGJ and ERL equally contributed to the conception and writing of this review. All authors contributed to the article and approved the submitted version.

Funding

ERL is supported by a research grant from the Leverhulme Trust (R102737-101). SGJ is supported by the W M Keck Science Department at the Claremont Colleges.

Acknowledgments

We thank Dr. Mary Tierney for supervising SGJ's dissertation, which provided foundational ideas and content for this review.

Conflict of interest

The authors declare that the research was conducted in the absence of any commercial or financial relationships that could be construed as a potential conflict of interest.

Publisher's note

References

Bai, Z., and Grant, B. D. (2015). A TOCA/CDC-42/PAR/WAVE functional module required for retrograde endocytic recycling. *Proc. Natl. Acad. Sci. U. States America* 112 (12), E1443–E1452. doi: 10.1073/pnas.1418651112

Bartuzi, P., Billadeau, D. D., Favier, R., Rong, S., Dekker, D., Fedoseienko, A., et al. (2016). CCC- and WASH-mediated endosomal sorting of LDLR is required for normal clearance of circulating LDL. *Nat. Commun.* 7 (1), 10961–10971. doi: 10.1038/ncomms10961

Bonifacino, J. S., and Hurley, J. H. (2008). Retromer. *Curr. Opin. Cell Biol.* 20 (4), 427–436. doi: 10.1016/j.ceb.2008.03.009

Braschi, E., Goyon, V., Zunino, R., Mohanty, A., Xu, L., and McBride, H. M. (2010). Vps35 mediates vesicle transport between the mitochondria and peroxisomes. *Curr. Biol.* 20 (14), 1310–1315. doi: 10.1016/j.cub.2010.05.066

Bugarcic, A., Zhe, Y., Kerr, M. C., Griffin, J., Collins, B. M., and Teasdale, R. D. (2011). Vps26A and Vps26B subunits define distinct retromer complexes. *Traffic* 12 (12), 1759–1773. doi: 10.1111/j.1600-0854.2011.01284.x

Burda, P., Padilla, S., Sarkar, S., and Emr, S. (2002). Retromer function in endosome-to-Golgi retrograde transport is regulated by the yeast Vps34 PtdIns 3-kinase. *J. Cell Sci.* 115, 3889–3900. doi: 10.1242/jcs.00090

Carlton, J. G., Bujny, M. V., Peter, B. J., Oorschot, V. M. J., Rutherford, A., Arkell, R. S., et al. (2005). Sorting nexin-2 is associated with tubular elements of the early endosome, but is not essential for retromer-mediated endosome-to-TGN transport. *J. Cell Sci.* 118 (Pt 19), 4527–4539. doi: 10.1242/jcs.02568

Chen, D., Xiao, H., Zhang, K., Wang, B., Gao, Z., Jian, Y., et al. (2010). Retromer is required for apoptotic cell clearance by phagocytic receptor recycling. *Science* 327 (5970), 1261–1264. doi: 10.1126/science.1184840

Collins, B. M. (2008). The structure and function of the retromer protein complex. *Traffic (Copenhagen Denmark)* 9 (11), 1811–1822. doi: 10.1111/j.1600-0854.2008.00777.x

Feng, Z., Inaba, J.-I., and Nagy, P. D. (2021). The retromer is co-opted to deliver lipid enzymes for the biogenesis of lipid-enriched tombusviral replication organelles. *Proc. Natl. Acad. Sci. U. States America* 118 (1), e2016066118. doi: 10.1073/pnas.2016066118

Gallon, M., Clairfeuille, T., Steinberg, F., Mas, C., Ghai, R., Sessions, R. B., et al. (2014). A unique PDZ domain and arrestin-like fold interaction reveals mechanistic details of endocytic recycling by SNX27-retromer. *Proc. Natl. Acad. Sci.* 111 (35), E3604–E3613. doi: 10.1073/pnas.1410552111

Gleason, R. J., Akintobi, A. M., Grant, B. D., and Padgett, R. W. (2014). BMP signaling requires retromer-dependent recycling of the type I receptor. *Proc. Natl. Acad. Sci.* 111 (7), 2578–2583. doi: 10.1073/pnas.1319947111

Haft, C. R., Sierra, M., de la, L., Bafford, R., Lesniak, M. A., Barr, V. A., et al. (2000). Human orthologs of yeast vacuolar protein sorting proteins Vps26, 29, and 35: assembly into multimeric complexes. *Mol. Biol. Cell* 11 (12), 4105–4116. doi: 10.1091/mbc.11.12.4105

Harbour, M. E., and Seaman, M. N. J. (2011). Evolutionary variations of VPS29, and their implications for the heteropentameric model of retromer. *Communicative Integr. Biol.* 4 (5), 619–622. doi: 10.4161/cib.4.5.16855

Harterink, M., Port, F., Lorenowicz, M. J., McGough, I. J., Silhankova, M., Betist, M. C., et al. (2011). A SNX3-dependent retromer pathway mediates retrograde transport of the wnt sorting receptor wntless and is required for wnt secretion. *Nat. Cell Biol.* 13 (8), 914–923. doi: 10.1038/ncb2281

Hashiguchi, Y., Niihama, M., Takahashi, T., Saito, C., Nakano, A., Tasaka, M., et al. (2010). Loss-of-function mutations of retromer large subunit genes suppress the phenotype of an arabidopsis zig mutant that lacks qb-SNARE VTI11. *Plant Cell* 22 (1), 159–172. doi: 10.1105/tpc.109.069294

Horazdovsky, B. F., Davies, B. A., Seaman, M. N., McLaughlin, S. A., Yoon, S., and Emr, S. D. (1997). A sorting nexin-1 homologue, Vps5p, forms a complex with Vps17p and is required for recycling the vacuolar protein-sorting receptor. *Mol. Biol. Cell* 8 (8), 1529–1541. doi: 10.1091/mbc.8.8.1529

Hu, S., Li, B., Wu, F., Zhu, D., Zouhar, J., Gao, C., et al. (2022). Plant ESCRT protein ALIX coordinates with retromer complex in regulating receptor-mediated sorting of soluble vacuolar proteins. *Proc. Natl. Acad. Sci.* 119 (20), e2200492119. doi: 10.1073/pnas.2200492119

Ivanov, R., Brumbarova, T., Blum, A., Jantke, A.-M., Fink-Straube, C., and Bauer, P. (2014). SORTING NEXIN1 is required for modulating the trafficking and stability of the arabidopsis IRON-REGULATED TRANSPORTER1. *Plant Cell* 26 (3), 1294–1307. doi: 10.1105/tpc.113.116244

Ivanov, R., and Robinson, D. G. (2020). EMAC, retromer, and VSRs: do they connect? *Protoplasma* 257 (6), 1725–1729. doi: 10.1007/s00709-020-01543-8

Jaillais, Y., Santambrogio, M., Rozier, F., Fobis-Loisy, I., Miège, C., and Gaude, T. (2007). The retromer protein VPS29 links cell polarity and organ initiation in plants. *Cell* 130 (6), 1057–1070. doi: 10.1016/j.cell.2007.08.040

Jha, S. G., Larson, E. R., Humble, J., Domozych, D. S., Barrington, D. S., and Tierney, M. L. (2018). Vacuolar protein sorting 26C encodes an evolutionarily conserved large retromer subunit in eukaryotes that is important for root hair growth in arabidopsis thaliana. *Plant J.* 94 (4), 595–611. doi: 10.1111/tpj.13880

Kleine-Vehn, J., Leitner, J., Zwiewka, M., Sauer, M., Abas, L., Luschnig, C., et al. (2008). Differential degradation of PIN2 auxin efflux carrier by retromer-dependent vacuolar targeting. *Proc. Natl. Acad. Sci. U. States America* 105 (46), 17812–17817. doi: 10.1073/pnas.0808073105

Koumandou, V. L., Klute, M. J., Herman, E. K., Nunez-Miguel, R., Dacks, J. B., and Field, M. C. (2011). Evolutionary reconstruction of the retromer complex and its function in trypanosoma brucei. *J. Cell Sci.* 124 (Pt 9), 1496–1509. doi: 10.1242/jcs.081596

Kvainickas, A., Jimenez-Orgaz, A., Nägele, H., Hu, Z., Dengjel, J., and Steinberg, F. (2017). Cargo-selective SNX-BAR proteins mediate retromer trimer independent retrograde transport. *J. Cell Biol.* 216 (11), 3677–3693. doi: 10.1083/jcb.201702137

Larson, E. R., Domozych, D. S., and Tierney, M. L. (2014). SNARE VTI13 plays a unique role in endosomal trafficking pathways associated with the vacuole and is essential for cell wall organization and root hair growth in arabidopsis. *Ann. Bot.* 114 (6), 1147–1159. doi: 10.1093/aob/mcu041

Law, K. C., Chung, K. K., and Zhuang, X. (2022). An update on coat protein complexes for vesicle formation in plant post-golgi trafficking. *Front. Plant Sci.* 13. doi: 10.3389/fpls.2022.826007

Li, H., Huang, R., Liao, Y., Yang, S., Feng, B., Qin, H., et al. (2023). A plant-unique protein BLISTER coordinates with core retromer to modulate endosomal sorting of plasma membrane and vacuolar proteins. *Proc. Natl. Acad. Sci.* 120 (1), e2211258120. doi: 10.1073/pnas.2211258120

Liang, C., Li, C., Wu, J., Zhao, M., Chen, D., Liu, C., et al. (2022). SORTING NEXIN2 proteins mediate stomatal movement and the response to drought stress by modulating trafficking and protein levels of the ABA exporter ABCG25. *Plant J.* 110 (6), 1603–1618. doi: 10.1111/tpj.15758

Ma, J., Nakagawa, Y., Kojima, I., and Shibata, H. (2014). Prolonged insulin stimulation down-regulates GLUT4 through oxidative stress-mediated retromer inhibition by a protein kinase CK2-dependent mechanism in 3T3-L1 adipocytes. *J. Biol. Chem.* 289 (1), 133–142. doi: 10.1074/jbc.M113.533240

McNally, K. E., Faulkner, R., Steinberg, F., Gallon, M., Ghai, R., Pim, D., et al. (2017). Retriever is a multiprotein complex for retromer-independent endosomal cargo recycling. *Nat. Cell Biol.* 19 (10), 1214–1225. doi: 10.1038/ncb3610

Munch, D., Teh, O.-K., Malinovsky, F. G., Liu, Q., Vetukuri, R. R., El Kasmi, F., et al. (2015). Retromer contributes to immunity-associated cell death in arabidopsis. *Plant Cell* 27 (2), 463–479. doi: 10.1105/tpc.114.132043

Niemes, S., Langhans, M., Viotti, C., Scheuring, D., San Wan Yan, M., Jiang, L., et al. (2010). Retromer recycles vacuolar sorting receptors from the trans-golgi network. *Plant J.: Cell Mol. Biol.* 61 (1), 107–121. doi: 10.1111/j.1365-313X.2009.04034.x

Nodzyński, T., Feraru, M. I., Hirsch, S., De Rycke, R., Niculaes, C., Boerjan, W., et al. (2013). Retromer subunits VPS35A and VPS29 mediate prevacuolar compartment (PVC) function in arabidopsis. *Mol. Plant* 6 (6), 1849–1862. doi: 10.1093/mp/sst044

Pourcher, M., Santambrogio, M., Thazar, N., Thierry, A.-M., Fobis-Loisy, I., Miège, C., et al. (2010). Analyses of SORTING NEXINs reveal distinct retromer-subcomplex functions in development and protein sorting in arabidopsis thaliana[C][W]. *Plant Cell* 22 (12), 3980–3991. doi: 10.1105/tpc.110.078451

Rodriguez-Furlan, C., Domozych, D., Qian, W., Enquist, P.-A., Li, X., Zhang, C., et al. (2019). Interaction between VPS35 and RABG3f is necessary as a checkpoint to control fusion of late compartments with the vacuole. *Proc. Natl. Acad. Sci.* 116 (42), 21291–21301. doi: 10.1073/pnas.1905321116

Salanenka, Y., Verstraeten, I., Löfke, C., Tabata, K., Naramoto, S., Glanc, M., et al. (2018). Gibberellin DELLA signaling targets the retromer complex to redirect protein trafficking to the plasma membrane. *Proc. Natl. Acad. Sci.* 115 (14), 3716–3721. doi: 10.1073/pnas.1721760115

Sanmartin, M., Ordóñez, A., Sohn, E., Robert, S., Sánchez-Serrano, J., Surpin, M., et al. (2007). Divergent functions of VTI12 and VTI11 in trafficking to storage and lytic vacuoles in arabidopsis. *Proc. Natl. Acad. Sci. U. States America* 104, 3645–3650. doi: 10.1073/pnas.0611147104

Seaman, M. N. J. (2004). Cargo-selective endosomal sorting for retrieval to the golgi requires retromer. *J. Cell Biol.* 165 (1), 111–122. doi: 10.1083/jcb.200312034

Seaman, M. N., McCaffery, J. M., and Emr, S. D. (1998). A membrane coat complex essential for endosome-to-Golgi retrograde transport in yeast. *J. Cell Biol.* 142 (3), 665–681. doi: 10.1083/jcb.142.3.665

Shirakawa, M., Ueda, H., Shimada, T., Nishiyama, C., and Hara-Nishimura, I. (2009). Vacuolar SNAREs function in the formation of the leaf vascular network by regulating auxin distribution. *Plant Cell Physiol.* 50 (7), 1319–1328. doi: 10.1093/pcp/pcp076

Simonetti, B., Danson, C. M., Heesom, K. J., and Cullen, P. J. (2017). Sequence-dependent cargo recognition by SNX-BARs mediates retromer-independent transport of CI-MPR. *J. Cell Biol.* 216 (11), 3695–3712. doi: 10.1083/jcb.201703015

Surpin, M., Zheng, H., Morita, M. T., Saito, C., Avila, E., Blakeslee, J. J., et al. (2003). The VTI family of SNARE proteins is necessary for plant viability and mediates different protein transport pathways. *Plant Cell* 15 (12), 2885–2899. doi: 10.1105/tpc.016121

Swarbrick, J. D., Shaw, D. J., Chhabra, S., Ghai, R., Valkov, E., Norwood, S. J., et al. (2011). VPS29 is not an active metallo-phosphatase but is a rigid scaffold required for retromer interaction with accessory proteins. *PloS One* 6 (5), e20420. doi: 10.1371/journal.pone.0020420

Tammineni, P., Jeong, Y. Y., Feng, T., Aikal, D., and Cai, Q. (2017). Impaired axonal retrograde trafficking of the retromer complex augments lysosomal deficits in alzheimer's disease neurons. *Hum. Mol. Genet.* 26 (22), 4352–4366. doi: 10.1093/hmg/ddx321

Temkin, P., Lauffer, B., Jäger, S., Cimermancic, P., Krogan, N. J., and von Zastrow, M. (2011). SNX27 mediates retromer tubule entry and endosome-to-plasma membrane trafficking of signalling receptors. *Nat. Cell Biol.* 13 (6), 715–721. doi: 10.1038/ncb2252

Thazar-Poulot, N., Miquel, M., Fobis-Loisy, I., and Gaude, T. (2015). Peroxisome extensions deliver the arabidopsis SDP1 lipase to oil bodies. *Proc. Natl. Acad. Sci. U. States America* 112 (13), 4158–4163. doi: 10.1073/pnas.1403322112

Wang, S., Tan, K. L., Agosto, M. A., Xiong, B., Yamamoto, S., Sandoval, H., et al. (2014). The retromer complex is required for rhodopsin recycling and its loss leads to photoreceptor degeneration. *PloS Biol.* 12 (4), e1001847. doi: 10.1371/journal.pbio.1001847

Wassmer, T., Attar, N., Harterink, M., van Weering, J. R. T., Traer, C. J., Oakley, J., et al. (2009). The retromer coat complex coordinates endosomal sorting and dynein-mediated transport, with carrier recognition by the trans-golgi network. *Dev. Cell* 17 (1), 110–122. doi: 10.1016/j.devcel.2009.04.016

Williams, E. T., Chen, X., and Moore, D. J. (2017). VPS35, the retromer complex and parkinson's disease. *J. Parkinson's Dis.* 7 (2), 219–233. doi: 10.3233/JPD-161020

Yamazaki, M., Shimada, T., Takahashi, H., Tamura, K., Kondo, M., Nishimura, M., et al. (2008). Arabidopsis VPS35, a retromer component, is required for vacuolar protein sorting and involved in plant growth and leaf senescence. *Plant Cell Physiol.* 49 (2), 142–156. doi: 10.1093/pcp/pcn006

Yang, Z., Hong, L. K., Follett, J., Wabitsch, M., Hamilton, N. A., Collins, B. M., et al. (2016). Functional characterization of retromer in GLUT4 storage vesicle formation and adipocyte differentiation. *FASEB J.* 30 (3), 1037–1050. doi: 10.1096/fj.15-274704

Zelazny, E., Santambrogio, M., and Gaude, T. (2013a). Retromer association with membranes: plants have their own rules! *Plant Signaling Behav.* 8 (9), e25312. doi: 10.4161/psb.25312

Zelazny, E., Santambrogio, M., Pourcher, M., Chambrier, P., Berne-Dedieu, A., Fobis-Loisy, I., et al. (2013b). Mechanisms governing the endosomal membrane recruitment of the core retromer in arabidopsis. *J. Biol. Chem.* 288 (13), 8815–8825. doi: 10.1074/jbc.M112.440503

Zhang, D., Isack, N. R., Glodowski, D. R., Liu, J., Chen, C. C.-H., Xu, X. Z. S., et al. (2012). RAB-6.2 and the retromer regulate glutamate receptor recycling through a retrograde pathway. *J. Cell Biol.* 196 (1), 85–101. doi: 10.1083/jcb.201104141

frontiers | Frontiers in Plant Science

TYPE Original Research
PUBLISHED 07 July 2023
DOI 10.3389/fpls.2023.1204889

OPEN ACCESS

EDITED BY
Cecilia Rodriguez-Furlan,
Washington State University, United States

REVIEWED BY
Arif Ashraf,
University of Massachusetts Amherst, United States
Mariana Romeiro Motta,
Université de Lyon, France
Xiaohui Li,
Purdue University, United States

*CORRESPONDENCE
Carolyn G. Rasmussen
crasmu@ucr.edu

†PRESENT ADDRESS
Anne W. Sylvester,
Marine Biological Laboratory, University of Chicago, Woods Hole, MA, United States

RECEIVED 12 April 2023
ACCEPTED 24 May 2023
PUBLISHED 07 July 2023

CITATION
Allsman LA, Bellinger MA, Huang V, Duong M, Contreras A, Romero AN, Verboonen B, Sidhu S, Zhang X, Steinkraus H, Uyehara AN, Martinez SE, Sinclair RM, Soriano GS, Diep B, Byrd V. D, Noriega A, Drakakaki G, Sylvester AW and Rasmussen CG (2023) Subcellular positioning during cell division and cell plate formation in maize. *Front. Plant Sci.* 14:1204889. doi: 10.3389/fpls.2023.1204889

Subcellular positioning during cell division and cell plate formation in maize

Lindy A. Allsman[1], Marschal A. Bellinger[1], Vivian Huang[1], Matthew Duong[1], Alondra Contreras[1], Andrea N. Romero[1], Benjamin Verboonen[1], Sukhmani Sidhu[1], Xiaoguo Zhang[2], Holly Steinkraus[2], Aimee N. Uyehara[1], Stephanie E. Martinez[1], Rosalie M. Sinclair[3], Gabriela Salazar Soriano[1], Beatrice Diep[1], Dawson Byrd V.[1], Alexander Noriega[1], Georgia Drakakaki[3], Anne W. Sylvester[2†] and Carolyn G. Rasmussen[1*]

[1]Department of Botany and Plant Sciences, Center for Plant Cell Biology, University of California, Riverside, Riverside, CA, United States, [2]Department of Molecular Biology, University of Wyoming, Laramie, WY, United States, [3]Department of Plant Sciences, University of California, Davis, Davis, CA, United States

Introduction: During proliferative plant cell division, the new cell wall, called the cell plate, is first built in the middle of the cell and then expands outward to complete cytokinesis. This dynamic process requires coordinated movement and arrangement of the cytoskeleton and organelles.

Methods: Here we use live-cell markers to track the dynamic reorganization of microtubules, nuclei, endoplasmic reticulum, and endomembrane compartments during division and the formation of the cell plate in maize leaf epidermal cells.

Results: The microtubule plus-end localized protein END BINDING1 (EB1) highlighted increasing microtubule dynamicity during mitosis to support rapid changes in microtubule structures. The localization of the cell-plate specific syntaxin KNOLLE, several RAB-GTPases, as well as two plasma membrane localized proteins was assessed after treatment with the cytokinesis-specific callose-deposition inhibitor Endosidin7 (ES7) and the microtubule-disrupting herbicide chlorpropham (CIPC). While ES7 caused cell plate defects in *Arabidopsis thaliana*, it did not alter callose accumulation, or disrupt cell plate formation in maize. In contrast, CIPC treatment of maize epidermal cells occasionally produced irregular cell plates that split or fragmented, but did not otherwise disrupt the accumulation of cell-plate localized proteins.

Discussion: Together, these markers provide a robust suite of tools to examine subcellular trafficking and organellar organization during mitosis and cell plate formation in maize.

KEYWORDS

mitosis, maize, cell plate, phragmoplast, microtubule

Introduction

Division is an essential step in cell proliferation and contributes to plant development. The proper re-organization of the cytoskeleton, organelles, and endomembrane networks are essential for cell division. Before plant cells divide, chromosomes are duplicated while cells often reach a size threshold minimum (Sablowski, 2016; Jones et al., 2017; D'Ario et al., 2021). The nucleus also migrates towards the future division plane and influences the positioning of subsequent mitotic cytoskeletal structures (Facette and Smith, 2012; Wada, 2017; Facette et al., 2019). In addition to interphase microtubules and the mitotic spindle, plants have two additional microtubule structures: the preprophase band (PPB) and the phragmoplast. The PPB comprises a ring of microtubules, and actin filaments that accumulate at the cell cortex before mitosis (Pickett-Heaps and Northcote, 1966). Many proteins additionally co-localize with the PPB, including microtubule-binding proteins (Van Damme et al., 2004). The PPB is not required for divisions, but when formed, it accurately predicts the future division site in many land plant divisions (Rasmussen and Bellinger, 2018; Livanos and Müller, 2019). The location of the PPB is just under the plasma membrane, known as the cortical division zone (Van Damme and Geelen, 2008; Smertenko et al., 2017). In telophase, the phragmoplast, a microtubule and microfilament structure, forms from spindle remnants (Lee and Liu, 2013; Smertenko, 2018). The phragmoplast directs formation of the cell plate during cytokinesis (Gu and Rasmussen, 2022; Sinclair et al., 2022). Cell plate assembly requires movement of vesicles along the phragmoplast, as well as vesicle fusion in the phragmoplast midline (Jürgens et al., 2015; Müller and Jürgens, 2016).

Cellular functions, such as chromosome separation during mitosis and formation of the new cell wall during cytokinesis, depend on proper regulation of microtubule dynamics. Microtubule dynamics are modulated by microtubule-associated proteins (MAPs) (Hashimoto, 2015). A subset of functionally diverse MAPs that bind to the plus end of microtubules are called plus-end-tracking proteins. The conserved eukaryotic protein END-BINDING PROTEIN (EB1) is a microtubule-plus-end tracking protein that binds growing microtubule ends, interacts with other proteins, and stabilizes the plus end (Van Damme et al., 2004; Nehlig et al., 2017). In *Arabidopsis thaliana*, EB1 localizes to microtubule plus ends and accumulate in mitotic structures (Chan et al., 2003; Mathur et al., 2003; Dixit et al., 2006; Bisgrove et al., 2008; Komaki et al., 2010).

A critical change that occurs before the onset of mitosis is the movement of the nucleus either to the middle of the cell for a symmetric division or towards one side of the cell during asymmetric division. Premitotic nuclear positioning in *A. thaliana* stomatal precursor cells depends on microtubules (Muroyama et al., 2020). In contrast, actin filaments, but not microtubules, are essential for premitotic nuclear migration of the first division of the *A. thaliana* zygote (Kimata et al., 2016). Actin-based nuclear movement also occurs prior to asymmetric divisions during stomatal development in maize (Kennard and Cleary, 1997). Nuclear migration is partially dependent on the interaction of actin with a protein in the linker of nucleoskeleton and cytoskeleton (LINC) complex in *A. thaliana* called SINE2 and in maize called MAIZE LINC KASH SINE-LIKE2 (MLKS2) (Gumber et al., 2019b), (Zhou et al., 2014). In maize, *mlks2* mutants have asymmetric division defects (McKenna et al., 2021) due to defective nuclear positioning that causes defects in PPB positioning (Arif Ashraf et al., 2022). A typical live cell marker used to explore nuclear dynamics and chromosome movement in *A. thaliana* is HISTONE2B fused to Yellow Fluorescent Protein (H2B:YFP) (Boisnard-Lorig et al., 2001). In maize, HISTONE2B fused to m-Cherry labels chromosomes in mitotic, interphase, and meiotic cells (Howe et al., 2012). The HISTONE1.1-YFP marker described below allows additional flexibility in combination with other fluorescent marker lines.

The nuclear envelope can be visualized by the localization of RAN GTPase activating Protein1 (RANGAP1). RANGAP increases RAN GTPase activity to generate the inactive GDP-bound form. In *A. thaliana*, RANGAP1 (AT3G63130) localizes to the division site throughout mitosis and cytokinesis (Xu et al., 2008). RANGAP1 performs essential GAP functions redundantly with RANGAP2 (Xu et al., 2008). The GAP activity of RANGAP1 is essential while its localization to mitotic structures and the division site is dispensable (Boruc et al., 2015). In contrast to continuous localization of RANGAP1 in *A. thaliana* at the division site, in onion cells, RANGAP1 is localized just below the PPB towards the cytoplasmic side. Further, onion RANGAP1 is not retained at the division site during the transition to metaphase (Yabuuchi et al., 2015).

During metaphase, the dynamic movement of organelles and subcellular structures promotes their proper segregation into daughter cells. The spindle assembles after nuclear envelope breakdown in metaphase (Dixit and Cyr, 2002) and chromosomes are separated in anaphase. On entry into metaphase, the endoplasmic reticulum (ER) dynamically reorganizes to the spindle poles, observed both using electron microscopy (Porter and Machado, 1960) and confocal microscopy of live cells with ER-retained HDEL-GFP (Nebenführ et al., 2000; Gupton et al., 2006). During division, ER organization is thought to be mediated by microtubules, whereas in interphase cells, plant ER organization primarily depends on interactions with actin microfilaments (Zachariadis et al., 2003; Gupton et al., 2006). Two highly conserved proteins that label the ER are PROTEIN DISULFIDE ISOMERASE1 (PDI1) and GLOSSY8. PDI1 plays a crucial role in mediating disulfide bond formation required for proper protein folding within the ER lumen (Li and Larkins, 1996). In contrast, GLOSSY8 is a beta-ketoacyl reductase enzyme required for cuticular wax synthesis found within ER membrane fractions (Xu et al., 1997; Xu et al., 2002). These proteins label the ER lumen and ER membrane, respectively.

During cytokinesis, plasma membrane localized proteins are sometimes localized at the cell plate, potentially to aid partitioning into the plasma membrane after cytokinesis is completed. Two examples that localize to the cell plate are the related auxin efflux transporters PINFORMED1 (PIN1) and PIN2 in Arabidopsis. PIN1 localizes to the cell plate where it interacts with DYNAMIN RELATED PROTEIN1A (DRP1A) (Mravec et al., 2011). Similarly, Arabidopsis PIN2 localizes to the cell plate during late

telophase (Men et al., 2008). In maize, two related kinase-dead receptor-like kinases have varied accumulation at the cell plate: PANGLOSS1 (PAN1) localizes to the cell plate, while another unrelated receptor-like kinase, PAN2, does not accumulate in the cell plate (Sutimantanapi et al., 2014). Together, this suggests that cell plate accumulation is a common, but not default localization, for plasma membrane proteins. PLASMA MEMBRANE INTRINSIC PROTEIN2 (PIP2), a protein that mediates water transport, localizes to the plasma membrane in maize (Zelazny et al., 2007; Berny et al., 2016; Martinez et al., 2018), but little is known about PIP2 localization during cytokinesis.

Other proteins that localize to the cell plate are essential for cell plate formation. These include SNARE proteins that facilitate vesicle docking and fusion. Mutations in genes that disrupt cell plate formation lead to defects in cytokinesis that result in lethality or tiny club-shaped seedlings (Söllner et al., 2002; Gillmor et al., 2016). KNOLLE is a cytokinesis-specific syntaxin that localizes to the cell plate during telophase (Lukowitz et al., 1996; Lauber et al., 1997). KNOLLE accumulates in small motile particles starting in late G2 as it is trafficked through the ER, the Golgi, and the Trans-Golgi Network (TGN) towards the cell plate (Reichardt et al., 2007; Karnahl et al., 2017). Once it localizes to the cell plate, KNOLLE forms SNARE complexes with the syntaxin regulator KEULE to promote proper fusion of Golgi-derived vesicles containing cargo used to construct the cell plate (Waizenegger et al., 2000). KNOLLE is recycled into vacuoles at the end of cytokinesis (Reichardt et al., 2007).

Another class of proteins, small GTPases in the Rab (Rat sarcoma (Ras) in brain, Rab) superfamily, play critical roles in vesicle transport and tethering throughout the endomembrane system and often localize to the forming cell plate (Elliott et al., 2020). The RAB-GTPases used in this study are RAB1A, RAB2A and RAB11D. Maize *RAB1A* is most closely related to *AtRABD2a* (Zhang et al., 2007; Okekeogbu et al., 2019), which is involved in ER to Golgi transport (Rutherford and Moore, 2002). The maize *RAB2A* was named to reflect its similarity to the yeast homolog *RAB2*. The closest homolog of maize *RAB2A* in *A. thaliana*, *RABB1c/RABB1*^{b}, encodes a protein that co-localizes with the Golgi, but does not label the cell plate (Rutherford and Moore, 2002; Chow et al., 2008). Maize RAB2A is enriched in the Golgi fraction (Okekeogbu et al., 2019), however its subcellular localization using microscopy has not been determined. The two RAB-GTPases most closely related to maize RAB11D are *AtRABA4d* and *AtRABA4a*, which have specific roles in polarized growth in pollen tubes and root hairs, respectively. RABa4d localizes towards the growing tip in motile particles. *raba4d* mutant pollen tubes grow abnormally, have reduced pectin accumulation, and result in reduced fertility *via* improper pollen tube guidance (Szumlanski and Nielsen, 2009; Zhou et al., 2020). In Arabidopsis and tobacco, the *RAB11D* homologs encode proteins that localize to the TGN where the proteins are organized and packaged in preparation for delivery through the cell (Dunkley et al., 2006; Toyooka et al., 2009). In maize, RAB11D is enriched in the Golgi fraction, but its localization during division is unknown (Okekeogbu et al., 2019).

Here we characterize the localization of proteins and organelles during maize cell division using confocal microscopy and disruption of cell plate formation using two chemicals with distinct activities. Since these images were taken using confocal microscopy, we acknowledge that spatial resolution is limited. The well-described live cell microtubule marker lines (YFP-TUBULIN and CFP-TUBULIN) were imaged together with proteins that label microtubule plus ends, chromosomes, the ER, the plasma membrane, and the cell plate. We show that the ER aligns with mitotic structures. RAB-GTPases are required for vesicle-target docking, and the cytokinesis-specific syntaxin KNOLLE is required for vesicle fusion. Several RAB-GTPases and KNOLLE localize to the cell plate and motile particles. We incubated maize leaves with Endosidin 7 (ES7), a chemical that inhibits cytokinesis-specific callose deposition in Arabidopsis (Park et al., 2014) and disrupts cytokinesis in algae (Davis et al., 2020). ES7 pulse treatments did not affect accumulation of cell plate localized proteins or disrupt cell plate morphology in maize. Longer 5-day ES7 incubation did not cause obvious cell plate defects in maize roots. Maize epidermal cells were also treated with chlorpropham (CIPC), a herbicide that disrupts microtubules. CIPC treatment generated multiple phragmoplasts and fragmented the cell plate but did not typically alter protein accumulation at the cell plate. Together, these data provide a framework for understanding dynamic movement of organelles and proteins during mitosis and cytokinesis.

Materials and methods

Maize plants were grown in 2-quart pots in standard greenhouse conditions (temperature setpoint between 31 - 33 C) with supplementary lighting ~400 μE m^{-2} s^{-1} from 1000Watt high pressure sodium bulbs (Gravita Pro Plus 1000W). Plants were grown for three to five weeks from seeds. Maize transgenic plants were identified by painting the leaf with 0.4% glufosinate (Basta Finale) in 0.05% tween or by genotyping using specific primers, listed in Supplementary Table 1. Leaf tissue was ground using a TissueLyser (Qiagen) for DNA extractions and PCR was performed using MyTaq (Bioline) or KOD Hot Start polymerase (EMD Millipore) according to manufacturer's conditions supplemented with 7% (vol/vol) DMSO.

Microscopy was performed using an Eclipse TE inverted stand (Nikon) with a W1 spinning disk (Yokagawa), EM-CCD camera (Hamamatsu 9100c), standard solid-state lasers (Obis from 40 mW to 100 mW), and an ASI Piezo stage controlled with micromanager software (www.micromanager.org) built by Solamere Technology. Standard emission filters were used (Chroma Technology). For YFP–TUBULIN, PDI-YFP, YFP-KNOLLE, RANGAP-YFP, PIN1A-YFP, RAB1A-YFP, and RAB11D-YFP, a 514 nm laser with emission filter 540/30 was used. For CFP–TUBULIN, RAB1A-CFP, PIP2a-CFP, and aniline blue-stained samples, a 445 nm laser with emission filter 480/40 was used. For EB1-mCherry and GLOSSY8-RFP, a 561 nm laser with emission filter 620/60 was used. A 100X oil immersion lens (1.48 NA) was used with

immersion oil (Type FF, Cargille) for leaf epidermal tissue and a 40X oil immersion lens (1.15 NA) was used with immersion oil (Series AAA 1.330 Refractive Index Liquid, Cargille) for root imaging.

Time-lapse and other imaging experiments were performed using a Rose chamber or glass slides, vacuum grease, and coverslips with a temperature between 20 - 22°C (Rasmussen, 2016). Three to five-week-old maize plants were used and leaves were removed until the ligule height was < 2 mm, and abaxial symmetrically dividing leaf epidermal samples were imaged. While imaging PIN1-YFP, the developing ligule was selected for imaging, as described (Neher et al., 2023). Samples were mounted in water. Mitotic structures were identified using a live cell marker for microtubules (either CFP-TUBULIN or YFP-TUBULIN) as previously described (Mohanty et al., 2009). Drift in the time lapse was corrected using the StackReg tool in FIJI (ImageJ) using the translation option (Thévenaz, 1998). Time intervals of 2.5 and 3 seconds were used for EB1-mCherry and YFP-TUBULIN microtubule time lapse imaging respectively. Kymographs were generated using Fiji's Multi-kymograph tool to track EB1-mCherry particles and microtubules (Zanic, 2016). Mann-Whitney *U* test (GraphPad Prism) was used for statistical analysis for graphs in Figure 1.

Time intervals of 1 to 4 seconds were used to capture YFP-KNOLLE, RAB11D-YFP, RAB1A-CFP, and RAB2A-YFP particle trafficking. Initial imaging intervals of 4 seconds were used and then changed to 1 and 2 second intervals for more efficient particle tracking. Time intervals: YFP-KNOLLE: 2 and 4 seconds, RAB11D-YFP: 2 and 3 seconds, RAB1A-CFP: 2 seconds, RAB2A-YFP: 1 and 2 seconds. 30-118 seconds timelapses were used for particle tracking. Particles were tracked with the FIJI plugin Mosaic with the following parameters: kernel radius = 2.0, cutoff radius = 0.2, percentile = 0.5, displacement = 10, link range = 2 and Brownian Motion (Sbalzarini and Koumoutsakos, 2005). The particle coordinates were exported onto Excel or Google Sheets and converted from pixels to microns. The slope of the particle movement between frames was calculated using the slope formula

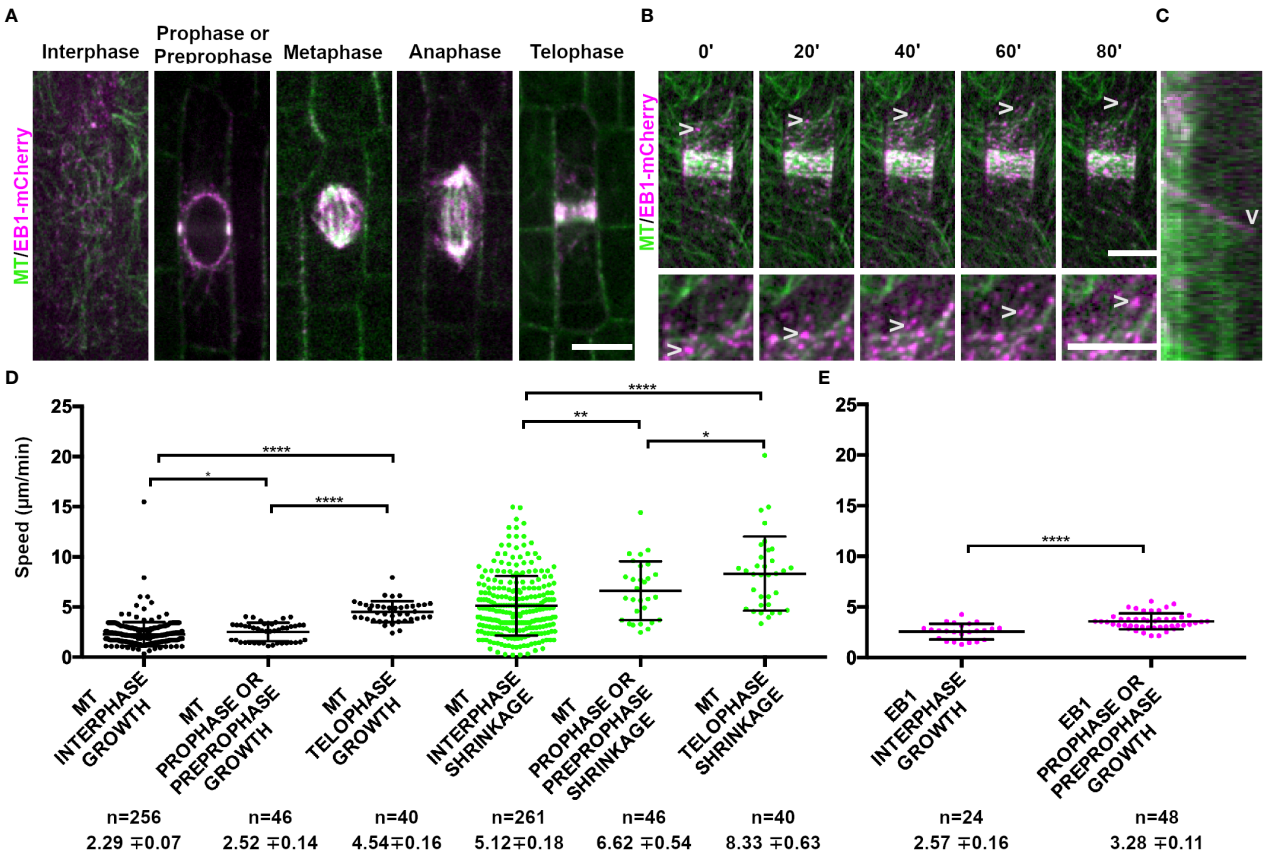

FIGURE 1
Microtubule binding protein END BINDING1 (EB1-mCherry) localizes to microtubule plus-ends and extensively co-localizes with YFP-TUBULIN during mitosis. Microtubules (false-colored green) from the abaxial side of maize leaves in regions with symmetrically dividing cells were imaged with YFP-TUBULIN and EB1 is false-colored magenta. **(A)** EB1-mCherry labels the plus-end of growing microtubules. **(B)** Timelapse of a cell in prophase. Arrowheads mark the EB1-mCherry protein. Zoom images of a prophase cell to visualize EB1. Arrowheads point at EB1-mCherry as the microtubule grows in the timelapse. Background subtraction was used in FIJI. Scale bars are 10µm. **(C)** Kymograph of EB1-mCherry protein tracking plus-end of microtubule. EB1-mCherry disappears followed by microtubule shrinkage (arrowhead). **(D)** Microtubule growth and catastrophe speed (µm/min) in wild-type maize leaf epidermal cells from 4 plants in interphase (n = 29 cells), prophase and preprophase (n = 2 cells) and telophase cells (n = 2 cells). **(E)** EB1 particle speed (µm/min) in wild-type maize leaf epidermal cells from 2 plants in interphase (n = 7 cells) and pre-prophase and prophase cells (n = 10 cells). P-values * < 0.05, ** < 0.01, **** < 0.0001 by Mann-Whitney *U* test.

($m = (y_2-y_1)/(x_2-x_1)$) before taking the absolute value of all the numbers. The values were then divided by the interval of the time lapse (in seconds) to account for the time elapsed between each frame. Afterwards, the speeds were averaged to generate an average speed of that particle. The particle speeds between non-telophase and telophase stages within the same marker and across markers were compared using a t-test with the Bonferroni correction.

Fluorescence intensity of YFP-KNOLLE, RAB11D-YFP, RAB2A-YFP and RAB1A-CFP was measured using a set ROI in Fiji based on the size of the smallest particle, a RAB2A particle. To avoid the photobleached parts of the time lapse or changes in the intensity, measurements were only taken from one frame per image. Five sets of data points were measured in different parts of the cell, including the background, cell plate, and particles found in dividing and non-dividing cells, respectively, and then averaged. The average of the cell plate or particle was subtracted from the average of the background, respectively. A log of the ratio of the cell plate and particle fluorescence intensities was generated to determine whether the cell plate or the particles had stronger fluorescence intensity.

For maize pulse-treatment with CIPC and Endosidin 7 (ES7), matched samples were used in which one side of each leaf (from the midrib) was incubated with the treatment, while the other side was incubated with a corresponding amount of DMSO. For CIPC treatments, 4-week-old plants were used, and dissections were taken from symmetrically dividing leaf blades where the ligule was less than 2 mm in height. Leaf sections were then placed in a coverslip with either 20 µL of 0.02% DMSO or 2 µM CIPC for 2-4 hours at room temperature (~21 °C). For treatment with ES7, 1 mM ES7 was used, and matched negative control samples were incubated with DMSO (2%). Samples were then loaded into a Rose Chamber and the abaxial side was imaged.

To measure the long-term effect of ES7 on maize roots, maize kernels were germinated for 5 days between two layers of germination paper soaked in 50 ml of 0.02% DMSO (negative control) or 10 µM ES7 in 6-quart bins (Sterilite). Three technical replicates were done, where one secondary root was chosen from 4 plants for each treatment. Secondary roots were imaged because primary roots were too thick to effectively image. Roots were stained for 5 minutes in propidium iodide (10µg/mL, Fisher Scientific) and loaded into a Rose chamber for imaging using a 40X objective (NA = 1.15).

For *Arabidopsis thaliana* ES7 treatments, wild-type (Col-0/Ws) seeds were sterilized with chlorine gas for 2 h at room temperature (~21°C) (Lindsey et al., 2017). ¼ strength MS media (Murashige and Skoog, 1962), 1% sucrose, pH 5.7, 0.8% (w/v) agar plates with either no treatment, 10 µM in 0.02% DMSO Endosidin7, or 0.02% DMSO, were used. Plants were placed in the dark for 2 days at 4 °C and then moved to the light for 5 days at 21 °C. After staining for 1 minute in propidium iodide (10 µg/mL), seedling roots were imaged using a Rose chamber and 40x objective in 20 µl H_2O. To measure root lengths of ES7 and DMSO treated samples, 40 plants per treatment from two separate replicates were measured using the segmented line tool in FIJI. Datapoints were pooled after determining that there was no significant difference between replicates using Mann-Whitney *U* test. Pulse treatments were done using wild-type plants (Col-0/Ws) with CFP-TUBULIN grown on ¼ MS plates for 5 days with no treatment, then transferred into 2 ml of ¼ MS with either 50 µM ES7 or 0.1% DMSO treatment for 2 hours. After staining for 30 minutes in FM4-64 (2 µM), 3 replicates of 3-4 seedling roots were imaged. Three different cell plate morphologies were observed: normal, gap (gaps in the cell plate), and stub (when the cell plate is incomplete).

To assess the accumulation of callose in cell plates during pulse treatments, four day old Arabidopsis Col-0 seedlings were treated with 50 µM ES7 (ChemBridge Corporation, San Diego, CA, USA) in 0.1% DMSO in ¼ Murashige and Skoog (MS) liquid medium, or 0.1% DMSO in ¼ MS liquid medium for two hours (Park et al., 2014) and imaged as described below. For FM4-64 imaging, 4-d-old seedlings were incubated for 5 min in the dark with ¼ MS medium supplemented with 2 µM FM4-64, followed by a quick washing step in FM4-64–free medium (Rigal et al., 2015; Rosquete et al., 2019). Callose staining was performed in 0.03 mg/mL dilution of Aniline Blue fluorochrome in water for 3-5 minutes (Biosupplies, Melbourne, Australia), washed once in water, and directly imaged (Davis et al., 2020). A Zeiss LSM 980 Airyscan 2 was used in Airyscan Fast mode (SR8Y) to image root cells co-stained with Aniline Blue and FM4-64 following chemical treatment. For multicolor imaging, the sequential line-scanning mode was employed. Fluorescent signal of FM4-64 was excited using a 488 nm laser and emission was collected above 493 nm using a plate as SBS. Aniline blue fluorochrome was excited with a 405 nm laser and emission was collected with a SP 550 nm SBS. The Airyscan GaAsP-PMT detector was used with an offset set of 0, a detector gain of 850V and a digital gain of 1.0. All images were collected using the LD LCI Plan -Apochromat 40X/1.2 Imm Korr M27 objective. Z-stacks were collected using bidirectional scanning.

To assess the accumulation of callose in maize, callose staining was performed as described (Zavaliev and Epel, 2015). CIPC, ES7, or DMSO treated samples that were imaged for either YFP-KNOLLE or RAB11D-YFP were subsequently fixed in 96% ethanol for three hours. Samples were rehydrated in deionized water for 30 minutes. Samples were then stained with 0.01% aniline blue by vacuum infiltration (-30 kPa for 10 minutes), then incubated at room temperature in the dark for two hours. Tiled imaging was used to sample evenly and to prevent bias. Samples treated with either CIPC, ES7 or DMSO were imaged to 1) observe the presence of callose in cell plates and 2) observe the morphology of the cell plate present in the samples. Three different cell plate morphologies were observed: normal, stub (when the cell plate is incomplete), and split (a cell plate with multiple ends).

The EB1-mCherry construct was assembled using triple template PCR (KOD hot start, Sigma Aldrich) to generate the full genomic sequence (primers ZmEB1A_3GWp1.3: GGGGACAAGTTTGTACAAAAAAGCAGGCTCAGAG CACAGGCAAGAGTGG and ZmEB1A_3GWp4 GGG GACAACTTTGTATAGAAAAGTTGGGTG CTCGGTTTCATTTGAGAACAAGC, and ZmEB1A_3GWp3 GGGGACAACTT GTATAATAAAGTTGAGTGAGA TGTGCGGCTACATGA and ZmEB1A_3GWp2 GGGG ACCACTTTGTACAAGAAAGCTGGGTAGAAAGC CGTATTGGCATCAC) with the m-Cherry insert (in pDONR P3r-P4r) at the C terminal end, flanked by linker peptides to minimize

folding interference. The PCR products were cloned using the Gateway system (Gateway LR Clonase II Plus, Invitrogen) into the donor vectors, pDONR P1-P4 and pDONR P3-P2.

YFP-KNOLLE was generated by a 939-bp genomic DNA fragment including the entire KNOLLE coding region and 5.7 kb of 5′ sequence amplified from B73 genomic DNA with primers KNOLLE-3GWp1 (Primer sequence = GGGGACAAG TTTGTACAAAAAAGCAGGCTCAGAGAGGAGGTGACC AAGC) and Knolle-3GWp4 (Primer sequence = GGGGA CAACTTTGTATAGAAAAGTTGATCCAAATCTACAACC GGCAGG). A 305-bp fragment immediately 3′ of the KNOLLE coding region was amplified from B73 genomic DNA with KNOLLE-3GWp3 (Primer sequence = GGGGACAACTT GT ATAATAAAGTTGATGAACGACCTCATGACCAAGT CCTTCATGAGC) and KNOLLE -3GWp2 (Primer sequence = GGGGACCACTTTGTACAAGAAAGCTGGGTATCCAGTGA TCGGCACTATG). Citrine variant YFP was amplified as described previously (Mohanty et al., 2009). These three fragments were assembled in pDONR221 (Invitrogen) to insert YFP in frame with KNOLLE at its N terminus with the 3′ KNOLLE flanking sequence downstream using a MultiSite Gateway three-fragment vector (Invitrogen) following the manufacturer's instructions. Both EB1-mCherry and YFP-KNOLLE constructs were recombined into the binary vector pAM1006 (Mohanty et al., 2009), transformed into *Agrobacterium tumefaciens* strain EHA101 and transformed into maize A188/B73 hybrid embryo callus by the Iowa State Plant Transformation Facility. Transformed plants were crossed into the inbred line B73.

Results

The conserved microtubule plus end localized protein, END-BINDING1 (EB1; Zm00001eb068860), fused to a monomeric red fluorescent protein (EB1-mCherry), localized to all mitotic structures (Figure 1A) and labeled microtubule plus ends (arrowheads, Figure 1B). For additional information about genes, including likely orthologs in Arabidopsis, predicted or known localization, and additional references, see Table 1. As expected, EB1-mCherry localization tracked the microtubule plus end, but was lost when the microtubule started shrinking (Figure 1C). Interestingly, both microtubule growth and shrinkage speeds increased from interphase (growth = 2.29 ± 0.07 μm/min standard deviation (SD), n = 256 microtubules; shrinkage = 5.12

TABLE 1 The gene name and ID used in this study and the putative Arabidopsis ortholog, and references.

Gene name and ID	Putative Arabidopsis orthologous gene id	Predicted or known localization and function	Reference
END BINDING1, Zm00001eb068860 GRMZM5G824964	*EB1a* AT3G47690	Microtubule plus ends. Stabilizes microtubules and to mediates interactions with other microtubule binding proteins.	(Chan et al., 2003; Mathur et al., 2003; Van Damme et al., 2004; Dixit et al., 2006; Bisgrove et al., 2008; Komaki et al., 2010)
HISTONE1.1, Zm00001d034479 GRMZM2G164020	*HISTONE1.2* AT2G30620	Chromosomes. Linker histone H1a, interacts with ZmSUN2 by IP/MS.	(Boisnard-Lorig et al., 2001; (Gumber et al., 2019a)
RANGAP1, Zm00001d051112 GRMZM2G079817	*RANGAP1* AT3G63130	Nuclear envelope, division site. GTPase activating protein for RAN monomeric GTPase.	(Xu et al., 2008; Yabuuchi et al., 2015)
GLOSSY8, Zm00001eb246270	*KCR1* AT1G67730	Endoplasmic reticulum membranes. Very long chain fatty acid production, beta-ketoacyl reductase.	(Xu et al., 1997; Xu et al., 2002; Dunkley et al., 2006; Kirienko et al., 2012; Okekeogbu et al., 2019)
PDI1, Zm00001eb168910, GRMZM2G091481	*PDI1* AT1G21750	Endoplasmic reticulum lumen. Isomerase.	(Li and Larkins, 1996; Dunkley et al., 2006; Kirienko et al., 2012)
KNOLLE, Zm00001d033919	*KNOLLE* AT1G08560	Cell plate. Syntaxin, SYP111.	(Lukowitz et al., 1996)
RAB11D, Zm00001d028002 GRMZM2G164527	*RABA4a* AT5G65270	TGN, post-Golgi vesicles, plasma membrane. Monomeric GTPase involved in vesicle trafficking.	(Vernoud et al., 2003; Dunkley et al., 2006; Szumlanski and Nielsen, 2009; Okekeogbu et al., 2019)
RAB1A, Zm00001d017456; GRMZM2G097746	*RABD2a* AT1G02130	Membranous particles distinct from FM4-64 in Arabidopsis. Required for pollen tube growth.	(Peng et al., 2011; Okekeogbu et al., 2019)
RAB2A, Zm00001eb080090 GRMZM2G330430	*RABB1C or RABB1*[b] AT4G17170	Golgi localization, does not localize to the cell plate in Arabidopsis.	(Chow et al., 2008; Okekeogbu et al., 2019)
PIP2-1, Zm00001eb306380	*PIP2;4* AT5G60660	Localizes to the plasma membrane in maize. Aquaporin, water transport.	(Zelazny et al., 2007; Berny et al., 2016; Martinez et al., 2018)
PIN1, Zm00001eb372180	*PIN1* AT1G73590	Auxin efflux transporter, localizes to the plasma membrane.	(Mravec et al., 2011)

± 0.18 μm/min SD, n = 261 microtubules, 4 plants each) to prophase (growth = 2.52 ± 0.14 μm/min SD, n = 46 microtubules; shrinkage = 6.62 ± 0.54 μm/min SD, n = 46 microtubules, 2 plants each) to telophase (growth = 4.54 ± 0.16 μm/min SD, n = 40 microtubules; shrinkage = 8.33 ± 0.63 μm/min SD, n = 40 microtubules, 2 plants, Figure 1D). Similar increases in EB1-mCherry particle movement was also detected between interphase (2.57 ± 0.16 μm/min SD, n = 24 microtubules, 3 plants) and prophase (3.58 ± 0.11 μm/min SD, n = 48 microtubules, 3 plants, Figure 1E). We were unable to assess EB1-mCherry dynamics in metaphase or anaphase because the EB1-mCherry particle density was too high in the spindle to clearly track. Together, this suggests that EB1 dynamics are similar to microtubule dynamics, and that microtubule dynamicity increases as the cell progresses through mitosis, similar to observations in tobacco cultured cells (Vos et al., 2004).

We next examined chromosome movement during mitosis using the chromosome binding protein HISTONE1.1 fused to a yellow fluorescent protein (HISTONE1.1-YFP, Zm00001e006785). HISTONE1.1-YFP localized to the nucleus during interphase (n ≥ 100 cells, 2 plants) and prophase (n = 24 cells), specifically labeling chromosomes (Figure 2A). As expected, chromosomes accumulated at the metaphase plate (n = 10 cells), were separated during anaphase (n = 9 cells) and were in the nucleus when the nuclear envelope re-formed during telophase (n = 14 cells). The HISTONE1.1-YFP signal intensity varied extensively and was sometimes too faint to image clearly in mitotic cells. However, the location of chromosomes and nuclei can be inferred from other marker lines described below.

The nuclear envelope protein RANGAP1 fused to YFP (RANGAP1-YFP, Zm00001d051112) labeled the nuclear envelope and the cell periphery during most cell cycle stages in maize epidermal leaves (Figure 2B), as previously described (Wu et al., 2013; Arif Ashraf et al., 2022). During preprophase or prophase, RANGAP1-YFP uniquely labeled the region directly adjacent to the PPB away from the plasma membrane. RANGAP1-YFP labeled all mitotic structures as well (Figure 2B). During late G2 (preprophase) and prophase, RANGAP1-YFP localized close to the PPB, slightly offset towards the cytoplasmic side (91%, n = 43/47 cells from 2 plants, Supplementary Figure 1). Further, RANGAP1-YFP always labeled the nuclear envelope during interphase, preprophase, and prophase. After nuclear envelope breakdown, RANGAP1-YFP no longer labeled the cortical division zone, but consistently co-localized with the entire metaphase spindle (n = 13 cells), the anaphase spindle (n = 4 cells) and the phragmoplast (n = 23 cells). This localization pattern is similar to that observed with immunolocalization of RANGAP1 in onion root cells (Yabuuchi et al., 2015). Similar localization patterns within both maize and onion RANGAP1 suggests potentially conserved monocot function that may diverge from dicot RANGAP1, which localizes consistently at the division site in Arabidopsis (Xu et al., 2008).

Several proteins that label the endoplasmic reticulum (ER) accumulate near mitotic structures. To assess ER localization during mitosis, PROTEIN DISULFIDE-ISOMERASE 1 fused to

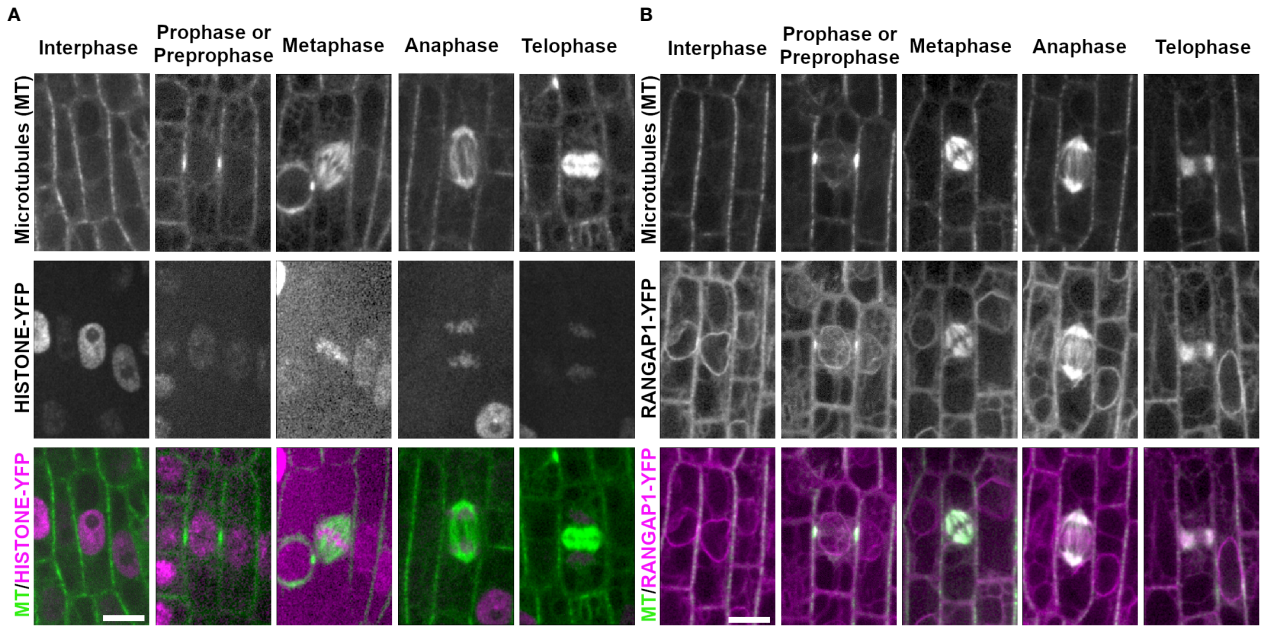

FIGURE 2
Chromosome marker HISTONE1.1-YFP and nuclear envelope marker RANGAP1-YFP with CFP-TUBULIN during the cell cycle. Microtubules from the abaxial side of maize leaves in regions with symmetrically dividing cells were imaged with CFP-TUBULIN (top row). In the merged images, microtubules are colored green, while HISTONE1.1-YFP or RANGAP1-YFP are colored magenta. **(A)** Chromosomes are labeled with HISTONE1.1-YFP (middle row). **(B)** RANGAP1-YFP labels the cell periphery, the nuclear envelope during interphase and preprophase/prophase, and localizes close to the PPB during prophase/preprophase. During mitosis, RANGAP1-YFP evenly labels all microtubule structures but is not at the division site. Preprophase/prophase RANGAP1-YFP and CFP-TUBULIN images are maximum-projections of Z stacks covering 7.5 microns to more clearly illustrate RANGAP1-YFP localization near the PPB. Scale bar is 10μm, all images are the same size.

YFP (PDI1-YFP; (Kirienko et al., 2012)), an enzyme within the ER lumen (Li and Larkins, 1996), and GLOSSY8-mRFP (Kirienko et al., 2012), an enzyme isolated from ER membranes (Xu et al., 2002), were imaged together with CFP-TUBULIN (Figure 3). In epidermal cells within the proliferative dividing zone, interphase PDI and GLOSSY8 localization appeared around the cell periphery and the nucleus, highlighting typical ER localization in this type of cell (Figure 3A, B, n = > 100 cells, 5 plants each). In premitotic and mitotic cells, PDI accumulated at the nuclear envelope when it was intact (n ≥ 100 cells). PDI1-YFP labeled a region just distal to the spindle in metaphase (n = 19 cells) and anaphase (n = 13 cells). During telophase, it accumulated near the cell plate and co-localized with the phragmoplast (n = 34 cells, Figure 3B). GLOSSY8-mRFP localized similarly to PDI1-YFP during prophase (n = 52 cells), at distal spindle regions in metaphase (n = 17 cells) and anaphase (n = 14 cells) and accumulated near the cell plate in telophase (n = 30 cells) (Figure 3A).

Next, we examined several proteins that accumulate in the cell plate, including the cell plate specific syntaxin KNOLLE fused to YFP (YFP-KNOLLE, Zm00001d033919, Figure 4A). YFP-KNOLLE accumulated only during mitosis and early G1, with undetectable fluorescence accumulation in interphase cells (n ≥ 100 cells, n = 3 plants). YFP-KNOLLE localized throughout the cell as motile particles presumably labeling TGN during prophase (n ≥ 100 cells), metaphase (n = 31 cells) and anaphase (n = 30 cells, Figure 4A). The average speed of particles from prophase to anaphase was 0.53 μm/s ± 0.41 SD (n = 9 particles from 4 plants, 8 cells, Figure 4E). During telophase, YFP-KNOLLE accumulated strongly at the cell plate (5 plants, n > 100 cells). Distinct YFP-KNOLLE particles were also observed in telophase and had an average speed of 0.69 μm/s ± 0.53 SD, (n = 21 particles from 4 plants, 12 cells, and an example of particle movement is shown in Supplementary Figure 2). Occasionally, some of these particles moved into the cell plate. YFP-KNOLLE also faintly labeled the plasma membrane in mitotic cells. This is consistent with movement and localization of KNOLLE in Arabidopsis (Reichardt et al., 2007; Boutté et al., 2010).

Two monomeric GTPases, RAB11D fused to YFP (RAB11D-YFP, Zm00001d028002) and RAB1A fused to CFP or YFP (RAB1A-CFP or RAB1A-YFP, Zm00001d017456), localized as motile particles and in the cytoplasm in both interphase (5 and 3 plants respectively, n ≥ 100 cells) and mitotic cells (prophase n = 95 cells, metaphase n = 25 cells, anaphase n = 10 cells and prophase n = 25 cells, metaphase n = 12 cells, anaphase n = 13 cells respectively), and accumulated at the cell plate during telophase (n = 143 cells and n = 19 cells respectively, Figures 4B, C). The apparent diameter of RAB11D-YFP fluorescent foci were 0.81 μm ± 0.13 SD (n = 30 particles, 3 plants). RAB11D-YFP non-telophase motile particles moved with an average speed of 0.8 μm/sec ± 0.4 μm/s SD (n = 21 particles from 19 non-telophase cells from 5 plants, Figure 4E). During telophase, the average particle speed of RAB11D-YFP was 1.10 μm/sec ± 0.64 μm/sec SD, (n = 9 particles from 6 telophase cells from 5 plants) and there was strong cell plate accumulation. RAB1A-CFP also accumulated at the cell plate although fluorescence intensity measurements suggest that it accumulates more in motile particles (Figure 4F). Motile particles of RAB1A-CFP were found scattered throughout the cells between prophase and anaphase, but RAB1A-CFP also localized to the cell plate

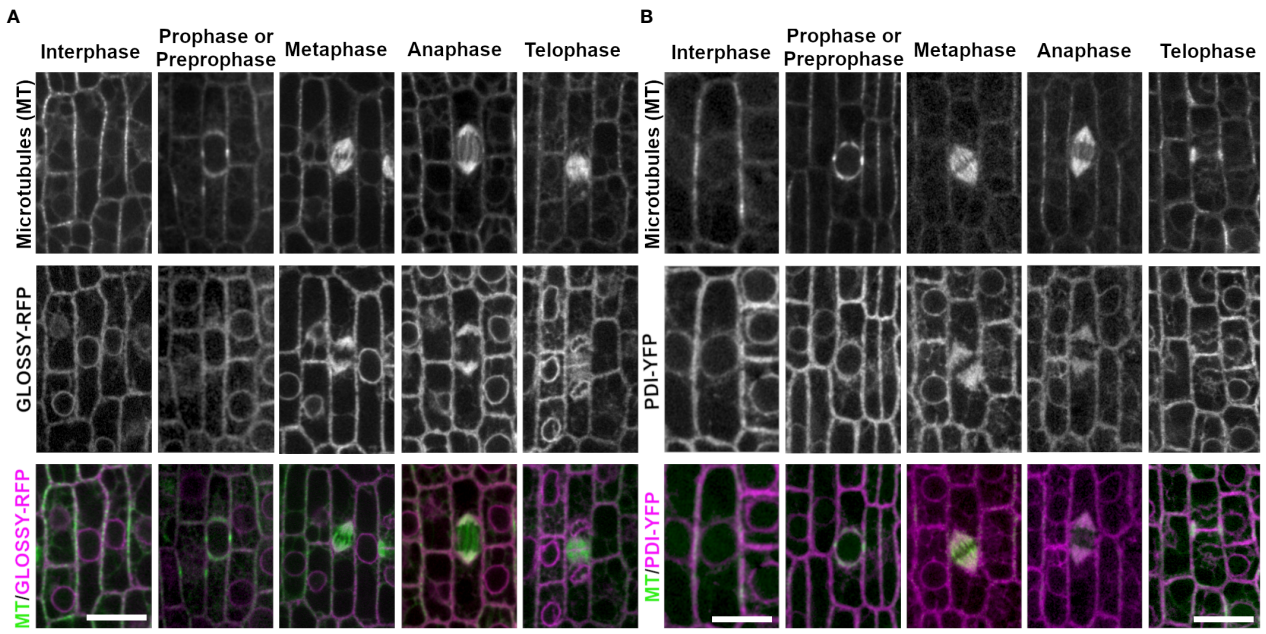

FIGURE 3
ER membrane marker GLOSSY8-mRFP and ER lumen marker PDI1- YFP with CFP-TUBULIN. Microtubules from the abaxial side of maize leaves in regions with symmetrically dividing cells were imaged with CFP-TUBULIN (top row). Microtubules are labeled green, while GLOSSY8-mRFP and PDI1-YFP are labeled magenta, in the merged photos (bottom row). **(A)** Endoplasmic reticulum membrane is labeled with GLOSSY8-mRFP. GLOSSY8-mRFP co-localizes with distal spindle regions during metaphase and anaphase. GLOSSY8-mRFP accumulates at the cell plate during telophase. **(B)** PDI1-YFP localization labels the endoplasmic reticulum lumen. PDI1-YFP localizes to distal spindle regions during metaphase and anaphase. Accumulation of PDI1-YFP is present near or in the cell plate and in the phragmoplast during telophase. Scale bar is 10μm.

10.3389/fpls.2023.1204889

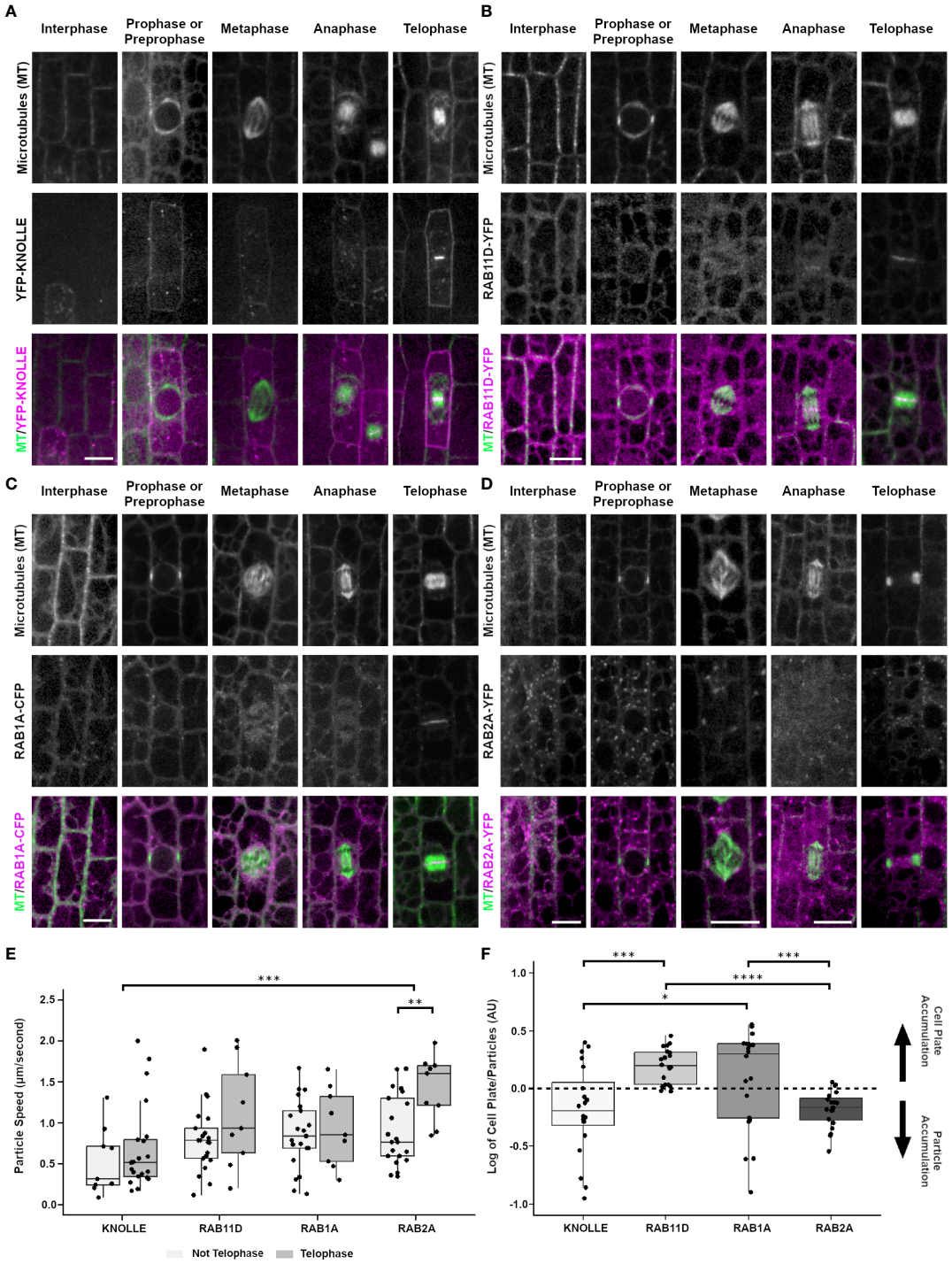

FIGURE 4
Localization of cell plate specific syntaxin KNOLLE (YFP-KNOLLE), likely trans-golgi marker RAB11D (RAB11D-YFP), vesicle tethering protein RAB1A (RAB1A-CFP), and golgi marker RAB2A (RAB2A-YFP) from the abaxial side of maize leaves in regions with symmetrically dividing cells. Microtubules (top row), marker (middle) and merged (bottom, microtubules in green and marker in magenta). Microtubules were imaged with CFP-TUBULIN in **(A, B, D)**. Microtubules were imaged with YFP-TUBULIN in **(C)**. **(A)** YFP-KNOLLE accumulates in motile particles, the plasma membrane and cell plate in mitotic cells. **(B)** RAB11D-YFP localizes as motile particles at all stages and accumulates in the cell plate. **(C)** RAB1A-CFP accumulates in motile particles and in the cell plate at telophase. **(D)** RAB2A-YFP accumulates in motile particles throughout interphase and mitosis. During telophase, RAB2A-YFP weakly accumulates in the cell plate. Scale bars for panels **(A-D)** are 10µm; if unlabeled, the micrograph has the same scale as the interphase cell. **(E)** Particle speeds of YFP-KNOLLE, RAB11D-YFP, RAB1A-CFP, and RAB2A-YFP in telophase vs. non-telophase cells. A t-test with Bonferroni Correction of the various marker comparisons shows that there are no significant differences in particle speeds in interphase cells. For dividing cells, there are no significant differences in particle speeds besides KNOLLE and RAB2A, ***$p < 0.001$, and RAB2A telophase and non-telophase cells **$p < 0.01$. **(F)** Relative fluorescence accumulation of YFP-KNOLLE, RAB11D-YFP, RAB1A-CFP and RAB2A was measured in cell plates versus in particles. 20 cell plates and 100 particles were measured for each marker from at least four plants. After determining that datasets were normally distributed (Jarque-Bera test) one-way Anova tests with the Bonferroni Correction were used to identify significant differences in relative fluorescence accumulation at the cell plate or particles between KNOLLE and RAB11D, RAB11D and RAB2A, as well as RAB1A and RAB2A. *$p < 0.05$, ***$p < 0.001$, ****$p < 0.0001$. Other comparisons had no significant differences in their fluorescence intensity log ratios.

10.3389/fpls.2023.1204889

during telophase (Figure 4C). The apparent particle diameter was measured to 0.75 μm ± 0.11 SD (30 particles analyzed from 3 plants). RAB1A-CFP particle speed averaged 0.86 μm/sec ± 0.42 SD (n = 21 particles, 21 non-telophase cells from 3 plants, Figure 4E). RAB1A-CFP particles that localized to the cell plate during telophase had an average speed of 0.94 μm/sec ± 0.47 SD (n = 9 particles, 6 telophase cells from 3 plants, Figure 4E). Only RAB2A showed significant differences in particle speeds between telophase and non-telophase cells. Comparisons within and between the markers were done using an unpaired t-test with a Bonferroni correction. Fluorescence intensity measurements of YFP-KNOLLE and RAB2A-YFP show more accumulation at the particles than at the cell plate whereas RAB11D-YFP and RAB1A-CFP show more accumulation at the cell plate (Figure 4F). A total of 20 telophase cells were measured from 5 plants with YFP-KNOLLE, 5 plants with RAB11D-YFP, 5 plants with RAB2A-YFP, 7 plants with RAB1A-CFP.

Similar to the two monomeric GTPases discussed above, the monomeric GTPase RAB2A-YFP also localized to motile particles during interphase and mitosis (4 plants, interphase n ≥ 100 cells, prophase n = 87 cells, metaphase n = 24 cells, anaphase n = 26 cells, Figure 4D). In contrast to the other RAB-GTPases, RAB2A-YFP only faintly accumulated in the cell plate during telophase (n = 59 cells, 4 plants), suggesting that RAB2A-YFP may not be directly targeted to the cell plate (Figure 4E). In non-dividing cells, RAB2A-YFP particles had an average speed of 0.91 μm/s ± 0.43 SD (n = 21 particles from 21 cells from 3 plants). During telophase, RAB2A-YFP particles had an average speed of 1.43 μm/s ± 0.40 SD (n = 9 particles, 6 cells from 3 plants).

PINIFORMED1 (PIN1) and PLASMA MEMBRANE INTRINSIC PROTEIN 2-1 (PIP2A) are both plasma membrane localized proteins that are required for transport of molecules across the plasma membrane. In all cell cycle stages examined, PIN1-YFP (3 plants, interphase, n ≥ 100 cells, prophase n = 19 cells, metaphase n = 14 cells, anaphase n = 5 cells, telophase n = 19 cells) and PIP2A-CFP (3 plants, interphase n ≥ 100 cells, prophase n = 33 cells, metaphase n = 22 cells, anaphase n = 6 cells, and telophase n = 39 cells) localized to the plasma membrane. In addition, during telophase, both PIN1-YFP and PIP2A-CFP weakly accumulated in the cell plate as compared to parental cell wall sites. Accumulation at each cell was measured as a fluorescence intensity ratio of fluorescence at the cell plate: fluorescence at the plasma membrane. The ratio was 0.794 ± 0.634 for PIP2-CFP (n = 3 plants, 13 cell plates) and 0.461 ± 0.375 for PIN1-YFP (n = 2 plants, 10 cell plates). PIN1-YFP accumulated in the cell plate 100% in both early telophase (n = 7/7 cells) and 90% in late telophase (n = 9/10 cells from 2 plants, Figure 5A). PIP2A-CFP also accumulated in cell plates, 91% in early telophase (n = 11/12 cells) and 100% in late telophase (n = 27 cells from 3 plants, Figure 5B).

To determine whether cell-plate localization of the proteins described above was contingent on proper cell plate formation, maize epidermal cells were treated with the herbicide chlorpropham (CIPC, 2μM). CIPC binds tubulin and generates fragmented phragmoplasts and fragmented or split cell plates *in vivo* (Young and Lewandowski, 2000; Buschmann et al., 2006). CIPC indeed generated fragmented phragmoplasts and split cell plates. However, despite generating aberrant cell plates, two cell plate associated proteins, YFP-KNOLLE and RAB11D-YFP still accumulated

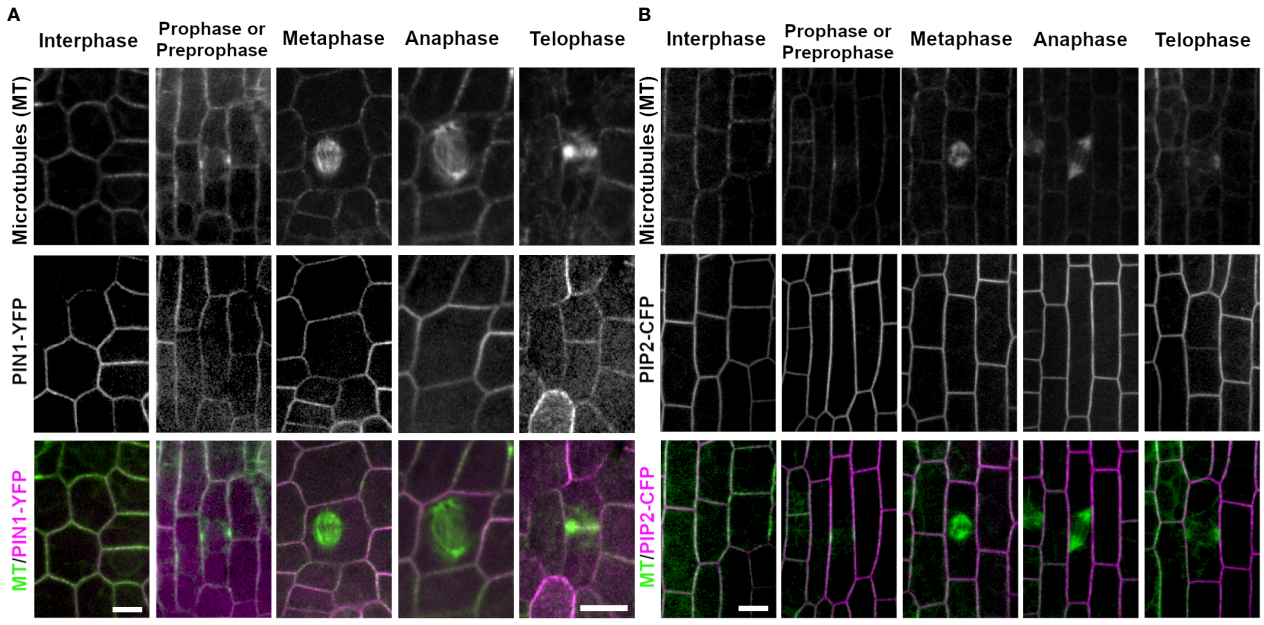

FIGURE 5
Plasma membrane markers PIN1 (PIN1-YFP) and PIP2 (PIP2-CFP). Microtubules were imaged with CFP-TUBULIN (left panels) and YFP-TUBULIN (right panels) in the top row. PIN1-YFP was imaged in the early fringe within the ligule and PIP2-CFP was imaged from the abaxial side of maize leaves in regions with symmetrically dividing cells in the middle row. Microtubules are labeled green and markers in magenta in the merged photos (bottom row). **(A)** PIN1-YFP localizes to the plasma membrane during interphase and all stages of mitosis. PIN1-YFP accumulates at the cell plate during telophase. **(B)** PIP2-CFP accumulates at the plasma membrane during interphase and all stages of mitosis in dividing epidermal tissue, and accumulates in the cell plate. Scale bars are 10μm.

10.3389/fpls.2023.1204889

normally at the cell plate (Figures 6A, B, YFP-KNOLLE (n = 3 plants, n = 88 cells with CIPC treatment, n = 38 cells with DMSO treatment) RAB11D-YFP (n = 3 plants, n = 29 cells with CIPC treatment, n = 36 cells with DMSO treatment). To further assess how CIPC disrupted cell plate formation, callose accumulation was visualized using aniline blue. Callose is a major polysaccharide deposited at the cell plate (Samuels et al., 1995). In CIPC treated samples, cell plate morphologies were often disrupted with approximately 50% of cells in telophase showing abnormal cell plates (n = 2 plants, n = 61 cells Figure 6). Abnormal cell plates observed in CIPC treatments were broken into three categories: cell plate stubs (n = 11/61 cells), split cell plates (n = 21/61 cells), and normal cell plates (n = 29/61 cells). In DMSO treated samples, cell plates were rarely disrupted (2% split cell plate, n = 1/59 cells, unpaired t-test, p-value < 0.01). These results indicate that CIPC does not disrupt the accumulation of vesicles and their cargo to the cell plate, but generated split and aberrant cell plates due to fragmented phragmoplasts.

Since CIPC disrupted cell plate morphology but did not alter accumulation of cell-plate associated proteins, we treated maize epidermal cells with Endosidin 7 (ES7) a drug that inhibits callose

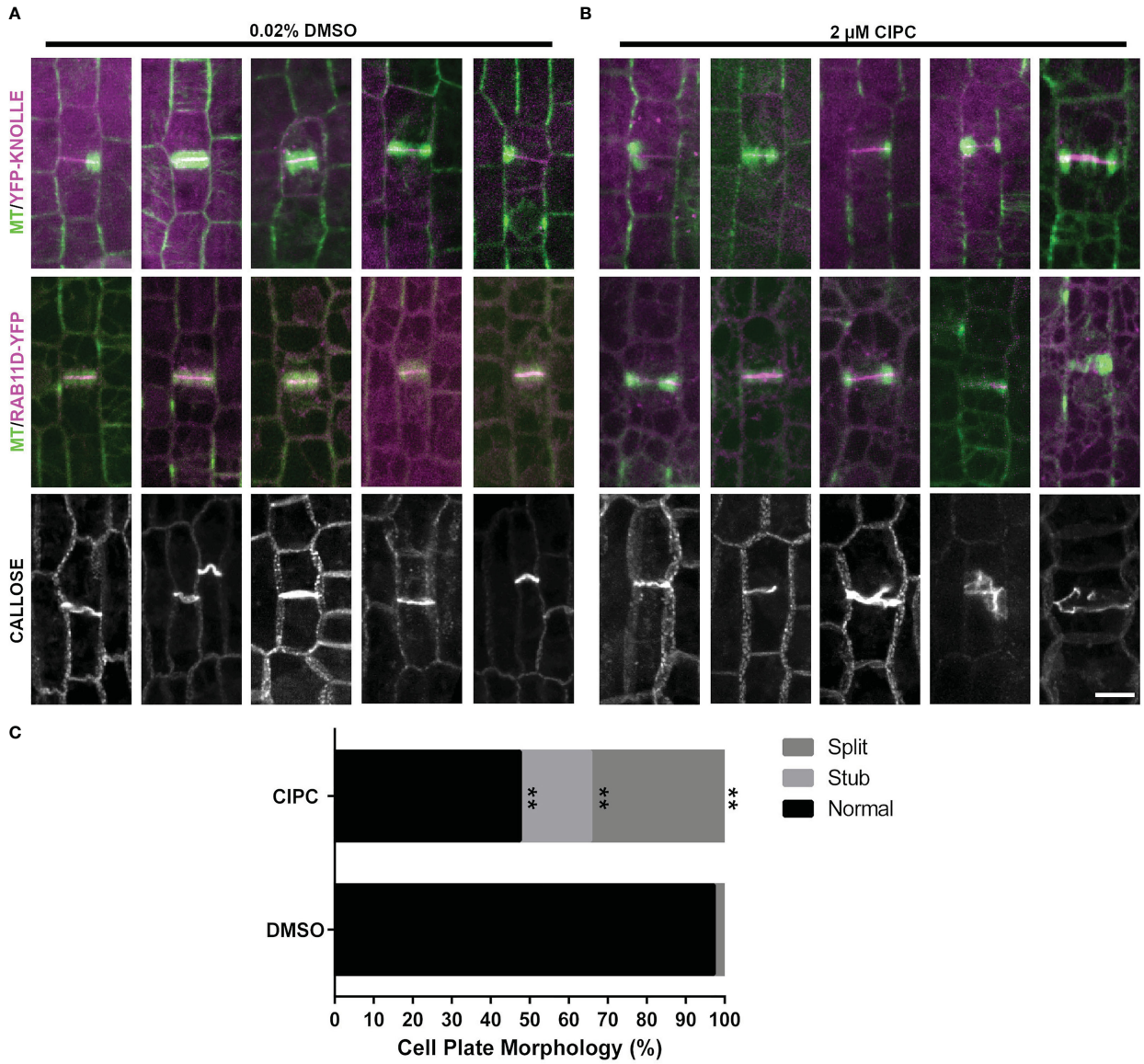

FIGURE 6
Effect of CIPC on the accumulation of YFP-KNOLLE, RAB11D-YFP, and callose to the cell plate. Microtubules imaged with the CFP-TUBULIN are labeled in green, with YFP-KNOLLE or RAB11D-YFP labeled in magenta, in the top and middle panels from the abaxial side of maize leaves in regions with symmetrically dividing cells. **(A)** Effect of 0.02% DMSO treatment on the accumulation of YFP-KNOLLE, RAB11D-YFP, and callose to the cell plate. **(B)** Effect of 2µM CIPC treatment on the accumulation of YFP-KNOLLE, RAB11D-YFP, and callose to the cell plate. **(C)** Percentage of cell plate morphology seen after callose staining on samples treated with either 0.02% DMSO or 2µM CIPC. DMSO: Stub = 0%, Split = 2%, Normal= 95%; CIPC: Stub = 18%, Split = 34%, Normal = 48%. Number of plants = 2, CIPC number of cells = 61, DMSO number of cells = 59. Scale bar is 10µm. For callose staining both YFP-KNOLLE and RAB11D-YFP number of plants = 3. In the YFP-KNOLLE plants cells in telophase n = 89 in the CIPC treatment, while for the DMSO treatment cells in telophase n = 37 cells. In the RAB11D-YFP plants, a total of telophase cells n = 36 were seen when treated with CIPC, while telophase n = 29 cells in the DMSO treatment. **p ≤ 0.01 unpaired t-test.

deposition at the cell plate, affects KNOLLE localization at late cell plate stages in Arabidopsis and disrupts cytokinesis in algae (Park et al., 2014; Davis et al., 2020). Maize epidermal cells were treated with different ES7 concentrations ranging from 25 µM to 1 mM. After 2-3 hours of incubation with ES7, we assessed YFP-KNOLLE accumulation at the cell plate (Supplementary Figure 3A). Fluorescence intensity measurements of YFP-KNOLLE in cell plates were similar between the negative control 2% DMSO treated plants (n = 3 plants, n = 21 cells) and 1 mM ES7 treated plants (n = 3 plants, n = 12 cells) and were not significantly different (Welch's two sample t-test, p-value = 0.31, Supplementary Figure 3C). We further stained for callose in the ES7 treated plants (Supplementary Figure 3A, bottom panel). Callose staining patterns were not significantly different between cells treated with 1 mM ES7 for 3 hours (11.4% abnormal, n = 20/175 cells) and negative control treated with 2% DMSO (6.4% abnormal, n = 9/141 cells, Fisher's exact test, p-value = 0.1694 (Supplementary Figure 3D).

In addition to pulse-treating maize leaf samples with ES7, we also grew maize seedlings for 5 days on germination paper supplemented with either 10 µM ES7 or 0.02% DMSO (Supplementary Figure 4). Root lengths of 10 µM ES7 treated plants (n = 3 replicates, 71 plants) were 5.6 cm ±1.6 and 5.8 cm ± 1.7 in the 0.02% DMSO negative control (n = 4 replicates, 58 plants, Supplementary Figure 4A). There was no statistically significant difference in the root length 5 days after germination between the two treatments (Supplementary Figure 4B, Mann-Whitney *U* test, p-value > 0.1). No cell wall stubs were seen in ES7 or DMSO treated maize roots stained with propidium iodide (Supplementary Figure 2C).

To ensure that we were using active and correctly diluted ES7, we used ES7 to treat Arabidopsis seedlings, as previously described (Park et al., 2014). The ES7 treatment slowed root growth and generated cell wall stubs, similar to previous reports (Supplementary Figure 5) (Park et al., 2014). We grew Arabidopsis (Col-0/Ws) seedlings for 5 days after stratification in 10 µM ES7. 10 µM ES7 treated plants had shorter roots (Supplementary Figure 5A) with an average of 0.18 cm ± 0.08 compared to the 0.02% DMSO negative control average length 0.81 cm ± 0.13 (Supplementary Figure 5B, Mann-Whitney *U* test, p-value < 0.0001). Arabidopsis seedlings were stained with propidium iodide and cell wall stubs were frequently observed in roots of seedlings grown in 10 µM ES7 for 5 days (Supplementary Figure 5C, right panel) in comparison to the 0.02% DMSO negative control (5C left panel). Alternatively, wild-type (Col-0/Ws) with CFP-TUBULIN seedlings were pulse-treated for 2 hours with 50 µM ES7 or 0.1% DMSO and stained with FM4-64 (2 µM) (Supplementary Figure 5D). When treated with 50 µM ES7, 19 incomplete cell plates or cell wall stubs were observed in 8 plants, versus 0 incomplete cell plates or cell wall stubs in 8 plants in 0.1% DMSO control (Fisher's exact test, p < 0.05, 3 replicates, 8 plants, n = 0/1206 cells in 0.1% DMSO and n = 19/1055 cells in 50 µM ES7). Pulse treatment with 50 µM ES7 affected callose accumulation when compared to 0.1% DMSO in 4-day old seedlings (n = 10 seedlings per treatment, Supplementary Figure 6). There was no detectable callose deposition in aberrant cell plates (Supplementary Figures 6D-F). Overall, this indicates that ES7 affects Arabidopsis as expected, but does not affect maize roots or leaves with the conditions used here.

Discussion

The localization of organelles, plasma membrane localized proteins, plus-end microtubule associated proteins, and proteins involved in vesicle transport are described in symmetrically dividing maize epidermal cells. First, we assessed how EB1, a protein that localizes to the plus-ends of microtubules, localizes in maize. Maize EB1 labels the growing plus-end of microtubules, disappearing as microtubules shrink. EB1 localization to microtubule plus-ends is similar to that seen in Arabidopsis, yeast, and human cells (Tirnauer and Bierer, 2000; Chan et al., 2003; Bisgrove et al., 2008; Komaki et al., 2010). Maize contains two *EB1* homologs (Zm00001eb068860 and Zm00001eb044540) which encode proteins with 64% amino acid identity. Both maize *EB1* homologs are most similar to *AtEB1a* and *AtEB1b*. Maize EB1(Zm00001eb068860) localization is more similar to AtEB1a and AtEB1b than AtEB1c, which localizes conspicuously in the nucleus in addition to the microtubule plus end (Komaki et al., 2010). Recently, maize EB1 (Zm00001eb068860) was shown to interact with TUBULIN FOLDING COFACTOR B, a protein that promotes tubulin folding and dimerization. Maize EB1 localized to plus-ends when expressed in *A. thaliana* protoplasts (Zhou et al., 2023). EB1 binds to and stabilizes an extended region past the microtubule plus end tip consisting of GTP-GDP-Pi-microtubules (Nehlig et al., 2017). Both EB1 and microtubule dynamics increased in cells in late G2 and prophase containing a PPB. Microtubule dynamicity continued to increase in telophase cells. In Arabidopsis, interphase microtubule plus-end growth rates in epidermal cells are ~3.7 µm/min (Shaw et al., 2003) and similar in cultured Arabidopsis cells ~3.5 µm/min (Chan et al., 2003). Maize interphase microtubule growth rates are slower, ~2.6 µm/min but both growth and shrinkage rates increased as cells formed PPBs and entered mitosis. Similar increased dynamicity is observed in cultured tobacco (BY-2) cells when cells had PPBs (Vos et al., 2004). In addition, faster growth and shrinkage was seen during telophase in maize epidermal cells, similar to previous reports (Bellinger et al., 2023). This increased microtubule dynamicity during mitosis may reflect alterations in the balance of microtubule associated proteins or in the relative amount of tubulin captured in various mitotic structures.

Maize ER and nuclear-envelope localized proteins dynamically repositioned during mitosis, similar to previous reports using live cell markers in Arabidopsis and tobacco cultured cells (Gupton et al., 2006; Oda and Fukuda, 2011; Meier et al., 2017). ER accumulation near mitotic structures has also been observed in monocots using transmission electron microscopy (Porter and Machado, 1960; Pickett-Heaps and Northcote, 1966). While maize ER and nuclear envelope localized proteins have similar localization during interphase, localization differences between RANGAP1, PDI1 and GLOSSY8 occur mainly during late G2 and mitosis. While RANGAP1 evenly labels the spindle, both PDI1 and

GLOSSY8 accumulate strongly at spindle poles, but do not strongly accumulate at the spindle midzone. In Arabidopsis, RANGAP labels the division site, and kinetochores, but does not label the spindle poles (Xu et al., 2008). However, its localization is dispensable for function, as tested by removing motifs required for interaction with nuclear envelope proteins (Boruc et al., 2015). In both onion epidermal cells and maize, RANGAP1 localizes to a region just inside the PPB, but disappears from the division site on entry into metaphase (Yabuuchi et al., 2015). The function of the two ER-localized proteins examined here, PDI1 and GLOSSY8, have been well characterized in maize and Arabidopsis (Li and Larkins, 1996; Xu et al., 1997; Lu and Christopher, 2008; Kirienko et al., 2012).

Many of the proteins examined here localize to the cell plate during telophase and cytokinesis and to motile particles that may be Golgi, *Trans*-Golgi Network (TGN), or vesicle populations. We used the well-characterized YFP-KNOLLE to assess cell plate formation and associated vesicle trafficking. In Arabidopsis, this mitotic syntaxin mediates homotypic cell fusion: *knolle* mutants have cytokinesis defects and an accumulation of unfused vesicles at the cell plate (Lukowitz et al., 1996; Lauber et al., 1997). KNOLLE is expressed solely during mitosis (Lauber et al., 1997). Similarly, maize YFP-KNOLLE was not observed in interphase cells but accumulated as motile particles during mitosis that then accumulated in the developing cell plate. YFP-KNOLLE accumulation in the cell plate was not reduced when cells were treated with CIPC or ES7. Both PIN1 and PIP2A, two plasma membrane localized transport proteins, accumulated in the cell plate.

The protein RAB1A is involved in vesicle tethering in both plants and mammals. In metazoans, the TRAPPIII complex activates RAB1 involved in ER-Golgi traffic and autophagy (Yang et al., 2016; Galindo and Munro, 2022). During mitosis in mammals, RAB1A localizes at distal regions of mitotic spindles (Marie et al., 2012). In Arabidopsis, RAB1A (AtRABD2a) plays a role in autophagosome formation in addition to promoting polarized growth (Zeng et al., 2021). AtRABD2a localizes to the Golgi and TGN/early endosomes, unlike the mammalian counterparts (Pinheiro et al., 2009). While most of the RAB-GTPAses in this study accumulated in the cell plate, RAB2A did not accumulate strongly in the cell plate, localizing more prominently in motile particles that may be Golgi bodies. These results are similar to that observed in Arabidopsis, where it co-localizes with a Golgi marker, and consistent with Golgi accumulation in maize biochemical fractionation experiments (Chow et al., 2008; Okekeogbu et al., 2019). In addition, in contrast to the other RABs or KNOLLE, RAB2A particle movements were faster and further increased during late stages of mitosis. In the future, it will be interesting to determine if this reflects Golgi movements during mitosis and cytokinesis.

The tubulin-binding herbicide CIPC generates split or multiple phragmoplasts which produce split or multiple cell plates (Clayton and Lloyd, 1984; Doonan et al., 1985; Eleftheriou and Bekiari, 2000; Young and Lewandowski, 2000). In our experimental conditions, CIPC treatment did not alter the recruitment of YFP-KNOLLE or RAB11D-YFP to the cell plate suggesting their localization may be independent of microtubule function or dynamics. However, CIPC caused significant defects in cell plate morphology detected by examining callose accumulation. In the future, it may be interesting to assess how microtubule dynamics are altered in CIPC treated cells.

Endosidin7 (ES7) is a chemical that inhibits cytokinetic specific callose deposition and cell plate maturation, often visualized as cell plate gaps. As a result, ES7 treatment disrupts the cell plate localization of KNOLLE and the RAB GTPase RABA2a during late cell stages of cell plate development (Park et al., 2014; Jawaid et al., 2022). Of the 12 callose synthases in Arabidopsis, CALLOSE SYNTHASE1/GLUCAN SYNTHASE-LIKE6 (CalS1/GSL6), CalS10/GSL8, and GSL10 are likely involved in cytokinesis (Záveská Drábková and Honys, 2017). In Arabidopsis, CalSI forms a complex with UDP-glucose transferase and localizes to the cell plate when expressed in tobacco cells (Hong et al., 2001). However, *cals1* mutants do not have defects in cell plate formation, while *gsl8* and *gls10* mutants have both reduced callose accumulation and defects in cytokinesis (Chen et al., 2009; Saatian et al., 2018). Although ES7 has a profound effect on cytokinesis in Arabidopsis and algae (Park et al., 2014; Davis et al., 2020), ES7 treated maize cells did not have defects in callose accumulation, cell plate morphology or altered YFP-KNOLLE or RAB11D-YFP accumulation. While earlier studies suggest that ES7 indirectly inhibits callose deposition (Park et al., 2014), the target of ES7 is still unknown. Whether lack of cell plate and root growth defects in maize roots and leaves are a result of poor ES7 uptake, lower affinity binding or other reasons is also unknown. Future experiments will clarify whether or not maize contains the ES7 target or whether it is sensitive to higher ES7 concentrations in germination treatments.

As demonstrated here, cell division in maize epidermal cells is a dynamic process that can be visualized at high spatial and temporal resolution. These markers highlight both conserved and potentially unique roles of proteins involved in cell division across the diversity of plants. Further experimental and functional studies using these markers will help clarify the role of these proteins and the spatial and temporal control of maize cell divisions.

Data availability statement

The original contributions presented in the study are included in the article/Supplementary Material. Further inquiries can be directed to the corresponding author.

Author contributions

LA, MB, VH, MD, AC, AR, BV, SS, AU, SM, CR designed and performed experiments, prepared the figures, and wrote the draft. GD provided ES7 and edited the manuscript, RS took images for ES7 experiments in Arabidopsis. GS, BD, DBV, and AN contributed to interphase microtubule measurements. CR conceptualized and designed the research, provided supervision, acquired funding and wrote the final manuscript. HS, XZ, and AS designed and generated fluorescent protein constructs EB1-mCherry and YFP-KNOLLE. All authors contributed to the article and approved the submitted version.

Funding

Funding from NSF-MCB #1716972 and NSF-CAREER #1942734 to CGR. Funding from DOE-GAANN #P200A150300 to MB, Office of Undergraduate Education Minigrant Program, Bernarr J. Hall Agricultural Scholarship and UCR School of Medicine Medical Scholars Research Program to SS. AC, GS, DB, and AN were partially supported by USDA-NIFA U-SPARC 2017-38422-27135, BD was awarded a Chancellor's Fellowship, MD was awarded a RISE fellowship from UCR, VH was awarded a Chancellor's Minigrant. SM and AU received funding from NSF DBI-1922642. AS acknowledges funding from NSF-DBI 0501862 and NSF-IOS 1027445 as part of the Maize Cell Genomics project and gratefully acknowledges the contributions of Anding Luo. GD acknowledges funding from NSF-MCB #1818219.

Acknowledgments

Thank you to Lourdes Flores for initial microtubule dynamics analysis.

Conflict of interest

The authors declare that the research was conducted in the absence of any commercial or financial relationships that could be construed as a potential conflict of interest.

Publisher's note

All claims expressed in this article are solely those of the authors and do not necessarily represent those of their affiliated organizations, or those of the publisher, the editors and the reviewers. Any product that may be evaluated in this article, or claim that may be made by its manufacturer, is not guaranteed or endorsed by the publisher.

Supplementary material

The Supplementary Material for this article can be found online at: https://www.frontiersin.org/articles/10.3389/fpls.2023.1204889/full#supplementary-material

References

Arif Ashraf, M., Liu, L., and Facette, M. R. (2022). An outer nuclear membrane protein promotes a polarized nuclear position and the future division plane during asymmetric cell division. *bioRxiv*, 505454. doi: 10.1101/2022.08.26.505454

Bellinger, M. A., Uyehara, A. N., Allsman, L., Martinez, P., McCarthy, M. C., and Rasmussen, C. G. (2023). Cortical microtubules contribute to division plane positioning during telophase in maize. *Plant Cell.* 35 (5), 1496–1512. doi: 10.1093/plcell/koad033

Berny, M. C., Gilis, D., Rooman, M., and Chaumont, F. (2016). Single mutations in the transmembrane domains of maize plasma membrane aquaporins affect the activity of monomers within a heterotetramer. *Mol. Plant* 9, 986–1003. doi: 10.1016/j.molp.2016.04.006

Bisgrove, S. R., Lee, Y.-R. J., Liu, B., Peters, N. T., and Kropf, D. L. (2008). The microtubule plus-end binding protein EB1 functions in root responses to touch and gravity signals in arabidopsis. *Plant Cell* 20, 396–410. doi: 10.1105/tpc.107.056846

Boisnard-Lorig, C., Colon-Carmona, A., Bauch, M., Hodge, S., Doerner, P., Bancharel, E., et al. (2001). Dynamic analyses of the expression of the HISTONE:: YFP fusion protein in arabidopsis show that syncytial endosperm is divided in mitotic domains. *Plant Cell* 13, 495–509. doi: 10.1105/tpc.13.3.495

Boruc, J., Griffis, A. H. N., Rodrigo-Peiris, T., Zhou, X., Tilford, B., Van Damme, D., et al. (2015). GAP activity, but not subcellular targeting, is required for arabidopsis RanGAP cellular and developmental functions. *Plant Cell* 27, 1985–1998. doi: 10.1105/tpc.114.135780

Boutté, Y., Frescatada-Rosa, M., Men, S., Chow, C.-M., Ebine, K., Gustavsson, A., et al. (2010). Endocytosis restricts arabidopsis KNOLLE syntaxin to the cell division plane during late cytokinesis. *EMBO J.* 29, 546–558. doi: 10.1038/emboj.2009.363

Buschmann, H., Chan, J., Sanchez-Pulido, L., Andrade-Navarro, M. A., Doonan, J. H., and Lloyd, C. W. (2006). Microtubule-associated AIR9 recognizes the cortical division site at preprophase and cell-plate insertion. *Curr. Biol.* 16, 1938–1943. doi: 10.1016/j.cub.2006.08.028

Chan, J., Calder, G. M., Doonan, J. H., and Lloyd, C. W. (2003). EB1 reveals mobile microtubule nucleation sites in arabidopsis. *Nat. Cell Biol.* 5, 967–971. doi: 10.1038/ncb1057

Chen, X.-Y., Liu, L., Lee, E., Han, X., Rim, Y., Chu, H., et al. (2009). The arabidopsis callose synthase gene GSL8 is required for cytokinesis and cell patterning. *Plant Physiol.* 150, 105–113. doi: 10.1104/pp.108.133918

Chow, C.-M., Neto, H., Foucart, C., and Moore, I. (2008). Rab-A2 and rab-A3 GTPases define a trans-golgi endosomal membrane domain in arabidopsis that contributes substantially to the cell plate. *Plant Cell* 20, 101–123. doi: 10.1105/tpc.107.052001

Clayton, L., and Lloyd, C. W. (1984). The relationship between the division plane and spindle geometry in allium cells treated with CIPC and griseofulvin: an anti-tubulin study. *Eur. J. Cell Biol.* 34, 248–253.

D'Ario, M., Tavares, R., Schiessl, K., Desvoyes, B., Gutierrez, C., Howard, M., et al. (2021). Cell size controlled in plants using DNA content as an internal scale. *Science* 372, 1176–1181. doi: 10.1126/science.abb4348

Davis, D. J., Wang, M., Sørensen, I., Rose, J. K. C., Domozych, D. S., and Drakakaki, G. (2020). Callose deposition is essential for the completion of cytokinesis in the unicellular alga, penium margaritaceum. *J. Cell Sci.*, 122580. doi: 10.1101/2020.05.28.122580

Dixit, R., Chang, E., and Cyr, R. (2006). Establishment of polarity during organization of the acentrosomal plant cortical microtubule array. *Mol. Biol. Cell* 17, 1298–1305. doi: 10.1091/mbc.E05-09-0864

Dixit, R., and Cyr, R. J. (2002). Spatio-temporal relationship between nuclear-envelope breakdown and preprophase band disappearance in cultured tobacco cells. *Protoplasma* 219, 116–121. doi: 10.1007/s007090200012

Doonan, J. H., Cove, D. J., and Lloyd, C. W. (1985). Immunofluorescence microscopy of microtubules in intact cell lineages of the moss, physcomitrella patens. i. normal and CIPC-treated tip cells. *J. Cell Sci.* 75, 131–147.

Dunkley, T. P. J., Hester, S., Shadforth, I. P., Runions, J., Weimar, T., Hanton, S. L., et al. (2006). Mapping the *Arabidopsis* organelle proteome. *Proc. Natl. Acad. Sci. U. S. A.* 103, 6518–6523. doi: 10.1073/pnas.0506958103

Eleftheriou, E. P., and Bekiari, E. (2000). Ultrastructural effects of the herbicide chlorpropham (CIPC) in root tip cells of wheat. *Plant Soil* 226, 11–19.

Elliott, L., Moore, I., and Kirchhelle, C. (2020). Spatio-temporal control of post-golgi exocytic trafficking in plants. *J. Cell Sci.* 133. doi: 10.1242/jcs.237065

Facette, M. R., Rasmussen, C. G., and Van Norman, J. M. (2019). A plane choice: coordinating timing and orientation of cell division during plant development. *Curr. Opin. Plant Biol.* 47, 47–55. doi: 10.1016/j.pbi.2018.09.001

Facette, M. R., and Smith, L. G. (2012). Division polarity in developing stomata. *Curr. Opin. Plant Biol.* 15, 585–592. doi: 10.1016/j.pbi.2012.09.013

Galindo, A., and Munro, S. (2022). The TRAPP complexes: oligomeric exchange factors that activate the small GTPases Rab1 and Rab11. *FEBS Lett.* 597 (6), 734–749. doi: 10.1002/1873-3468.14553

Gillmor, C. S., Roeder, A. H. K., Sieber, P., Somerville, C., and Lukowitz, W. (2016). A genetic screen for mutations affecting cell division in the arabidopsis thaliana embryo identifies seven loci required for cytokinesis. *PloS One* 11, e0146492. doi: 10.1371/journal.pone.0146492

Gu, Y., and Rasmussen, C. G. (2022). Cell biology of primary cell wall synthesis in plants. *Plant Cell* 34, 103. doi: 10.1093/plcell/koab249

Gumber, H. K., McKenna, J. F., Estrada, A. L., Tolmie, A. F., Graumann, K., and Bass, H. W. (2019a). Identification and characterization of genes encoding the nuclear envelope LINC complex in the monocot species zea mays. *J. Cell Sci.* 132. doi: 10.1242/jcs.221390

Gumber, H. K., McKenna, J. F., Tolmie, A. F., Jalovec, A. M., Kartick, A. C., Graumann, K., et al. (2019b). MLKS2 is an ARM domain and f-actin-associated KASH protein that functions in stomatal complex development and meiotic chromosome segregation. *Nucleus* 10, 144–166. doi: 10.1080/19491034.2019.1629795

Gupton, S. L., Collings, D. A., and Allen, N. S. (2006). Endoplasmic reticulum targeted GFP reveals ER organization in tobacco NT-1 cells during cell division. *Plant Physiol. Biochem.* 44, 95–105. doi: 10.1016/j.plaphy.2006.03.003

Hashimoto, T. (2015). Microtubules in plants. *Arabidopsis Book* 13, e0179. doi: 10.1199/tab.0179

Hong, Z., Delauney, A. J., and Verma, D. P. S. (2001). A cell plate–specific callose synthase and its interaction with phragmoplastin. *Plant Cell* 13, 755–768. doi: 10.1105/tpc.13.4.755

Howe, E. S., Clemente, T. E., and Bass, H. W. (2012). Maize histone H2B-mCherry: a new fluorescent chromatin marker for somatic and meiotic chromosome research. *DNA Cell Biol.* 31, 925–938. doi: 10.1089/dna.2011.1514

Jawaid, M. Z., Sinclair, R., Bulone, V., Cox, D. L., and Drakakaki, G. (2022). A biophysical model for plant cell plate maturation based on the contribution of a spreading force. *Plant Physiol.* 188, 795–806. doi: 10.1093/plphys/kiab552

Jones, A. R., Forero-Vargas, M., Withers, S. P., Smith, R. S., Traas, J., Dewitte, W., et al. (2017). Cell-size dependent progression of the cell cycle creates homeostasis and flexibility of plant cell size. *Nat. Commun.* 8, 15060. doi: 10.1038/ncomms15060

Jürgens, G., Park, M., Richter, S., Touihri, S., Krause, C., El Kasmi, F., et al. (2015). Plant cytokinesis: a tale of membrane traffic and fusion. *Biochem. Soc Trans.* 43, 73–78. doi: 10.1042/BST20140246

Karnahl, M., Park, M., Mayer, U., Hiller, U., and Jürgens, G. (2017). ER assembly of SNARE complexes mediating formation of partitioning membrane in arabidopsis cytokinesis. *Elife* 6, e25327. doi: 10.7554/eLife.25327

Kennard, J. L., and Cleary, A. L. (1997). Pre-mitotic nuclear migration in subsidiary mother cells of tradescantia occurs in G1 of the cell cycle and requires f-actin. *Cell Motil. Cytoskeleton* 36, 55–67. doi: 10.1002/(SICI)1097-0169(1997)36:1<55::AID-CM5>3.0.CO;2-G

Kimata, Y., Higaki, T., Kawashima, T., Kurihara, D., Sato, Y., Yamada, T., et al. (2016). Cytoskeleton dynamics control the first asymmetric cell division in arabidopsis zygote. *Proc. Natl. Acad. Sci. U. S. A.* 113, 14157–14162. doi: 10.1073/pnas.1613979113

Kirienko, D. R., Luo, A., and Sylvester, A. W. (2012). Reliable transient transformation of intact maize leaf cells for functional genomics and experimental study. *Plant Physiol.* 159, 1309–1318. doi: 10.1104/pp.112.199737

Komaki, S., Abe, T., Coutuer, S., Inzé, D., Russinova, E., and Hashimoto, T. (2010). Nuclear-localized subtype of end-binding 1 protein regulates spindle organization in arabidopsis. *J. Cell Sci.* 123, 451–459. doi: 10.1242/jcs.062703

Lauber, M. H., Waizenegger, I., Steinmann, T., Schwarz, H., Mayer, U., Hwang, I., et al. (1997). The arabidopsis KNOLLE protein is a cytokinesis-specific syntaxin. *J. Cell Biol.* 139, 1485–1493. doi: 10.1083/jcb.139.6.1485

Lee, Y.-R. J., and Liu, B. (2013). The rise and fall of the phragmoplast microtubule array. *Curr. Opin. Plant Biol.* 16, 757–763. doi: 10.1016/j.pbi.2013.10.008

Li, C. P., and Larkins, B. A. (1996). Expression of protein disulfide isomerase is elevated in the endosperm of the maize floury-2 mutant. *Plant Mol. Biol.* 30, 873–882. doi: 10.1007/BF00020800

Lindsey, B. E.3rd, Rivero, L., Calhoun, C. S., Grotewold, E., and Brkljacic, J. (2017). Standardized method for high-throughput sterilization of arabidopsis seeds. *J. Vis. Exp.* (128), 56587. doi: 10.3791/56587

Livanos, P., and Müller, S. (2019). Division plane establishment and cytokinesis. *Annu. Rev. Plant Biol.* 70, 239–267. doi: 10.1146/annurev-arplant-050718-100444

Lu, D.-P., and Christopher, D. A. (2008). Endoplasmic reticulum stress activates the expression of a sub-group of protein disulfide isomerase genes and AtbZIP60 modulates the response in arabidopsis thaliana. *Mol. Genet. Genomics* 280, 199–210. doi: 10.1007/s00438-008-0356-z

Lukowitz, W., Mayer, U., and Jürgens, G. (1996). Cytokinesis in the arabidopsis embryo involves the syntaxin-related KNOLLE gene product. *Cell* 84, 61–71.

Marie, M., Dale, H. A., Kouprina, N., and Saraste, J. (2012). Division of the intermediate compartment at the onset of mitosis provides a mechanism for golgi inheritance. *J. Cell Sci.* 125, 5403–5416. doi: 10.1242/jcs.108100

Martinez, P., Allsman, L. A., Brakke, K. A., Hoyt, C., Hayes, J., Liang, H., et al. (2018). Predicting division planes of three-dimensional cells by soap-film minimization. *Plant Cell* 30, 2255–2266. doi: 10.1105/tpc.18.00401

Mathur, J., Mathur, N., Kernebeck, B., Srinivas, B. P., and Hülskamp, M. (2003). A novel localization pattern for an EB1-like protein links microtubule dynamics to endomembrane organization. *Curr. Biol.* 13, 1991–1997. doi: 10.1016/j.cub.2003.10.033

McKenna, J. F., Gumber, H. K., Turpin, Z. M., Jalovec, A. M., Kartick, A. C., Graumann, K., et al. (2021). Maize (Zea mays l.) nucleoskeletal proteins regulate nuclear envelope remodeling and function in stomatal complex development and pollen viability. *Cold Spring Harbor Lab.*, 424208. doi: 10.1101/2020.12.23.424208

Meier, I., Richards, E. J., and Evans, D. E. (2017). Cell biology of the plant nucleus. *Annu. Rev. Plant Biol.* 68, 139–172. doi: 10.1146/annurev-arplant-042916-041115

Men, S., Boutté, Y., Ikeda, Y., Li, X., Palme, K., Stierhof, Y.-D., et al. (2008). Sterol-dependent endocytosis mediates post-cytokinetic acquisition of PIN2 auxin efflux carrier polarity. *Nat. Cell Biol.* 10, 237–244. doi: 10.1038/ncb1686

Mohanty, A., Luo, A., DeBlasio, S., Ling, X., Yang, Y., Tuthill, D. E., et al. (2009). Advancing cell biology and functional genomics in maize using fluorescent protein-tagged lines. *Plant Physiol.* 149, 601–605. doi: 10.1104/pp.108.130146

Mravec, J., Petrášek, J., Li, N., Boeren, S., Karlova, R., Kitakura, S., et al. (2011). Cell plate restricted association of DRP1A and PIN proteins is required for cell polarity establishment in arabidopsis. *Curr. Biol.* 21, 1055–1060. doi: 10.1016/j.cub.2011.05.018

Müller, S., and Jürgens, G. (2016). Plant cytokinesis–no ring, no constriction but centrifugal construction of the partitioning membrane. *Semin. Cell Dev. Biol.* 53, 10–18. doi: 10.1016/j.semcdb.2015.10.037

Murashige, T., and Skoog, F. (1962). A revised medium for rapid growth and bioassays with tobacco tissue cultures. physiology plant, v. 15. *Physiol. Plant* 15, 473–497.

Muroyama, A., Gong, Y., and Bergmann, D. C. (2020). Opposing, polarity-driven nuclear migrations underpin asymmetric divisions to pattern arabidopsis stomata. *Curr. Biol.* 30 (22), 4549–4552. doi: 10.1016/j.cub.2020.08.100

Nebenführ, A., Frohlick, J. A., and Staehelin, L. A. (2000). Redistribution of golgi stacks and other organelles during mitosis and cytokinesis in plant cells. *Plant Physiol.* 124, 135–151.

Neher, W., Rasmussen, C. G., Braybrook, S. A., Lažetić, V., Stowers, C. E., Mooney, P. T., et al. (2023). The maize preligule band is subdivided into distinct domains with contrasting cellular properties prior to ligule outgrowth. *bioRxiv*, 527228. doi: 10.1101/2023.02.06.527228

Nehlig, A., Molina, A., Rodrigues-Ferreira, S., Honoré, S., and Nahmias, C. (2017). Regulation of end-binding protein EB1 in the control of microtubule dynamics. *Cell. Mol. Life Sci.* 74, 2381–2393. doi: 10.1007/s00018-017-2476-2

Oda, Y., and Fukuda, H. (2011). Dynamics of arabidopsis SUN proteins during mitosis and their involvement in nuclear shaping: dynamics and functions of arabidopsis SUN proteins. *Plant J.* 66, 629–641. doi: 10.1111/j.1365-313X.2011.04523.x

Okekeogbu, I. O., Aryal, U. K., Fernández-Niño, S. M. G., Penning, B. W., Heazlewood, J. L., McCann, M. C., et al. (2019). Differential distributions of trafficking and signaling proteins of the maize ER-golgi apparatus. *Plant Signal. Behav.* 14, 1672513. doi: 10.1080/15592324.2019.1672513

Park, E., Díaz-Moreno, S. M., Davis, D. J., Wilkop, T. E., Bulone, V., and Drakakaki, G. (2014). Endosidin 7 specifically arrests late cytokinesis and inhibits callose biosynthesis, revealing distinct trafficking events during cell plate maturation. *Plant Physiol.* 165, 1019–1034. doi: 10.1104/pp.114.241497

Peng, J., Ilarslan, H., Wurtele, E. S., and Bassham, D. C. (2011). AtRabD2b and AtRabD2c have overlapping functions in pollen development and pollen tube growth. *BMC Plant Biol.* 11, 25. doi: 10.1186/1471-2229-11-25

Pickett-Heaps, J. D., and Northcote, D. H. (1966). Organization of microtubules and endoplasmic reticulum during mitosis and cytokinesis in wheat meristems. *J. Cell Sci.* 1, 109–120.

Pinheiro, H., Samalova, M., Geldner, N., Chory, J., Martinez, A., and Moore, I. (2009). Genetic evidence that the higher plant rab-D1 and rab-D2 GTPases exhibit distinct but overlapping interactions in the early secretory pathway. *J. Cell Sci.* 122, 3749–3758. doi: 10.1242/jcs.050625

Porter, K. R., and Machado, R. D. (1960). Studies on the endoplasmic reticulum. IV. its form and distribution during mitosis in cells of onion root tip. *J. Biophys. Biochem. Cytol.* 7, 167–180.

Rasmussen, C. G. (2016). "Using live-cell markers in maize to analyze cell division orientation and timing," in *Plant cell division: methods and protocols methods in molecular biology*. Ed. M.-C. Caillaud (New York, NY: Springer New York), 209–225. doi: 10.1007/978-1-4939-3142-2_16

Rasmussen, C. G., and Bellinger, M. (2018). An overview of plant division-plane orientation. *New Phytol.* 219 (2), 505–512. doi: 10.1111/nph.15183

Reichardt, I., Stierhof, Y.-D., Mayer, U., Richter, S., Schwarz, H., Schumacher, K., et al. (2007). Plant cytokinesis requires *de novo* secretory trafficking but not endocytosis. *Curr. Biol.* 17, 2047–2053. doi: 10.1016/j.cub.2007.10.040

Rigal, A., Doyle, S. M., and Robert, S. (2015). Live cell imaging of FM4-64, a tool for tracing the endocytic pathways in arabidopsis root cells. *Methods Mol. Biol.* 1242, 93–103. doi: 10.1007/978-1-4939-1902-4_9

Rosquete, M. R., Worden, N., Ren, G., Sinclair, R. M., Pfleger, S., Salemi, M., et al. (2019). AtTRAPPC11/ROG2: a role for TRAPPs in maintenance of the plant trans-golgi Network/Early endosome organization and function. *Plant Cell* 31, 1879–1898. doi: 10.1105/tpc.19.00110

Rutherford, S., and Moore, I. (2002). The arabidopsis rab GTPase family: another enigma variation. *Curr. Opin. Plant Biol.* 5, 518–528. doi: 10.1016/s1369-5266(02)00307-2

Saatian, B., Austin, R. S., Tian, G., Chen, C., Nguyen, V., Kohalmi, S. E., et al. (2018). Analysis of a novel mutant allele of GSL8 reveals its key roles in cytokinesis and symplastic trafficking in arabidopsis. *BMC Plant Biol.* 18, 295. doi: 10.1186/s12870-018-1515-y

Sablowski, R. (2016). Coordination of plant cell growth and division: collective control or mutual agreement? *Curr. Opin. Plant Biol.* 34, 54–60. doi: 10.1016/j.pbi.2016.09.004

Samuels, A. L., Giddings, T. H.Jr., and Staehelin, L. A. (1995). Cytokinesis in tobacco BY-2 and root tip cells: a new model of cell plate formation in higher plants. *J. Cell Biol.* 130, 1345–1357.

Sbalzarini, I. F., and Koumoutsakos, P. (2005). Feature point tracking and trajectory analysis for video imaging in cell biology. *J. Struct. Biol.* 151, 182–195. doi: 10.1016/j.jsb.2005.06.002

Shaw, S. L., Kamyar, R., and Ehrhardt, D. W. (2003). Sustained microtubule treadmilling in arabidopsis cortical arrays. *Science* 300, 1715–1718. doi: 10.1126/science.1083529

Sinclair, R., Hsu, G., Davis, D., Chang, M., Rosquete, M., Iwasa, J. H., et al. (2022). Plant cytokinesis and the construction of new cell wall. *FEBS Lett.* 596, 2243–2255. doi: 10.1002/1873-3468.14426

Smertenko, A. (2018). Phragmoplast expansion: the four-stroke engine that powers plant cytokinesis. *Curr. Opin. Plant Biol.* 46, 130–137. doi: 10.1016/j.pbi.2018.07.011

Smertenko, A., Assaad, F., Baluška, F., Bezanilla, M., Buschmann, H., Drakakaki, G., et al. (2017). Plant cytokinesis: terminology for structures and processes. *Trends Cell Biol.* 27, 885–894. doi: 10.1016/j.tcb.2017.08.008

Söllner, R., Glässer, G., Wanner, G., Somerville, C. R., Jürgens, G., and Assaad, F. F. (2002). Cytokinesis-defective mutants of arabidopsis. *Plant Physiol.* 129, 678–690. doi: 10.1104/pp.004184

Sutimantanapi, D., Pater, D., and Smith, L. G. (2014). Divergent roles for maize PAN1 and PAN2 receptor-like proteins in cytokinesis and cell morphogenesis. *Plant Physiol.* 164, 1905–1917. doi: 10.1104/pp.113.232660

Szumlanski, A. L., and Nielsen, E. (2009). The rab GTPase RabA4d regulates pollen tube tip growth in arabidopsis thaliana. *Plant Cell* 21, 526–544. doi: 10.1105/tpc.108.060277

Thévenaz, P. (1998). StackReg: an ImageJ plugin for the recursive alignment of a stack of images. *Biomed. Imaging Group Swiss Federal Instit. Technol. Lausanne* 2012.

Tirnauer, J. S., and Bierer, B. E. (2000). EB1 proteins regulate microtubule dynamics, cell polarity, and chromosome stability. *J. Cell Biol.* 149, 761–766. doi: 10.1083/jcb.149.4.761

Toyooka, K., Goto, Y., Asatsuma, S., Koizumi, M., Mitsui, T., and Matsuoka, K. (2009). A mobile secretory vesicle cluster involved in mass transport from the golgi to the plant cell exterior. *Plant Cell* 21, 1212–1229. doi: 10.1105/tpc.108.058933

Van Damme, D., Bouget, F.-Y., Van Poucke, K., Inzé, D., and Geelen, D. (2004). Molecular dissection of plant cytokinesis and phragmoplast structure: a survey of GFP-tagged proteins: GFP survey of cell division genes. *Plant J.* 40, 386–398. doi: 10.1111/j.1365-313X.2004.02222.x

Van Damme, D., and Geelen, D. (2008). Demarcation of the cortical division zone in dividing plant cells. *Cell Biol. Int.* 32, 178–187. doi: 10.1016/j.cellbi.2007.10.010

Vernoud, V., Horton, A. C., Yang, Z., and Nielsen, E. (2003). Analysis of the small GTPase gene superfamily of arabidopsis. *Plant Physiol.* 131, 1191–1208. doi: 10.1104/pp.013052

Vos, J. W., Dogterom, M., and Emons, A. M. C. (2004). Microtubules become more dynamic but not shorter during preprophase band formation: a possible "search-and-capture" mechanism for microtubule translocation. *Cell Motil. Cytoskeleton* 57, 246–258. doi: 10.1002/cm.10169

Wada, M. (2017). Nuclear movement and positioning in plant cells. *Semin. Cell Dev. Biol.* 82, 17–24. doi: 10.1016/j.semcdb.2017.10.001

Waizenegger, I., Lukowitz, W., Assaad, F., Schwarz, H., Jürgens, G., and Mayer, U. (2000). The arabidopsis KNOLLE and KEULE genes interact to promote vesicle fusion during cytokinesis. *Curr. Biol.* 10, 1371–1374.

Wu, Q., Luo, A., Zadrozny, T., Sylvester, A., and Jackson, D. (2013). Fluorescent protein marker lines in maize: generation and applications. *Int. J. Dev. Biol.* 57, 535–543. doi: 10.1387/ijdb.130240qw

Xu, X., Dietrich, C. R., Delledonne, M., Xia, Y., Wen, T. J., Robertson, D. S., et al. (1997). Sequence analysis of the cloned glossy8 gene of maize suggests that it may code for a beta-ketoacyl reductase required for the biosynthesis of cuticular waxes. *Plant Physiol.* 115, 501–510. doi: 10.1104/pp.115.2.501

Xu, X., Dietrich, C. R., Lessire, R., Nikolau, B. J., and Schnable, P. S. (2002). The endoplasmic reticulum-associated maize GL8 protein is a component of the acyl-coenzyme a elongase involved in the production of cuticular waxes. *Plant Physiol.* 128, 924–934. doi: 10.1104/pp.010621

Xu, X. M., Zhao, Q., Rodrigo-Peiris, T., Brkljacic, J., He, C. S., Müller, S., et al. (2008). RanGAP1 is a continuous marker of the arabidopsis cell division plane. *Proc. Natl. Acad. Sci. U. S. A.* 105, 18637–18642. doi: 10.1073/pnas.0806157105

Yabuuchi, T., Nakai, T., Sonobe, S., Yamauchi, D., and Mineyuki, Y. (2015). Preprophase band formation and cortical division zone establishment: RanGAP behaves differently from microtubules during their band formation. *Plant Signal. Behav.* 10, e1060385. doi: 10.1080/15592324.2015.1060385

Yang, X.-Z., Li, X.-X., Zhang, Y.-J., Rodriguez-Rodriguez, L., Xiang, M.-Q., Wang, H.-Y., et al. (2016). Rab1 in cell signaling, cancer and other diseases. *Oncogene* 35, 5699–5704. doi: 10.1038/onc.2016.81

Young, D. H., and Lewandowski, V. T. (2000). Covalent binding of the benzamide RH-4032 to tubulin in suspension-cultured tobacco cells and its application in a cell-based competitive-binding assay. *Plant Physiol.* 124, 115–124. doi: 10.1104/pp.124.1.115

Zachariadis, M., Quader, H., Galatis, B., and Apostolakos, P. (2003). Organization of the endoplasmic reticulum in dividing cells of the gymnosperms pinus brutia and pinus nigra, and of the pterophyte asplenium nidus. *Cell Biol. Int.* 27, 31–40.

Zanic, M. (2016). Measuring the effects of microtubule-associated proteins on microtubule dynamics *In vitro*. *Methods Mol. Biol.* 1413, 47–61. doi: 10.1007/978-1-4939-3542-0_4

Zavaliev, R., and Epel, B. L. (2015). Imaging callose at plasmodesmata using aniline blue: quantitative confocal microscopy. *Methods Mol. Biol.* 1217, 105–119. doi: 10.1007/978-1-4939-1523-1_7

Záveská Drábková, L., and Honys, D. (2017). Evolutionary history of callose synthases in terrestrial plants with emphasis on proteins involved in male gametophyte development. *PloS One* 12, e0187331. doi: 10.1371/journal.pone.0187331

Zelazny, E., Borst, J. W., Muylaert, M., Batoko, H., Hemminga, M. A., and Chaumont, F. (2007). FRET imaging in living maize cells reveals that plasma membrane aquaporins interact to regulate their subcellular localization. *Proc. Natl. Acad. Sci. U. S. A.* 104, 12359–12364. doi: 10.1073/pnas.0701180104

Zeng, Y., Li, B., Ji, C., Feng, L., Niu, F., Deng, C., et al. (2021). A unique AtSar1D-AtRabD2a nexus modulates autophagosome biogenesis in *Arabidopsis thaliana*. *Proc. Natl. Acad. Sci. U. S. A.* 118. doi: 10.1073/pnas.2021293118

Zhang, J., Hill, D. R., and Sylvester, A. W. (2007). Diversification of the RAB guanosine triphosphatase family in dicots and monocots. *J. Integr. Plant Biol.* 49, 1129–1141. doi: 10.1111/j.1672-9072.2007.00520.x

Zhou, Q., Fu, Z., Li, M., Shen, Q., Sun, C., Feng, Y., et al. (2023). Maize tubulin folding cofactor b is required for cell division and cell growth through modulating microtubule homeostasis. *New Phytol.* doi: 10.1111/nph.18839

Zhou, X., Graumann, K., Wirthmueller, L., Jones, J. D. G., and Meier, I. (2014). Identification of unique SUN-interacting nuclear envelope proteins with diverse functions in plants. *J. Cell Biol.* 205, 677–692. doi: 10.1083/jcb.201401138

Zhou, Y., Yang, Y., Niu, Y., Fan, T., Qian, D., Luo, C., et al. (2020). The tip-localized phosphatidylserine established by arabidopsis ALA3 is crucial for rab GTPase-mediated vesicle trafficking and pollen tube growth. *Plant Cell* 32, 3170–3187. doi: 10.1105/tpc.19.00844

frontiers | Frontiers in Plant Science

TYPE Original Research
PUBLISHED 01 August 2023
DOI 10.3389/fpls.2023.1212806

OPEN ACCESS

EDITED BY
Thorsten Seidel,
Bielefeld University, Germany

REVIEWED BY
Rui Malhó,
University of Lisbon, Portugal
Jinbo Shen,
Zhejiang Agriculture and Forestry University, China

*CORRESPONDENCE
Simón Ruiz-Lara
sruiz@utalca.cl

RECEIVED 26 April 2023
ACCEPTED 04 July 2023
PUBLISHED 01 August 2023

CITATION
Salinas-Cornejo J, Madrid-Espinoza J, Verdugo I, Norambuena L and Ruiz-Lara S (2023) A SNARE-like protein from *Solanum lycopersicum* increases salt tolerance by modulating vesicular trafficking in tomato. *Front. Plant Sci.* 14:1212806. doi: 10.3389/fpls.2023.1212806

A SNARE-like protein from *Solanum lycopersicum* increases salt tolerance by modulating vesicular trafficking in tomato

Josselyn Salinas-Cornejo[1], José Madrid-Espinoza[1], Isabel Verdugo[1], Lorena Norambuena[2] and Simón Ruiz-Lara[1]*

[1]Laboratorio de Genómica Funcional, Instituto de Ciencias Biológicas, Universidad de Talca, Talca, Chile, [2]Departamento de Biología, Facultad de Ciencias, Universidad de Chile, Santiago, Chile

Intracellular vesicular trafficking ensures the exchange of lipids and proteins between endomembrane compartments. This is relevant under high salinity conditions, since both the removal of transporters and ion channels from the plasma membrane and the compartmentalization of toxic ions require the formation of vesicles, which can be maintained as multivesicular bodies or be fused to the central vacuole. SNARE proteins (Soluble N-ethylmaleimide-sensitive factor attachment receptor) participate in the vesicle fusion process and give specificity to their destination. Plant genome studies have revealed a superfamily of genes that encode for proteins called SNARE-like. These proteins appear to be participating in vesicular trafficking with similar functions to those of SNARE proteins. A SNARE-like, named SlSLSP6, in *Solanum lycopersicum* plants has been shown to be induced under high salinity conditions. A phylogenetic relationship of SlSLSP6 with SNARE-like proteins of salinity-tolerant plants, including *Salicornia brachiata*, *Zostera marina* and *Solanum pennelli*, was determined. Considering its amino acid sequence, a putative clathrin adapter complex domain and palmitoylation site was predicted. Subcellular localization analysis evidenced that SlSLSP6 is mostly localized in the plasma membrane. Using transgenic tomato plants, we identified that overexpression of *SlSLSP6* increased tolerance to salt stress. This tolerance was evident when we quantified an improvement in physiological and biochemical parameters, such as higher chlorophyll content, performance index, efficiency of photosystem II and relative water content, and lower malondialdehyde content, compared to control plants. At the subcellular level, the overexpression of *SlSLSP6* reduced the presence of H_2O_2 in roots and increased the compartmentalization of sodium in vacuoles during salt stress. These effects appear to be associated with the higher endocytic rate of FM4-64, determined in the plant root cells. Taken together, these results indicate that SlSLSP6 increases tolerance to salt stress by modulating vesicular trafficking through over-induction of the endocytic pathway. This work contributes to understanding the role of this type of SNARE-like protein during salt stress and could be a potential candidate in breeding programs for tolerance to salt stress in tomato plants.

KEYWORDS

SNARE-like superfamily protein, vesicular trafficking, *Solanum lycopersicum*, endocytosis, sodium compartmentalization, salt stress

1 Introduction

In eukaryotes, the endomembrane system is composed of a series of compartments that are interconnected through diverse and specific trafficking pathways (Saito and Ueda, 2009; Pizarro and Norambuena, 2014). The direction of transported cargo and its location depend on the balance of all the pathways that affect its movement. The balance of the different pathways will determine the amount of protein in each of the compartments. The ability to change this balance could be useful when the presence of certain proteins changes in a particular compartment in response to a stimulus or disturbance (Uemura and Ueda, 2014; Zhao et al., 2020), as observed in plants subjected to salt stress conditions (Baral et al., 2015a; Baral et al., 2015b). Since the transport of lipids and proteins between the different cellular compartments is carried out mainly through membranous vesicles, the regulation of intracellular vesicular traffic becomes highly important during salt stress, since the cellular requirements must be maintained to cope with the stress that threatens the viability of the plant (Pizarro and Norambuena, 2014). In plants exposed to high salinity, an osmotic and ionic imbalance occurs inside their cells that compromises physiological, biochemical, and molecular activities and leads to a loss of plant viability (Macková et al., 2013). Removal of transporters and ion channels from the plasma membrane through the process of endocytosis, followed by degradation in vacuoles, has been suggested as a common mechanism to prevent toxicity in plants under salt stress conditions (Baral et al., 2015a; Ivanov and Vert, 2021). Most of the endocytosed cargo converges in the vacuole and is subjected to degradation, another part is recycled back to the plasma membrane and a less common part is reoriented and maintained in prevacuolar structures. For this to happen, a series of proteins are involved in the anchoring and fusion of vesicles, for the recognition and direction of membrane fusion (Barlow and Dacks, 2018; Shimizu and Uemura, 2022). Among them, it has been described that SNARE and SNARE-like proteins play a critical role in this process (Saito and Ueda, 2009; Singh et al., 2016; Rosquete and Drakakaki, 2018). Therefore, its function is essential in these multiple vesicular trafficking routes involved during saline stress (Saito and Ueda, 2009; Pizarro and Norambuena, 2014).

It has been reported that overexpression of *GsSNAP33*, a gene that codes for a protein of the plasma membrane Qb+Qc-SNARE type, in *Arabidopsis thaliana*, significantly increases tolerance to salt stress (Nisa et al., 2017). Additionally, it has been identified that the overexpression of the *AtSFT12* gene, which codes for a Qc-SNARE located in the Golgi complex, confers tolerance to salt stress in *A. thaliana* plants, since the overexpressing plants accumulate a greater amount of sodium in the vacuole (Tarte et al., 2015). Also, the silencing of two genes for vacuole-localized SNAREs, *VAMP711* and *SYP22*, increase tolerance to salt stress through compartmentalization of reactive oxygen species (ROS) and sodium ions in multivesicular bodies, respectively (Leshem et al., 2006; Hamaji et al., 2009). Indeed, in the mutants of *vamp711* and *syp22*, the fusion of vesicles with the vacuole would be blocked. In *vamp711*, the tolerance to salt stress has been associated with the endocytosis of plasma membrane NADPH oxidases (e.g., RbohD, among others), resulting in the production of hydrogen peroxide inside the vesicles, preventing the mobilization of ROS towards the vacuole (Leshem et al., 2006). Although, ROS play a fundamental role under many stresses since they activate different regulatory pathways to promote tolerance (Hao et al., 2014). Under salt stress, excessive levels of these induces programmed cell death (Apel and Hirt, 2004). To counteract this and generate tolerance to salt stress, RbohD is removed from the plasma membrane and compartmentalized in multivesicular bodies to maintain lower levels of cytoplasmic ROS (Martinière et al., 2019). This reduction of ROS decreases the oxidative damage of the vacuole and prevents its alkalinization. Therefore, this would promote the functioning of the H^+ gradient and the vacuolar sequestration of excess cytoplasmic sodium (Leshem and Levine, 2007; Baral et al., 2015b).

Despite its agronomic importance, studies on vesicular traffic in *Solanum lycopersicum* plants are not very extensive, which makes it a potential plant model to study salt stress response genes. Recently, the identification and transcriptional analysis of tomato SNARE proteins in response to salt stress were determined. Among them, *SlVAMP721.2*, *SlSYP71.1* and *SlSNAP33.2* showed strong induction (Salinas-Cornejo et al., 2019). Hence, they could be considered as future candidates in studies associated with abiotic stress. Precisely, the evaluation of *SlSNAP33.2* showed to improve the tolerance to salt stress by increasing the rate of endocytosis and the physiological and biochemical parameters of tomato plants grown under greenhouse conditions (Salinas-Cornejo et al., 2021). Regarding, the SNARE-like proteins in tomato are unknown. Recent studies showed that a *SNARE-like* gene, *SbSLSP*, that codes a plasma membrane protein of the halophytic plant *Salicornia brachiata*, confers tolerance to salt stress when is overexpressed in tobacco plants. *SbSLSP* in transgenic plants maintains cellular homeostasis, increases the detoxification of ROS, and improves physiological and biochemical parameters, under stress conditions (Singh et al., 2016). Even though a model of intracellular functioning of this protein was proposed, the characterization of this functionality has not been demonstrated. The question is whether this tolerance is generated by being SNARE-like from a halophyte plant or by the intracellular behavior of this type of protein. Advance knowledge of the intracellular role played by SNARE-like proteins under salt stress conditions would be essential to answer this question. According to this, we studied the effects of overexpression of a *SNARE-like* gene on vesicular trafficking in *S. lycopersicum* plants subjected to high salinity conditions. Consequently, the putative gene that codes for a SNARE-like in the genome of *S. lycopersicum* was identified and its expression levels during salt stress were analyzed. Then, the effects of its overexpression on salt stress tolerance in *S. lycopersicum* plants were evaluated by measuring physiological and biochemical parameters. Subsequently, the subcellular localization of SNARE-like was determined, to then analyze the endocytic rate, the accumulation of hydrogen peroxide and the vacuolar sodium content under salt stress conditions. These results allow us to suggest that the tolerance conferred by these SNARE-like proteins is due to the modulation of intracellular vesicular traffic induced by a high endocytic rate. In addition, it will serve as a basis to carry out evaluations on the use of this type of genes in programs associated with genetic improvement and tolerance to salt stress in tomato plants.

2 Materials and methods

2.1 Plant material and culture conditions

For this research, we used tomato seeds (*Solanum lycopersicum* cv. Moneymaker) which were sown in a 0.5 L plastic pot with a mixture of 1:1:1 of perlite, vermiculite, and peat as substrate. After 15 days post germination, seedlings were transferred to 2 L plastic pots containing the same substrate. The plants were watered once a week with a nutrient solution containing 1.1 g/L of Murashige and Skoog salts (MS; Murashige and Skoog, 1962). Tomato plants were cultivated and propagated in growth chambers at 25°C with a long-day photoperiod (16/8 hours light/dark). After 10-12 weeks, tomato plants were subjected to saline stress treatments by adding 400 mL of 300 mM NaCl for 72 hours. Three plants for each condition were considered. Leaf and root were collected separately for each plant in the periods 0, 3, 6, 12, 24, 48 and 72 hours of treatment with salt stress, to measure transcript levels. The collected tissue was quickly frozen with liquid nitrogen and stored at -80°C for further analysis.

2.2 *In silico* analysis of the genes that code for SNARE-like in tomato plants

The Solgenomic database (http://www.solgenomics.net) was used to search for *S. lycopersicum* protein displaying sequence identity with the SNARE-like protein from *S. brachiata* (accession number KF111691). The sequence of the gene *Solyc06g068080.2* (*SlSLSP6*) was selected by the highest score of similarity of the gene product. Sequences were aligned using the MUSCLE software (https://www.ebi.ac.uk/Tools/msa/muscle/). Comparative analyses were performed for each protein with the BLASTp program (http://www.ncbi.nlm.nih.gov), InterPro (https://www.ebi.ac.uk/interpro/) and Pfam databases. A phylogenetic tree was built using the MEGA7 (http://www.megasoftware.net) (Kumar et al., 2016) with the neighbor-joining method (Saitou and Nei, 1987) and bootstrap analysis of 1000 replications.

2.3 Isolation and purification of total RNA and cDNA synthesis

Total RNA was extracted from leaves and roots of *S. lycopersicum* plants using the SV Total RNA Isolation System commercial kit (Promega, Madison, WI, USA). Each sample was treated with DNase I (Ambion® TURBO DNA-free™) to remove remaining genomic DNA. RNA concentration and purity were estimated in a NanoQuant spectrophotometer (UV-160A, Kyoto, Japan).

First-strand cDNA synthesis was performed with 1–2 µg of isolated RNA using the Maxima H Minus First Strand cDNA Synthesis kit (Thermofisher, Massachusetts, USA). cDNA samples were stored at -20°C.

2.4 PCR and quantitative real-time PCR (RT-qPCR)

The PCR reactions were carried out in a final volume of 25 µL which contained DNA, 1X PCR buffer, $MgCl_2$, dNTPs, the corresponding oligonucleotides (Supplementary Table 1) and the Taq polymerase enzyme (Promega Corporation). The PCR product was analyzed in agarose gel electrophoresis (1X TAE Buffer). RT-qPCR analysis was carried out using the Brilliant SYBR Green qPCR MasterMix System (Stratagene, La Jolla, CA) according to the manufacturer's instructions on a DNA engine Opticon 2 Cycler System (MJ Research, Watertown, MA). For each sample, RT-qPCR was carried out in triplicate (technical replicates). The $2^{-\Delta\Delta Ct}$ method was applied to calculate the fold change of gene transcript levels (Livak and Schmittgen, 2001). *Ubiquitin3* gene (accession X58253) was used as a housekeeping gene (Yáñez et al., 2009).

2.5 Gene transformation of tomato plants

For the transformation of tomato plants, the coding sequence of *SlSLSP6* was amplified from cDNA of leaves using the primers described in Supplementary Table 1. After the amplification reaction, the DNA fragments were cloned into pGEM-T vector (Promega) and sequenced. Then, the complete cDNA of the *SlSLSP6* was inserted between the XbaI-BamHI restriction sites, replacing *β-glucuronidase* gene (GUS gene) of the binary vector pBI121 (Clontech, Palo Alto, CA, USA), and staying under the control of the constitutive promoter CaMV 35S, generating the 35S:: SlSLSP6 cassette. Tomato plants were transformed with the 35S:: SlSLSP6 cassette and with the unmodified pBI121 for control plants (Vector). Chemo-competent *Agrobacterium tumefaciens* GV3101 was cultured in YM solid medium (0.04% w/v yeast extract, 1% w/v mannitol, 1.7 mM NaCl, 0.8 mM $MgSO_4.7H_2O$ and 1.5 w/v of agar) and grown at 28°C for 48 hours with the followed antibiotics: kanamycin (50 mg/mL), gentamicin (100 mg/mL) and rifampin (100 mg/mL). The colonies were analyzed by PCR. A culture of the PCR-confirmed strains was used to transform tomato cotyledons from 10-day-old seedlings, according to the method of Fillati et al. (1987). After six months of organogenesis, the shoots obtained were individualized. The plants were selected in kanamycin antibiotic (50 mg/mL) and characterized by PCR and RT-qPCR. Sixteen *SlSLSP6* overexpressor lines were selected (L1-L16).

2.6 Determination of performance and tolerance to salt stress

SlSLSP6 overexpressing plants (L9 and L10) and control plants (WT and Vector) with similar size and number of leaves were subjected to salt stress conditions grown in pots with perlite and vermiculite substrate (1:1). These plants were subjected to irrigation

with 200 mL of a 300 mM NaCl saline solution every 72 hours. Plant performance and tolerance parameters were evaluated after 5, 15 and 25 days of stress treatment. Each time of the experimental trial considers 3 plants as biological replicates. Relative water content (RWC) was estimated according to the modified protocol of Maggio et al. (2007) and Vasquez-Robinet et al. (2008), where RWC = [(FW – DW)/(TW – DW)] x 100. Three leaves of about the same size and location on the plant were weighed (fresh weight, FW) and then incubated in distilled water for 24 hours at room temperature in darkness. Then, the tissue was weighed to calculate the turgid weight (TW) and finally, the samples were dried at 60°C for 48 hours for the determination of the dry weight (DW). Additionally, the efficiency of photosystem II represented as Fv/Fm and the performance index (PI) were evaluated. These measurements were obtained using a pocket fluorometer (Hansatech, King's Lynn, Norfolk, England) following the procedure described by Giorio (2011). The chlorophyll content was evaluated in leaf discs following the previously described protocols (Orellana et al., 2010; Salinas-Cornejo et al., 2021). According to this, the leaf discs were ground with 80% acetone (v/v) and the extract was centrifuged. The absorbance of the supernatant was measured using the NanoQuant spectrophotometer (UV-160A, Kyoto, Japan), using the method described by Lichtenthaler and Wellburn (1983).

To determine lipid damage, the lipid peroxidation marker (MDA) was determined according to the modified protocol of Dionisio-Sese and Tobita (1998) and Ghanem et al. (2008). The concentration was obtained by subtracting the absorbance between 600 and 532 nm. Then, the value was multiplied using the molar extinction coefficient of 155 $mmol^{-1}cm^{-1}$. In addition, the ROS accumulation was observed in cells of the apical zone of the root (root length of 0.5 cm) of transgenic tomato plants (L9 and L10 lines) and control plants (WT and Vector). Tomato seedlings exposed for 40 minutes to liquid MS medium supplemented with 200 mM NaCl were subsequently incubated for 20 minutes with the fluorescent tracer H_2DCFDA 10 µM (2',7'-dichlorodihydrofluorescein diacetate, ThermoFisher Scientific, Massachusetts, USA) as described by Leshem et al. (2006) and Zhao et al. (2009). To delimit the plasma membrane of each cell, the seedlings were stained with FM4-64 5 µM for 15 minutes in darkness at 4°C. Then, the roots were visualized immediately.

2.7 SlSLSP6 subcellular localization

The subcellular accumulation of SlSLSP6 was performed in 10-day-old *Arabidopsis thaliana* seedling lines expressing different organelle markers described by Geldner et al., 2009. Each line was transiently transformed using the 35S::GFP-SlSLSP6 construct, contained in the pAM1 vector. The *SlSLSP6* gene, amplified as described in section 2.5, was inserted into the pAM1 vector in the C-terminal orientation of the GFP gene. We use an adaptation of the technique carried out by Wu et al. (2014), called AGROBEST. The Arabidopsis marker lines RabG3f-mCherry (Germplasm ID CS781670; late endosome/tonoplast), RabF2a-mCherry (Germplasm ID CS781672; late endosome/prevacuolar compartments), VAMP711-mCherry (Germplasm ID CS781673; tonoplast), VTI12-mCherry (Germplasm ID CS781675; early endosome/TGN), SYP32-mCherry (Germplasm ID CS781677; Golgi complex) and PIP1;4-mCherry (Germplasm ID CS781687; plasma membrane) were grown in similar MS agar plates in growth chambers.

2.8 Endocytosis rate analysis

The rate of plasma membrane internalization was determined in root apical zone cells (root length 0.5 cm) of both transgenic tomato seedlings (L9 and L10 lines) and control plants (WT and Vector) using the membrane tracer FM4-64 (Molecular Probes, Eugene, OR). Roots were stained with FM4-64 (5 µM) in a solution of MS liquid medium at 4°C for 20 minutes in darkness. At 5-, 15-, and 30-minutes at room temperature, different seedlings were by imaged. To determine the effect of salt stress on the endocytic rate, a group of seedlings, previously stained with FM4-64 (5µM), was subjected to salt stress by incubation with liquid MS medium supplemented with 200 mM NaCl for 30 minutes at room temperature.

2.9 Analysis of intracellular sodium accumulation

The accumulation of sodium into the vacuole was determined using the Na^+ indicator Sodium Green™ (ThermoFisher Scientific, Massachusetts, USA). Tomato seedlings with root length of 0.5 cm were incubated in MS medium supplemented with 200 mM NaCl for a period of 16 hours. After treatment, the seedlings were incubated with 5 µM Sodium Green™ for 2 hours and a non-ionic surfactant Pluronic F-127 20% w/v (ThermoFisher Scientific, Massachusetts, USA) to improve the uptake of the dye, following an adaptation of the method described by Tarte et al., 2015 (San Martín-Davison et al., 2017; Salinas-Cornejo et al., 2021). Then, the roots were stained for 20 minutes with FM4-64 5 µM (in the dark at 4°C) to delimit the plasma membrane and visualized.

2.10 Quantification of fluorescent markers

To quantify colocalization data, colocalization between GFP-SlSLSP6 and mCherry markers was quantified using the square of Pearson correlation coefficient (R^2). The colocalization between GFP-SlSLSP6 and PIP1;4-mCherry was scored from a defined region of interest (ROI) for calculation of the Pearson correlation coefficient. R^2 was estimated considering 10 images using the Zeiss Zen 2010 software (zeiss.com).

The FM4-64 fluorescence was quantified manually at the intracellular and plasma membrane compartments using ImageJ software (http://rsb.info.nih.gov/ij/). FM4-64 internalization rate was determined as the ratio of both signals in each cell, using the equation described by Varma and Mayor (1998) and Baral et al. (2015a).

The quantification of the signal of H_2DCFDA and Sodium Green markers was performed using ImageJ software. The mean of fluorescence was scored from a manually defined ROI in each

image. Images were processed using a color-coded intensity, with the lowest fluorescence intensity corresponding to blue and highest fluorescence intensity corresponding to green color.

To quantify the fluorescence intensities, laser, gain and pinhole settings of the confocal microscope were identical and constant among different treatments. All confocal experiments were independently repeated at least three times, considering for each experiment at least 25 cells from 5 roots of 5 different plants for each genotype.

2.11 Confocal microscopy

Root cells were visualized with Zeiss-LSM 710 confocal microscope (Zeiss Axio Observer Z1 equipped with LSM700 module and PTM detector). An Fluar 40x/1.30 oil M27 objective or N-Achroplan 10x/0.25 M27 lens were used. Digital zoom 1X or 4X. The parameters were: laser 555 nm/emission>588–596 nm for FM4-64 or fluorescent protein mCherry, laser 488 nm/emission 517–561 nm for the fluorescent protein GFP, Sodium-Green or H_2DCFDA (filter SP 555 Zeiss), pixel dwell of 25.2 µs, 488/555 nm lasers set at 2%, pinhole diameter of 70 µm, and beam splitter MBS 405/488/555/639.

2.12 Statistical analysis

Statistical analyzes were performed using the R program (version 1.7). Statistical significance was determined by one-way ANOVA analysis ($p < 0.05$).

3 Results

3.1 Identification of a SNARE-like superfamily gene from *Solanum lycopersicum*

Using the Solgenomics database, the sequence coding for a putative SNARE-like in *Solanum lycopersicum* was identified. This gene was named *SlSLSP6* (Solyc06g068080.2), which has not been previously characterized. The analysis using NCBI Blastp tool indicated that the amino acid sequence of SbSLSP from *Salicornia brachiata* (Accession AGV05388) displayed an 84.35% identity to the sequence SlSLSP6 from *Solanum lycopersicum* (Accession XP_010322672). SlSLSP6 is a protein of 147 amino acids with no transmembrane domains in its structure as expected for a SNARE protein. However, SlSLSP6 displayed putative palmitoylation site at the cysteine residue located at position 115 (Cys115) at the LDKYGKICLCLDEIV motif that may allow it to interact with membranes (Supplementary Figure 1). Multiple alignment and comparison of the amino acid sequences of SlSLSP6 with SNARE-like from *Arabidopsis thaliana* (AtSLSP), *Salicornia brachiata* (SbSLSP) and two other sequences identified in *Solanum lycopersicum* (SlSLSP3 and SlSLSP11) revealed a high identity score as well as the presence of conserved domains as a SNARE-like superfamily protein (Supplementary Figure 1). The phylogenetic analysis of plants SNARE-like proteins showed that SlSLSP6 clustered with proteins from the halophytic plants *S. brachiata* and *Zostera marina* (Park et al., 2016; Singh et al., 2016) (Supplementary Figure 2). SISLSP6 is grouped also with the proteins from *Nicotiana tomentosiformis* and *Solanum pennelli*, considered salt-tolerant plants. Consequently, based on the high sequence identity and the presence of the structural domains of the SNARE-like superfamily proteins, the SlSLSP6 is predicted to function as a SNARE-like protein in *S. lycopersicum*.

3.2 *SlSLSP6* responds to salt stress

The *S. lycopersicum* plants were subjected to saline stress (300 mM NaCl) for 72 hours, to evaluate whether the *SlSLSP6* responds to such a challenge (Figure 1). The salt treatment indeed was a stressful condition since the salt stress-marker-genes *AREB1* (Orellana et al., 2010; Madrid-Espinoza et al., 2019) and *TSW12* (Torres-Schumann et al., 1992; San Martín-Davison et al., 2017) responded as expected, increasing their transcript level along the treatment (Figures 1B, C). Interestingly, *SlSLSP6* transcript levels increased at 3 hours of salt stress in both roots and leaves. This increase was maintained as far as 12 hours of treatment (Figure 1A). After 24 hours of salt stress, the *SlSLSP6* transcript level becomes similar to the beginning of the trial (time 0) in both tissues. These results indicate that *SlSLSP6* is induced under salt stress in leaves and roots suggesting the participation of the *SlSLSP6* gene product in the primary response of *S. lycopersicum* to saline stress.

3.3 The overexpression of *SlSLSP6* in *S. lycopersicum* confers tolerance to salt stress

To evaluate the participation of *SlSLSP6* in the response to salt stress, we study the effects of its overexpression in *S. lycopersicum*. Then, cDNA of the *SlSLSP6* gene was cloned into the binary vector pBI121 to express the coding sequence under the 35S promoter in plants. *S. lycopersicum* cv. Moneymaker was transformed mediated by *Agrobacterium tumefaciens* and transformant explants were selected by kanamycin resistance and verified by PCR. The same protocol was followed transforming tomato plants with the empty vector to be used as a control (Vector) for the following experiments. The expression levels of *SlSLSP6* were evaluated by qRT-PCR on the *SlSLSP6* transformant plants. Three lines were identified as overexpressors of *SlSLSP6* (Supplementary Figure 3). Two of them, L9 and L10 were selected for the further characterization.

The response to salt stress of *SlSLSP6* overexpressor plants was evaluated and compared to control plants as well as wild type plants. Two-month-old tomato plants were irrigated every 72 hours with a solution of 300 mM NaCl. Plant performance parameters were evaluated just before starting the trial and after 5, 15 and 25 days of salt treatment. After 15 days of treatment, the macroscopic symptoms as yellow leaves induced by salt stress began to appear in wild type and Vector plants; however, they are less abundant on

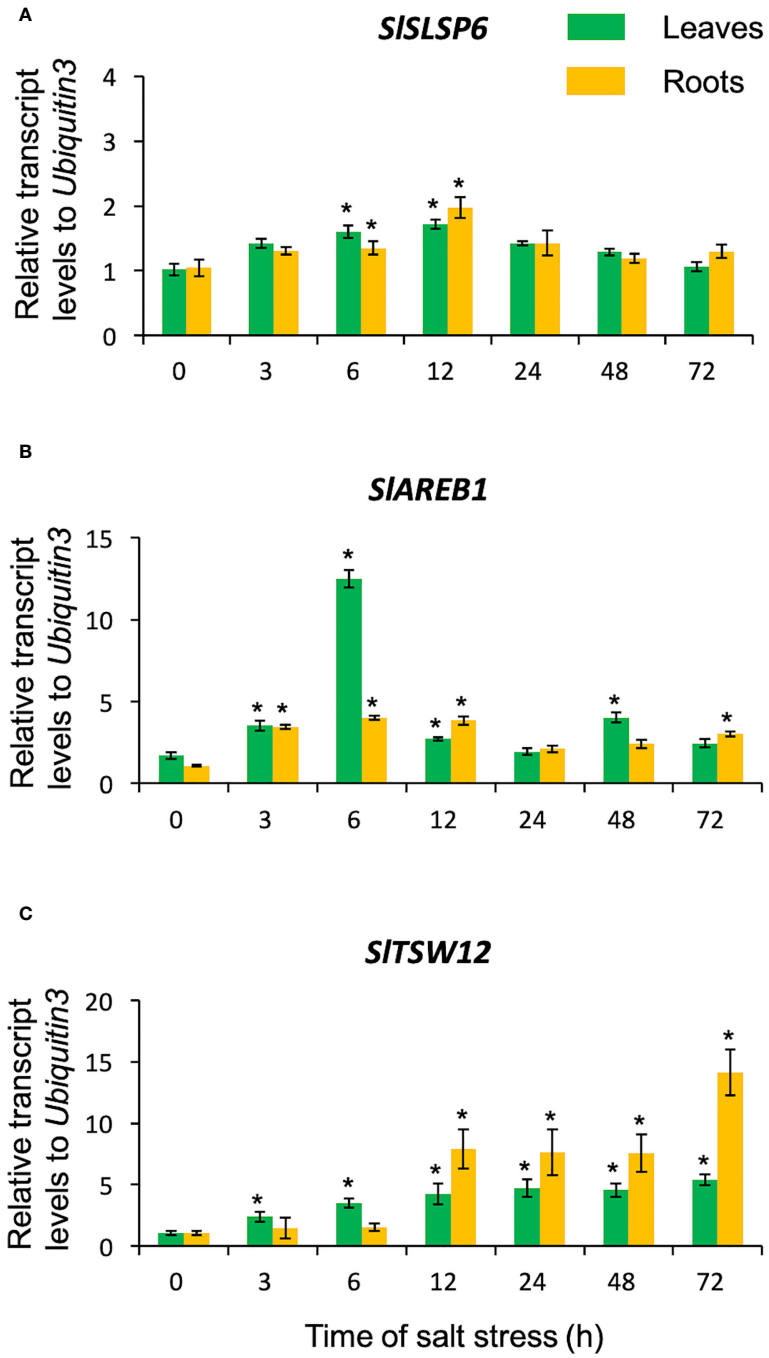

FIGURE 1
Transcript levels of *SlSLSP6* in *S. lycopersicum* exposed to salt stress. Ten-twelve-week-old tomato plants were watered with 300 mM NaCl solution for 3, 6, 12, 24, 48 and 72 hours. Roots and leaves were collected separately for RNA isolation. The transcript levels of *SlSLSP6* **(A)**, *SlAREB1* **(B)** and *SlTSW12* **(C)** were measured by RTqPCR. Results are expressed as relative expression considering *Ubiquitin3* as the gene of reference. Mean and standard errors of three biological replicates are shown. Asterisks above the bars indicate statistically significant difference to the level before starting the salt treatment (time 0) determined by one-way ANOVA (p-value < 0.05).

L9 and L10 lines. After 25 days of salt stress, there were evident differences between the control plants and L9 and L10 plants. The symptoms of chlorosis and wilting were dramatic on WT and Vector plants showing a significant loss of the older leaves. However, L9 and L10 plants exhibited less chlorotic leaves and displayed several green leaves after the same period of salt stress treatment, suggesting an increase of salt tolerance due to the higher level of *SlSLSP6* gene product (Figure 2A). Consistently, the RWC of L9 and L10 lines reached 74% and 64%, respectively while in wild type plants decreased to 56% after 25 days of salt stress (Figure 2B). This suggests that there is greater turgidity in the leaves of the overexpressing lines, which is consistent with the better appearance of the plants (Figure 2A). The applied salt stress treatment resulted in 70% reduction of chlorophyll levels in wild type and Vector

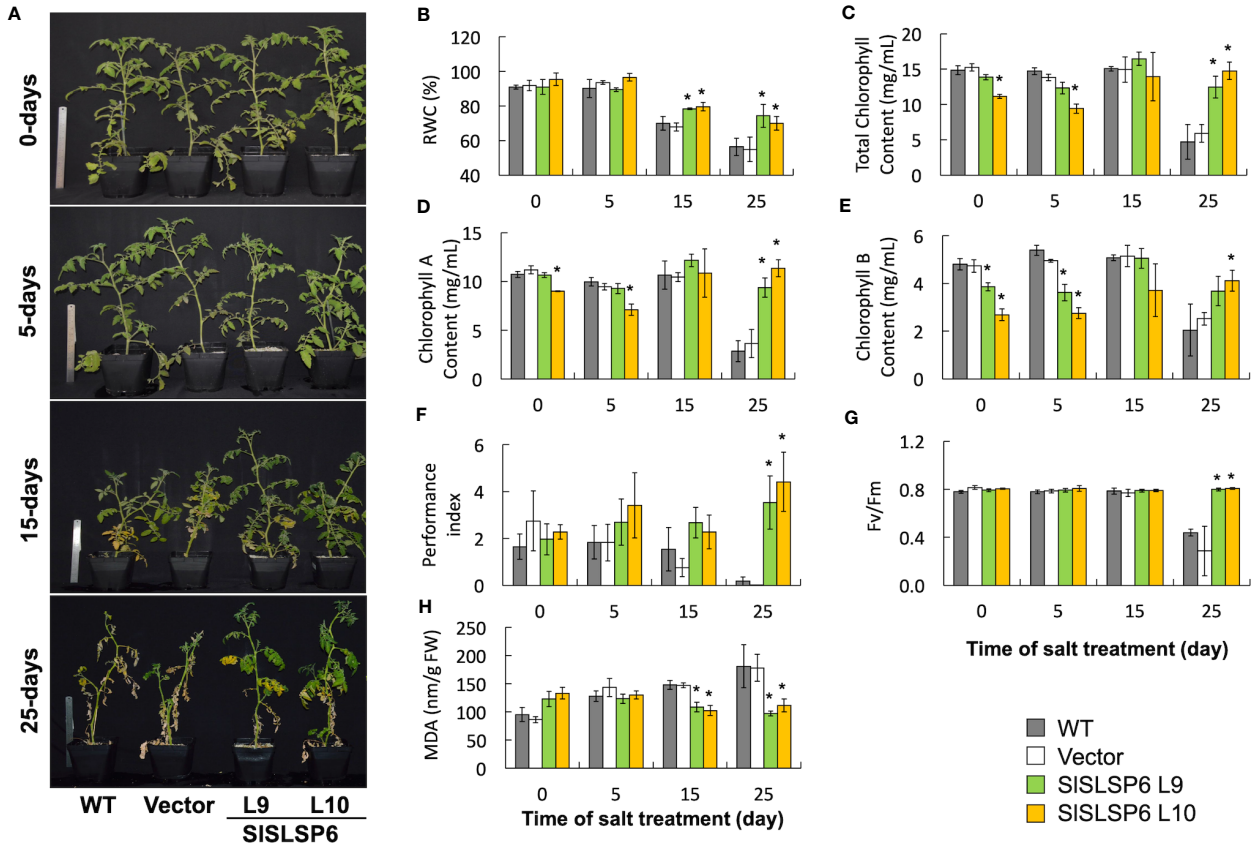

FIGURE 2
The response of plants transformed with *SlSLSP6* shows a greater tolerance to high salinity conditions. Tomato plants (WT, Vector and *SlSLSP6* overexpression lines) were watered with 300 mM NaCl solution every 72 hours for a period of 25 days. Plants performance and tolerance parameters were evaluated at the beginning of the trial (time 0) and after 5, 15 and 25-days of salt stress. **(A)** Representative images of each line of tomato plants. **(B)** Relative water content (RWC). **(C)** Total chlorophyll content. **(D)** Chlorophyll A content. **(E)** Chlorophyll B content. **(F)** Performance Index (PI). **(G)** PSII Maximum quantum efficiency analysis (Fv/Fm). **(H)** Malondialdehyde (MDA) content. Mean and standard error of three plants in three independent experiments are shown. Asterisks indicate statistically significant differences between WT and transgenic plants (p-value < 0.05) determined by one-way ANOVA.

plants. However, the overexpression of *SlSLSP6* rescued the drop on chlorophyll (chlorophyll A and chlorophyll B) content induced by 25 days of salt stress (Figures 2C–E). These results suggest that the high levels of *SlSLSP6* somehow increase the plant tolerance. To confirm that *SlSLSP6* overexpression plants are more tolerant to salt stress, we evaluate physiological state of the plants by measuring the performance index (PI) and the efficiency of photosystem II (PSII), represented by the maximum quantum efficiency of the PSII (Fv/Fm). The PI values in the *SlSLSP6* overexpressor lines were significantly higher compared to control plants, which decreased by approximately 75% after 25 days of stressful conditions (Figure 2F). As expected, the ratio Fv/Fm dropped drastically to 0.4 in control plants after 25 days of salt stress (Figure 2G). In contrast, *SlSLSP6* overexpressors lines kept the levels of Fv/Fm as plants without any salt stress condition. Consistently, there was no membrane damage on overexpressor plants as result of the salt stress while in control plants lipid peroxidation increases along the salt treatment (1.8 times higher after 25 days) (Figure 2G). In addition, we used the fluorescent marker H_2DCFDA to determine the level of ROS in tomato roots under normal conditions (Supplementary Figure 4) and subjected to 200 mM NaCl. The L9 line showed to be less tolerant since it had a similar result to the control plants. Instead, the L10 line showed 15 - 30% decrease of ROS accumulation compared to control plants (Figures 3A, B). Overall, the overexpression of *SlSLSP6* prevents the detrimental effects of salt stress improving plant performance at the physiological and cellular level. These results demonstrate that the overexpression of *SlSLSP6* improves the tolerance of the tomato plants to high salinity conditions.

3.4 SlSLSP6 is localized at the plasma membrane of root cells of *A. thaliana*

SbSLSP from *S. brachiata*, a SNARE-like protein, is localized within the endomembrane system (Singh et al., 2016). Similar to SbSLSP, SlSLSP6 from *S. lycopersicum* would have a conserved function in the endomembrane system. Although SlSLSP6 does not display a transmembrane domain most likely it is able to be recruited to membranes in order to accomplish its function. To determine the subcellular localization of SlSLSP6, we overexpress transiently a GFP-SlSLSP6 construct in a collection of *A. thaliana*

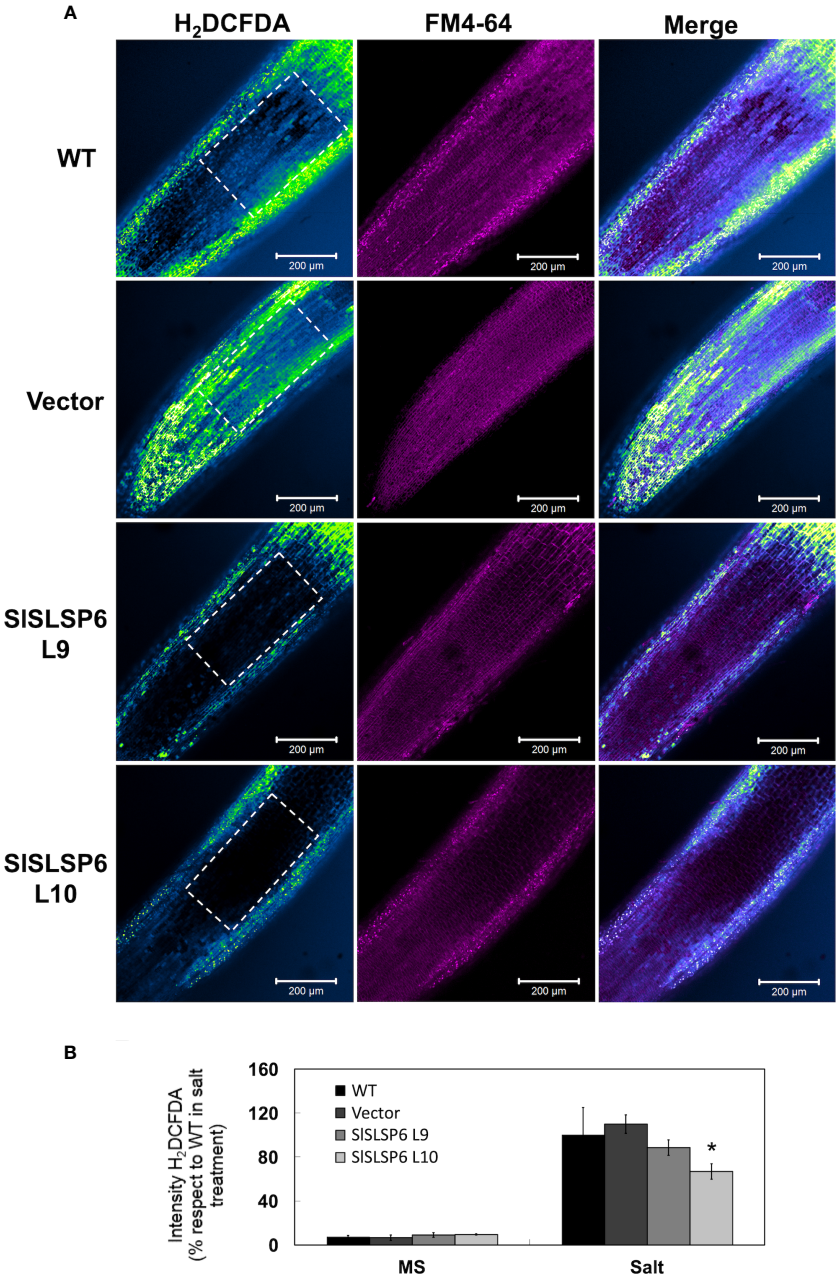

FIGURE 3
H_2O_2 content in *Solanum lycopersicum* roots under salt stress conditions. **(A)** Representative images of H_2O_2 production in control tomato seedlings and *SlSLSP6* overexpressing lines under 200 mM NaCl and observed by confocal microscopy. The ROI delimited by the white dashed lines was considered for quantification. Tomato roots were treated with H_2DCFDA (color-coded intensity, with the lowest fluorescence intensity corresponding to blue and highest fluorescence intensity corresponding to green color) and FM4-64 tracer (in magenta). Images of the differentiation and elongation zones of the roots were obtained. The bar indicates a scale of 200 µm. **(B)** Quantification of fluorescence intensity of H_2DCFDA. The values indicate the percentage relative to 100% fluorescence intensity evaluated in the WT plants under salt stress. Data indicate mean values and standard errors. Asterisks indicate statistically significant differences between control lines and transgenic plants (p-value < 0.05), using one-way ANOVA.

that express fluorescent endomembrane compartment markers (Geldner et al., 2009). The following mCherry markers were selected: plasma membrane (AtPIP1;4), early endosome/TGN (AtVTI12), Golgi complex (AtSYP32), late endosome/prevacuolar compartments (AtRabF2a), late endosome/tonoplast (AtRabG3f) and tonoplast (AtVAMP711). *A. thaliana* roots were transiently transformed using a protocol adapted from the AGROBEST technique (Wu et al., 2014; Wang et al., 2018), with two different constructions: the plasmid pAM1 carrying the sequence to express GFP : SlSLSP6 (35S::GFP-SlSLSP6) or with the empty vector (35S::GFP), as a negative control. The results indicated that GFP-SlSLSP6 signal overlapped with the mCherry AtPIP1;4 protein, located in the plasma membrane (yellow arrow Figure 4 and Supplementary Figure 5), strongly suggesting that

10.3389/fpls.2023.1212806

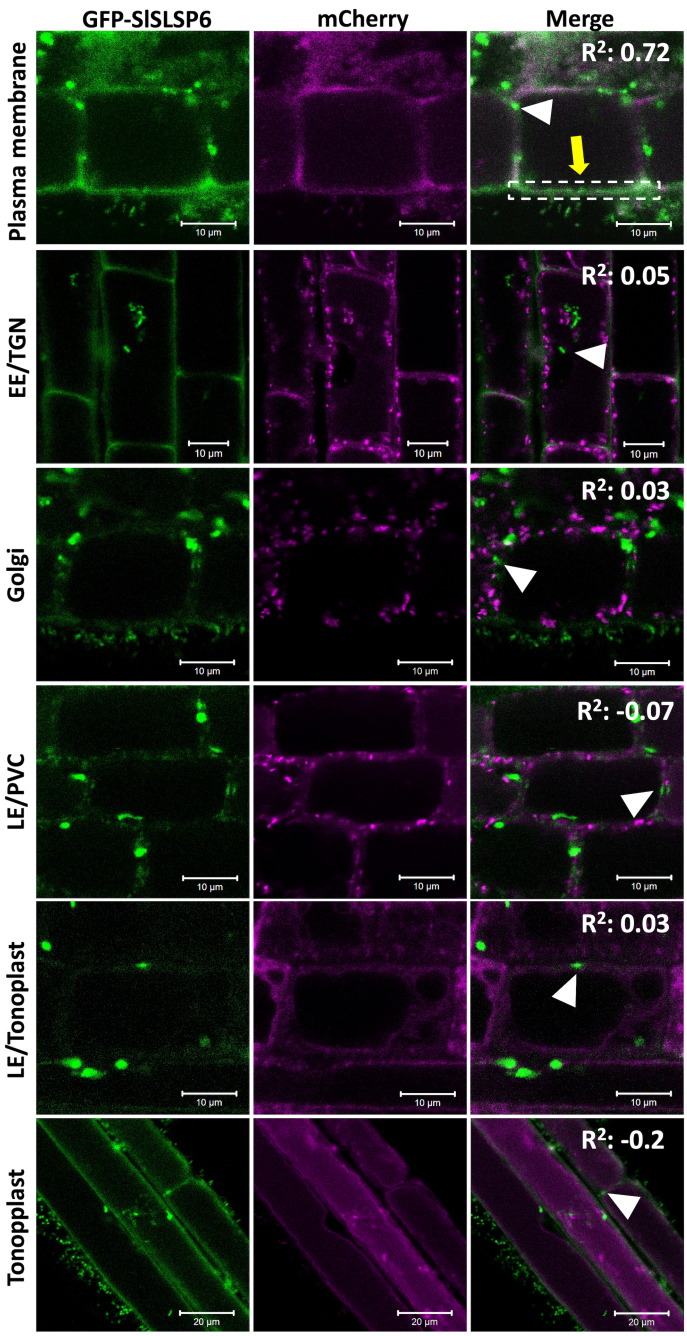

FIGURE 4
SlSLSP6 resides in the plasma membrane of *A. thaliana* root cells. 10-day-old *Arabidopsis thaliana* mCherry-marker lines of different endomembrane compartments were transiently transformed with the vector that allows to express a GFP-fusion to SlSLSP6 version. GFP and mCherry (in magenta) fluorescence in root cells were visualized by confocal microscopy. For each marker line, 25 cells of 15 plants were evaluated. Images of the differentiation or elongation zone of the roots were obtained. The square of Pearson correlation coefficient is indicated (R^2). In the colocalization with plasma membrane, the ROI delimited by the white dashed lines was considered for quantification. Markers: Plasma membrane, PIP1;4-mCherry; EE/TGN, VTI12-mCherry; Golgi, SYP32-mCherry; LE/PVC, RabF2a-mCherry; LE/tonoplast, RabG3f-mCherry; Tonoplast, VAMP711-mCherry.

SlSLSP6 is accumulated in the plasma membrane. In contrast, the GFP-SlSLSP6 distribution did not colocalize with the markers of the vacuole and Golgi complex. In addition to the plasma membrane distribution, GFP-SlSLSP6 displayed a punctate pattern (white arrowheads Figure 4) with similar characteristics to endosomes or PVCs. However, these bodies did not colocalize with the AtVTI12 nor AtRabF2a proteins, indicating there are different compartments than the early endosome/TGN nor LE/PVC. Therefore, these results suggest that the SlSLSP6 protein would be participating in processes linked to the plasma membrane, such as endocytosis, and may participate in pathways to the early or late endosome.

3.5 The overexpression of *S. lycopersicum SlSLSP6* increases the endocytosis under normal and salt stress conditions

Endocytic trafficking has been proved to be important for salt stress tolerance (San Martín-Davison et al., 2017). In fact, an increased rate of endocytosis has been shown to increase plant tolerance under salt stress conditions (Salinas-Cornejo et al., 2021). As SlSLSP6 could be participating in processes linked to the plasma membrane, we hypothesized that this SNARE-like would have an active role in endocytosis. To test the rate of endocytosis, the internalization of the tracer FM4-64 was analyzed in *SlSLSP6* overexpression lines (L9 and L10) and compared to wild type and Vector tomato seedling roots. The L10 overexpressing line grown in control conditions displayed a higher internalization rate than control plant: FM4-64 internalization after 15 and 30 minutes increased 1.6 and 2.0 times higher, respectively, compared to what was observed in the roots of the control plant (Figures 5A, C). Surprisingly, the L9 overexpressing line displayed similar levels of FM4-64 internalization than control plants although displayed higher levels of *SlSLSP6* transcripts. This result confirms the functional role of SlSLSP6 on endomembrane trafficking as a SNARE-like protein at the plasma membrane. It has been shown that salt stress induces endocytosis in root cells (Salinas-Cornejo et al., 2021). Therefore, we tested whether such a challenge would stimulate further membrane internalization in *SlSLSP6* overexpression lines. Then, tomato seedlings were subjected to 30 minutes of salt stress (200 mM NaCl) before the endocytosis rate was evaluated (Figure 5B). Indeed, salt treatment induced FM4-64 internalization on control plants (Figure 5B). Under this condition, the overexpressing lines L9 and L10 showed a higher internalization rate than control plants: 1.2 and 1.4, respectively, compared to 1.0 (Figures 5B, D). These results strongly suggest that the high level of *SlSLSP6* gene product resulted in modulation of vesicular trafficking increasing the rate of endocytosis playing an important role on the mechanisms by which plants manage the salt stress.

3.6 *SlSLSP6* overexpression induces sodium compartmentalization into the vacuoles

An increase in the endocytosis rate promotes a greater compartmentalization of sodium in the vacuoles contributing to plant tolerance against salt stress conditions (Salinas-Cornejo et al., 2021). To verify this relationship, sodium accumulation was monitored using the Sodium Green™ fluorescent indicator in tomato roots of plants under normal conditions (Supplementary Figure 6) and subjected to 200 mM NaCl for 16 hours. Both *SlSLSP6* overexpressing lines L9 and L10 displayed a higher level of signal of Sodium Green than control plants (Figures 6A, B). Indeed, the L9 line displayed an increase of about 60% of fluorescent signal than control plants while L10 displayed the double amount of control plants. It was also observed that the accumulation of sodium occurs inside the vacuoles, both in the epidermal and cortical zone of the tomato roots, unlike what was identified in the control plants, where the accumulation is mainly in epidermal cells. Along with this, we observed that there was a strong accumulation of the sodium marker in structures with a pattern different from that of the vacuoles, whose composition and nature are unknown. These structures were also labeled with FM4-64 (white arrows Figure 6A). It could be speculated that they correspond to endosomal aggregates from the plasma membrane *via* the endocytic pathway, but this requires further investigation. Consequently, these results suggest that the greater compartmentalization of sodium in the vacuoles and in endosomal aggregates could be due to a greater endocytic dynamic of the transgenic plants that overexpress *SlSLSP6*, allowing to explain their enhanced tolerance under high salinity conditions.

4 Discussion

SNARE proteins are fundamental components in the vesicular trafficking machinery, playing a central role in the anchoring and fusion of vesicles with their acceptor membranes and in many biological processes, such as signaling in response to abiotic stress conditions (Leshem et al., 2006; Tarte et al., 2015; Nisa et al., 2017; Salinas-Cornejo et al., 2019; Won and Kim, 2020). They are relatively small proteins, in the range of 200-400 amino acids, where the SNARE domain is susceptible to form coiled-coil structures (Lipka et al., 2007). Most of the SNARE proteins described have transmembrane domains. However, some SNARE proteins are anchored to membranes through lipid modifications (Saito and Ueda, 2009). The homologous proteins of SNAP-25, a protein of the Qb+Qc-SNARE type, have a site in its sequence where a post-translational modification known as palmitoylation occurs, which would contribute to the stability of its association with the plasma membrane (Gonzalo and Linder, 1998; Greaves and Chamberlain, 2011; Won and Kim, 2020). In this sense, a *SNARE-like* gene, called *SlSLSP6* in tomato, has been identified and characterized, determining that the SlSLSP6 protein possesses a putative transmembrane domain, predicted as a palmitoylation signaling site. This type of reversible post-translational modification would allow a pivotal role in associations with membranes or interactions with other proteins, regulating their traffic or modulating their stability, anchoring proteins in the membrane in response to environmental conditions (Singh et al., 2016; Won and Kim, 2020). For another SNARE-like, it has been described the presence of sequences where lipid modifications occur, increasing the affinity of soluble proteins for membranes, allowing their insertion. Such is the case of SbSLSP from the halophyte plant *Salicornia brachiata*, in which a myristoylation site has been predicted (Singh et al., 2016). In addition, the predictive analysis of sites of putative lipid-type modifications on the SNARE-like sequence of *Arabidopsis thaliana* was performed, showing sites of possible palmitoylations or myristoylation (Supplementary Figure 1), which suggests that post-translational modifications increase the affinity of SNARE-like to the membrane or to certain proteins. In addition, the SlSLSP6 protein also presented a conserved domain associated with clathrins

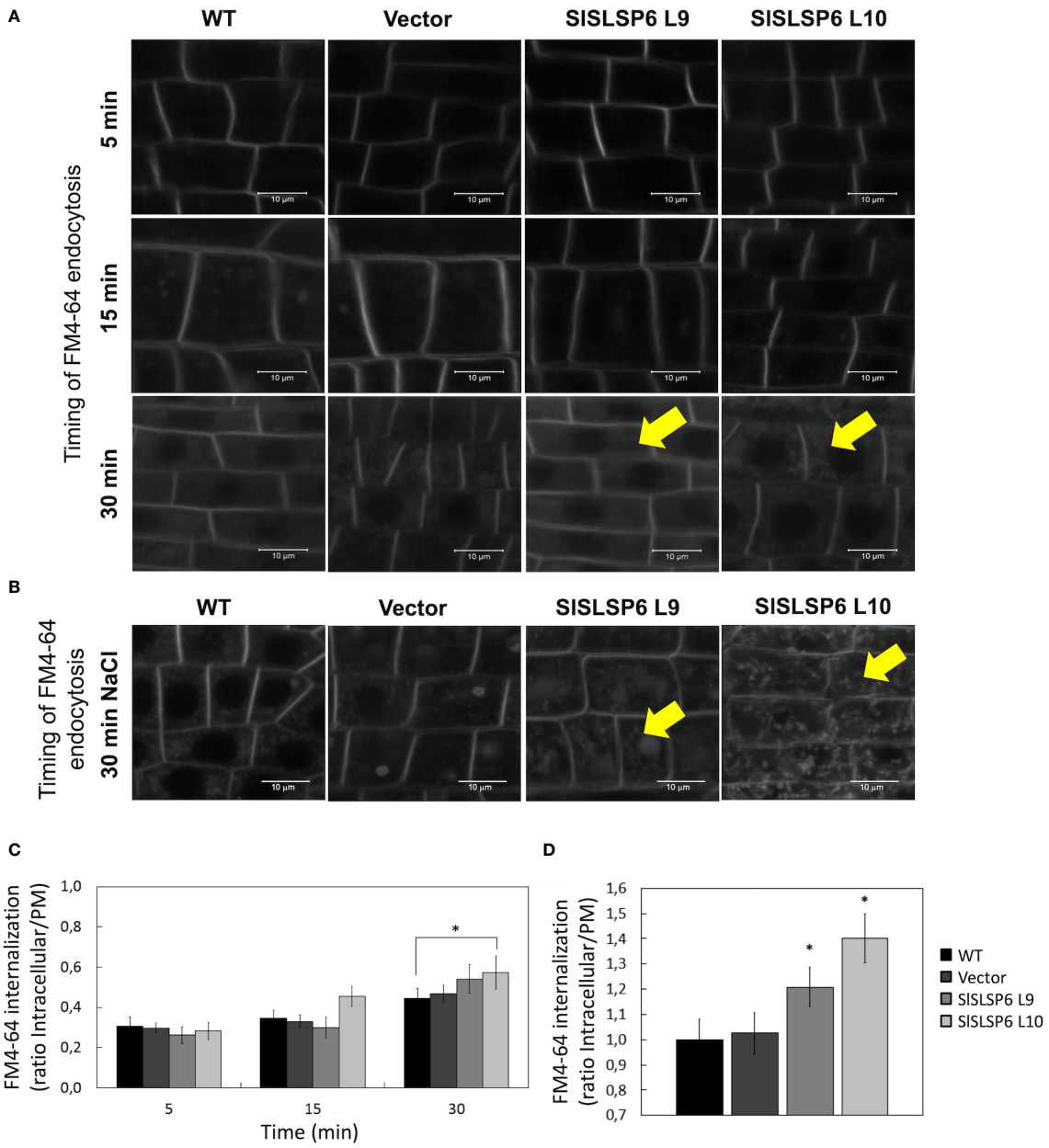

FIGURE 5
Endocytosis in wild type and transgenic *Solanum lycopersicum* roots. The endocytosis rate was evaluated on root cells with root length of 0.5 cm from WT, Vector and tomato plants that overexpress *SlSLSP6* (L9 and L10 lines) using the FM4-64 tracer. **(A)** Internalization of FM4-64 (in grayscale) was evaluated by confocal microscopy at 5, 15 and 30 minutes. Representative images of the differentiation zone of the root of three independent experiments (n=25 cells) are shown. Yellow arrows indicate representative FM4-64-stained endosomes. **(B)** FM4-64 internalization (in grayscale) on root plants treated previously with 200mM NaCl. Yellow arrows indicate representative FM4-64-stained endosomes. **(C)** Internalization rate of FM4-64 was evaluated in the experiment on **(A)** Mean and standard error are shown; n=25 cells. Asterisks indicate statistically significant differences between WT and transgenic plants (p-value < 0.05), using one-way ANOVA. **(D)** FM4-64 internalization rate of plants in **(B)** Results are expressed as the ratio between intracellular and plasma membrane signal. Mean and standard errors are shown. Asterisks indicate statistically significant differences between WT and transgenic plants (p-value < 0.05), using one-way ANOVA.

(Supplementary Figure 1), a protein complex that is involved in the assembly of clathrin coated vesicles (CCVs) budding from the plasma membrane. They are important in the selection and direction of cargo that will be transported. It has been described that these CCVs are part of the transport of membrane proteins through the endocytosis pathway (Reynolds et al., 2018). In this context, some plasma membrane proteins with typical SNARE-like features have been described in plants, including LOLITA (Longin-like protein interacts with TPLATE adaptor) from *A. thaliana* (Gadeyne et al., 2014) and SbSLSP (SNARE-like Superfamily Protein) from *S. brachiata* (Singh et al., 2016). LOLITA acts as an adapter protein together with other seven proteins, forming the TPLATE complex. This TPLATE complex directs clathrin-mediated endocytosis (Gadeyne et al., 2014; Yperman et al., 2021), is specific to plants and essential for their survival. However, its role under salt stress has not been described. On the

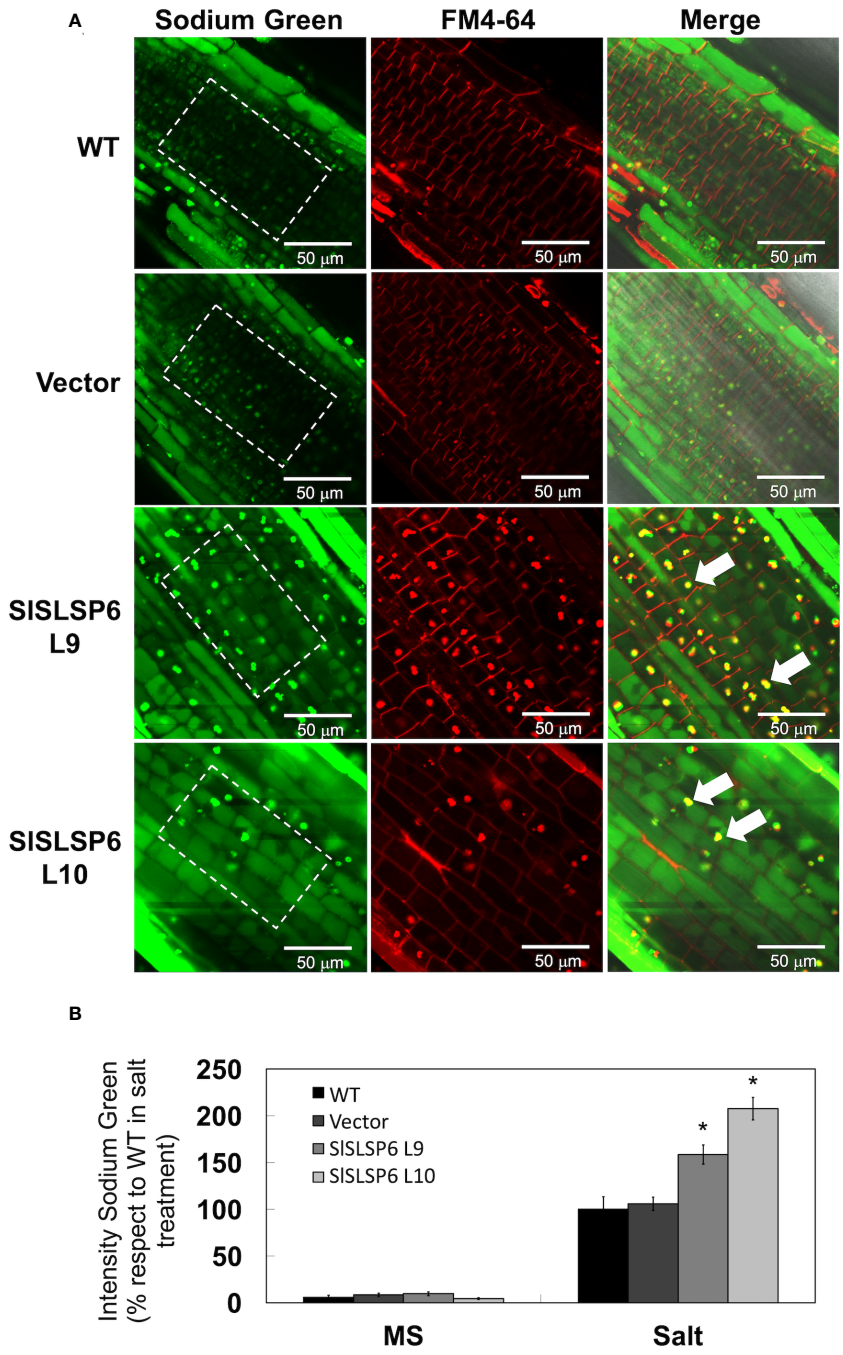

FIGURE 6
Sodium compartmentalization in *Solanum lycopersicum* root cell vacuoles under salt stress conditions. **(A)** Representative images of sodium accumulation in control tomato seedlings and lines overexpressing *SlSLSP6* under 200 mM NaCl and observed by confocal microscopy. The differentiation zone of the root was imaged. Tomato roots were treated with Sodium Green™ (green signal) and FM4-64 tracer (red signal). The bar indicates a scale of 50 µm. The ROI delimited by the white dashed lines was considered for quantification. **(B)** Quantification of fluorescence intensity of Sodium Green™ under normal conditions (MS) and salt stress (NaCl). The values indicate the percentage relative to 100% fluorescence intensity evaluated in the WT plants under salt stress. Data indicate mean values and standard errors. Asterisks indicate statistically significant differences between control lines and transgenic plants (p-value < 0.05), using one-way ANOVA.

other hand, SbSLSP has been associated with clathrin-mediated endocytosis regulation mechanisms and in response to salt and osmotic stress, as observed in transgenic tobacco plants that overexpressed *SbSLSP*, which improved their tolerance (Singh et al., 2016). Additionally, the analysis performed using the AGROBEST technique allowed us to observe the subcellular colocalization of the SlSLSP6 protein with different organelle markers (Figure 4). This analysis showed that this SNARE-like was located predominantly in the plasma membrane, supporting the *in silico* analysis. Also, we identified the presence of small structures in the vicinity of the plasma membrane, of unknown nature (Figure 4). The trans-Golgi network has been described as an

essential hub from which multiple vesicle trafficking pathways branch, including the secretory and vacuolar pathway (Uemura et al., 2019). Although no colocalization was observed with VTI12, an EE/TGNE marker, it cannot be assumed that these unknown structures could correspond to endosomal aggregates that participate in a different pathway. Along with this, since the proteins SbSLSP and LOLITA are also located in the plasma membrane, the localization of SlSLSP6 in tomato could indicate the maintenance of the mechanism of action of this type of SNARE-like. Additionally, the relative expression analysis carried out for the identification of SNARE-like proteins in tomato (Figure 1) suggests that *SlSLSP6* could be playing an important role under salt stress conditions. Accordingly, genes such as *GsSNAP33* from *Glycine soja* (Nisa et al., 2017), *SlSNAP33* from *S. lycopersicum* (Salinas-Cornejo et al., 2021), *AtSFT12* from *A. thaliana* (Tarte et al., 2015) and *SbSLSP* from *S. brachiata* (Singh et al., 2016) are induced above basal levels of gene expression when plants are subjected to different salt concentrations and participate in the activation of tolerance mechanisms. Therefore, all these antecedents allow us to speculate that the function of this tomato SNARE-like, abundantly associated with the plasma membrane, could be generating an increase in vesicular traffic and modulating clathrin-mediated endocytosis, being a candidate capable of contributing to the response of plants to adverse conditions, such as salinity stress.

This investigation revealed that *SlSLSP6* overexpression improved the physiological and biochemical parameters of tomato plants subjected to salt stress. In previous studies, it was observed that wild-type tomato plants subjected to 300 mM NaCl presented evident symptoms of stress around 15 days, decreasing the relative water content and photosynthesis, which was attributed to a disruption of normal functioning and maintenance of the cell structure (Orellana et al., 2010). The salt treatment caused a constant and marked inhibition of the photosynthetic machinery in the control plants, unlike what was observed in the *SlSLSP6* overexpressing lines, which maintained proper functioning and demonstrated a better photosynthetic rate (Figure 2G). The overexpression of *G. soja GsSNAP33* in *A. thaliana* plants also generated tolerance under abiotic stress conditions, where the transgenic genotypes presented a higher survival rate, higher biomass production and a higher photosynthetic rate (Nisa et al., 2017). Under salt stress or due to water deficiency, a closure of the stomata occurs, which limits the concentration of CO_2 and damages the photochemical machinery of the leaves, strongly depressing photosynthesis (Chaves et al., 2009; Keisham et al., 2018). In addition, it was observed that *A. thaliana* plants that overexpressed *AtSFT12* presented a higher fresh weight and greener leaves compared to control plants, when they were subjected to salt stress conditions (Tarte et al., 2015). This suggests a change in the distribution of some proteins that reside in the plasma membrane, such as aquaporins, which could be involved in the reduction of intracellular water loss (Baral et al., 2015b). Likewise, a hyperosmotic condition disorganizes the balance of cell membranes. Cell volume decreases, which leads to an excess of plasma membrane that must be endocytosed to reestablish cell turgor (Zwiewka et al., 2015; Zhang et al., 2019). Vesicular traffic is the indispensable process in the life of plants, which allows the movement of cellular materials inside small vesicles. Specifically, endocytosis plays a fundamental role in the removal and/or relocation of proteins, lipids, and other materials from the plasma membrane (Baral et al., 2015b; Dragwidge and VAN Damme, 2020). It has been reported that during salt stress there is an increase in endocytosis in *A. thaliana* (Baral et al., 2015a). In this investigation, an increase in endocytosis was evidenced in the overexpressing tomato lines, compared to the control plants, considering both normal and salt stress conditions (Figure 5). Other evidence indicates the consistency of these results, as is the case of salt stress tolerant plants that overexpress *SchRabGDI1* (San Martín-Davison et al., 2017) or *SlSNAP33* (Salinas-Cornejo et al., 2021), suggesting an acceleration of endocytosis in the roots of tomato plants overexpressing *SlSLSP6*. Similarly, it is hypothesized that overexpression of *SbSLSP* from *S. brachiata* would increase clathrin-mediated endocytosis, improving the stability and integrity of membranes and modifying the distribution of transporters in the plasma membrane (Singh et al., 2016). The increase in endocytosis observed in the transgenic lines could be contributing to the internalization of the plasma membrane, to restore the turgidity of the cells (Zwiewka et al., 2015), and to the removal of proteins from the plasma membrane, such as aquaporins, to allow osmotic adjustment within cells. This mechanism would be activated under salt stress conditions and other types of abiotic stress, improving tolerance in tomato plants.

To mitigate the consequences produced by salt stress at the physiological, cellular and molecular level, plants respond by activating different mechanisms. A high concentration of Na^+ ions will cause an ionic imbalance, triggering a massive entry of toxic ions into the cells and will also produce changes at the lipid level (Baral et al., 2015b; Orlova et al., 2019). Along with this, salinity stimulates the accumulation of ROS, which in high concentrations are toxic to cells. At low concentrations, these molecules help mitigate salt stress through a series of signal transduction mechanisms (Mangal et al., 2022). The evidence obtained in this investigation indicated that the overexpressing lines showed less damage at the level of cell membranes (Figure 2H). Previous studies have reported that tobacco plants that overexpress *SbSLSP* present lower levels of MDA in response to stress (Singh et al., 2016). Related to this, the overexpression of *SlSNAP33* has also been shown to provide tolerance to salt stress in tomato plants presenting less damage to cell membranes (Salinas-Cornejo et al., 2021). When plants are subjected to hyperosmotic conditions, caused by salt stress for example, the response of the cells is associated with the production of ROS and the compartmentalization of toxic ions in the vacuoles, between other mechanisms (Zwiewka et al., 2015). Here, using the H_2DCFDA fluorescent tracer, it has been shown that the overexpression of *SlSLSP6* in tomato plants causes a significant reduction in hydrogen peroxide, observed mainly in the L10 transgenic line (Figure 3). This response has also been reported in tomato plants that overexpress *SlSNAP33*, which has been associated with the endocytosis of plasma membrane NADPH oxidases, generating a lower production of ROS in root cells (Salinas-Cornejo et al., 2021). In addition, in *A. thaliana* it has also been reported that the internalization of NADPH oxidases, such as RbohD, causes the production of ROS inside vesicles, decreasing its levels in cells (Leshem et al., 2006). This is interesting, since this decrease in the accumulation of ROS in the vacuoles would generate a greater

compartmentalization of vacuolar sodium when plants are subjected to salt stress. It is suggested that there would be a decrease in oxidative damage in the tonoplast and in v-ATPases, helping to maintain the proton gradient and promoting the sequestration of cytoplasmic sodium inside the vacuole (Leshem and Levine, 2007). In this context, the results obtained showed that the transgenic plants had a greater accumulation of sodium in the vacuoles compared to the control plants (Figure 6). Similar results were presented by Tarte et al., 2015 and Salinas-Cornejo et al., 2021, where it was shown that the *AtSFT12* overexpressing plants of *A. thaliana* subjected to 100 mM NaCl and the *SlSNAP33* overexpressing tomato plants subjected to 200 mM NaCl compartmentalized more sodium in the vacuoles, which was monitored with the fluorescent tracer Sodium Green™. Interestingly, along with sodium accumulation in the vacuoles, Sodium Green™ staining was observed in rounded compartments within the cells of unknown nature (Figure 6). Since these structures were stained with the membrane marker FM4-64, it could be assumed that they are bordered by a lipid membrane. These compartments were observed in plants subjected to salt stress, stained with both FM4-64 and Sodium Green™. In overexpressing plants, it seems that these structures are accumulating more sodium than in WT plants. It could be speculated that these compartments have characteristics similar to endosomal or prevacuolar bodies, which would be sequestering sodium ions from the cytosol, mediated by the Na^+/H^+ antiporters NHX5 and NHX6, which reside in mobile endosomal structures (Bassil et al., 2011). Similar characteristics were described by Hamaji et al., 2009, where they observed the formation of vesicles that surrounded the vacuoles in *A. thaliana* root cells. These vesicles were marked with the fluorescent tracer Sodium Green™, which allows us to assume that it is sodium accumulation inside these compartments. In any case, to give certainty to these speculations, more research is required. Therefore, from this research arise the approaches that imply that an acceleration of endocytosis would occur, activating the removal of transporters from the plasma membrane. Because of the above, an increase in exocytosis would be generated, allowing the replacement of damaged lipids from the membrane. Moreover, the traffic towards the vacuole would increase, removing the excess sodium from the cytosol in a greater proportion to avoid its intracellular toxic effects, to finally obtain an improved tolerance of *SlSLSP6* overexpressing tomato plants to salt stress.

5 Conclusion

Here, we identified and characterized a *SNARE-like* gene, called *SlSLSP6* in tomato, determining its possible relationship with tolerance to salt stress. We can speculate that the function of this tomato SNARE-like fulfills its role in the plasma membrane, could be increasing the vesicular traffic and modulating clathrin-mediated endocytosis. This increase in endocytosis could be impacting in the replacement of lipids and in the removal of proteins from the plasma membrane. Furthermore, the traffic towards the vacuole would increase, removing the excess of toxic ions from the cytosol. These mechanisms would be activated against salt stress, improving the physiological and biochemical parameters of tomato plants. Finally, these results provide the knowledge to understand the role of this type of SNARE-like protein during salt stress and could be a suitable candidate to contribute to breeding programs to improve tolerance in tomato plants.

Data availability statement

The original contributions presented in the study are included in the article/Supplementary Material. Further inquiries can be directed to the corresponding author.

Author contributions

Conceived and designed experiments, JS-C, JM-E, IV, and SR-L; writing—original draft preparation, JS-C, JM-E, LN, and SR-L; writing—review and editing, JS-C, JM-E, LN, and SR-L; visualization, JS-C; project administration and funding acquisition, SR-L. All authors contributed to the article and approved the submitted version.

Funding

This research was supported by FONDECYT (grants 1170554 and 1211180) and the Universidad de Talca doctoral fellowship (JS-C).

Acknowledgments

We are grateful for the comments and scientific discussion of editors and reviewers.

Conflict of interest

The authors declare that the research was conducted in the absence of any commercial or financial relationships that could be construed as a potential conflict of interest.

Publisher's note

Supplementary material

The Supplementary Material for this article can be found online at: https://www.frontiersin.org/articles/10.3389/fpls.2023.1212806/full#supplementary-material

References

Apel, K., and Hirt, H. (2004). Reactive oxygen species: metabolism, oxidative stress, and signal transduction. *Annu. Rev. Plant Biol.* 55, 373–399. doi: 10.1146/annurev.arplant.55.031903.141701

Baral, A., Irani, N. G., Fujimoto, M., Nakano, A., Mayor, S., and Mathew, M. K. (2015a). Salt-induced remodeling of spatially restricted clathrin-independent endocytic pathways in Arabidopsis root. *Plant Cell* 27 (4), 1297–1315. doi: 10.1105/tpc.15.00154

Baral, A., Shruthi, K. S., and Mathew, M. K. (2015b). Vesicular trafficking and salinity responses in plants. *IUBMB Life* 67 (9), 677–686. doi: 10.1002/iub.1425

Barlow, L. D., and Dacks, J. B. (2018). Seeing the endomembrane system for the trees: Evolutionary analysis highlights the importance of plants as models for eukaryotic membrane-trafficking. *Semin. Cell Dev. Biol.* 80, 142–152. doi: 10.1016/j.semcdb.2017.09.027

Bassil, E., Ohto, M. A., Esumi, T., Tajima, H., Zhu, Z., Cagnac, O., et al. (2011). The Arabidopsis intracellular Na^+/H^+ antiporters NHX5 and NHX6 are endosome associated and necessary for plant growth and development. *Plant Cell* 23 (1), 224–239. doi: 10.1105/tpc.110.079426

Chaves, M. M., Flexas, J., and Pinheiro, C. (2009). Photosynthesis under drought and salt stress: regulation mechanisms from whole plant to cell. *Ann. Bot.* 103 (4), 551–560. doi: 10.1093/aob/mcn125

Dionisio-Sese, M., and Tobita, S. (1998). Antioxidant response of rice seedlings to salinity stress. *Plant Sci.* 135 (1), 1–9. doi: 10.1016/S0168-9452(98)00025-9

Dragwidge, J. M., and VAN Damme, D. (2020). Visualising endocytosis in plants: past, present, and future. *J. Microsc.* 280 (2), 104–110. doi: 10.1111/jmi.12926

Fillati, J., Kiser, J., and Rose, R. (1987). Efficient transfer of a glyphosate tolerance gene into tomato using a binary tumefaciens vector. *Bio/Technology* 5, 726–730. doi: 10.1038/nbt0787-726

Gadeyne, A., Sánchez-Rodríguez, C., Vanneste, S., Di Rubbo, S., Zauber, H., Vanneste, K., et al. (2014). The TPLATE adaptor complex drives clathrin-mediated endocytosis in plants. *Cell* 156 (4), 691–704. doi: 10.1016/j.cell.2014.01.039

Geldner, N., Dénervaud-Tendon, V., Hyman, D. L., Mayer, U., Stierhof, Y. D., and Chory, J. (2009). Rapid, combinatorial analysis of membrane compartments in intact plants with a multicolor marker set. *Plant J.* 59 (1), 169–178. doi: 10.1111/j.1365-313X.2009.03851.x

Ghanem, M. E., Albacete, A., Martínez-Andújar, C., Acosta, M., Romero-Aranda, R., Dodd, I. C., et al. (2008). Hormonal changes during salinity-induced leaf senescence in tomato (*Solanum lycopersicum* L.). *J. Exp. Bot.* 59 (11), 3039–3050. doi: 10.1093/jxb/ern153

Giorio, P. (2011). Black leaf-clips increased minimum fluorescence emission in clipped leaves exposed to high solar radiation during dark adaptation. *Photosynthetica* 49 (371), 371–379. doi: 10.1007/s11099-011-0040-0

Gonzalo, S., and Linder, M. E. (1998). SNAP-25 palmitoylation and plasma membrane targeting require a functional secretory pathway. *Mol. Biol. Cell* 9 (3), 585–597. doi: 10.1091/mbc.9.3.585

Greaves, J., and Chamberlain, L. H. (2011). DHHC palmitoyl transferases: substrate interactions and (patho)physiology. *Trends Biochem. Sci.* 36 (5), 245–253. doi: 10.1016/j.tibs.2011.01.003

Hamaji, K., Nagira, M., Yoshida, K., Ohnishi, M., Oda, Y., Uemura, T., et al. (2009). Dynamic aspects of ion accumulation by vesicle traffic under salt stress in Arabidopsis. *Plant Cell Physiol.* 50 (12), 2023–2033. doi: 10.1093/pcp/pcp143

Hao, H., Fan, L., Chen, T., Li, R., Li, X., He, Q., et al. (2014). Clathrin and membrane microdomains cooperatively regulate RbohD dynamics and activity in Arabidopsis. *Plant Cell* 26 (4), 1729–1745. doi: 10.1105/tpc.113.122358

Ivanov, R., and Vert, G. (2021). Endocytosis in plants: Peculiarities and roles in the regulated trafficking of plant metal transporters. *Biol. Cell* 113 (1), 1–13. doi: 10.1111/boc.202000118

Keisham, M., Mukherjee, S., and Bhatla, S. C. (2018). Mechanisms of sodium transport in plants—progresses and challenges. *Int. J. Mol. Sci.* 19 (3), 647. doi: 10.3390/ijms19030647

Kumar, S., Stecher, G., and Tamura, K. (2016). MEGA7: molecular evolutionary genetics analysis version 7.0 for bigger datasets. *Mol. Biol. Evol.* 33 (7), 1870–1874. doi: 10.1093/molbev/msw054

Leshem, Y., and Levine, A. (2007). Intracellular ROS: What Does it Do There? *Plant Signal Behav.* 2 (3), 155–156. doi: 10.4161/psb.2.3.3685

Leshem, Y., Melamed-Book, N., Cagnac, O., Ronen, G., Nishri, Y., Solomon, M., et al. (2006). Suppression of Arabidopsis vesicle-SNARE expression inhibited fusion of H_2O_2-containing vesicles with tonoplast and increased salt tolerance. *Proc. Natl. Acad. Sci. U.S.A.* 103 (47), 18008–18013. doi: 10.1073/pnas.0604421103

Lichtenthaler, H., and Wellburn, A. (1983). Determination of total carotenoids and chlorophyll a and b of leaf extract in different solvents. *Biochem. Soc. Trans.* 11 (5), 591–592. doi: 10.1042/bst0110591

Lipka, V., Kwon, C., and Panstruga, R. (2007). SNARE-ware: the role of SNARE-domain proteins in plant biology. *Annu. Rev. Cell Dev. Biol.* 23, 147–174. doi: 10.1146/annurev.cellbio.23.090506.123529

Livak, K. J., and Schmittgen, T. D. (2001). Analysis of relative gene expression data using real-time quantitative PCR and the $2^{-\Delta\Delta CT}$ method. *Methods* 25 (4), 402–408. doi: 10.1006/meth.2001.1262

Macková, H., Hronková, M., Dobrá, J., Turečková, V., Novák, O., Lubovská, Z., et al. (2013). Enhanced drought and heat stress tolerance of tobacco plants with ectopically enhanced cytokinin oxidase/dehydrogenase gene expression. *J. Exp. Bot.* 64 (10), 2805–2815. doi: 10.1093/jxb/ert131

Madrid-Espinoza, J., Salinas-Cornejo, J., and Ruiz-Lara, S. (2019). The RabGAP gene family in tomato (*Solanum lycopersicum*) and wild relatives: identification, interaction networks, and transcriptional analysis during plant development and in response to salt stress. *Genes (Basel)* 10 (9), 638. doi: 10.3390/genes10090638

Maggio, A., Raimondi, G., Martino, A., and De Pascale, S. (2007). Salt stress response in tomato beyond the salinity tolerance threshold. *Environ. Exp. Bot.* 59 (3), 276–282. doi: 10.1016/j.envexpbot.2006.02.002

Mangal, V., Lal, M. K., Tiwari, R. K., Altaf, M. A., Sood, S., Kumar, D., et al. (2022). Molecular insights into the role of reactive oxygen, nitrogen and sulphur species in conferring salinity stress tolerance in plants. *J. Plant Growth Regul.* 42, 1–21. doi: 10.1016/bs.ircmb.2015.07.004

Martinière, A., Fiche, J. B., Smokvarska, M., Mari, S., Alcon, C., Dumont, X., et al. (2019). Osmotic stress activates two reactive oxygen species pathways with distinct effects on protein nanodomains and diffusion. *Plant Physiol.* 179 (4), 1581–1593. doi: 10.1104/pp.18.01065

Murashige, T., and Skoog, F. (1962). A revised medium for rapid growth and bio assays with tobacco tissue cultures. *Physiol. Plant* 15 (3), 473–497. doi: 10.1111/j.1399-3054.1962.tb08052.x

Nisa, Z. U., Mallano, A. I., Yu, Y., Chen, C., Duan, X., Amanullah, S., et al. (2017). GsSNAP33, a novel *Glycine soja* SNAP25-type protein gene: Improvement of plant salt and drought tolerances in transgenic *Arabidopsis thaliana*. *Plant Physiol. Biochem.* 119, 9–20. doi: 10.1016/j.plaphy.2017.07.029

Orellana, S., Yañez, M., Espinoza, A., Verdugo, I., González, E., Ruiz-Lara, S., et al. (2010). The transcription factor SlAREB1 confers drought, salt stress tolerance and regulates biotic and abiotic stress-related genes in tomato. *Plant Cell Environ.* 33 (12), 2191–2208. doi: 10.1111/j.1365-3040.2010.02220.x

Orlova, Y. V., Sergienko, O. V., Khalilova, L. A., Voronkov, A. S., Fomenkov, A. A., Nosov, A. V., et al. (2019). Sodium transport by endocytic vesicles in cultured *Arabidopsis thaliana* (L.) Heynh. cells. *In Vitro Cell. Dev. Biol. – Plant* 55 (4), 359–370. doi: 10.1007/s11627-019-10005-7

Park, H. J., Kim, W. Y., and Yun, D. J. (2016). A new insight of salt stress signaling in plant. *Mol. Cells* 39 (6), 447. doi: 10.14348/molcells.2016.0083

Pizarro, L., and Norambuena, L. (2014). Regulation of protein trafficking: posttranslational mechanisms and the unexplored transcriptional control. *Plant Sci.* 225, 24–33. doi: 10.1016/j.plantsci.2014.05.004

Reynolds, G. D., Wang, C., Pan, J., and Bednarek, S. Y. (2018). Inroads into internalization: five years of endocytic exploration. *Plant Physiol.* 176 (1), 208–218. doi: 10.1104/pp.17.01117

Rosquete, M. R., and Drakakaki, G. (2018). Plant TGN in the stress response: a compartmentalized overview. *Curr. Opin. Plant Biol.* 46, 122–129. doi: 10.1186/s12870-019-1814-y

Saito, C., and Ueda, T. (2009). Chapter 4: functions of RAB and SNARE proteins in plant life. *Int. Rev. Cell Mol. Biol.* 274, 183–233. doi: 10.1016/S1937-6448(08)02004-2

Saitou, N., and Nei, M. (1987). The neighbor-joining method: a new method for reconstructing phylogenetic trees. *Mol. Biol. Evol.* 4 (4), 406–425. doi: 10.1093/oxfordjournals.molbev.a040454

Salinas-Cornejo, J., Madrid-Espinoza, J., and Ruiz-Lara, S. (2019). Identification and transcriptional analysis of SNARE vesicle fusion regulators in tomato (*Solanum lycopersicum*) during plant development and a comparative analysis of the response to salt stress with wild relatives. *J. Plant Physiol.* 242, 153018. doi: 10.1016/j.jplph.2019.153018

Salinas-Cornejo, J., Madrid-Espinoza, J., Verdugo, I., Pérez-Díaz, J., Martín-Davison, A. S., Norambuena, L., et al. (2021). The exocytosis associated SNAP25-type protein, SlSNAP33, increases salt stress tolerance by modulating endocytosis in tomato. *Plants (Basel)* 10 (7), 1322. doi: 10.3390/plants10071322

San Martín-Davison, A., Pérez-Díaz, R., Soto, F., Madrid-Espinoza, J., González-Villanueva, E., Pizarro, L., et al. (2017). Involvement of SchRabGDI1 from *Solanum chilense* in endocytic trafficking and tolerance to salt stress. *Plant Sci.* 263, 1–11. doi: 10.1016/j.plantsci.2017.06.007

Shimizu, Y., and Uemura, T. (2022). The sorting of cargo proteins in the plant trans-Golgi network. *Front. Plant Sci.* 13. doi: 10.3389/fpls.2022.957995

Singh, D., Yadav, N. S., Tiwari, V., Agarwal, P. K., and Jha, B. (2016). A SNARE-like superfamily protein SbSLSP from the halophyte *Salicornia brachiata* confers salt and drought tolerance by maintaining membrane stability, K(+)/Na(+) ratio, and antioxidant machinery. *Front. Plant Sci.* 7. doi: 10.3389/fpls.2016.00737

Tarte, V. N., Seok, H. Y., Woo, D. H., Le, D. H., Tran, H. T., Baik, J. W., et al. (2015). Arabidopsis Qc-SNARE gene AtSFT12 is involved in salt and osmotic stress responses

and Na(+) accumulation in vacuoles. *Plant Cell Rep.* 34 (7), 1127–1138. doi: 10.1007/s00299-015-1771-3

Torres-Schumann, S., Godoy, J. A., and Pintor-Toro, J. A. (1992). A probable lipid transfer protein gene is induced by NaCl in stems of tomato plants. *Plant Mol. Biol.* 18 (4), 749–757. doi: 10.1007/BF00020016

Uemura, T., Nakano, R., Takagi, J., Wang, Y., Kramer, K., Finkemeier, I., et al. (2019). A golgi-released subpopulation of the trans-golgi network mediates protein secretion in Arabidopsis. *Plant Physiol.* 179 (2), 519–532. doi: 10.1104/pp.18.01228

Uemura, T., and Ueda, T. (2014). Plant vacuolar trafficking driven by RAB and SNARE proteins. *Curr. Opin. Plant Biol.* 22, 116–121. doi: 10.1016/j.pbi.2014.10.002

Varma, R., and Mayor, S. (1998). GPI-anchored proteins are organized in submicron domains at the cell surface. *Nature.* 394 (6695), 798–801. doi: 10.1038/29563

Vasquez-Robinet, C., Mane, S. P., Ulanov, A. V., Watkinson, J. I., Stromberg, V. K., De Koeyer, D., et al. (2008). Physiological and molecular adaptations to drought in Andean potato genotypes. *J. Exp. Bot.* 59 (8), 2109–2123. doi: 10.1093/jxb/ern073

Wang, Y. C., Yu, M., Shih, P. Y., Wu, H. Y., and Lai, E. M. (2018). Stable pH suppresses defense signaling and is the key to enhance Agrobacterium-mediated transient expression in Arabidopsis seedlings. *Sci. Rep.* 8 (1), 1–9. doi: 10.1038/s41598-018-34949-9

Won, K. H., and Kim, H. (2020). Functions of the plant Qbc SNARE SNAP25 in cytokinesis and biotic and abiotic stress responses. *Mol. Cells* 43 (4), 313–322. doi: 10.14348/molcells.2020.2245

Wu, H. Y., Liu, K. H., Wang, Y. C., Wu, J. F., Chiu, W. L., Chen, C. Y., et al. (2014). AGROBEST: an efficient Agrobacterium-mediated transient expression method for versatile gene function analyses in Arabidopsis seedlings. *Plant Methods* 10 (1), 1–16. doi: 10.1186/1746-4811-10-19

Yáñez, M., Cáceres, S., Orellana, S., Bastías, A., Verdugo, I., Ruiz-Lara, S., et al. (2009). An abiotic stress-responsive bZIP transcription factor from wild and cultivated tomatoes regulates stress-related genes. *Plant Cell Rep.* 28 (10), 1497–1507. doi: 10.1007/s00299-009-0749-4

Yperman, K., Wang, J., Eeckhout, D., Winkler, J., Vu, L. D., Vandorpe, M., et al. (2021). Molecular architecture of the endocytic TPLATE complex. *Sci. Adv.* 7 (9), eabe7999. doi: 10.1126/sciadv.abe7999

Zhang, L., Xing, J., and Lin, J. (2019). At the intersection of exocytosis and endocytosis in plants. *New Phytol.* 224 (4), 1479–1489. doi: 10.1111/nph.16018

Zhao, C. R., Ikka, T., Sawaki, Y., Kobayashi, Y., Suzuki, Y., Hibino, T., et al. (2009). Comparative transcriptomic characterization of aluminum, sodium chloride, cadmium and copper rhizotoxicities in *Arabidopsis thaliana*. *BMC Plant Biol.* 9, 32. doi: 10.1186/1471-2229-9-32

Zhao, C., Zhang, H., Song, C., Zhu, J. K., and Shabala, S. (2020). Mechanisms of plant responses and adaptation to soil salinity. *Innovation* 1 (1), 100017. doi: 10.1016/j.xinn.2020.100017

Zwiewka, M., Nodzyński, T., Robert, S., Vanneste, S., and Friml, J. (2015). Osmotic stress modulates the balance between exocytosis and clathrin-mediated endocytosis in *Arabidopsis thaliana*. *Mol. Plant* 8 (8), 1175–1187. doi: 10.1016/j.molp.2015.03.007

frontiers | Frontiers in Plant Science

TYPE Review
PUBLISHED 11 August 2023
DOI 10.3389/fpls.2023.1226498

OPEN ACCESS

EDITED BY
Cecilia Rodriguez-Furlan,
Washington State University, United States

REVIEWED BY
Daniel Garcia Cabanillas,
Morgridge Institute for Research,
United States
Guanwei Wu,
Ningbo University, China

*CORRESPONDENCE
Jan Zouhar
zouhar@mendelu.cz

†These authors have contributed equally to this work

RECEIVED 21 May 2023
ACCEPTED 25 July 2023
PUBLISHED 11 August 2023

CITATION
Jovanović I, Frantová N and Zouhar J (2023) A sword or a buffet: plant endomembrane system in viral infections. *Front. Plant Sci.* 14:1226498. doi: 10.3389/fpls.2023.1226498

A sword or a buffet: plant endomembrane system in viral infections

Ivana Jovanović[1†], Nicole Frantová[1†] and Jan Zouhar[2*]

[1]Department of Crop Science, Breeding and Plant Medicine, Faculty of AgriSciences, Mendel University in Brno, Brno, Czechia, [2]Central European Institute of Technology, Faculty of AgriSciences, Mendel University in Brno, Brno, Czechia

The plant endomembrane system is an elaborate collection of membrane-bound compartments that perform distinct tasks in plant growth and development, and in responses to abiotic and biotic stresses. Most plant viruses are positive-strand RNA viruses that remodel the host endomembrane system to establish intricate replication compartments. Their fundamental role is to create optimal conditions for viral replication, and to protect replication complexes and the cell-to-cell movement machinery from host defenses. In addition to the intracellular antiviral defense, represented mainly by RNA interference and effector-triggered immunity, recent findings indicate that plant antiviral immunity also includes membrane-localized receptor-like kinases that detect viral molecular patterns and trigger immune responses, which are similar to those observed for bacterial and fungal pathogens. Another recently identified part of plant antiviral defenses is executed by selective autophagy that mediates a specific degradation of viral proteins, resulting in an infection arrest. In a perpetual tug-of-war, certain host autophagy components may be exploited by viral proteins to support or protect an effective viral replication. In this review, we present recent advances in the understanding of the molecular interplay between viral components and plant endomembrane-associated pathways.

KEYWORDS

plant virus, endomembrane system, endoplasmic reticulum, virus replication, autophagy

1 Introduction

Plant cells contain a sophisticated system of membrane-limited subcellular compartments that guarantee a spatial-temporal separation of their specific functions and chemical compositions, called the endomembrane system. The endoplasmic reticulum (ER) is one of the largest structures in eukaryotic cells, comprising interconnected tubules, cisternae, and three-way junctions (Sparkes et al., 2009). The constricted tubules pass through plasmodesmata, making endoplasmic reticulum a *bona fide* multicellular organelle (Nicolas et al., 2017). Regarding its function, endoplasmic reticulum is a gateway involved in lipid metabolism, and synthesis and folding of proteins. Each plant cell may contain hundreds

of individual Golgi stacks that actively move along the cytoskeleton (Boevink et al., 1998). The cellular functions of plant Golgi include synthesis and trafficking of complex carbohydrates for the cell wall, and participation in transport and modifications of proteins destined for other organelles, such as vacuoles and chloroplasts (Villarejo et al., 2005; Oikawa et al., 2013; Di Sansebastiano et al., 2017). The *trans*-Golgi network (TGN) is a major sorting station in plant cells, governing cargo delivery to the plasma membrane and participating in post-Golgi trafficking to endosomes and the vacuole (Ruiz Rosquete et al., 2018). In addition, plant TGN also functions as an early endosome, receiving endocytosed cargo from the plasma membrane (Viotti et al., 2010). The exact contribution of various post-Golgi compartments and their resident proteins to protein sorting constitutes still an unresolved area of plant cell biology. To conciliate the contradictory experimental data, a unified model was recently proposed (Zouhar et al., 2023). It states that a distinct population of TGN, termed late TGN, is converted into early multivesicular bodies (MVBs). These early MVBs then gradually mature into late MVBs that finally fuse with the tonoplast, delivering its content into the vacuolar lumen. Vacuole represents a dominant structure in plant cells that can occupy up to 90% of the cell volume (Zhang et al., 2014). It is a multifunctional organelle and in vegetative cells, its primary lytic function resembles that of yeast vacuoles and lysosomes in metazoans. However, certain cell types may contain protein storage vacuoles (PSVs) with neutral pH, structures that are unique to plants (Frigerio et al., 2008). Plants as sessile organisms mastered the use of their endomembrane system pathways to respond to various environmental stresses. Experimental data indicate a critical role of the plant endoplasmic reticulum (Park and Park, 2019), the *trans*-Golgi network (Ruiz Rosquete and Drakakaki, 2018), the autophagosomes and multivesicular bodies (Wang et al., 2020) in responses to both abiotic and biotic stresses.

Plant RNA and DNA viruses represent half of the disease-causing pathogens with a tremendous economic impact on agriculture (Nicaise, 2014). Positive-sense single-strand (+ss) RNA viruses are among the most economically damaging pathogens. Within this group, viruses of the *Closterovirus*, *Cucumovirus*, *Luteovirus*, *Potyvirus* and *Sobemovirus* genera cause serious diseases in various crops, including crucial cereals, vegetables but also in high-value fruit crops, such as citrus and papaya (Tatineni and Hein, 2023). Upon infection, RNA viruses induce formation of specialized cytoplasmic viral replication organelles (VROs) to facilitate their replication, to achieve cell-to-cell movement and to shelter their replication complexes from host antiviral defense. The endoplasmic reticulum is a primary target for plant RNA viruses, but they frequently remodel additional cellular compartments, such as chloroplasts and peroxisomes (Richardson, 2019). Begomoviruses constitute a remarkably successful group of emerging viruses and carry a monopartite or bipartite single-strand (ss) DNA genome (Fiallo-Olivé and Navas-Castillo, 2023). Their replication does not require a drastic host endomembrane remodeling and takes place in the nucleus. Eleven species within the *Cassava mosaic virus* (genus *Begomovirus*) group infect cassava, a daily staple in the diet of more than half a billion people in Africa and India (Legg et al., 2015).

To control virus infections, plants deploy two major strategies. The highly conserved primary antiviral response is the RNA interference (RNAi), initiated by plant DICER-LIKE enzymes (DCLs) that cleave long double-strand RNAs or RNA hairpins into small interfering RNAs (siRNAs) of distinct lengths. The siRNAs associate with ARGONAUTE proteins, catalytic components of the silencing complexes, which mediate methylation of viral DNAs, silencing of viral RNAs, or an inhibition of the viral RNA translation (Yang and Li, 2018). The crucial role of RNAi is emphasized by the fact that as a counter-acting measure, viruses evolved silencing suppressors that act at various steps of antiviral silencing but may also play other roles during infection (Csorba et al., 2015). The second major antiviral strategy is represented by effector-triggered immunity (ETI). During ETI-based antiviral response, host resistance proteins (R) recognize viral avirulence (Avr) factors, resulting in production of reactive oxygen species (ROS), induction of salicylic acid and expression of defense-related genes (Huang, 2021). Recent discoveries of a selective viral protein degradation by autophagy and the ubiquitin-proteasome pathway, and the reevaluation of the role of membrane-localized receptor-like kinases in antiviral defense exposed plant responses to viral infections as a complex multilayered system (Teixeira et al., 2019; Wu et al., 2019b; Dubiella and Serrano, 2021; Wu et al., 2021; Yang and Liu, 2022).

In this review, we summarize some of the important discoveries in the field of molecular plant virology related to plant endomembrane system. In the first section, we present examples of a misappropriation of various endomembrane compartments and their resident proteins by distinct viral genera to create viral replication organelles and an involvement of these novel membrane entities in the cell-to-cell viral movement. In the second part, we focus on membrane-localized receptors of viral molecular patterns, their putative localizations, and the identity of molecules they likely recognize. Finally, the third section introduces a dual role of plant selective autophagy during viral infections. Specific degradation of viral proteins often leads to an infection arrest, but plant viruses evolved mechanisms to utilize host autophagy processes to promote viral replication.

2 Hijacking the plant endomembrane system

Positive-strand RNA viruses perform their life cycle in the cytoplasm of an infected host cell, where they are met by the antiviral defense systems and unfavorable conditions for genome replication. Therefore, the virus must create an intracellular environment where viral and host proteins concentrate, facilitating its replication. In eukaryotic cells, such spatial and functional isolation is guaranteed in membrane-limited compartments. Indeed, RNA viruses induce biogenesis of such membranous replication entities, which display two basic topologies. The first type of viral replication organelles (VROs) is represented by membrane invaginations, also called spherules, while the second type is formed by membrane protrusions to

generate tubules or vesicles (He et al., 2023). This is made possible by the ability of viral proteins to induce membrane deformations or to seize host proteins with similar capabilities (Agaoua et al., 2021). For optimal biogenesis and functioning of replication organelles, the RNA viruses coopt host proteins and modify or trigger host cellular pathways to fine tune the lipid and protein composition of these newly formed compartments (Ketter and Randall, 2019; He et al., 2023).

2.1 Manipulating host cellular pathways to support viral infection

Positive-strand RNA viruses often disrupt ER homeostasis as a first step in the formation of viral replication organelles that contain viral replication complexes (VRCs) and sites of viral particle assembly and maturation (Laliberté and Sanfaçon, 2010). One of the ER-associated pathways that is activated and utilized by plant viruses is the unfolded protein response (UPR) that represents a conserved eukaryotic reaction to a presence of misfolded proteins in the lumen of the endoplasmic reticulum. In Arabidopsis, the accumulation of misfolded proteins triggers INOSITOL REQUIRING ENZYME1 (IRE1)-mediated splicing of *bZIP60* mRNA that then encodes an active transcription factor (Nagashima et al., 2011). Similarly, upon detection of misfolded proteins, ER membrane-localized bZIP17 and bZIP28 proteins are transported to Golgi, where they are proteolytically processed to yield functional transcription factors that regulate expression of ER resident enzymes and chaperons to increase folding capacity in the ER (Che et al., 2010).

Potato virus X (PVX, +ssRNA, genus *Potexvirus*) infection triggers upregulation of many genes associated with the UPR, with the membrane-localized triple gene block protein 3 (TGBp3) identified as the responsible factor (Ye et al., 2011). Supporting a proposed proviral role of UPR in the PVX infection, silencing of *bZIP60* inhibits viral replication and delays virus accumulation in *Nicotiana benthamiana* (Ye et al., 2011). The 6K2 transmembrane protein of *Turnip mosaic virus* (TuMV, +ssRNA, genus *Potyvirus*) was also identified as a potent inducer of *bZIP60* splicing. Both *bzip60* and *ire1* mutants displayed alleviated viral pathogenesis, suggesting that IRE1-mediated *bZIP60* splicing is essential for the TuMV infection (Zhang et al., 2015). It was hypothesized that both TGBp3 and 6K2 trigger the UPR pathway because they might be considered chronically misfolded proteins by the host UPR sensors (Bao and Howell, 2017). Regarding the target genes upregulated by the UPR-generated transcription factors, tobacco plants infected with *Cucumber mosaic virus* (CMV, +ssRNA, genus *Cucumovirus*), *Soybean mosaic virus* (SMV, +ssRNA, genus *Potyvirus*), *Pepper mottle virus* (PepMoV, +ssRNA, genus *Potyvirus*) and *Potato virus X* (*Potexvirus*) demonstrated a significant up-regulation of genes encoding ER lumen-localized IMMUNOGLOBULIN BINDING PROTEIN 1 and 2 (BiP1 and BiP2), members of the heat shock protein 70 (HSP70) family. Tobacco BiP2 chaperon was identified as an interacting partner of potyviral nuclear inclusion protein b (NIb), which functions as the RNA-dependent RNA polymerase responsible for viral replication (Widyasari et al., 2023). Considering that NIb is a very active recruiter of various proviral host proteins (Shen et al., 2020), we may speculate that the observed UPR-mediated induction of BiP molecular chaperones has likely a direct role in folding of proteins essential for successful viral infection.

The virus-triggered UPR upregulation is not exclusive to viruses with +ssRNA genomes. The membrane-associated viral proteins NSvc2 and NSvc4 of *Rice stripe virus* (RSV, -ssRNA, genus *Tenuivirus*) activate the bZIP17/28 pathway in *N. benthamiana*. Silencing *bZIP17/28* delayed RSV infection and decreased virus accumulation, indicating that RSV triggers UPR to specifically promote its infection (Li et al., 2022). The βC1 protein of *Tomato yellow leaf curl China virus* (TYLCCNV, ssDNA, genus *Begomovirus*) is a significant inducer of UPR and can upregulate the *bZIP60* expression. Transient expression of bZIP60-regulated BiP and calreticulin molecular chaperones in *N. benthamiana* resulted in higher accumulation of viral DNA and more severe viral symptoms, suggesting that these chaperones positively assist the TYLCCNV infection (Zhang et al., 2023).

Biological membranes represent an essential platform for viral replication. While some viruses form their viral replication compartments from preexisting host membranes, others trigger general membrane proliferation and/or accumulation of specific lipids at the VROs (Verchot, 2011). Endoplasmic reticulum is a major cellular compartment responsible for lipid biosynthesis (Jacquemyn et al., 2017). As the formation of viral replication organelles requires a significant amount of new membranes, it is not surprising that ER membrane proliferation is a common phenotype observed during various plant virus infections (Schaad et al., 1997; Lee and Ahlquist, 2003; Turner et al., 2004). In plants, ER membrane proliferation is regulated by phosphatidate phosphohydrolase (PAH) (Craddock et al., 2015). The disruption of PAH leads to accumulation of phosphatidic acid (PA) and massive proliferation of ER membranes that can be efficiently utilized for the viral replication organelle formation (Zhang et al., 2018). It was shown that overexpression of Arabidopsis PAH in tobacco leads to decreased accumulation of *Tomato bushy stunt virus* (TBSV, +ssRNA, genus *Tombusvirus*), *Red clover necrotic mosaic virus* (RCNMV, +ssRNA, genus *Dianthovirus*), *Brome mosaic virus* (BMV, +ssRNA, genus *Bromovirus*) and *Tobacco mosaic virus* (TMV, +ssRNA, genus *Tobamovirus*) (Chuang et al., 2014; Zhang et al., 2018). However, no direct downregulation of PAH initiated by viral proteins has been reported yet. Interestingly, *Red clover necrotic mosaic virus* (*Dianthovirus*) induces a high accumulation of PA by recruiting host phospholipases D into viral replication complexes (Hyodo et al., 2015). Phosphatidic acid is not the only phospholipid that supports an efficient viral replication. When *Brome mosaic virus* (*Bromovirus*) infects yeast cells, the BMV 1a replication protein recruits Cho2p (choline requiring 2) enzyme to synthesize phosphatidylcholine (PC) at the site of viral replication (Zhang et al., 2016). Similar accumulation of PC at the viral replication sites was observed also for human poliovirus and hepatitis C virus, revealing a conserved attribute among +ssRNA viruses (Zhang et al., 2016). Considering the complexity of lipid metabolic pathways, plant viruses may constitute an invaluable tool in studying the lipid biosynthesis regulation in plants.

2.2 Establishing the viral replication organelles

For the formation of VROs, some plant RNA viruses specifically target particular membrane compartments, such as the ER, chloroplasts, and vacuoles. In contrast, other RNA viruses do not have these strict requirements and either target several membrane populations in the course of the infection or they appropriate other available membrane types as an alternative (Xu and Nagy, 2014).

Brome mosaic virus (*Bromovirus*) establishes its VROs through invaginations of the ER membrane. The formation of approx. 70 nm lumenal spherules requires the Endosomal Sorting Complex Required for Transport (ESCRT). The ESCRT machinery has membrane curvature-inducing properties and in later stage narrows the neck connecting the spherule with cytoplasm. BMV recruits the ESCRT proteins transiently through interaction with 1a replication protein (Diaz et al., 2015). *Beet black scorch virus* (BBSV, +ssRNA, genus *Betanecrovirus*) auxiliary replication protein p23 plays a crucial role in establishing ER-derived spherules in *N. benthamiana*. In a rare topology arrangement, these spherules are connected to each other by tubules (Cao et al., 2015).

Biogenesis of the *Potato virus X* (*Potexvirus*) VRO requires three partially overlapping open reading frames (ORFs), termed the triple gene block (TGB) (Morozov and Solovyev, 2003). In the PVX infected cell, VRCs localize to large perinuclear structures called X-bodies (Tilsner et al., 2012). The core of the X-body is formed by TGBp1 aggregates, surrounded by dense reticulated network of ER membranes recruited by the TGBp2/TGBp3 complex. The replication complexes are associated with the TGBp1 and TGBp2 aggregates, while the virions localize to the periphery of the X-bodies (Wu et al., 2019a).

Barley stripe mosaic virus (BSMV, +ssRNA, genus *Hordeivirus*) builds its VRO on chloroplasts and causes dramatic morphological changes of these organelles (Carroll, 1970). The BSMV replication complexes are associated with peripheral outer membrane-invaginated spherules and large cytoplasmic invaginations (CIs) (Carroll, 1970; Lin and Langenberg, 1985; Torrance et al., 2006). The peripheral spherules are often clustered within inner membrane-derived packets, and they are connected to the cytoplasm *via* neck-like structures (Jin et al., 2018). The CIs are associated with the later stage of BSMV infection. The transmission electron tomography revealed that the invagination of the chloroplast membranes progresses gradually in the course of the infection, resulting in the CIs of diverse morphologies (Jin et al., 2018).

The initial stage of the *Turnip mosaic virus* (*Potyvirus*) VRO biogenesis includes remodeling of the ER, mediated by 6K2 viral protein (Cotton et al., 2009). A detailed time-course analysis of the 6K2-driven biogenesis of the replication compartments revealed early accumulation of convoluted ER membranes, followed by a formation of single-membrane vesicle-like (SMVL) structures (Wan et al., 2015a). These highly motile compartments represent functional VROs that move on actin filaments through thin tubular structures that traverse the vacuole (Cotton et al., 2009; Grangeon et al., 2013). During the TuMV VRO biogenesis, the 6K2 transmembrane protein coopts the SEC24A subunit of the COPII coatomer at the ER exit sites (ERES), affecting the conventional ER-to-Golgi anterograde trafficking of the host cargo proteins (Wei and Wang, 2008; Jiang et al., 2015). Importantly, 6K2 also interacts with ROOT HAIR DEFECTIVE 3 (RHD3) at the endoplasmic reticulum membrane (Movahed et al., 2019b). RHD3 is a plant dynamin-like GTPase that is required for efficient homotypic fusion of ER membranes (Chen et al., 2011). Interaction of RHD3 with 6K2 is essential for the formation and maturation of the TuMV motile VROs, as mutations in the RHD3-interacting GxxxG domain of 6K2 result in the accumulation of 6K2 in the Golgi stacks, representing a nonproductive pathway for viral infection (Cabanillas et al., 2018; Movahed et al., 2019b). In agreement with the identified crucial role of RHD3 in the TuMV life cycle, the *rhd3* mutant plants exhibit compromised viral replication and cell-to-cell movement (Movahed et al., 2019b). The 6K2-induced motile VROs then target chloroplasts, multivesicular bodies (MVBs), vacuoles or plasma membrane to establish a secondary subset of VROs (Wei et al., 2010a; Wei et al., 2010b; Wan et al., 2015a; Cabanillas et al., 2018; Li et al., 2020a). At an early stage of infection, the 6K2 VROs are localized at the periphery of the chloroplasts, while later, TuMV-infected cells display tubular structures, consisting of approx. 20 chloroplasts with 6K2-containing VROs localized between adjacent chloroplasts (Wei et al., 2013). This unique localization may provide an ideal energy- and resource-rich environment for the TuMV replication. Formation of the tubular chloroplast aggregates depends on the SYP71 Qc-SNARE protein, which normally regulates membrane fusion processes at the ER and plasma membrane. However, as SYP71 is not essential for targeting of the 6K2 VROs to the chloroplast outer membrane, its molecular role in chloroplast clustering needs to be further elucidated (Wei et al., 2013). Chloroplasts are sites of salicylic and jasmonic acid biosynthesis and sources of ROS and calcium bursts, which makes them important organelles in antiviral responses (Littlejohn et al., 2021). In *N. benthamiana*, chloroplasts frequently migrate to perinuclear position during plant-pathogen interactions (Ding et al., 2019). This rearrangement likely facilitates an efficient regulation of expression of defense related genes *via* retrograde signaling (Chan et al., 2016). In a counteractive measure, the TuMV silencing suppressor protein VPg interacts with the chloroplast NADH dehydrogenase-like (NDH) complex M subunit (NdhM), resulting in a suppression of the antiviral chloroplast perinuclear clustering in *N. benthamiana* (Zhai et al., 2021). In Arabidopsis, targeting of the 6K2 VROs to the multivesicular bodies utilizes the VTI11 Qb-SNARE protein and VACUOLAR SORTING RECEPTOR4, bypassing the *trans*-Golgi network, a post-Golgi sorting organelle (Cabanillas et al., 2018; Wu et al., 2022a). In addition to the highly motile 6K2-labelled VROs and the secondary sites of viral replication, the TuMV infected cell contains a large perinuclear structure, which comprises amalgamated Golgi stacks, the endoplasmic reticulum, chloroplasts, COPII coatomers, and viral and host proteins necessary for replication (Grangeon et al., 2012). Elegant photoactivation experiments revealed that the perinuclear structure is both a target

and a source of motile 6K2 VROs (Grangeon et al., 2012). The TuMV infection process is also accompanied by a formation of double-membrane tubules (DMTs), which were observed by transmission electron tomography. The DMTs function likely as the ultrastructure underlying the perinuclear compartment and the sites of the TuMV particle assembly (Wan et al., 2015a).

The key viral protein in the establishment of the *Tomato bushy stunt virus* (*Tombusvirus*) replication organelle is the p33 RNA chaperone, which interacts with approx. 100 host proteins (Nagy et al., 2012). The TBSV VROs are established by invaginations of the peroxisomal membranes (Fernández De Castro et al., 2017). This inward vesiculation is executed by the host ESCRT proteins recruited by p33 protein (Barajas et al., 2009). However, the tombusvirus replication requires an appropriation of numerous additional resources of the host cell (Nagy and Feng, 2021). Their efficient and rapid delivery to the VRO is ensured by p33 inhibition of cofilin, a major modulator of actin filament disassembly, resulting in the microfilament stabilization (Nawaz-Ul-Rehman et al., 2016). The p33-mediated establishment of ER-peroxisome membrane contact sites allows for generation of sterol-rich membrane environments, crucial for a successful TBSV replication (Barajas et al., 2014). TBSV also subverts ER-derived anterograde vesicles *via* p33 interaction with Rab1 GTPase, resulting in the accumulation of COPII vesicles at the replication compartments (Inaba et al., 2019). Interestingly, interactions of p33 with small GTPases extend beyond the Rab1 clade. The p33 protein interacts with the host Rab7 small GTPase, causing its relocalization into the VROs (Feng et al., 2021b). The change of Rab7 localization leads to mislocalization of the core retromer complex and mistargeting of multiple host lipid enzymes, including phosphatidylinositol 3-kinase, phosphatidylinositol 4-kinase and phosphatidylserine decarboxylase, into the replication organelle (Feng et al., 2021a). The enrichment of phosphatidylinositol-3-phosphate and phosphatidylinositol-4-phosphate in the VRO membrane is crucial for efficient TBSV replication (Feng et al., 2019; Sasvari et al., 2020). In addition, p33 mediates recruitment of Rab5-positive endosomes that leads to the enrichment of phosphatidylethanolamine in the VRO membranes (Xu and Nagy, 2016).

The tonoplast is appropriated for the VRO formation during infection of *Cucumber mosaic virus* (*Cucumovirus*). Confocal microscopy and electron tomography approaches revealed that CMV replication proteins 1a and 2a trigger formation of spherules 50–70 nm in diameter at the vacuolar membrane. The interior of these spherules communicates with cytosol through neck-like channels (Wang et al., 2021). Recently identified interaction of 126kDa protein of *Tobacco mosaic virus* (*Tobamovirus*) with the SYP2 Qa-SNARE proteins and decreased accumulation of TMV in plants lacking the SYP2 syntaxins indicate that the vacuolar membrane plays an important role in the *Tobacco mosaic virus* life cycle (Ibrahim et al., 2020).

2.3 Cell-to-cell movement

For efficient intercellular movement, viral replication complexes of many +ssRNA viruses are targeted to plasmodesmata (PD). The colocalization of the viral replication machinery with viral movement proteins (MPs) to the PD greatly increases the chance of the MP interaction with virions or viral RNAs and decreases the host mRNA interaction with the movement proteins (Wu and Cheng, 2020).

Movement proteins of the *Tobamovirus* genus interact with SYNAPTOTAGMIN A (SYTA), a resident of the plasma membrane–endoplasmic reticulum contact sites, and trigger relocalization of SYTA to the PD (Yuan et al., 2018). The MP–SYTA complex causes remodeling of the PD to establish virus replication sites and changes the PD permeability, thus enabling virus cell-to-cell movement (Levy et al., 2015). In the *syta* mutant, intercellular movement is reduced not only for tobamoviruses, but also for viruses from the *Begomovirus* and *Potyvirus* genera, suggesting a general proviral role of SYTA (Lewis and Lazarowitz, 2010; Uchiyama et al., 2014; Cabanillas et al., 2018).

At the endoplasmic reticulum, TGBp2 protein of *Potato virus X* (*Potexvirus*) induces the formation of mobile vesicles that sequentially recruit viral replication complexes, TGBp3 and TGBp1, resulting in the formation of mobile VROs (mVROs) (Ju et al., 2005; Samuels et al., 2007; Tilsner et al., 2013; Wu et al., 2019a). Intracellular transport of mVROs towards the plasmodesmata is likely mediated by microfilaments, indicated by the TGBp2 colocalization with actin and the need of intact actin filaments for efficient intercellular movement (Ju et al., 2005; Harries et al., 2009). At the plasmodesmata, the three TGB movement proteins orchestrate formation of replication compartments that functionally relate to perinuclear X-bodies described in the previous subsection. The TGBp2 and TGBp3 are responsible for remodeling ER membranes at the PD orifice (Tilsner et al., 2013; Wu et al., 2019a). The necessary modification of the PD size exclusion limit is likely mediated by TGBp2, which is capable of inducing ER tubule constrictions in a reticulon-like manner (Lazareva et al., 2021). Specific antibody-based labelling of the PVX virions in the plasmodesmata connecting infected cells elegantly demonstrated that virions represent the probable infectious entity in the cell-to-cell transport (Santa Cruz et al., 1998). The multifunctional TGBp1 protein is essential for loading the PVX virions into the plasmodesmal cavity (Tilsner et al., 2013).

The *Turnip mosaic virus* (*Potyvirus*) cell-to-cell movement depends on the 6K2 motile VROs, indicated by its inhibition by brefeldin A and concanamycin A, compounds that disturb pre- and post-Golgi trafficking pathways (Agbeci et al., 2013). The TuMV intercellular movement is also inhibited by actin-depolymerizing drugs and the expression of a dominant-negative mutant of myosin XI-2, demonstrating that the 6K2 VRO trafficking is mediated by actin filaments (Agbeci et al., 2013). The TuMV movement protein, P3N-PIPO, guides the cylindrical inclusion (CI) viral protein to plasmodesmata, where CI forms conical structures that are essential for intercellular movement (Wei et al., 2010b). Due to a polymerase slippage within the P3 cistron, P3N-PIPO is a chimeric protein that consists of N-terminal portion of P3 protein and a small ORF termed PIPO, for Pretty Interesting *Potyviridae* ORF (Rodamilans et al., 2015). The multipartite interactions among 6K2, P3, P3N-PIPO and CI are indispensable for recruitment of the 6K2 motile VROs to the PD (Chai et al., 2020). However, the identity of the infectious material that is transferred between the adjacent cells remains an unresolved issue. The coat protein (CP) deletion or point mutations within its

core domain abolished the TuMV intercellular movement but they did not affect viral replication (Dai et al., 2020). The observed requirement of the native coat protein for efficient cell-to-cell movement suggests that the transported infectious entities may be virions (Dai et al., 2020; Wang, 2021). In contrast, detection of 6K2 intercellular movement implies that the viral RNA complex may be transported in a membrane-mediated manner (Grangeon et al., 2013). Using an infection-free movement assay, CI and P3N-PIPO were identified as sufficient to support the intercellular movement of the 6K2-induced vesicles (Movahed et al., 2017). The 6K2 cell-to-cell movement was abolished when CI carried a mutation in the 6K2-interacting domain, indicating that CI serves as a docking platform for the 6K2 vesicles (Movahed et al., 2017). In a similar way, the 6K2 replication vesicles, released into the extracellular space during membrane fusion of multivesicular bodies with the plasma membrane, may represent vehicles for systemic TuMV infection (Wan et al., 2015b; Movahed et al., 2019a). To unite these contradictory models of the TuMV cell-to-cell movement, we may hypothesize that the PD-localized coat protein may represent an essential factor in the movement of the 6K2-containing replication vesicles through plasmodesmata, presumably by interaction with certain components of the transported vesicles. Further analyses of the coat protein function at plasmodesmata may resolve this puzzling issue. Interestingly, the TuMV multifunctional cylindrical inclusion (CI) protein and the viral genome-linked protein (VPg), which are essential for intercellular movement, also participate in viral replication and are retrieved from the plasma membrane to endosomes by clathrin-mediated endocytosis. This uptake of viral proteins is regulated by the DYNAMIN-RELATED PROTEIN family of GTPases that assists in the endocytic vesicle budding (Wu et al., 2018). The expression of a dominant-negative form of DRP1A suppresses TuMV replication, indicating that the dynamic partitioning of CI and VPg between plasma membrane and early/late endosomes likely represents an important regulatory mechanism (Wu et al., 2020). The CI and VPg viral proteins are recognized by the β subunit of the AP2 clathrin adaptor complex, as the corresponding *ap2β* knockout impairs intracellular endosomal trafficking of both viral cargoes and inhibits TuMV replication (Wu et al., 2020). In more detail, the endocytic uptake of CI depends on the interaction of its dileucine motif with the AP2β subunit (Wu et al., 2022b). Similar endocytosis-assisted cycling of viral proteins between the plasma membrane and early endosomes has been reported also for movement proteins of *Ourmia melon virus* (OuMV, +ssRNA, genus *Ourmiavirus*) and *Cauliflower mosaic virus* (CaMV, dsDNA, genus *Caulimovirus*) (Carluccio et al., 2014; Ozber et al., 2022).

In conclusion, positive-strand RNA viruses are master manipulators of the endomembrane system in plants. They appropriate not only existing host endomembrane compartments but also other organelles, such as chloroplasts or peroxisomes, to establish intricate viral replication organelles (Figure 1). To do so, they hijack numerous host proteins involved in membrane shaping or fusion, and activate host cellular pathways, including the unfolded protein response, to successfully perform their replication.

3 Plant viruses and membrane-mediated immunity

In this section, we discuss a paradigm shift regarding the role of membrane-localized receptor-like kinases, their associated proteins and the subsequent signaling cascades in plant antiviral immunity. In continuation, we discuss two important questions - what molecules may represent the viral molecular patterns that are recognized by these receptor complexes and where may this recognition take place.

3.1 Membrane-localized pattern recognition receptor complexes

Viruses are obligate intracellular parasites and plant antiviral immunity was accordingly thought to be mediated mainly by RNA interference and intracellular effector-triggered immunity (Nicaise, 2014). Therefore, detection of extracellular pathogen- and danger-associated molecular patterns (PAMPs and DAMPs) was not considered noteworthy for virus pathogenesis. This detection is mediated by cell surface-localized pattern recognition receptors (PRRs) that are represented by either receptor-like kinases (RLKs) or receptor-like proteins (RLPs) (He et al., 2018). Both types of receptors recognize PAMPs or DAMPs *via* diverse extracellular domains and require assistance of co-receptors for signal transduction, resulting in calcium (Ca^{2+}) influx, reactive oxygen species burst, activation of calcium-dependent kinases (CDPKs) and mitogen-activated protein kinases (MAPKs), hormone signaling, and changes in gene expression, all directed at confinement of the infection (Tang et al., 2017; Zhang and Zhang, 2022). This extracellular signal-based response is known as the pattern-triggered immunity (PTI). In the last decade, however, it was demonstrated that mutants in SOMATIC EMBRYOGENESIS RECEPTOR-LIKE KINASEs (SERKs) show increased susceptibility to several RNA viruses. SERKs represent quintessential components of pattern-triggered immunity and function as coreceptors of the PRR proteins (Ma et al., 2016). Not surprisingly, the discovery of their involvement in plant antiviral responses initiated search for a novel model of plant antiviral immunity. Arabidopsis plants lacking SERK3, better known as BRI1-ASSOCIATED KINASE 1 (BAK1), or SERK4, also known as BAK1-LIKE 1 (BKK1), showed enhanced susceptibility to *Turnip crinkle virus* (TCV, +ssRNA, genus *Betacarmovirus*) infection (Yang et al., 2010). Higher viral accumulation and classical virus-induced symptoms were also detected in the *bak1* Arabidopsis mutant plants infected with *Tobacco mosaic virus* (*Tobamovirus*) and *Oilseed rape mosaic virus* (ORMV, +ssRNA, genus *Tobamovirus*) (Kørner et al., 2013). For some viral species, BAK1 and BKK1 may contribute redundantly to antiviral immunity, as it was demonstrated for *Plum pox virus* (PPV, +ssRNA, genus *Potyvirus*). Only Arabidopsis plants carrying both *bak1* and *bkk1* mutations displayed a massive increase in PPV accumulation (Nicaise and Candresse, 2017).

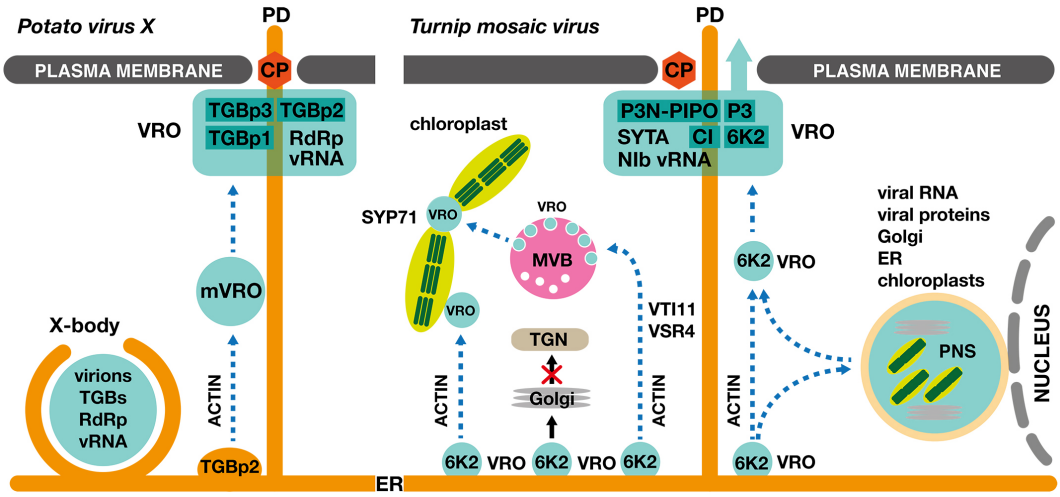

FIGURE 1
Establishment of viral replication organelles and viral cell-to-cell movement in PVX- and TuMV-infected plant cells. Left panel: *Potato virus X* (*Potexvirus*) induces formation of an intricate perinuclear replication compartment called the X-body, containing triple gene block proteins (TGBp1, TGBp2 and TGBp3), viral RNA (vRNA) and viral RNA-dependent RNA polymerase (RdRp). In addition, ER-derived TGBp2 vesicles establish mobile viral replication organelles (mVROs) that contribute to the biogenesis of a static replication compartment localized to the plasmodesmata for efficient viral intercellular movement, mediated by the PVX coat protein (CP). The intracellular movement of the TGBp2 vesicles and the mVROs is mediated by the actomyosin system. Right panel: ER-derived viral replication organelles of *Turnip mosaic virus* (*Potyvirus*), labeled with 6K2 viral protein, form secondary VROs at chloroplasts and multivesicular bodies (MVBs). The formation of the interplastidial VROs requires SYP71, a plant-specific Qc-SNARE. The 6K2-containing VROs, which enter the Golgi apparatus *via* a conventional COPII-mediated anterograde transport pathway, represent a nonproductive population. The TuMV-infected cell contains a large static perinuclear structure (PNS), which comprises amalgamated Golgi stacks, the endoplasmic reticulum, chloroplasts, and viral replication machinery. The PNS receives but also releases motile VROs. The 6K2-labelled motile VROs also contribute to the formation of dynamic replication compartments in the proximity of the plasmodesmata, containing viral RNA (vRNA), viral RNA-dependent RNA polymerase (NIb), viral movement protein (P3N-PIPO), viral protein P3, cylindrical inclusion viral protein (CI) and the host SYNAPTOTAGMIN A (SYTA). Cell-to-cell movement can be mediated either by virions containing the coat protein (CP) or by direct movement of the 6K2-containing VRO through plasmodesmata. The intracellular movement of the 6K2 VROs is mediated by the actomyosin system.

During bacterial and fungal infections, the key PTI proteins are targets of intracellular effectors that aim to shut down the associated defense pathways. It is conceivable that plant viruses may employ a similar *modus operandi*. Indeed, the first evidence came from *in planta* expression of the PPV capsid protein (CP), which was found to strongly impair PTI responses. The induction of the bacterial flagellin-induced marker genes was suppressed in CP-expressing samples in both *N. benthamiana* and Arabidopsis (Nicaise and Candresse, 2017). PTI-suppressing activity was also detected for the movement protein of *Cucumber mosaic virus* (*Cucumovirus*). Expression of the CMV movement protein in Arabidopsis and *N. benthamiana* suppresses reactive oxygen species (ROS) production triggered by multiple pathogen-associated molecular patterns (PAMPs), including bacterial flagellin and EF-Tu, and fungal-derived chitin (Kong et al., 2018).

Infection of *Tomato yellow leaf curl China virus* (*Begomovirus*) induces the activation of a host mitogen-activated protein kinase (MAPK) cascade, which represents a characteristic PTI readout. To counter these responses, the βC1 protein of TYLCCNV interacts with MKK2 and MPK4 and inhibits their kinase activity (Hu et al., 2019). A coat protein of *Beet black scorch virus* (*Betanecrovirus*) was also identified as a potent inhibitor of MAPK-mediated antiviral defense. The viral effector does not bind the kinase itself but interferes with the binding of 14-3-3a protein to MAPKKKα, resulting in the MAPKKKα protein instability (Gao et al., 2022). The molecular role of MAPK cascade in suppression of viral infections was demonstrated for *Barley yellow striate mosaic virus* (BYSMV, -ssRNA, genus *Cytorhabdovirus*). Barley MPK3 interacts with the BYSMV nucleoprotein (N) and phosphorylates it, causing formation of unstable N–RNA complexes and subsequently abolishing virus infection (Ding et al., 2022).

In addition to virus-triggered classic PTI responses listed above, the plant antiviral defense seems to involve an additional strategy. This novel layer of the antiviral defense depends on the transmembrane receptor-like kinase NSP-INTERACTING KINASE 1 (NIK1). Tomato and soybean NIK1 proteins were first identified as interacting partners of the nuclear shuttle proteins (NSP) of bipartite geminiviruses *Tomato golden mosaic virus* (TGMV, ssDNA, genus *Begomovirus*) and *Tomato crinkle leaf yellows virus* (TCrLYV, ssDNA, genus *Begomovirus*) through yeast two-hybrid assays and *in vitro* protein binding experiments (Mariano et al., 2004). Arabidopsis genome encodes three homologs, designated NIK1, NIK2 and NIK3 (Fontes et al., 2004). Taking advantage of genetic tools available for Arabidopsis and the fact that bipartite geminivirus *Cabbage leaf curl virus* (CaLCuV, ssDNA, genus *Begomovirus*) infects Arabidopsis, it was shown that binding of the CaLCuV NSP to NIKs inhibited their kinase activity and that *nik* single mutant plants were susceptible to geminivirus infection (Fontes et al., 2004). It was demonstrated that the kinase domain of NIK1 binds Arabidopsis RIBOSOMAL PROTEIN L10 A (rpL10A) (Rocha et al., 2008). The NIK1-dependent phosphorylation promotes translocation of rpL10A to the nucleus

(Carvalho et al., 2008), where it interacts with a MYB-like protein, L10-INTERACTING MYB DOMAIN-CONTAINING PROTEIN (LIMYB). These two proteins in concert fully repress the expression of *RIBOSOMAL PROTEIN* (*RP*) genes, resulting in decreased viral RNA association with polysome fractions and enhanced tolerance to geminivirus infection (Zorzatto et al., 2015). The C4 protein of monopartite geminivirus *Tomato yellow leaf curl virus* (TYLCV, ssDNA, genus *Begomovirus*) can broadly interact with various subfamilies of plant receptor-like kinases (RLKs) (Garnelo Gómez et al., 2019), suggesting that C4 of a monopartite begomovirus may exert the NSP role. Given the structural similarity of NIK proteins to SERKs (Teixeira et al., 2019), it is tempting to speculate that NIKs may function as coreceptors of yet-unidentified receptors of virus-associated molecular patterns. Supporting this hypothesis, NIK1 was found to interact with the bacterial flagellin receptor FLS2. The NIK1-overexpressing Arabidopsis plants show enhanced susceptibility to bacterial infections, likely caused by the NIK1 interference with the formation of a functional FLS2 complex (Li et al., 2019).

3.2 Virus-associated molecular patterns

The BAK1-dependent responses were observed upon induction with crude extracts from tobamovirus infected *N. benthamiana* plants but not with purified virions, indicating that some internal viral components or replication/transcription intermediates, such as proteins or certain types of nucleic acids, may be responsible for the PTI induction (Kørner et al., 2013). In addition, viral nucleic acid extracts from *Cabbage leaf curl virus*-infected Arabidopsis plants were able to activate NIK1-mediated responses. Using *nik1* and *nik2* single and double mutant plants, it was also demonstrated that this elicitation is dependent on NIK1 and/or NIK2 (Teixeira et al., 2019).

Double-strand RNAs (dsRNAs) can be generated in life cycles of ssRNA, dsRNA and DNA viruses and may thus represent general molecular patterns recognized by the antiviral PTI machinery. In mammalian cells, dsRNA is recognized by the endosomal TLR3 Toll-like receptor that triggers antiviral cellular responses (Lester and Li, 2014). It was proposed that fusion of the autophagosome containing apoptotic cell debris with the TLR3-containing endosome allows viral dsRNA recognition (Fitzgerald and Kagan, 2020). In plants, purified dsRNAs from the *Oil seed rape mosaic virus*-infected plants and the synthetic dsRNA analog polyinosinic–polycytidylic acid (poly(I:C)) triggered typical PTI responses, such as activation of MAP kinases and accumulation of pathogenesis-related phytohormones (Niehl et al., 2016). Ethylene production, a well-known marker of PTI, was impaired only in the *serk1* mutants, but not in *bak1/serk3* a *bkk1/serk4* plants, suggesting a putative specificity within the SERK family in antiviral responses. Importantly, the PTI responses listed above were observed in plants lacking the two major DICER-LIKE proteins, indicating that dsRNA represents a *bona fide* viral PAMP that functions independently from the RNAi pathway (Niehl et al., 2016). Strikingly, the poly(I:C) treatment of *N. benthamiana* infected with *Tobacco mosaic virus* reduced viral cell-to-cell movement, while viral replication and accumulation remain unaffected (Huang et al., 2023). Subsequent analyses revealed that the poly(I:C) molecular pattern is recognized by a receptor complex that contains SERK1 and the signal is further transmitted by receptor-like cytoplasmic kinases BIK1 and PBL1, leading to callose deposition at plasmodesmata and thus decreased viral intercellular movement. Interestingly, the poly(I:C) induced callose deposition is inhibited by movement proteins derived from +ssRNA tobamoviruses *Tobacco mosaic virus*, *Oilseed rape mosaic virus* and *Turnip vein clearing virus*, but the exact molecular mechanism of such inhibition is currently unknown (Huang et al., 2023). It remains to be tested whether other members of the SERK protein family also participate in the dsRNA sensing or whether their corresponding receptor complexes detect other yet-unidentified viral molecular patterns.

Considering that mammalian TLR signal presence of foreign nucleic acids from endosomal compartments (Tan et al., 2018), can plant virus-specific PRRs also function from endosomes? Plant receptors of bacterial PAMPs, such as FLS2 or EFR (receptor of bacterial elongation factor EF-Tu), internalize into endosomal compartments only after ligand perception (Mbengue et al., 2016), unlike structurally-similar brassinosteroid receptor BRI1 that cycles between the PM and endosomes independently of its ligand (Geldner et al., 2007). Interestingly, observed endocytosis of FLS2 seems crucial for certain PTI processes, such as callose deposition and stomatal closure, but not for others, including activation of MAP kinases or production of reactive oxygen species, suggesting that FLS2 may activate certain responses after its internalization into endosomal membranes (Mbengue et al., 2016). It was recently reported that external application of nonself nucleic acids resulted in their rapid internalization by endocytosis in Arabidopsis (Chiusano et al., 2021). Such observation provides a suitable explanation for the previously reported PTI activation by externally applied dsRNAs, poly(I:C) and viral extracts (Kørner et al., 2013; Niehl et al., 2016). In addition, NSP from *Cabbage leaf curl virus* (*Begomovirus*) was found to interact not only with NIKs but also with a novel SNARE-like protein, designated NSP-INTERACTING SYNTAXIN DOMAIN-CONTAINING PROTEIN (NISP). NISP, which harbors a syntaxin-6 domain at the N-terminus and a transmembrane segment at the C-terminus, exhibits a proviral function as the *nisp1* mutant is less susceptible to begomovirus infection. Using fluorescent molecular markers and FM4-64 labeling, NISP-GFP was localized to early endosomes (Gouveia-Mageste et al., 2021). These findings suggest that NISP may function in recruitment of begomoviral NSPs to the early endosomal membrane where they may, among other functions, inhibit the NIK-containing PRR complexes.

In conclusion, we hypothesize that viral PAMPs, likely represented by double-strand RNA molecules and certain viral proteins, are recognized by the yet-unidentified membrane-localized receptor complexes. After detection, the PRR proteins and their coreceptors from the SERK family initiate classic PTI responses, including ethylene production, callose deposition and MAP kinase activation. Alternatively, the receptor complexes

containing the NIK1 family of putative coreceptors trigger general translational attenuation, leading to decreased virus accumulation. The viral PAMP-specific receptor complexes may be localized to endosomal compartments, in a topology analogous to the dsRNA-specific receptors in metazoans, but the virus-associated molecular patterns may be recognized also in the extracellular space, in a similar manner as the bacterial and fungal PAMPs (Figure 2). The recently identified MVB-derived vesicles, released during *Turnip mosaic virus* (*Potyvirus*) infection into the apoplast in Arabidopsis and *N. benthamiana*, contain viral nucleic acids and proteins, and may thus facilitate detection of viral PAMPs by their corresponding plasma membrane-localized receptors (Movahed et al., 2019a).

4 Autophagy in plant virus interactions

In this section, we will present selective autophagy as a critical component of plant antiviral defense processes. We will also discuss how viruses utilize autophagy as a proviral tool to selectively target and degrade functional host factors to evade plant defense responses.

4.1 Antiviral functions of selective plant autophagy

Autophagy facilitates the vacuole-dependent unspecific (bulk) or highly selective degradation of cellular components, mediated by conserved AUTOPHAGY-RELATED (ATG) proteins (Marshall and Vierstra, 2018). A membrane structure named phagophore is formed upon activation of autophagy and progresses into a double-membrane compartment, containing the autophagy cargo, known as the autophagosome (Wun et al., 2020). In plants, autophagy activation is positively regulated by the SUCROSE NON-FERMENTING1-RELATED PROTEIN KINASE1 (SnRK1) protein family and repressed by the TARGET OF RAPAMYCIN complexes (Soto-Burgos et al., 2018). The Arabidopsis ATG1–ATG13 kinase complex is required for the phagophore initiation and represents both the regulator and the target of autophagic recycling, thus allowing the plant cell to reset the phagophore initiation process (Suttangkakul et al., 2011). The ATG1–ATG13 complex promotes ATG9–ATG2–ATG18-mediated delivery of lipids to the growing phagophore (Zhuang et al., 2017). Simultaneously, the phagophore membrane is enriched in phosphatidylinositol 3-phosphate by the phosphatidylinositol 3-

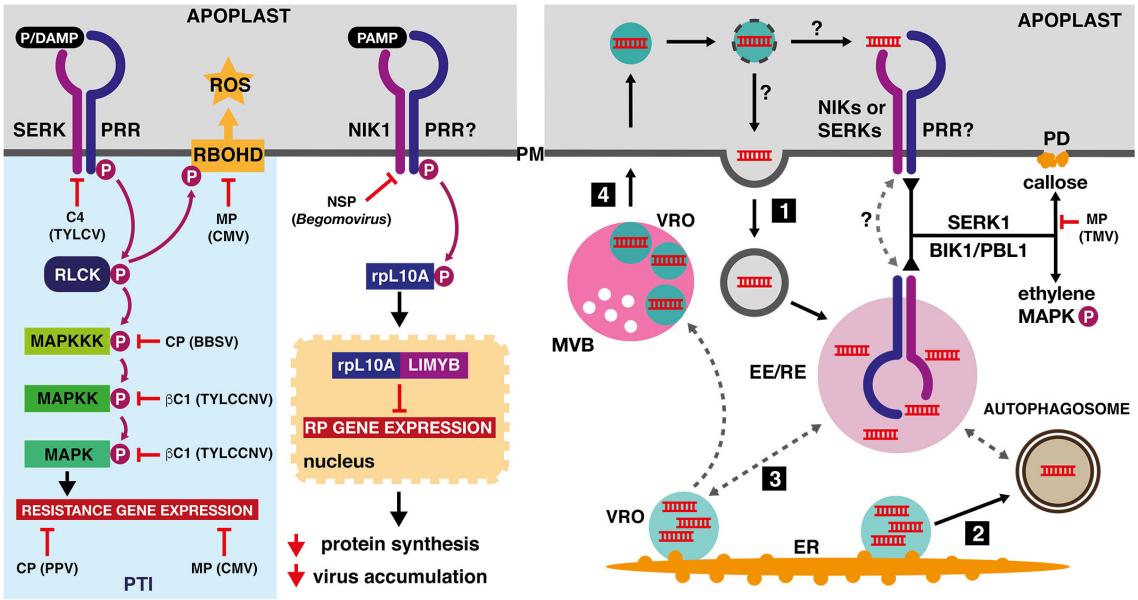

FIGURE 2
Effects of viral proteins on pathogen-triggered immunity and possible ways of viral dsRNA sensing in plants. Left panel: The coat protein (CP) of *Plum pox virus* (PPV, *Potyvirus*) and the movement protein (MP) of *Cucumber mosaic virus* (CMV, *Cucumovirus*) repress transcriptional reprogramming induced by pattern-triggered immunity (PTI). The C4 protein of *Tomato yellow leaf curl virus* (TYLCV, *Begomovirus*) and the nuclear shuttle protein (NSP) of various *Begomovirus* species inhibit membrane-localized receptor-like kinases from the SERK and NIK families. Activation of the NIK1-containing receptor complex leads to binding of phosphorylated ribosomal protein rpL10A to MYB-like transcription factor (LIMYB). The resulting protein complex represses expression of ribosomal protein genes, leading to an enhanced tolerance to viral infection. The coat protein of *Beet black scorch virus* (BBSV, *Betanecrovirus*) and the βC1 virulence factor of *Tomato yellow leaf curl China virus* (TYLCCNV, *Begomovirus*) are inhibitors of MAPK-mediated defense processes. The CMV movement protein was identified as a potent suppressor of the reactive oxygen species (ROS) production, mediated by plasma-membrane localized RESPIRATORY BURST OXIDASE HOMOLOGUE D (RBOHD). Right panel: PRR complexes, which are localized to the early or recycling endosomes (EE/RE) or cycle between the EE/RE and the plasma membrane, may detect dsRNA that was endocytosed from the extracellular space (1), delivered to the certain endosome population by means of autophagosomes (2) or by contact with the viral replication organelles (3). Alternatively, plasma membrane-localized PRR complexes may detect dsRNA delivered to the apoplast by extracellular vesicles, derived from intralumenal secondary replication organelles formed by motile ER-derived VROs in the prevacuolar compartments of the TuMV-infected plant cells (4). The viral PAMP signal, represented by dsRNA and detected by the SERK1-containing receptor complex, is further transmitted by receptor-like cytoplasmic kinases (RLCKs) BIK1 and PBL1, resulting in callose deposition, ethylene production and MAPK activation. The callose deposition is inhibited by the movement proteins (MP) of *Tobacco mosaic virus* (TMV) and other tobamoviruses.

kinase protein complex (Liu et al., 2020). The ubiquitin-fold protein ATG8 is conjugated to phosphatidylethanolamine by the ATG12–ATG5–ATG16 complex and this lipidation allows for its phagophore membrane insertion (Chung et al., 2010). At the engulfing phagophore, the ATG8–PE conjugate acts as a tethering platform for the selective autophagy. ATG8 can bind autophagy cargo directly or *via* a range of the ATG8-interacting motif (AIM)-containing proteins that function as highly selective autophagy receptors (Liu et al., 2021). While bulk autophagy does not require actin filaments, the selective autophagy receptors colocalize with actin, suggesting that the selective autophagy cargo needs to be actively transported and concentrated at the phagophore (Zientara-Rytter and Sirko, 2014; Zheng et al., 2019). Subsequently, the double membrane structure is sealed by the ESCRT proteins (Zhou et al., 2019). The autophagosome eventually fuses with the tonoplast, releasing its content for degradation by vacuolar hydrolases (Gao et al., 2015; Kalinowska and Isono, 2018). However, the direct fusion of the autophagosome and the vacuole has been recently challenged. It was shown that the interaction of the autophagosome-localized CELL DEATH RELATED ENDOSOMAL FYVE/SYLF PROTEIN 1 (CFS1) adaptor with an MVB-localized subunit of the ESCRT complex has a crucial role in the autophagic flux, as the delivery of autophagosomes to the vacuole is disrupted in the *cfs1* Arabidopsis plants (Sutipatanasomboon et al., 2017; Zhao et al., 2022). It was proposed that CFS1 mediates formation of plant amphisomes, which were previously identified in metazoans, and that plant amphisomes may serve as sorting hubs for multivesicular bodies and autophagosomes before fusing with the vacuole (Zhao et al., 2022).

The first direct interaction of a viral protein and the selective plant autophagy machinery was demonstrated for the βC1 virulence factor of *Cotton leaf curl Multan virus* (CLCuMuV, ssDNA, genus *Begomovirus*) (Haxim et al., 2017). Using a yeast two-hybrid approach (Y2H), pull-down assays and bimolecular fluorescence complementation (BiFC) experiments, ATG8f proteins from tomato (*Solanum lycopersicum*) and tobacco (*Nicotiana benthamiana*) were identified as βC1 interacting partners. The specific interaction between ATG8f and βC1 was attributed to an 11-amino acid motif within the βC1 viral protein. A mutation in this motif resulted in higher accumulation of CLCuMuV in tobacco. Silencing autophagy-related genes *ATG5* and *ATG7* caused reduced plant resistance to begomoviruses *Cotton leaf curl Multan virus*, *Tomato yellow leaf curl virus* and *Tomato yellow leaf curl China virus*, whereas activating autophagy led to enhanced plant resistance (Haxim et al., 2017). The C1 nucleoprotein of *Tomato leaf curl Yunnan virus* (TLCYnV, ssDNA, genus *Begomovirus*) is also degraded by autophagy *via* a direct interaction with ATG8 (Li et al., 2020b). This interaction, mediated by the AIM motif in the C1 protein, was demonstrated using the *ATG8h* coding sequence from *S. lycopersicum* in both the Y2H assay and the BiFC experiments. Silencing *ATG8h*, *ATG5*, and *ATG7* genes in *S. lycopersicum* and *N. benthamiana* inhibits the degradation of C1, which in turn promotes TLCYnV infection. Importantly, karyopherin EXPORTIN1 (XPO1) from tomato and tobacco is necessary for the transfer of the C1-ATG8h complex from the nucleus to the cytoplasm to facilitate the C1 degradation (Li et al., 2020b). Another direct interaction with ATG8 was reported for a movement protein of *Citrus leaf blotch virus* (CLBV, +ssRNA, genus *Citrivirus*) (Niu et al., 2021). The identified AIM motif within the CLBV MP interacts specifically with the ATG8C1 isoform, while additional binding domains at the N-terminus of the CLBV MP were hypothesized for an interaction with the ATG8i isoform in tobacco (Niu et al., 2021). The requirements of a particular ATG8 isoform for a successful degradation of distinct viral proteins suggests a coevolution-driven selectivity.

However, autophagy in plants involves not only direct targeting of the viral component by the core autophagy protein ATG8 but mainly requires cargo receptors as intermediaries. A central role plays an autophagy receptor NEXT TO BRCA1 GENE 1 (NBR1)/JOKA2, which selectively brings the autophagy cargo to the phagophore through interaction with ATG8. NBR1-dependent selective autophagy promotes degradation of the non-assembled virus capsid protein P4 of *Cauliflower mosaic virus* (*Caulimovirus*), which restricts viral infection in Arabidopsis (Hafrén et al., 2017). Upon CaMV infection, Arabidopsis *atg5* and *atg7* autophagy-defective mutants exhibit more severe symptoms than wild-type plants and accumulate higher amounts of the P4 capsid protein, while the levels of other viral proteins remain unaltered. In a typical tug-of-war strategy, the CaMV P6 protein sequesters viral particles to inclusion bodies, where they are protected from the autophagy machinery (Hafrén et al., 2017). NBR1-mediated selective autophagy has been also shown to target the RNA silencing suppressor (RSS) helper-component protease HCpro from TuMV (Hafrén et al., 2018). Arabidopsis autophagy mutants show stronger TuMV disease symptoms including severe stunting and accelerated leaf senescence, compared to the wild type plants. Intriguingly, the TuMV seems to counteract NBR1-dependent autophagy during infection using other viral proteins, thereby limiting its antiviral potential (Hafrén et al., 2018). The silencing suppressors such as HCpro of *Tobacco etch virus* (TEV, +ssRNA, genus *Potyvirus*) or 2b from *Cucumber mosaic virus* (*Cucumovirus*) or *Tomato aspermy virus* (TAV, +ssRNA, genus *Cucumovirus*) are not recognized by NBR1, but instead bind calmodulin-like protein rgs-CaM and the resulting protein complex is subsequently degraded by autophagy (Nakahara et al., 2012). The unambiguous role of autophagy in the HCpro–rgs-CaM complex degradation is indicated by its sensitivity to 3-methyladenine, which represents a potent inhibitor of the autophagosome biogenesis (Nakahara et al., 2012). A recently identified autophagy cargo receptor, P3 INTERACTING PROTEIN in *N. benthamiana* (NbP3IP), facilitates the degradation of the P3 protein, an RNA silencing suppressor encoded by the *Rice stripe virus* (*Tenuivirus*) (Jiang et al., 2021). Using BiFC and pull-down assays, it was demonstrated that NbP3IP interacts with NbATG8f. While silencing *ATG5* and *ATG7* in *N. benthamiana* promoted RSV infection, tobacco plants with activated autophagy contained lower amounts of virus (Jiang et al., 2021).

ATG6/BECLIN1 represents another potential cargo receptor, interacting with NIb, the TuMV RNA-dependent RNA polymerase (RdRp) (Li et al., 2018). Deficiency of ATG6 or ATG8a in *N. benthamiana* increases NIb accumulation and promotes viral

infection. A noteworthy aspect is that ATG6 also interacts with RdRps from other potyviruses, such as *Plum pox virus*, *Soybean mosaic virus*, and *Tobacco etch virus*, as well as RdRps from *Cucumber green mottle mosaic virus* (CGMMV, +ssRNA, genus *Tobamovirus*) and *Pepino mosaic virus* (PepMV, +ssRNA, genus *Potexvirus*) (Li et al., 2018). These findings suggest that the ATG6-mediated targeting of RdRps could be a general mechanism for restricting viral infection in plants. However, a recent report challenged the strict antiviral role of selective autophagy in TuMV infection and suggested an additional function in promoting viral replication (Li et al., 2020a).

4.2 Plant autophagy in promoting viral infection

The proviral role of receptor-independent bulk autophagy was proposed to be linked to the suppression of virus-associated senescence that leads to a significant extension of the virus production timespan and to better chances for virus particle acquisition by aphid vectors (Hafrén et al., 2017). However, an increasing number of reports identified a proviral role of selective autophagy. A small viral membrane protein 6K2 of *Turnip mosaic virus*, described in the previous section as a key protein in the formation of viral replication compartments, upregulates the *NBR1* gene expression through the IRE1/bZIP60 pathway. It was demonstrated that overexpression of NBR1 stimulates TuMV replication, while its deficiency inhibits virus infection (Li et al., 2020a). The upregulated NBR1 competes with BECLIN1 for interaction with NIb, the TuMV RNA polymerase, and binds ATG8f of both *Nicotiana benthamiana* and Arabidopsis. The resulting NIb–NBR1–ATG8f complex colocalizes with 6K2 to the vacuolar membrane. At the tobacco tonoplast, ATG8f interacts with TONOPLAST INTRINSIC PROTEIN 1 (NbTIP1), resulting in the formation of numerous viral replication complexes (Li et al., 2020a). An interesting example of proviral autophagy functions was shown to be mediated by P0 protein from *Turnip yellows virus* (TuYV, +ssRNA, genus *Polerovirus*). P0 is an F-box protein that interacts with S PHASE KINASE-ASSOCIATED PROTEIN 1 (SKP1), a core component of the SKP1–CULLIN1–F-box protein (SCF) E3 ubiquitin ligase complex (Bortolamiol et al., 2007). The SCF complex ubiquitinates ARGONAUTE1 (AGO1), a key component of the RNA-induced silencing complex (RISC) in Arabidopsis, but the AGO1 ubiquitination does not cause its 26S proteasome degradation (Baumberger et al., 2007). Instead, ubiquitinated AGO1 and P0 interact with ATG8-INTERACTING PROTEIN1 (ATI1) at the endoplasmic reticulum and the resulting protein complex is degraded by ATG5/ATG7-mediated autophagy (Michaeli et al., 2019).

In conclusion, autophagy may play both antiviral and proviral roles during viral replication in plant cells (Figure 3). Regarding the regulation of the autophagy processes, recent findings indicate that autophagy activation is tightly linked to the unfolded protein

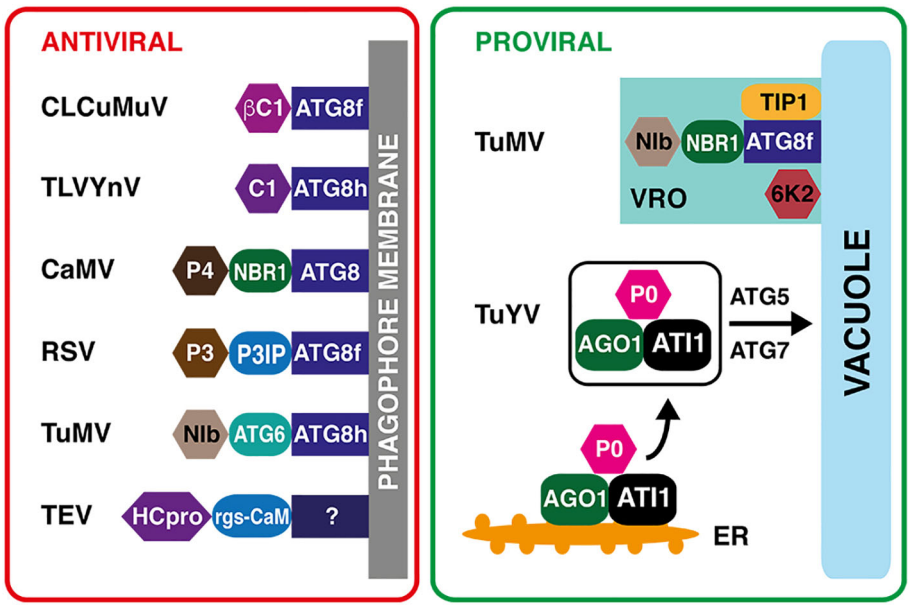

FIGURE 3
Proviral and antiviral roles of plant selective autophagy. Left panel: Virus–host protein interactions with the antiviral outcome. The βC1 virulence factor of *Cotton leaf curl Multan virus* (CLCuMuV, *Begomovirus*) and the C1 nucleoprotein of *Tomato leaf curl Yunnan virus* (TLCYnV, *Begomovirus*) are recognized directly by the phagophore-localized ATG8 protein. The non-assembled virus capsid protein P4 of *Cauliflower mosaic virus* (CaMV, *Caulimovirus*) is recognized by the NEXT TO BRCA1 GENE 1 (NBR1) specific autophagy receptor. The P3 INTERACTING PROTEIN (P3IP) autophagy cargo receptor binds the P3 RNA silencing suppressor of *Rice stripe virus* (RSV, *Tenuivirus*). The autophagy protein ATG6 serves as a receptor for the NIb RNA-dependent RNA polymerase of *Turnip mosaic virus* (TuMV, *Potyvirus*). The selective autophagy of the HCPro silencing suppressor of *Tobacco etch virus* (TEV) requires calmodulin-like protein rgs-CaM as an intermediary. The rgs-CaM binding partner on the phagophore is unknown. Right panel: Two examples of proviral functions of selective autophagy. During TuMV infection, the NIb viral RNA polymerase interacts with the NBR1 autophagy receptor and ATG8f, and associates with TONOPLAST INTRINSIC PROTEIN 1 (TIP1) and viral 6K2 proteins. This complex triggers a formation of tonoplast-bound replication compartments, protected from plant defenses. The P0 viral protein of *Turnip yellows virus* (TuYV, *Polerovirus*) forms a complex with ubiquitinated ARGONAUTE1, a key component of RNA interference pathway, and ATG8-INTERACTING PROTEIN1 (ATI1), which is subsequently degraded by ATG5/ATG7-mediated autophagy, resulting in a decreased RNA interference activity.

response, which is triggered by various plant viruses. In a process termed IRE1-dependent decay of messenger RNA (RIDD), IRE1b degrades the RNA transcripts of factors that interfere with the induction of autophagy in Arabidopsis (Liu et al., 2012; Yang et al., 2016). In addition, the activation of UPR is directly linked to upregulation of genes encoding selective autophagy receptors (Li et al., 2020a). However, a limited information is available on the contribution of the two major autophagy regulatory hubs, represented by the TOR complexes and kinases from the SnRK1 family, on plant–virus interactions. The current available data indicate that TOR inhibition causes increased resistance to *Watermelon mosaic virus* (WMV, +ssRNA, genus *Potyvirus*) and *Tobacco mosaic virus* (*Tobamovirus*) (Ouibrahim et al., 2015; Marash et al., 2022).

5 Concluding remarks

Plant cells contain a diverse population of membrane structures that perform distinct tasks in plant development and in responses to environmental cues. Understanding the molecular mechanisms of the host endomembrane system misappropriation by positive-strand RNA viruses provides invaluable insights into processes of viral replication, assembly, and intercellular movement. Recent reports on the participation of membrane-localized receptor-like kinases in detection of viral nucleic acids indicate that the classical pattern-triggered immunity, crucial for detection of bacterial and fungal pathogens, comprises an important part of antiviral defenses in plant cells. The emerging knowledge of plant selective autophagy indicates its dual role in plant–virus interactions. Selective autophagy targets viral components for degradation to restrict viral accumulation, while being manipulated by viral proteins to promote viral infection. The detailed comprehension of molecular mechanisms discussed partly in this review will likely lead to the development of potential biotechnology strategies to enhance and engineer crop resistance to viral infections.

Author contributions

IJ, NF and JZ wrote sections of the manuscript and prepared the figures. All authors contributed to the article and approved the submitted version.

Acknowledgments

We acknowledge Dr. Guillermo Ruano Blanco for critically reading the manuscript. We apologize to those colleagues whose important contributions may have been omitted due to negligence, focus or space constraints.

Conflict of interest

The authors declare that the research was conducted in the absence of any commercial or financial relationships that could be construed as a potential conflict of interest.

Publisher's note

References

Agaoua, A., Bendahmane, A., Moquet, F., and Dogimont, C. (2021). Membrane trafficking proteins: A new target to identify resistance to viruses in plants. *Plants (Basel)* 10, 2139. doi: 10.3390/plants10102139

Agbeci, M., Grangeon, R., Nelson, R. S., Zheng, H., and Laliberté, J. F. (2013). Contribution of host intracellular transport machineries to intercellular movement of Turnip mosaic virus. *PloS Pathog.* 9, e1003683. doi: 10.1371/journal.ppat.1003683

Bao, Y., and Howell, S. H. (2017). The unfolded protein response supports plant development and defense as well as responses to abiotic stress. *Front. Plant Sci.* 8. doi: 10.3389/fpls.2017.00344

Barajas, D., Jiang, Y., and Nagy, P. D. (2009). A unique role for the host ESCRT proteins in replication of *Tomato bushy stunt virus*. *PloS Pathog.* 5, e1000705. doi: 10.1371/journal.ppat.1000705

Barajas, D., Xu, K., De Castro Martín, I. F., Sasvari, Z., Brandizzi, F., Risco, C., et al. (2014). Co-opted oxysterol-binding ORP and VAP proteins channel sterols to RNA virus replication sites *via* membrane contact sites. *PloS Pathog.* 10, e1004388. doi: 10.1371/journal.ppat.1004388

Baumberger, N., Tsai, C. H., Lie, M., Havecker, E., and Baulcombe, D. C. (2007). The Polerovirus silencing suppressor P0 targets ARGONAUTE proteins for degradation. *Curr. Biol.* 17, 1609–1614. doi: 10.1016/j.cub.2007.08.039

Boevink, P., Oparka, K., Santa Cruz, S., Martin, B., Betteridge, A., and Hawes, C. (1998). Stacks on tracks: the plant Golgi apparatus traffics on an actin/ER network. *Plant J.* 15, 441–447. doi: 10.1046/j.1365-313x.1998.00208.x

Bortolamiol, D., Pazhouhandeh, M., Marrocco, K., Genschik, P., and Ziegler-Graff, V. (2007). The Polerovirus F box protein P0 targets ARGONAUTE1 to suppress RNA silencing. *Curr. Biol.* 17, 1615–1621. doi: 10.1016/j.cub.2007.07.061

Cabanillas, D. G., Jiang, J., Movahed, N., Germain, H., Yamaji, Y., Zheng, H., et al. (2018). Turnip mosaic virus uses the SNARE protein VTI11 in an unconventional route for replication vesicle trafficking. *Plant Cell* 30, 2594–2615. doi: 10.1105/tpc.18.00281

Cao, X., Jin, X., Zhang, X., Li, Y., Wang, C., Wang, X., et al. (2015). Morphogenesis of endoplasmic reticulum membrane-invaginated vesicles during *beet black scorch virus* infection: role of auxiliary replication protein and new implications of three-dimensional architecture. *J. Virol.* 89, 6184–6195. doi: 10.1128/JVI.00401-15

Carluccio, A. V., Zicca, S., and Stavolone, L. (2014). Hitching a ride on vesicles: cauliflower mosaic virus movement protein trafficking in the endomembrane system. *Plant Physiol.* 164, 1261–1270. doi: 10.1104/pp.113.234534

Carroll, T. W. (1970). Relation of barley stripe mosaic virus to plastids. *Virology* 42, 1015–1022. doi: 10.1016/0042-6822(70)90350-8

Carvalho, C. M., Santos, A. A., Pires, S. R., Rocha, C. S., Saraiva, D. I., MaChado, J. P., et al. (2008). Regulated nuclear trafficking of rpL10A mediated by NIK1 represents a defense strategy of plant cells against virus. *PloS Pathog.* 4, e1000247. doi: 10.1371/journal.ppat.1000247

Chai, M., Wu, X., Liu, J., Fang, Y., Luan, Y., Cui, X., et al. (2020). P3N-PIPO interacts with P3 *via* the shared N-terminal domain to recruit viral replication vesicles for cell-to-cell movement. *J. Virol.* 94, e01898-01819. doi: 10.1128/JVI.01898-19

Chan, K. X., Phua, S. Y., Crisp, P., Mcquinn, R., and Pogson, B. J. (2016). Learning the languages of the chloroplast: retrograde signaling and beyond. *Annu. Rev. Plant Biol.* 67, 25–53. doi: 10.1146/annurev-arplant-043015-111854

Che, P., Bussell, J. D., Zhou, W., Estavillo, G. M., Pogson, B. J., and Smith, S. M. (2010). Signaling from the endoplasmic reticulum activates brassinosteroid signaling and promotes acclimation to stress in *Arabidopsis*. *Sci. Signal* 3, ra69. doi: 10.1126/scisignal.2001140

Chen, J., Stefano, G., Brandizzi, F., and Zheng, H. (2011). *Arabidopsis* RHD3 mediates the generation of the tubular ER network and is required for Golgi distribution and motility in plant cells. *J. Cell Sci.* 124, 2241–2252. doi: 10.1242/jcs.084624

Chiusano, M. L., Incerti, G., Colantuono, C., Termolino, P., Palomba, E., Monticolo, F., et al. (2021). *Arabidopsis thaliana* response to extracellular DNA: self versus nonself exposure. *Plants (Basel)* 10, 1744. doi: 10.3390/plants10081744

Chuang, C., Barajas, D., Qin, J., and Nagy, P. D. (2014). Inactivation of the host lipin gene accelerates RNA virus replication through viral exploitation of the expanded endoplasmic reticulum membrane. *PloS Pathog.* 10, e1003944. doi: 10.1371/journal.ppat.1003944

Chung, T., Phillips, A. R., and Vierstra, R. D. (2010). ATG8 lipidation and ATG8-mediated autophagy in Arabidopsis require ATG12 expressed from the differentially controlled *ATG12A* and *ATG12B* loci. *Plant J.* 62, 483–493. doi: 10.1111/j.1365-313X.2010.04166.x

Cotton, S., Grangeon, R., Thivierge, K., Mathieu, I., Ide, C., Wei, T., et al. (2009). Turnip mosaic virus RNA replication complex vesicles are mobile, align with microfilaments, and are each derived from a single viral genome. *J. Virol.* 83, 10460–10471. doi: 10.1128/JVI.00819-09

Craddock, C. P., Adams, N., Bryant, F. M., Kurup, S., and Eastmond, P. J. (2015). Regulation of endomembrane biogenesis in arabidopsis by phosphatidic acid hydrolase. *Plant Signal Behav.* 10, e1065367. doi: 10.1080/15592324.2015.1065367

Csorba, T., Kontra, L., and Burgyán, J. (2015). Viral silencing suppressors: Tools forged to fine-tune host-pathogen coexistence. *Virology* 479-480, 85–103. doi: 10.1016/j.virol.2015.02.028

Dai, Z., He, R., Bernards, M. A., and Wang, A. (2020). The *cis*-expression of the coat protein of turnip mosaic virus is essential for viral intercellular movement in plants. *Mol. Plant Pathol.* 21, 1194–1211. doi: 10.1111/mpp.12973

Diaz, A., Zhang, J., Ollwerther, A., Wang, X., and Ahlquist, P. (2015). Host ESCRT proteins are required for bromovirus RNA replication compartment assembly and function. *PloS Pathog.* 11, e1004742. doi: 10.1371/journal.ppat.1004742

Ding, Z. H., Gao, Q., Tong, X., Xu, W. Y., Ma, L., Zhang, Z. J., et al. (2022). MAPKs trigger antiviral immunity by directly phosphorylating a rhabdovirus nucleoprotein in plants and insect vectors. *Plant Cell* 34, 3110–3127. doi: 10.1093/plcell/koac143

Ding, X., Jimenez-Gongora, T., Krenz, B., and Lozano-Duran, R. (2019). Chloroplast clustering around the nucleus is a general response to pathogen perception in *Nicotiana benthamiana*. *Mol. Plant Pathol.* 20, 1298–1306. doi: 10.1111/mpp.12840

Di Sansebastiano, G. P., Barozzi, F., Piro, G., Denecke, J., and De Marcos Lousa, C. (2017). Trafficking routes to the plant vacuole: connecting alternative and classical pathways. *J. Exp. Bot.* 69, 79–90. doi: 10.1093/jxb/erx376

Dubiella, U., and Serrano, I. (2021). The ubiquitin proteasome system as a double agent in plant-virus interactions. *Plants (Basel)* 10, 928. doi: 10.3390/plants10050928

Feng, Z., Inaba, J., and Nagy, P. D. (2021a). The retromer is co-opted to deliver lipid enzymes for the biogenesis of lipid-enriched tombusviral replication organelles. *Proc. Natl. Acad. Sci. U.S.A.* 118, e2016066118. doi: 10.1073/pnas.2016066118

Feng, Z., Inaba, J., and Nagy, P. D. (2021b). Tombusviruses target a major crossroad in the endocytic and recycling pathways *via* co-opting rab7 small GTPase. *J. Virol.* 95, e0107621. doi: 10.1128/JVI.01076-21

Feng, Z., Xu, K., Kovalev, N., and Nagy, P. D. (2019). Recruitment of Vps34 PI3K and enrichment of PI3P phosphoinositide in the viral replication compartment is crucial for replication of a positive-strand RNA virus. *PloS Pathog.* 15, e1007530. doi: 10.1371/journal.ppat.1007530

Fernández De Castro, I., Fernández, J. J., Barajas, D., Nagy, P. D., and Risco, C. (2017). Three-dimensional imaging of the intracellular assembly of a functional viral RNA replicase complex. *J. Cell Sci.* 130, 260–268. doi: 10.1242/jcs.181586

Fiallo-Olivé, E., and Navas-Castillo, J. (2023). Begomoviruses: what is the secret(s) of their success? *Trends Plant Sci.* 28, 715–727. doi: 10.1016/j.tplants.2023.01.012

Fitzgerald, K. A., and Kagan, J. C. (2020). Toll-like receptors and the control of immunity. *Cell* 180, 1044–1066. doi: 10.1016/j.cell.2020.02.041

Fontes, E. P., Santos, A. A., Luz, D. F., Waclawovsky, A. J., and Chory, J. (2004). The geminivirus nuclear shuttle protein is a virulence factor that suppresses transmembrane receptor kinase activity. *Genes Dev.* 18, 2545–2556. doi: 10.1101/gad.1245904

Frigerio, L., Hinz, G., and Robinson, D. G. (2008). Multiple vacuoles in plant cells: rule or exception? *Traffic* 9, 1564–1570. doi: 10.1111/j.1600-0854.2008.00776.x

Gao, Z., Zhang, D., Wang, X., Zhang, X., Wen, Z., Zhang, Q., et al. (2022). Coat proteins of necroviruses target 14-3-3a to subvert MAPKKKα-mediated antiviral immunity in plants. *Nat. Commun.* 13, 716. doi: 10.1038/s41467-022-28395-5

Gao, C., Zhuang, X., Cui, Y., Fu, X., He, Y., Zhao, Q., et al. (2015). Dual roles of an *Arabidopsis* ESCRT component FREE1 in regulating vacuolar protein transport and autophagic degradation. *Proc. Natl. Acad. Sci. U.S.A.* 112, 1886–1891. doi: 10.1073/pnas.1421271112

Garnelo Gómez, B., Zhang, D., Rosas-Díaz, T., Wei, Y., Macho, A. P., and Lozano-Durán, R. (2019). The C4 protein from tomato yellow leaf curl virus can broadly interact with plant receptor-like kinases. *Viruses* 1 (11), 1009. doi: 10.3390/v11111009

Geldner, N., Hyman, D. L., Wang, X., Schumacher, K., and Chory, J. (2007). Endosomal signaling of plant steroid receptor kinase BRI1. *Genes Dev.* 21, 1598–1602. doi: 10.1101/gad.1561307

Gouveia-Mageste, B. C., Martins, L. G. C., Dal-Bianco, M., MaChado, J. P. B., Da Silva, J. C. F., Kim, A. Y., et al. (2021). A plant-specific syntaxin-6 protein contributes to the intracytoplasmic route for the begomovirus CabLCV. *Plant Physiol.* 187, 158–173. doi: 10.1093/plphys/kiab252

Grangeon, R., Agbeci, M., Chen, J., Grondin, G., Zheng, H., and Laliberté, J. F. (2012). Impact on the endoplasmic reticulum and Golgi apparatus of turnip mosaic virus infection. *J. Virol.* 86, 9255–9265. doi: 10.1128/JVI.01146-12

Grangeon, R., Jiang, J., Wan, J., Agbeci, M., Zheng, H., and Laliberté, J. F. (2013). 6K2-induced vesicles can move cell to cell during turnip mosaic virus infection. *Front. Microbiol.* 4. doi: 10.3389/fmicb.2013.00351

Hafrén, A., Macia, J. L., Love, A. J., Milner, J. J., Drucker, M., and Hofius, D. (2017). Selective autophagy limits cauliflower mosaic virus infection by NBR1-mediated targeting of viral capsid protein and particles. *Proc. Natl. Acad. Sci. U.S.A.* 114, E2026–E2035. doi: 10.1073/pnas.1610687114

Hafrén, A., Üstün, S., Hochmuth, A., Svenning, S., Johansen, T., and Hofius, D. (2018). Turnip mosaic virus counteracts selective autophagy of the viral silencing suppressor HCpro. *Plant Physiol.* 176, 649–662. doi: 10.1104/pp.17.01198

Harries, P. A., Park, J. W., Sasaki, N., Ballard, K. D., Maule, A. J., and Nelson, R. S. (2009). Differing requirements for actin and myosin by plant viruses for sustained intercellular movement. *Proc. Natl. Acad. Sci. U.S.A.* 106, 17594–17599. doi: 10.1073/pnas.0909239106

Haxim, Y., Ismayil, A., Jia, Q., Wang, Y., Zheng, X., Chen, T., et al. (2017). Autophagy functions as an antiviral mechanism against geminiviruses in plants. *Elife* 6, e23897. doi: 10.7554/eLife.23897

He, R., Li, Y., Bernards, M. A., and Wang, A. (2023). Manipulation of the cellular membrane-cytoskeleton network for RNA virus replication and movement in plants. *Viruses* 15, 744. doi: 10.3390/v15030744

He, Y., Zhou, J., Shan, L., and Meng, X. (2018). Plant cell surface receptor-mediated signaling - a common theme amid diversity. *J. Cell Sci.* 131, jcs209353. doi: 10.1242/jcs.209353

Hu, T., Huang, C., He, Y., Castillo-González, C., Gui, X., Wang, Y., et al. (2019). βC1 protein encoded in geminivirus satellite concertedly targets MKK2 and MPK4 to counter host defense. *PloS Pathog.* 15, e1007728. doi: 10.1371/journal.ppat.1007728

Huang, C. (2021). From player to pawn: viral avirulence factors involved in plant immunity. *Viruses* 13, 688. doi: 10.3390/v13040688

Huang, C., Sede, A. R., Elvira-González, L., Yan, Y., Rodriguez, M., Mutterer, J., et al. (2023). DsRNA-induced immunity targets plasmodesmata and is suppressed by viral movement proteins. *Plant Cell*. koad176. doi: 10.1093/plcell/koad176

Hyodo, K., Taniguchi, T., Manabe, Y., Kaido, M., Mise, K., Sugawara, T., et al. (2015). Phosphatidic acid produced by phospholipase D promotes RNA replication of a plant RNA virus. *PloS Pathog.* 11, e1004909. doi: 10.1371/journal.ppat.1004909

Ibrahim, A., Yang, X., Liu, C., Cooper, K. D., Bishop, B. A., Zhu, M., et al. (2020). Plant SNAREs SYP22 and SYP23 interact with *Tobacco mosaic virus* 126 kDa protein and SYP2s are required for normal local virus accumulation and spread. *Virology* 547, 57–71. doi: 10.1016/j.virol.2020.04.002

Inaba, J., Xu, K., Kovalev, N., Ramanathan, H., Roy, C. R., Lindenbach, B. D., et al. (2019). Screening *Legionella* effectors for antiviral effects reveals Rab1 GTPase as a proviral factor coopted for tombusvirus replication. *Proc. Natl. Acad. Sci. U.S.A.* 116, 21739–21747. doi: 10.1073/pnas.1911108116

Jacquemyn, J., Cascalho, A., and Goodchild, R. E. (2017). The ins and outs of endoplasmic reticulum-controlled lipid biosynthesis. *EMBO Rep.* 18, 1905–1921. doi: 10.15252/embr.201643426

Jiang, L., Lu, Y., Zheng, X., Yang, X., Chen, Y., Zhang, T., et al. (2021). The plant protein NbP3IP directs degradation of *Rice stripe virus* p3 silencing suppressor protein to limit virus infection through interaction with the autophagy-related protein NbATG8. *New Phytol.* 229, 1036–1051. doi: 10.1111/nph.16917

Jiang, J., Patarroyo, C., Garcia Cabanillas, D., Zheng, H., and Laliberté, J. F. (2015). The vesicle-forming 6K2 protein of turnip mosaic virus interacts with the COPII coatomer sec24a for viral systemic infection. *J. Virol.* 89, 6695–6710. doi: 10.1128/JVI.00503-15

Jin, X., Jiang, Z., Zhang, K., Wang, P., Cao, X., Yue, N., et al. (2018). Three-dimensional analysis of chloroplast structures associated with virus infection. *Plant Physiol.* 176, 282–294. doi: 10.1104/pp.17.00871

Ju, H. J., Samuels, T. D., Wang, Y. S., Blancaflor, E., Payton, M., Mitra, R., et al. (2005). The potato virus X TGBp2 movement protein associates with endoplasmic reticulum-derived vesicles during virus infection. *Plant Physiol.* 138, 1877–1895. doi: 10.1104/pp.105.066019

Kalinowska, K., and Isono, E. (2018). All roads lead to the vacuole-autophagic transport as part of the endomembrane trafficking network in plants. *J. Exp. Bot.* 69, 1313–1324. doi: 10.1093/jxb/erx395

Ketter, E., and Randall, G. (2019). Virus impact on lipids and membranes. *Annu. Rev. Virol.* 6, 319–340. doi: 10.1146/annurev-virology-092818-015748

Kong, J., Wei, M., Li, G., Lei, R., Qiu, Y., Wang, C., et al. (2018). The *cucumber mosaic virus* movement protein suppresses PAMP-triggered immune responses in Arabidopsis and tobacco. *Biochem. Biophys. Res. Commun.* 498, 395–401. doi: 10.1016/j.bbrc.2018.01.072

Kørner, C. J., Klauser, D., Niehl, A., Dominguez-Ferreras, A., Chinchilla, D., Boller, T., et al. (2013). The immunity regulator BAK1 contributes to resistance against diverse RNA viruses. *Mol. Plant Microbe Interact.* 26, 1271–1280. doi: 10.1094/MPMI-06-13-0179-R

Laliberté, J. F., and Sanfaçon, H. (2010). Cellular remodeling during plant virus infection. *Annu. Rev. Phytopathol.* 48, 69–91. doi: 10.1146/annurev-phyto-073009-114239

Lazareva, E. A., Lezzhov, A. A., Chergintsev, D. A., Golyshev, S. A., Dolja, V. V., Morozov, S. Y., et al. (2021). Reticulon-like properties of a plant virus-encoded movement protein. *New Phytol.* 229, 1052–1066. doi: 10.1111/nph.16905

Lee, W. M., and Ahlquist, P. (2003). Membrane synthesis, specific lipid requirements, and localized lipid composition changes associated with a positive-strand RNA virus RNA replication protein. *J. Virol.* 77, 12819–12828. doi: 10.1128/jvi.77.23.12819-12828.2003

Legg, J. P., Lava Kumar, P., Makeshkumar, T., Tripathi, L., Ferguson, M., Kanju, E., et al. (2015). Cassava virus diseases: biology, epidemiology, and management. *Adv. Virus Res.* 91, 85–142. doi: 10.1016/bs.aivir.2014.10.001

Lester, S. N., and Li, K. (2014). Toll-like receptors in antiviral innate immunity. *J. Mol. Biol.* 426, 1246–1264. doi: 10.1016/j.jmb.2013.11.024

Levy, A., Zheng, J. Y., and Lazarowitz, S. G. (2015). Synaptotagmin SYTA forms ER-plasma membrane junctions that are recruited to plasmodesmata for plant virus movement. *Curr. Biol.* 25, 2018–2025. doi: 10.1016/j.cub.2015.06.015

Lewis, J. D., and Lazarowitz, S. G. (2010). *Arabidopsis* synaptotagmin SYTA regulates endocytosis and virus movement protein cell-to-cell transport. *Proc. Natl. Acad. Sci. U.S.A.* 107, 2491–2496. doi: 10.1073/pnas.0909080107

Li, B., Ferreira, M. A., Huang, M., Camargos, L. F., Yu, X., Teixeira, R. M., et al. (2019). The receptor-like kinase NIK1 targets FLS2/BAK1 immune complex and inversely modulates antiviral and antibacterial immunity. *Nat. Commun.* 10, 4996. doi: 10.1038/s41467-019-12847-6

Li, F., Zhang, C., Li, Y., Wu, G., Hou, X., Zhou, X., et al. (2018). Beclin1 restricts RNA virus infection in plants through suppression and degradation of the viral polymerase. *Nat. Commun.* 9, 1268. doi: 10.1038/s41467-018-03658-2

Li, C., Zhang, T., Liu, Y., Li, Z., Wang, Y., Fu, S., et al. (2022). Rice stripe virus activates the bZIP17/28 branch of the unfolded protein response signalling pathway to promote viral infection. *Mol. Plant Pathol.* 23, 447–458. doi: 10.1111/mpp.13171

Li, F., Zhang, C., Tang, Z., Zhang, L., Dai, Z., Lyu, S., et al. (2020a). A plant RNA virus activates selective autophagy in a UPR-dependent manner to promote virus infection. *New Phytol.* 228, 622–639. doi: 10.1111/nph.16716

Li, F., Zhang, M., Zhang, C., and Zhou, X. (2020b). Nuclear autophagy degrades a geminivirus nuclear protein to restrict viral infection in solanaceous plants. *New Phytol.* 225, 1746–1761. doi: 10.1111/nph.16268

Lin, N. S., and Langenberg, W. G. (1985). Peripheral vesicles in proplastids of barley stripe mosaic virus-infected wheat cells contain double-stranded RNA. *Virology* 142, 291–298. doi: 10.1016/0042-6822(85)90337-x

Littlejohn, G. R., Breen, S., Smirnoff, N., and Grant, M. (2021). Chloroplast immunity illuminated. *New Phytol.* 229, 3088–3107. doi: 10.1111/nph.17076

Liu, Y., Burgos, J. S., Deng, Y., Srivastava, R., Howell, S. H., and Bassham, D. C. (2012). Degradation of the endoplasmic reticulum by autophagy during endoplasmic reticulum stress in *Arabidopsis*. *Plant Cell* 24, 4635–4651. doi: 10.1105/tpc.112.101535

Liu, F., Hu, W., Li, F., Marshall, R. S., Zarza, X., Munnik, T., et al. (2020). AUTOPHAGY-RELATED14 and its associated phosphatidylinositol 3-kinase complex promotes autophagy in Arabidopsis. *Plant Cell* 32, 3939–3960. doi: 10.1105/tpc.20.00285

Liu, W., Liu, Z., Mo, Z., Guo, S., Liu, Y., and Xie, Q. (2021). ATG8-interacting motif: evolution and function in selective autophagy of targeting biological processes. *Front. Plant Sci.* 12. doi: 10.3389/fpls.2021.783881

Ma, X., Xu, G., He, P., and Shan, L. (2016). SERKing coreceptors for receptors. *Trends Plant Sci.* 21, 1017–1033. doi: 10.1016/j.tplants.2016.08.014

Marash, I., Leibman-Markus, M., Gupta, R., Avni, A., and Bar, M. (2022). TOR inhibition primes immunity and pathogen resistance in tomato in a salicylic acid-dependent manner. *Mol. Plant Pathol.* 23, 1035–1047. doi: 10.1111/mpp.13207

Mariano, A. C., Andrade, M. O., Santos, A. A., Carolino, S. M., Oliveira, M. L., Baracat-Pereira, M. C., et al. (2004). Identification of a novel receptor-like protein kinase that interacts with a geminivirus nuclear shuttle protein. *Virology* 318, 24–31. doi: 10.1016/j.virol.2003.09.038

Marshall, R. S., and Vierstra, R. D. (2018). Autophagy: the master of bulk and selective recycling. *Annu. Rev. Plant Biol.* 69, 173–208. doi: 10.1146/annurev-arplant-042817-040606

Mbengue, M., Bourdais, G., Gervasi, F., Beck, M., Zhou, J., Spallek, T., et al. (2016). Clathrin-dependent endocytosis is required for immunity mediated by pattern recognition receptor kinases. *Proc. Natl. Acad. Sci. U.S.A.* 113, 11034–11039. doi: 10.1073/pnas.1606004113

Michaeli, S., Clavel, M., Lechner, E., Viotti, C., Wu, J., Dubois, M., et al. (2019). The viral F-box protein P0 induces an ER-derived autophagy degradation pathway for the clearance of membrane-bound AGO1. *Proc. Natl. Acad. Sci. U.S.A.* 116, 22872–22883. doi: 10.1073/pnas.1912222116

Morozov, S. Y., and Solovyev, A. G. (2003). Triple gene block: modular design of a multifunctional machine for plant virus movement. *J. Gen. Virol.* 84, 1351–1366. doi: 10.1099/vir.0.18922-0

Movahed, N., Cabanillas, D. G., Wan, J., Vali, H., Laliberte, J. F., and Zheng, H. (2019a). Turnip mosaic virus components are released into the extracellular space by vesicles in infected leaves. *Plant Physiol.* 180, 1375–1388. doi: 10.1104/pp.19.00381

Movahed, N., Patarroyo, C., Sun, J., Vali, H., Laliberté, J. F., and Zheng, H. (2017). Cylindrical inclusion protein of turnip mosaic virus serves as a docking point for the intercellular movement of viral replication vesicles. *Plant Physiol.* 175, 1732–1744. doi: 10.1104/pp.17.01484

Movahed, N., Sun, J., Vali, H., Laliberté, J. F., and Zheng, H. (2019b). A host ER fusogen is recruited by *turnip mosaic virus* for maturation of viral replication vesicles. *Plant Physiol.* 179, 507–518. doi: 10.1104/pp.18.01342

Nagashima, Y., Mishiba, K., Suzuki, E., Shimada, Y., Iwata, Y., and Koizumi, N. (2011). Arabidopsis IRE1 catalyses unconventional splicing of *bZIP60* mRNA to produce the active transcription factor. *Sci. Rep.* 1, 29. doi: 10.1038/srep00029

Nagy, P. D., Barajas, D., and Pogany, J. (2012). Host factors with regulatory roles in tombusvirus replication. *Curr. Opin. Virol.* 2, 691–698. doi: 10.1016/j.coviro.2012.10.004

Nagy, P. D., and Feng, Z. (2021). Tombusviruses orchestrate the host endomembrane system to create elaborate membranous replication organelles. *Curr. Opin. Virol.* 48, 30–41. doi: 10.1016/j.coviro.2021.03.007

Nakahara, K. S., Masuta, C., Yamada, S., Shimura, H., Kashihara, Y., Wada, T. S., et al. (2012). Tobacco calmodulin-like protein provides secondary defense by binding to and directing degradation of virus RNA silencing suppressors. *Proc. Natl. Acad. Sci. U.S.A.* 109, 10113–10118. doi: 10.1073/pnas.1201628109

Nawaz-Ul-Rehman, M. S., Prasanth, K. R., Xu, K., Sasvari, Z., Kovalev, N., De Castro Martín, I. F., et al. (2016). Viral replication protein inhibits cellular cofilin actin depolymerization factor to regulate the actin network and promote viral replicase assembly. *PloS Pathog.* 12, e1005440. doi: 10.1371/journal.ppat.1005440

Nicaise, V. (2014). Crop immunity against viruses: outcomes and future challenges. *Front. Plant Sci.* 5. doi: 10.3389/fpls.2014.00660

Nicaise, V., and Candresse, T. (2017). *Plum pox virus* capsid protein suppresses plant pathogen-associated molecular pattern (PAMP)-triggered immunity. *Mol. Plant Pathol.* 18, 878–886. doi: 10.1111/mpp.12447

Nicolas, W. J., Grison, M. S., Trépout, S., Gaston, A., Fouché, M., Cordelières, F. P., et al. (2017). Architecture and permeability of post-cytokinesis plasmodesmata lacking cytoplasmic sleeves. *Nat. Plants* 3, 17082. doi: 10.1038/nplants.2017.82

Niehl, A., Wyrsch, I., Boller, T., and Heinlein, M. (2016). Double-stranded RNAs induce a pattern-triggered immune signaling pathway in plants. *New Phytol.* 211, 1008–1019. doi: 10.1111/nph.13944

Niu, E., Liu, H., Zhou, H., Luo, L., Wu, Y., Andika, I. B., et al. (2021). Autophagy inhibits intercellular transport of citrus leaf blotch virus by targeting viral movement protein. *Viruses* 13, 2189. doi: 10.3390/v13112189

Oikawa, A., Lund, C. H., Sakuragi, Y., and Scheller, H. V. (2013). Golgi-localized enzyme complexes for plant cell wall biosynthesis. *Trends Plant Sci.* 18, 49–58. doi: 10.1016/j.tplants.2012.07.002

Ouibrahim, L., Rubio, A. G., Moretti, A., Montané, M. H., Menand, B., Meyer, C., et al. (2015). Potyviruses differ in their requirement for TOR signalling. *J. Gen. Virol.* 96, 2898–2903. doi: 10.1099/vir.0.000186

Ozber, N., Margaria, P., Anderson, C. T., Turina, M., and Rosa, C. (2022). Sorting motifs target the movement protein of ourmia melon virus to the trans-Golgi network and plasmodesmata. *Front. Virol.* 2. doi: 10.3389/fviro.2022.934011

Park, C. J., and Park, J. M. (2019). Endoplasmic reticulum plays a critical role in integrating signals generated by both biotic and abiotic stress in plants. *Front. Plant Sci.* 10. doi: 10.3389/fpls.2019.00399

Richardson, L. G. L. (2019). Hijacking the ER Membrane: Lessons from *Turnip mosaic virus*. *Plant Physiol.* 179, 367–368. doi: 10.1104/pp.18.01551

Rocha, C. S., Santos, A. A., MaChado, J. P., and Fontes, E. P. (2008). The ribosomal protein L10/QM-like protein is a component of the NIK-mediated antiviral signaling. *Virology* 380, 165–169. doi: 10.1016/j.virol.2008.08.005

Rodamilans, B., Valli, A., Mingot, A., San Leon, D., Baulcombe, D., López-Moya, J. J., et al. (2015). RNA polymerase slippage as a mechanism for the production of frameshift gene products in plant viruses of the *Potyviridae* family. *J. Virol.* 89, 6965–6967. doi: 10.1128/JVI.00337-15

Ruiz Rosquete, M., Davis, D. J., and Drakakaki, G. (2018). The plant trans-Golgi network: not just a matter of distinction. *Plant Physiol.* 176, 187–198. doi: 10.1104/pp.17.01239

Ruiz Rosquete, M., and Drakakaki, G. (2018). Plant TGN in the stress response: a compartmentalized overview. *Curr. Opin. Plant Biol.* 46, 122–129. doi: 10.1016/j.pbi.2018.09.003

Samuels, T. D., Ju, H. J., Ye, C. M., Motes, C. M., Blancaflor, E. B., and Verchot-Lubicz, J. (2007). Subcellular targeting and interactions among the *Potato virus X* TGB proteins. *Virology* 367, 375–389. doi: 10.1016/j.virol.2007.05.022

Santa Cruz, S., Roberts, A. G., Prior, D. A., Chapman, S., and Oparka, K. J. (1998). Cell-to-cell and phloem-mediated transport of potato virus X. The role of virions. *Plant Cell* 10, 495–510. doi: 10.1105/tpc.10.4.495

Sasvari, Z., Lin, W., Inaba, J. I., Xu, K., Kovalev, N., and Nagy, P. D. (2020). Co-opted cellular sac1 lipid phosphatase and PI(4)P phosphoinositide are key host factors during the biogenesis of the tombusvirus replication compartment. *J. Virol.* 94, e01979–e01919. doi: 10.1128/JVI.01979-19

Schaad, M. C., Jensen, P. E., and Carrington, J. C. (1997). Formation of plant RNA virus replication complexes on membranes: role of an endoplasmic reticulum-targeted viral protein. *EMBO J.* 16, 4049–4059. doi: 10.1093/emboj/16.13.4049

Shen, W., Shi, Y., Dai, Z., and Wang, A. (2020). The RNA-dependent RNA polymerase NIb of potyviruses plays multifunctional, contrasting roles during viral infection. *Viruses* 12, 77. doi: 10.3390/v12010077

Soto-Burgos, J., Zhuang, X., Jiang, L., and Bassham, D. C. (2018). Dynamics of autophagosome formation. *Plant Physiol.* 176, 219–229. doi: 10.1104/pp.17.01236

Sparkes, I. A., Frigerio, L., Tolley, N., and Hawes, C. (2009). The plant endoplasmic reticulum: a cell-wide web. *Biochem. J.* 423, 145–155. doi: 10.1042/BJ20091113

Sutipatanasomboon, A., Herberth, S., Alwood, E. G., Häweker, H., Müller, B., Shahriari, M., et al. (2017). Disruption of the plant-specific CFS1 gene impairs autophagosome turnover and triggers EDS1-dependent cell death. *Sci. Rep.* 7, 8677. doi: 10.1038/s41598-017-08577-8

Suttangkakul, A., Li, F., Chung, T., and Vierstra, R. D. (2011). The ATG1/ATG13 protein kinase complex is both a regulator and a target of autophagic recycling in *Arabidopsis*. *Plant Cell* 23, 3761–3779. doi: 10.1105/tpc.111.090993

Tan, X., Sun, L., Chen, J., and Chen, Z. J. (2018). Detection of microbial infections through innate immune sensing of nucleic acids. *Annu. Rev. Microbiol.* 72, 447–478. doi: 10.1146/annurev-micro-102215-095605

Tang, D., Wang, G., and Zhou, J. M. (2017). Receptor kinases in plant-pathogen interactions: more than pattern recognition. *Plant Cell* 29, 618–637. doi: 10.1105/tpc.16.00891

Tatineni, S., and Hein, G. L. (2023). Plant viruses of agricultural importance: current and future perspectives of virus disease management strategies. *Phytopathology* 113, 117–141. doi: 10.1094/PHYTO-05-22-0167-RVW

Teixeira, R. M., Ferreira, M. A., Raimundo, G., Loriato, V., Reis, P., and Fontes, E. P. B. (2019). Virus perception at the cell surface: revisiting the roles of receptor-like kinases as viral pattern recognition receptors. *Mol. Plant Pathol.* 20, 1196–1202. doi: 10.1111/mpp.12816

Tilsner, J., Linnik, O., Louveaux, M., Roberts, I. M., Chapman, S. N., and Oparka, K. J. (2013). Replication and trafficking of a plant virus are coupled at the entrances of plasmodesmata. *J. Cell Biol.* 201, 981–995. doi: 10.1083/jcb.201304003

Tilsner, J., Linnik, O., Wright, K. M., Bell, K., Roberts, A. G., Lacomme, C., et al. (2012). The TGB1 movement protein of *Potato virus X* reorganizes actin and endomembranes into the X-body, a viral replication factory. *Plant Physiol.* 158, 1359–1370. doi: 10.1104/pp.111.189605

Torrance, L., Cowan, G. H., Gillespie, T., Ziegler, A., and Lacomme, C. (2006). Barley stripe mosaic virus-encoded proteins triple-gene block 2 and γb localize to chloroplasts in virus-infected monocot and dicot plants, revealing hitherto-unknown roles in virus replication. *J. Gen. Virol.* 87, 2403–2411. doi: 10.1099/vir.0.81975-0

Turner, K. A., Sit, T. L., Callaway, A. S., Allen, N. S., and Lommel, S. A. (2004). Red clover necrotic mosaic virus replication proteins accumulate at the endoplasmic reticulum. *Virology* 320, 276–290. doi: 10.1016/j.virol.2003.12.006

Uchiyama, A., Shimada-Beltran, H., Levy, A., Zheng, J. Y., Javia, P. A., and Lazarowitz, S. G. (2014). The Arabidopsis synaptotagmin SYTA regulates the cell-to-cell movement of diverse plant viruses. *Front. Plant Sci.* 5. doi: 10.3389/fpls.2014.00584

Verchot, J. (2011). Wrapping membranes around plant virus infection. *Curr. Opin. Virol.* 1, 388–395. doi: 10.1016/j.coviro.2011.09.009

Villarejo, A., Burén, S., Larsson, S., Déjardin, A., Monné, M., Rudhe, C., et al. (2005). Evidence for a protein transported through the secretory pathway *en route* to the higher plant chloroplast. *Nat. Cell Biol.* 7, 1224–1231. doi: 10.1038/ncb1330

Viotti, C., Bubeck, J., Stierhof, Y. D., Krebs, M., Langhans, M., Van Den Berg, W., et al. (2010). Endocytic and secretory traffic in *Arabidopsis* merge in the trans-Golgi network/early endosome, an independent and highly dynamic organelle. *Plant Cell* 22, 1344–1357. doi: 10.1105/tpc.109.072637

Wan, J., Basu, K., Mui, J., Vali, H., Zheng, H., and Laliberté, J. F. (2015a). Ultrastructural characterization of turnip mosaic virus-induced cellular rearrangements reveals membrane-bound viral particles accumulating in vacuoles. *J. Virol.* 89, 12441–12456. doi: 10.1128/JVI.02138-15

Wan, J., Cabanillas, D. G., Zheng, H., and Laliberté, J. F. (2015b). *Turnip mosaic virus* moves systemically through both phloem and xylem as membrane-associated complexes. *Plant Physiol.* 167, 1374–1388. doi: 10.1104/pp.15.00097

Wang, A. (2021). Cell-to-cell movement of plant viruses *via* plasmodesmata: a current perspective on potyviruses. *Curr. Opin. Virol.* 48, 10–16. doi: 10.1016/j.coviro.2021.03.002

Wang, M., Li, X., Luo, S., Fan, B., Zhu, C., and Chen, Z. (2020). Coordination and crosstalk between autophagosome and multivesicular body pathways in plant stress responses. *Cells* 9, 119. doi: 10.3390/cells9010119

Wang, X., Ma, J., Jin, X., Yue, N., Gao, P., Mai, K. K. K., et al. (2021). Three-dimensional reconstruction and comparison of vacuolar membranes in response to viral infection. *J. Integr. Plant Biol.* 63, 353–364. doi: 10.1111/jipb.13027

Wei, T., Huang, T. S., Mcneil, J., Laliberté, J. F., Hong, J., Nelson, R. S., et al. (2010a). Sequential recruitment of the endoplasmic reticulum and chloroplasts for plant potyvirus replication. *J. Virol.* 84, 799–809. doi: 10.1128/JVI.01824-09

Wei, T., and Wang, A. (2008). Biogenesis of cytoplasmic membranous vesicles for plant potyvirus replication occurs at endoplasmic reticulum exit sites in a COPI- and COPII-dependent manner. *J. Virol.* 82, 12252–12264. doi: 10.1128/JVI.01329-08

Wei, T., Zhang, C., Hong, J., Xiong, R., Kasschau, K. D., Zhou, X., et al. (2010b). Formation of complexes at plasmodesmata for potyvirus intercellular movement is mediated by the viral protein P3N-PIPO. *PloS Pathog.* 6, e1000962. doi: 10.1371/journal.ppat.1000962

Wei, T., Zhang, C., Hou, X., Sanfaçon, H., and Wang, A. (2013). The SNARE protein Syp71 is essential for turnip mosaic virus infection by mediating fusion of virus-induced vesicles with chloroplasts. *PloS Pathog.* 9, e1003378. doi: 10.1371/journal.ppat.1003378

Widyasari, K., Bwalya, J., and Kim, K. H. (2023). Binding immunoglobulin 2 functions as a proviral factor for potyvirus infections in *Nicotiana benthamiana*. *Mol. Plant Pathol.* 24, 179–187. doi: 10.1111/mpp.13284

Wu, X., and Cheng, X. (2020). Intercellular movement of plant RNA viruses: Targeting replication complexes to the plasmodesma for both accuracy and efficiency. *Traffic* 21, 725–736. doi: 10.1111/tra.12768

Wu, G., Cui, X., Chen, H., Renaud, J. B., Yu, K., Chen, X., et al. (2018). Dynamin-like proteins of endocytosis in plants are coopted by potyviruses to enhance virus infection. *J. Virol.* 92, e01320–e01318. doi: 10.1128/JVI.01320-18

Wu, G., Cui, X., Dai, Z., He, R., Li, Y., Yu, K., et al. (2020). A plant RNA virus hijacks endocytic proteins to establish its infection in plants. *Plant J.* 101, 384–400. doi: 10.1111/tpj.14549

Wu, G., Jia, Z., Ding, K., Zheng, H., Lu, Y., Lin, L., et al. (2022a). Turnip mosaic virus co-opts the vacuolar sorting receptor VSR4 to promote viral genome replication in plants by targeting viral replication vesicles to the endosome. *PloS Pathog.* 18, e1010257. doi: 10.1371/journal.ppat.1010257

Wu, G., Jia, Z., Rui, P., Zheng, H., Lu, Y., Lin, L., et al. (2022b). Acidic dileucine motifs in the cylindrical inclusion protein of turnip mosaic virus are crucial for endosomal targeting and viral replication. *Mol. Plant Pathol.* 23, 1381–1389. doi: 10.1111/mpp.13231

Wu, X., Liu, J., Chai, M., Wang, J., Li, D., Wang, A., et al. (2019a). The potato virus X TGBp2 protein plays dual functional roles in viral replication and movement. *J. Virol.* 93, e01635–e01618. doi: 10.1128/JVI.01635-18

Wu, W., Luo, X., and Ren, M. (2021). Clearance or hijack: universal interplay mechanisms between viruses and host autophagy from plants to animals. *Front. Cell Infect. Microbiol.* 11. doi: 10.3389/fcimb.2021.786348

Wu, X., Valli, A., García, J. A., Zhou, X., and Cheng, X. (2019b). The tug-of-war between plants and viruses: great progress and many remaining questions. *Viruses* 11, 203. doi: 10.3390/v11030203

Wun, C. L., Quan, Y., and Zhuang, X. (2020). Recent advances in membrane shaping for plant autophagosome biogenesis. *Front. Plant Sci.* 11. doi: 10.3389/fpls.2020.00565

Xu, K., and Nagy, P. D. (2014). Expanding use of multi-origin subcellular membranes by positive-strand RNA viruses during replication. *Curr. Opin. Virol.* 9, 119–126. doi: 10.1016/j.coviro.2014.09.015

Xu, K., and Nagy, P. D. (2016). Enrichment of phosphatidylethanolamine in viral replication compartments *via* co-opting the endosomal rab5 small GTPase by a positive-strand RNA virus. *PloS Biol.* 14, e2000128. doi: 10.1371/journal.pbio.2000128

Yang, H., Gou, X., He, K., Xi, D., Du, J., Lin, H., et al. (2010). BAK1 and BKK1 in *Arabidopsis thaliana* confer reduced susceptibility to *turnip crinkle virus*. *Eur. J. Plant Pathol.* 127, 149–156. doi: 10.1007/s10658-010-9581-5

Yang, Z., and Li, Y. (2018). Dissection of RNAi-based antiviral immunity in plants. *Curr. Opin. Virol.* 32, 88–99. doi: 10.1016/j.coviro.2018.08.003

Yang, M., and Liu, Y. (2022). Autophagy in plant viral infection. *FEBS Lett.* 596, 2152–2162. doi: 10.1002/1873-3468.14349

Yang, X., Srivastava, R., Howell, S. H., and Bassham, D. C. (2016). Activation of autophagy by unfolded proteins during endoplasmic reticulum stress. *Plant J.* 85, 83–95. doi: 10.1111/tpj.13091

Ye, C., Dickman, M. B., Whitham, S. A., Payton, M., and Verchot, J. (2011). The unfolded protein response is triggered by a plant viral movement protein. *Plant Physiol.* 156, 741–755. doi: 10.1104/pp.111.174110

Yuan, C., Lazarowitz, S. G., and Citovsky, V. (2018). The plasmodesmal localization signal of TMV MP is recognized by plant synaptotagmin SYTA. *mBio* 9, e01314–e01318. doi: 10.1128/mBio.01314-18

Zhai, Y., Yuan, Q., Qiu, S., Li, S., Li, M., Zheng, H., et al. (2021). Turnip mosaic virus impairs perinuclear chloroplast clustering to facilitate viral infection. *Plant Cell Environ.* 44, 3681–3699. doi: 10.1111/pce.14157

Zhang, M., Cao, B., Zhang, H., Fan, Z., Zhou, X., and Li, F. (2023). Geminivirus satellite-encoded βC1 activates UPR, induces bZIP60 nuclear export, and manipulates the expression of bZIP60 downstream genes to benefit virus infection. *Sci. China Life Sci.* 66, 1408–1425. doi: 10.1007/s11427-022-2196-y

Zhang, L., Chen, H., Brandizzi, F., Verchot, J., and Wang, A. (2015). The UPR branch IRE1-*bZIP60* in plants plays an essential role in viral infection and is

complementary to the only UPR pathway in yeast. *PloS Genet.* 11, e1005164. doi: 10.1371/journal.pgen.1005164

Zhang, Z., He, G., Han, G. S., Zhang, J., Catanzaro, N., Diaz, A., et al. (2018). Host Pah1p phosphatidate phosphatase limits viral replication by regulating phospholipid synthesis. *PloS Pathog.* 14, e1006988. doi: 10.1371/journal.ppat.1006988

Zhang, C., Hicks, G. R., and Raikhel, N. V. (2014). Plant vacuole morphology and vacuolar trafficking. *Front. Plant Sci.* 5. doi: 10.3389/fpls.2014.00476

Zhang, M., and Zhang, S. (2022). Mitogen-activated protein kinase cascades in plant signaling. *J. Integr. Plant Biol.* 64, 301–341. doi: 10.1111/jipb.13215

Zhang, J., Zhang, Z., Chukkapalli, V., Nchoutmboube, J. A., Li, J., Randall, G., et al. (2016). Positive-strand RNA viruses stimulate host phosphatidylcholine synthesis at viral replication sites. *Proc. Natl. Acad. Sci. U.S.A.* 113, E1064–E1073. doi: 10.1073/pnas.1519730113

Zhao, J., Bui, M. T., Ma, J., Künzl, F., Picchianti, L., de la Concepcion, J. C., et al. (2022). Plant autophagosomes mature into amphisomes prior to their delivery to the central vacuole. *J. Cell Biol.* 221, e202203139. doi: 10.1083/jcb.202203139

Zheng, X., Wu, M., Li, X., Cao, J., Li, J., Wang, J., et al. (2019). Actin filaments are dispensable for bulk autophagy in plants. *Autophagy* 15, 2126–2141. doi: 10.1080/15548627.2019.1596496

Zhou, F., Wu, Z., Zhao, M., Murtazina, R., Cai, J., Zhang, A., et al. (2019). Rab5-dependent autophagosome closure by ESCRT. *J. Cell Biol.* 218, 1908–1927. doi: 10.1083/jcb.201811173

Zhuang, X., Chung, K. P., Cui, Y., Lin, W., Gao, C., Kang, B. H., et al. (2017). ATG9 regulates autophagosome progression from the endoplasmic reticulum in *Arabidopsis*. *Proc. Natl. Acad. Sci. U.S.A.* 114, E426–E435. doi: 10.1073/pnas.1616299114

Zientara-Rytter, K., and Sirko, A. (2014). Selective autophagy receptor Joka2 co-localizes with cytoskeleton in plant cells. *Plant Signal Behav.* 9, e28523. doi: 10.4161/psb.28523

Zorzatto, C., MaChado, J. P., Lopes, K. V., Nascimento, K. J., Pereira, W. A., Brustolini, O. J., et al. (2015). NIK1-mediated translation suppression functions as a plant antiviral immunity mechanism. *Nature* 520, 679–682. doi: 10.1038/nature14171

Zouhar, J., Cao, W., Shen, J., and Rojo, E. (2023). Retrograde transport in plants: Circular economy in the endomembrane system. *Eur. J. Cell Biol.* 102, 151309. doi: 10.1016/j.ejcb.2023.151309

frontiers | Frontiers in Plant Science

TYPE Review
PUBLISHED 17 August 2023
DOI 10.3389/fpls.2023.1240973

OPEN ACCESS

EDITED BY
Caiji Gao,
South China Normal University, China

REVIEWED BY
Viktor Zarsky,
Charles University, Czechia
Hao Wang,
South China Agricultural University, China

*CORRESPONDENCE
Cecilia Rodriguez-Furlan
c.rodriguezfurlan@wsu.edu

RECEIVED 15 June 2023
ACCEPTED 01 August 2023
PUBLISHED 17 August 2023

CITATION
Rodriguez-Furlan C, Borna R and Betz O (2023) RAB7 GTPases as coordinators of plant endomembrane traffic.
Front. Plant Sci. 14:1240973.
doi: 10.3389/fpls.2023.1240973

RAB7 GTPases as coordinators of plant endomembrane traffic

Cecilia Rodriguez-Furlan* , Rita Borna and Oliver Betz

School of Biological Sciences, Washington State University, Pullman, WA, United States

The ras gene from rat brain (RAB) family of small GTPases is highly conserved among eukaryotes and regulates endomembrane trafficking pathways. RAB7, in particular, has been linked to various processes involved in regulating endocytic and autophagic pathways. Plants have several copies of RAB7 proteins that reflect the intricacy of their endomembrane transport systems. RAB7 activity regulates different pathways of endomembrane trafficking in plants: (1) endocytic traffic to the vacuole; (2) biosynthetic traffic to the vacuole; and (3) recycling from the late endosome to the secretory pathway. During certain developmental and stress related processes another pathway becomes activated (4) autophagic trafficking towards the vacuole that is also regulated by RAB7. RAB7s carry out these functions by interacting with various effector proteins. Current research reveals many unexplored RAB7 functions in connection with stress responses. Thus, this review describes a comprehensive summary of current knowledge of plant RAB7's functions, discusses unresolved challenges, and recommends prospective future research directions.

KEYWORDS

Rab7, RabG, endosomes, vacuole, tethering, stress, GTPases

1 Introduction

Ras gene from rat brain (RAB) GTPases are a class of regulatory proteins essential for eukaryotic cell endomembrane trafficking (Touchot et al., 1987; Homma et al., 2021). RABs are found on different cellular membranes and function as molecular switches cycling between an active GTP-bound state and an inactive GDP-bound state. RABs assist transport between cellular compartments by controlling various endomembrane trafficking processes, including vesicle generation, mobility, tethering, and fusion. Overall, RABs are essential for maintaining the proper organization and function of the endomembrane systems in eukaryotic cells.

RAB GTPases exhibit a high degree of conservation across eukaryotic organisms, with twenty-three RAB subfamilies identified across species (Elias et al., 2012). The RAB plant sequences group in only eight clades encompassing six subfamilies common to both yeasts and mammals, which are RAB1, RAB5, RAB6, RAB7, RAB8, and RAB11 while three, RAB2, RAB18, and RAB22, are exclusively present in plants and mammals and are not detected in yeasts. Therefore, using the 57 Arabidopsis encoded RAB genomic sequences, another nomenclature was proposed for the Arabidopsis subclasses RABs (A-H). Based on

their sequence homology, the Arabidopsis categories are related to the original RAB subfamilies as follows: RABA=RAB11 and RAB25, RABB=RAB2, RABC=RAB18, RABD=RAB1, RABE=RAB8 and RAB10, RABF=RAB5 and RAB22, and RABG=RAB7 and H=RAB6 (Teh and Moore, 2007).

In Arabidopsis, RABA have been related the regulation of the late steps of secretion, RABB and RABD to the endoplasmic reticulum-Golgi transport, RABE to the regulation of vesicle secretion and early endocytosis, and RABF and RABG regulate traffic to the vacuoles. The RAB7 cluster in plants (RABG in Arabidopsis) has arisen as a subject of considerable attention in the scientific community due to its potential to significantly enhance plant resilience in the face of biotic and abiotic stress (Tripathy et al., 2021). Numerous studies across diverse plant species have consistently demonstrated that the overexpression of RAB7 proteins leads to a remarkable improvement in plant performance when subjected to various stress conditions. This phenomenon has stimulated a growing body of research into the underlying mechanisms through which RAB7 proteins benefit stress tolerance. This review will provide specific examples of how RAB7 affects various cellular activities, from functions common to animals and yeast to plant-specific functions. We will review our current knowledge of RAB7's impact on plant growth and stress responses. Finally, we will highlight the open questions and potential future research directions to expand our understanding of RAB7's function.

2 RAB7 functions as a molecular switch

RAB7 is a member of the RAB family of GTPases, which switches between an active guanosine triphosphate (GTP)-bound state and an inactive guanosine diphosphate (GDP)-bound form (Figure 1). The proteins controlling the RAB switch are conserved among different organisms. They associate with membranes that are prenylated at their C-terminal cysteine residues by a RAB geranylgeranyltransferase (RGT). In *Arabidopsis*, heterodimers RGTA1-RGTB1 and RGTA1-RGTB2 can prenylate a wide range of RABs, including RABGs (Shi et al., 2016). The prenylated RAB7 can then be delivered to a target membrane, where a guanine nucleotide exchange factor (GEF) triggers GDP release and loading of GTP, thereby stabilizing RAB7 in its active conformation and allowing for specific effector proteins to be recruited to the membrane (Vetter and Wittinghofer, 2001). Eventually, RAB7 becomes inactivated by interacting with GTPase-activating proteins (GAPs), triggering GTP hydrolysis. The GDP-bound RAB7 is then released from the membrane into the cytoplasm by a GDP dissociation inhibitor (GDI), which solubilizes the prenylated tail until reactivation by GEFs (Zárský et al., 1997; Ueda et al., 1998).

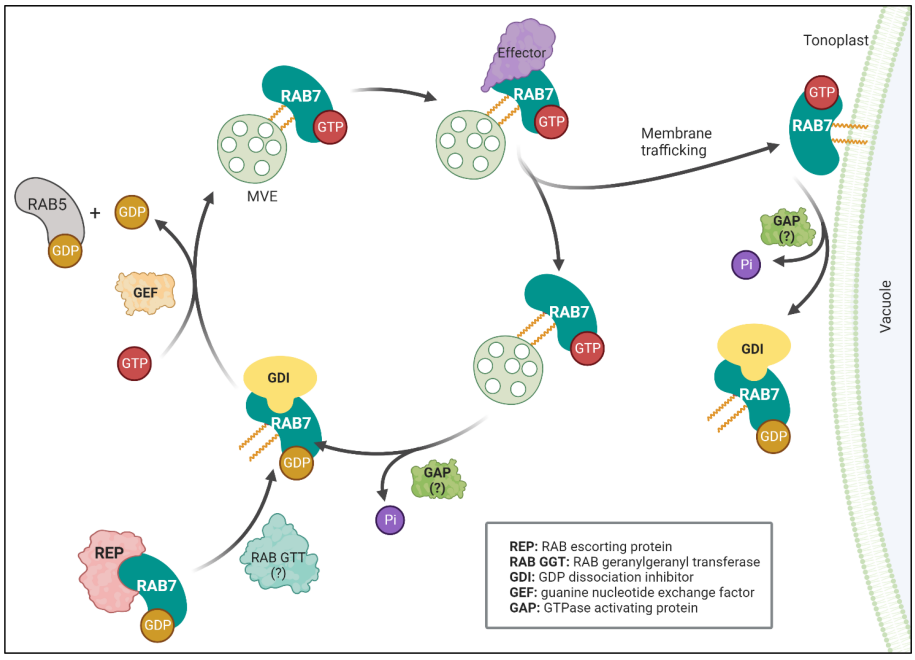

FIGURE 1
RAB7 functions as a molecular switch. RAB7 cycles between inactive (GDP-bound) and active (GTP-bound) states. A RAB escorting protein (REP) binds newly synthesized RAB7 associated to GDP and presents it to the geranylgeranyltransferase (RGT) and becomes prenylated. The prenylated protein can be solubilized in the cytosol by the GDP dissociation inhibitor (GDI), which protects the hydrophobic geranylgeranyl groups from the hydrophilic environment. A guanine nucleotide exchange factor (GEF) releases GDP and loads GTP to stabilize prenylated RAB7 in its active state to the MVE membrane. The GEF complex also acts as a GTPase activating protein (GAP) for RAB5 exchanging it for RAB7 at the maturating MVE. Once activated RAB7-GTP can interact with different effectors controlling membrane trafficking events like retrieval of proteins (recycling) or fusion with the vacuole (interaction with tethers). GTP hydrolysis by GTPase activating protein catalyzes RAB7 hydrolysis (GAPs interacting with RAB7 are still unidentified in plants, referred as:)?. Finally, a GDP dissociation inhibitor (GDI) releases the membrane bound RAB7 into the cytoplasm, reinitiating the cycle. Figure created with BioRender.com.

3 The RAB7 group in plants

In animals, the protein RAB7 is involved in the late stages of endocytic trafficking, including the maturation of late endosomes and lysosomes and the degradation of cellular waste material through autophagy (Guerra and Bucci, 2016). In yeast, the RAB7 ortholog Ypt7p is essential for the maturation and fusion of late endosomes with the vacuole and for the homotypic fusion of vacuoles (Nordmann et al., 2012). Plants exhibit a higher copy number of RAB7 proteins when compared with other organisms, which may reflect the higher complexity of plant endomembrane trafficking. For example, there are five RAB7 homologs in rice: OsRAB7a1, OsRAB7a2, OsRAB7b1, OsRAB7b2, and OsRAB7b3 (Nahm et al., 2003); five RAB7 homologs in the moss *Physcomitrella patens* (Uemura and Ueda, 2014); and eight RAB7 homologs have been described in the *Arabidopsis* genome: RABG1, RABG2, RABG3a, RABG3b, RABG3c, RABG3d, RABG3e, and RABG3f (Rutherford and Moore, 2002; Vernoud et al., 2003).

Studying individual functional contributions using knockout genetic approaches is challenging due to the large size of the RABG family in *Arabidopsis*. Individual mutants did not show a significant phenotype; however, quadruple, quintuple, and sextuple mutants exhibited dwarfism in the early developmental stages. These mutants were fertile and eventually grew to a size similar to the wild type (Singh et al., 2014). The quintuple mutants of RABG3b, c, d, e, and f and the sextuple mutants of RABG3a, b, c, d, e, and f show deficits in biosynthetic and endocytic protein transport to the vacuole. Furthermore, these mutants have fragmented vacuoles, affecting lytic and storage vacuoles. The abnormalities displayed by several RABG3 isoform mutations suggest that RABGs play a vital role in vacuole trafficking and biogenesis. However, these processes should be essential for plant growth and development, resulting in severe phenotypes. The mild phenotypes observed in the RABG3 sextuple mutant could be attributed to the partial reduction in RABG3f expression levels (the insertional mutant is not a null allele, instead it is a knockdown) and the remaining expression of the other family members RABG1 and RABG2.

To better assess the function of individual members, several publications used instead point mutations of the GTPase active site, to generate constitutively active or inactive RABG3 forms. RAB proteins feature two "switch regions" that accommodate the gamma phosphate of GTP, which causes significant conformational changes between their inactive and active states. Mutating S/T into N in the switch-I motif GXXXGK(S/T) disturbs the coordination of the gamma phosphate, thereby lowering GTP affinity (Gabe Lee et al., 2009). This GDP-locked RAB7 sequesters GDI and GEF proteins, acting as a dominant negative (DN). The DXXGQ motif in the switch-II region Q catalyzes GTP hydrolysis. The Q to L mutations impede GTP hydrolysis, making the protein GTP-locked and constitutively activated (CA) RAB7.

The overexpression of DN-RABG3c inhibits the vacuolar targeting of soluble and membrane proteins (Bottanelli et al., 2012). Additionally, CA-RABG3f overexpression results in enlarged pre-vacuolar compartments known as multivesicular bodies or endosomes (MVBs, MVEs), modified vacuole morphology, hindered protein vacuolar trafficking, and finally, affected whole plant development (Cui et al., 2014). Moreover, inducible DN-RABG3f overexpression showed vacuole protein traffic defects leading to inhibition of root development in a dexamethasone dose-dependent manner, co-related with a dose-dependent increase in expression of the DN protein. Therefore, in animals, yeast, and in plants RAB7s are central regulators of late endosome fusion with the lytic compartment. Additional functions regulating homotypic vacuole fusion and autophagy regulation are conserved. However, plant-specific functions like regulation of traffic to the specialized lytic and storage vacuoles has also been described (Cui et al., 2014; Singh et al., 2014).

4 RAB7's role in vesicle maturation during traffic to the vacuole

In plants, the trans-Golgi network (TGN) sorts biosynthetic cargo but also receives and sort materials internalized from the plasma membrane by endocytosis (acting as an early endosome) (Rosquete et al., 2018). The TGN cargo can be sorted into compartments that will mature by developing intraluminal vesicles and receive the name multivesicular endosomes (MVEs), also known as multivesicular bodies, late endosomes or pre-vacuolar compartments, to finally fuse with the vacuole membrane, i.e., the tonoplast. As soon as the MVEs leave the TGN, can be recognized by the presence at their membranes of the protein RAB5 (Ebine et al., 2014). In *Arabidopsis*, the RAB5 GTPase, RABF2b (also known as ARA7), bounds the membranes leaving the TGN until the complex MON1 (SAND1)-CZZ1AB recruits the RAB7/RABG3f (Cui et al., 2014; Singh et al., 2014).. The MON1 (SAND1)-CZZ1AB complex functions as a GEF activating RABG3f and as a GAP for RAB5 that is then released from the MVEs (Figure 1). Accordingly, DN-RABG3f has been detected to be associated with the MON1, CZZ1A, and B complexes (Rodriguez-Furlan et al., 2019). A proportion of DN-RABG3f is associated with membranes and restricted to MVEs, indicating that RABG3f activation is necessary for its arrival to the tonoplast (Cui et al., 2014). Similarly, in rice, it was shown that only when b2oth MON1 and CZZ1 are present, they can interact with OsRAB7b3, while MON1 by itself can interact with OsRAB5a (Pan et al., 2021). The available information suggests a model where MON1 recognizes RAB5 proteins while recruiting CZZ1 to act as a GAP for RAB5 while recruiting and activating RAB7 (Figure 1).

5 RAB7 association with the tethering complex HOPS

Once activated, RAB7 plays a crucial role in membrane fusion by interacting with tethering complexes that facilitate the initial contact between membranes. RAB7 interacts with the homotypic fusion and protein sorting (HOPS) complex formed by the vacuolar protein sorting (VPS) subunits VPS11, VPS16, VPS18, VPS33, VPS39, and VPS41 (Balderhaar and Ungermann, 2013). Then, the fusion events are made possible by the presence of soluble N-ethylmaleimide-sensitive factor attachment receptor (SNARE) proteins on both

membranes (Lipka et al., 2007). Q-SNAREs (such as syntaxins of plants, SYP) are present on the target membrane, and R-SNAREs (like vesicle-associated membrane proteins, VAMP) are observed on the vesicle. The Q- and R-SNAREs associate to enable fusion events. In *Arabidopsis*, the HOPS complex interacts with the Q-SNARE SYP22 and the R-SNARE VAMP713, allowing MVE-tonoplast fusion (Takemoto et al., 2018) (Figure 2).

VPS39 in yeast attaches to RAB7 (Ypt7) in endosomes. At the same time, VPS41 binds to a Ypt7 located at the tonoplast connecting both membranes (Lürick et al., 2017). In *Arabidopsis*, only partial information shows that VPS3, VPS33, VPS39 and VPS41 can co-immunoprecipitate with RABG3f (Takemoto et al., 2018; Rodriguez-Furlan et al., 2019). Similar to yeast, VPS41 and RAB7 (RABG3f or RABG3c) colocalize only in the tonoplast (Hao et al., 2016; Brillada et al., 2018; Jiang et al., 2022). Furthermore, VPS33 interacts directly with the Q-SNARE SYP22, probably recognizing the SNARE (Brillada et al., 2018). Therefore, the recruitment and architecture of the RAB7-HOPS-SNARE complex in plants still need to be fully elucidated.

Beyond its role in MVE-tonoplast fusion, the RABG3-HOPS complex interaction is required for vacuole formation and homotypic vacuole fusion, as evidenced by the HOPS and RABG3 mutants' fragmented vacuole phenotypes (Singh et al., 2014; Hao et al., 2016; Brillada et al., 2018). In this line of evidence, RABG3f and VPS39 can be detected colocalizing at contact points between adjacent vacuoles.

The HOPS complex was detected in autophagosomes, along with the autophagy-related protein ATG14, a phosphatidylinositol-3-phosphate kinase (Wang et al., 2022). ATG14 is co-immunoprecipitated and colocalized with RABG3a and RABG3f. Consistent with these findings, when DN-RABG3f or DN-RABG3a is overexpressed, cells accumulate autophagosomes in the cytoplasm (Lürick et al., 2017). Therefore, it is possible that RAB7 proteins observed in autophagosomes can be involved in HOPS complex assembly, thereby facilitating autophagosome fusion with the tonoplast (Figure 2). However, such a hypothesis still needs to be tested.

6 RAB7's association with the core retromer complex

RAB7 can interact with another complex, the core-retromer VPS35-VPS26-VPS29 (Figure 2). The VPS35 subunit interacts with RABG3f to anchor the cytosolic VPS35-VPS26-VPS29 complex to the MVEs (Zelazny et al., 2013). In *Arabidopsis*, the core-retromer has

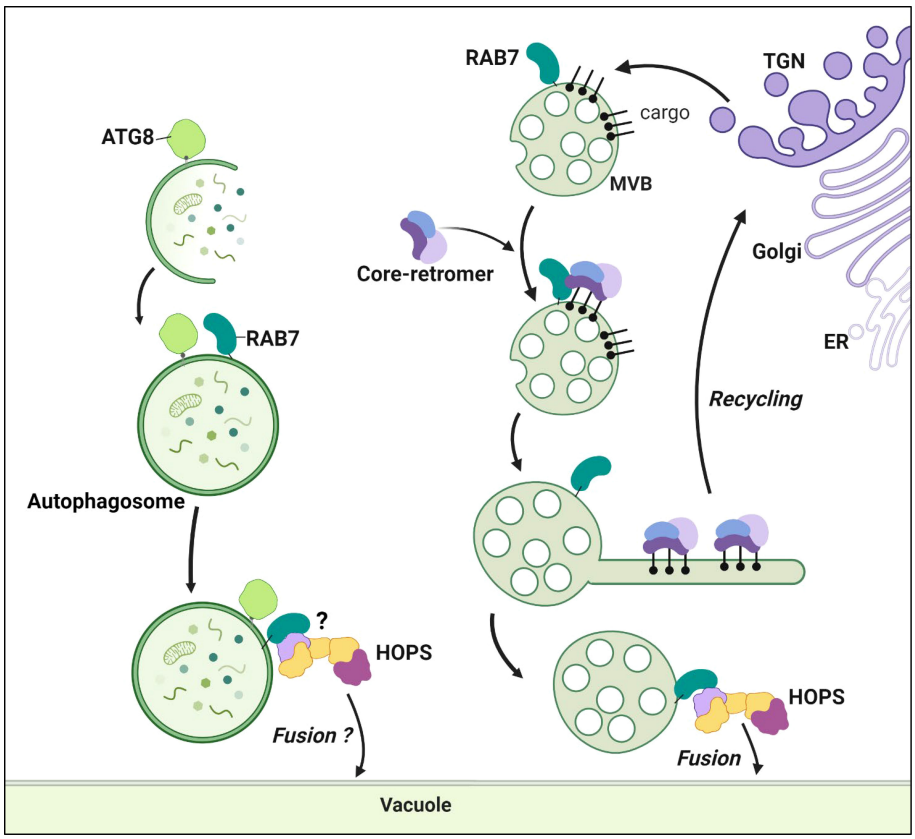

FIGURE 2
RAB7 at MVEs and autophagosomes. RAB7 anchors the core-retromer to the MVEs membrane. The core-retromer is formed by VPS35, VPS26 and VPS29 (depicted with three different colors in the figure). At the MVEs the retromer interacts with cargo proteins sorting them for recycling back to the TGN. In mammalians the retromer forms extensions or tubules rescuing the proteins from degradation, such structures have not been described in plants yet. RAB7 also interacts with the HOPS complex at the MVEs favoring the fusion of the vesicles with the tonoplast, releasing the contents in the vacuole lumen. RAB7 is co-localizing and co-immunoprecipitating with ATG8. However, its function at autophagosomes remains uncharacterized. The HOPS complex role facilitating fusion of autophagosomes with the tonoplast also remains to be studied (referred as)?. Figure created with BioRender.com.

extra copies of a few subunits, including VPS35A, VPS35B, VPS35C, VPS26A, VPS26B and VPS26C; however, there is only one copy for VPS29. Interestingly, the activation of RABG3f promotes the VPS35A-RABG3f interaction, as evidenced by the greater co-immunoprecipitation of VPS35A with CA-RABG3f compared to DN-RABG3f (Gabe Lee et al., 2009). The inhibition of the chemical interaction between RABG3f and VPS35A interrupted the trafficking of endocytic and synthetic cargo toward the vacuoles (Gabe Lee et al., 2009). Similar phenotypes are observed in mutants of the different subunits of VPS26, VPS29, and VPS35 (Nodzyński et al., 2013; Munch et al., 2015; Jha et al., 2018). Triple mutant *vps35a1b2c1*, double mutant *vps26a1b1*, and single mutant *vps29* all exhibited deleterious developmental phenotypes, highlighting the biological relevance of the different subunits (Yamazaki et al., 2008). However, VPS35A and C redundantly regulate vacuolar protein sorting, impacting PVC morphology, while VPS35B's role seems dispensable in these pathways (Munch et al., 2015). Therefore, multiple subcomplexes likely exist since all VPS35 isoforms interact with VPS26 and VPS29 (Zelazny et al., 2013). This interaction might be tissue- or process-specific, depending on the needs of the particular cell.

The core retromer is implicated in recycling vacuolar sorting receptors from the MVE to the TGN (Hu et al., 2022). The ALIX protein associates with the VPS26-VPS29 dimer in the cytosol, thereby stabilizing the interaction and recruiting VPS35. ALIX mutations show a defect in protein delivery to the vacuole and miss the localization of vacuolar sorting receptors. Therefore, a model where ALIX interaction precedes VPS35-RABG3f interaction is proposed. In this updated model, ALIX recruits VPS26-VPS29, and the three proteins then interact with VPS35, which is anchored to the MVEs by RABG3f. VPS35 can then interact with and recognize the vacuolar sorting receptors at the MVEs and recycle them back to the TGN (Figure 2).

Overall, the retromer-RAB7 interaction has particularities unique to plant systems. The identity and mechanistic of retromer cargo retrieval is still debated and is an interesting research topic in plant cells (Heucken and Ivanov, 2018).

7 RAB7 and plant cell death regulation during developmental processes

In plants, programmed cell death (PCD) plays a significant role in diverse growth, developmental processes. PCD can be triggered by different factors during development, including differentiation induction and age-related senescence. For example, differentiation-induced PCD is the final step in the maturation of specific cell types like the xylem tracheary elements, root cap, or anther tapetum layer (Plackett et al., 2011; Bollhöner et al., 2012; Fendrych et al., 2014; Olvera-Carrillo et al., 2015). Meanwhile, age-induced PCD occurs during the senescence of organs or the entire plant at the end of its life cycle (Thomas, 2013).

The role of RABG3b in regulating PCD has been hypothesized in the context of xylem-tracheary element differentiation (Ménard et al., 2015). CA-RABG3b overexpression was discovered to induce autophagy, as evidenced by the formation of autophagic structures in the cytoplasm of developing tracheary element cells (Kwon et al., 2010; Kwon et al., 2011). An increase in autophagy is linked to the disintegration of cellular contents and organelles, followed by vacuole collapse, releasing hydrolytic enzymes into the cytosol for total cellular breakdown (Hara-Nishimura and Hatsugai, 2011). In cells with deficient autophagy, such as *atg5-1* mutants, cells expressing DN-RABG3b, or cells with RNA interference-mediated RABG3b knockdown (RABG3bRNAi), vacuole collapse is either delayed or absent (Kwon et al., 2010). Before vacuole collapse, events such as increased vacuole size, transport and activation of vacuolar lytic enzymes, acidification of vacuoles, and the degradation of the material delivered by autophagy are observed (Van Doorn et al., 2011). These processes are linked to RABG3 activity, which implies that it may play a role in controlling the pathways leading to programmed cell death (Kwon et al., 2010).

8 RAB7 and plant cell death regulation during pathogen attack

PCD is also involved in stress, and immune responses. Upon pathogen detection the plant's immune system often induces a controlled PCD process usually called the hypersensitive response (HR). The term "hypersensitivity" arises from the unusually fast and extended cell death around the pathogen site of infection to prevent its spread (YIN et al., 2022). Interestingly, when exposed to PCD inducers, such as fungal toxin fumonisin B1 and the bacterial pathogens *Pst DC3000* (*AvrRpm1*) and *Pst DC3000* (*AvrRpt2*), CA-RABG3b overexpressing plants accumulated a large number of autophagic structures and displayed accelerated and expanded cell death (Kwon et al., 2010). Additionally, VPS35B retromer mutants are defective in autophagic degradation and immunity-associated PCD when exposed to *Pst DC3000 (AvrRpm1) and Pst DC3000 (AvrRpt2)* (Munch et al., 2015). Therefore, it is tempting to propose that RABG3b and retromer function positively contribute to immunity-associated PCD by activating autophagic cell death and containing the spread of the infection. Supporting this notion, knocking down the RAB7 (TaRAB7) gene expression in *Triticum aestivum* resulted in a higher abundance of the fungus *Puccinia striiformis f.* sp. *tritici* on infected leaves compared to control leaves, which suggests a role for TaRAB7 in controlling infection (Liu et al., 2012).

Another theory proposes a link between the enhanced autophagy that precedes PCD and the spatial confinement of cell death, thereby avoiding necrotic cell death and the spread of toxic signals that could induce PCD in nearby cells (Patel and Dinesh-Kumar, 2008; Escamez et al., 2016). This hypothesis explains the observed enhanced senescence and prolonged cell death upon overexpression of CA-RABG3b (Kwon et al., 2010; Kwon et al., 2013). However, further investigation is necessary to elucidate the precise role of RAB7 in regulating plant cell death.

9 Are RAB7 MVEs turned into exosomes during biotic interactions?

Numerous microorganisms that engage in symbiotic or pathogenic interactions with plants exhibit specialized cellular

structures that invade host cells and remain enveloped by membranes derived from the host (Ivanov et al., 2010). The same applies to *Phytophthora infestans*, whose hyphae penetrate plant cells and remain surrounded by an extrahaustorial membrane that interfaces the host and the pathogen. RAB7 (RABG3c) is found on the extrahaustorial membrane and is thought to participate in rerouting MVEs towards this membrane (Bozkurt et al., 2015). Another case is the *Rhizobium* bacteria that are individually internalized into symbiosome compartments. Symbiosomes are intracellular in nature but are considered apoplastic compartments separated by the plasma membrane (Ivanov et al., 2012; Coba de la Pena et al., 2018). As the symbiotic association develops, the symbiosome membrane also becomes labeled by RAB7 (Limpens et al., 2009).

Another case is the powdery mildew infection. Plant cells respond to the non-host pathogen's presence by repolarizing their secretory pathway, producing a structure named papillae composed of cell walls and antimicrobial components, and depositing it around the fungal haustoria to halt fungal growth (Underwood and Somerville, 2008). The *mon-1* mutants in the *Arabidopsis* No-0 ecotype form defective papillae structures, leading to penetration and infection by the powdery mildew *Golovinomyces orontii (Go)* (Liao et al., 2023). The data implies that MON1 is essential for activating RAB7 during papillae formation. Accordingly, during papillae formation when cells are attacked by the fungus *Blumeria graminis f.* sp. *hordei (Bgh)*, RABG3c interacts with the component of the EXOCYST complex EXO70B2 located at the papilla membrane (Ortmannová et al., 2022). Therefore, it has been hypothesized that EXO70B2 may act by tethering RAB7 MVEs to the plasma membrane during papilla and encasement formation.

In each of these hypotheses, RAB7 MVEs are thought to reroute and fuse with the plasma membrane rather than the vacuole. However, this theory needs additional testing. During the developmental stage in which RAB7 is detected, VPS39 and VPS41 proteins are not present in the membrane of the symbiosomes (Gavrin et al., 2014). This suggests that the presence of RAB7 at these membranes serves a different functional role or that another fusion machinery (possibly the EXOCYST complex) is involved in tethering RAB7 MVEs with the plasma membrane.

10 RAB7 is highjacked by pathogens to infect cells

RAB7 appears to be important in defense against infection, which may explain why several pathogens target its activity to better penetrate or replicate in plant cells. In barley, the *Blumeria graminis f.* sp. *hordei (Bgh)* effector CSEP0162 protein interacts with the heat shock proteins of the plant and MON1, thereby directing them into aggresomes (Liao et al., 2023). The aggresomes are intracellular depositions of misfolded proteins turned into cytoplasmic inclusions (Verchot, 2011). These aggresomes are believed to be degraded by autophagosomes (Lamark and Johansen, 2012). Therefore, by hijacking MON1, CSEP0162 activity prevents the formation of the papillae encasements favoring the powdery mildew fungus infection in barley (Liao et al., 2023).

Positive-strand RNA viruses, such as tomato bushy stunt virus (TBSV) and carnation Italian ringspot virus (CIRV), exploit RAB7 activity to facilitate the formation of viral replication organelles (VROs) in plant cells (Feng et al., 2021a). VROs are membranous intracellular structures containing viral proteins and viral RNAs that sequester subverted host factors to facilitate replication and prevent cellular degradation. The depletion of RAB7 significantly inhibits TBSV and CIRV replication. The viral p33 replication protein interacts with RAB7, leading to the redistribution of RAB7 into the VROs. Deleting MON1 or CCZ1 impedes TBSV RNA replication, suggesting that activated RAB7 plays a proviral role. Furthermore, p33 was shown to interact directly with the retromer components VPS35, VPS29, and VPS26 to recruit them into VROs (Feng et al., 2021b). Therefore, it is proposed that the retargeting of RAB7 and the core-retromer into VROs by p33 enables the delivery of various retromer cargos, including lipid enzymes, all of which possess proviral functions. These findings indicate tombusviruses exploit RAB7 to redirect endocytic and recycling trafficking pathways to support efficient virus replication.

11 RAB7's role in abiotic stress responses

Many research teams have overexpressed RAB7 in various plant species and have repeatedly observed an improvement in plant fitness in response to various abiotic stressful circumstances (Agarwal et al., 2007; George and Parida, 2011; Peng et al., 2014; Tripathy et al., 2017; El-Esawi and Alayafi, 2019). In *Arabidopsis*, overexpression of the RABG3e gene increases tolerance to osmotic and salt stress, decreases the formation of reactive oxygen species, and shows improved recovery from osmotic stress, thereby increasing stress response efficiency (Mazel et al., 2004). Similarly, RAB7 overexpression in rice enhanced the responses to salt stress by enlarging the vacuolar size in both the roots and the leaves, suggesting increased sodium sequestration as a stress response mechanism (Peng et al., 2014; Tripathy et al., 2017). In addition, these plants retained photosynthetic activity and grana integrity, which enabled proper chloroplast function under salt stress. In a different study, RAB7 overexpression in rice boosted water retention, growth rate, and oxidative stress responses to heat and drought (El-Esawi and Alayafi, 2019). These findings potentially indicate a role for RAB7 in sodium sequestration, cellular homeostasis maintenance, and ROS reduction to enable normal cellular function under abiotic stress conditions. Additionally, during ammonium stress roots of czza1b1 mutants show arrest of growth and accumulation of autophagosomes in the cytoplasm, consistent with a role of RAB7 regulating autophagy during stress (Robert et al., 2021). However, further research is required to dissect the mechanism behind the RAB7-orchestrated response.

12 RAB7 more than just tethering: future topics of exploration

Recent advances in our understanding of RAB7-mediated endomembrane traffic are summarized in this review, emphasizing

the diverse regulatory mechanisms that have evolved in land plants. The primary takeaway from this analysis is that there is still much to learn about RAB7 roles. This includes but is not limited to further characterization of the RAB7 compartments, understanding the biochemical interactions at play, and determining how RAB7 function contributes to the outcomes seen in mutant and overexpressing plants. Several promising directions for future study are suggested, as follows:

RAB7 has been detected in late MVEs (Cui et al., 2014) and autophagosomes (Kwon et al., 2013) and is even associated with TRAPPIII (Kalde et al., 2019), which is a complex detected in the TGN. The function of RAB7 in autophagosomes and potentially in TGN is still unknown. Further analyzing RAB7 interactions in different organelles will help us understand its function.

RAB7 it is in vesicles that likely fuse to the plasma membrane during a pathogen attack. However, the nature and contents of those compartments remain a matter of discussion. The mechanism by which such compartments are redirected and fused with the plasma membrane remains to be fully described.

RAB7-CA-overexpressing plants accumulate ubiquitinated proteins, autophagosomes, and MVEs and exhibit extensive cell death. An avenue of research could be analyzing the RAB7 contribution to containing PCD by facilitating the degradation of proteins and protein aggregates that can be toxic for cells.

RAB7 functions intricately connected to phosphatidylinositol 3-phosphate (PI3P), a vital membrane marker that is present in MVEs and autophagic compartments (Noack and Jaillais, 2017). In plants, PI3P synthesis occurs through the activity of the class III phosphatidylinositol 3-kinase (PI3K) complex, composed of the VPS34 kinase, ATG6, VPS15, and either VPS38 or ATG14 as the fourth subunit. Notably, an interaction between RAB7/RABG3a from *N. benthamiana* and the subunits ATG14 and VPS38 has been observed *in vitro* (Wang et al., 2022). However, the precise mechanisms underlying the association between PI3P and RAB7 in regulating autophagic traffic remain unresolved, representing another interesting research topic.

Creating conditional or inducible RAB7 mutants could help understand its specific role during abiotic stress responses in different plant species.

We are especially optimistic about the recent developments in proteomics, including proximity labeling technologies (Kim et al., 2019) that could give us spatial resolution (Han et al., 2018) and enough data to start answering many of these questions. Finally, we are particularly interested in examining the similarities and differences across various plant species. The fact that overexpressing RAB7 in numerous plant species widely improves their fitness under stress demonstrates the similarities shared by organisms with vastly different physiologies and evolutionary histories. Thus, improving our understanding of these critical pathways across the plant kingdom will pave the way to a complete picture of how the plant endomembrane system is regulated.

Author contributions

CR-F: conceptualized, wrote the entire review, prepared the figures. RB contributed to the writing process of four sections of the manuscript. OB contributed to the abiotic stress section writing. All authors contributed to the article and approved the submitted version.

Funding

This manuscript was financed by School of Biological Sciences, Washington State University, PG00020979 Startup.

Acknowledgments

We thank all the members of the Rodriguez-Furlan lab for discussions of the project and feedback on the manuscript while it was in preparation. We apologize to those colleagues whose important work we were unable to incorporate due to space restrictions.

Conflict of interest

The authors declare that the research was conducted in the absence of any commercial or financial relationships that could be construed as a potential conflict of interest.

Publisher's note

References

Agarwal, P. K., Agarwal, P., Jain, P., Jha, B., Reddy, M. K., and Sopory, S. K. (2007). Constitutive overexpression of a stress-inducible small GTP-binding protein PgRab7 from Pennisetum glaucum enhances abiotic stress tolerance in transgenic tobacco. *Plant Cell Rep.* >27 (1), 105–115. doi: 10.1007/s00299-007-0446-0

Balderhaar, H. J. K., and Ungermann, C. (2013). CORVET and HOPS tethering complexes–coordinators of endosome and lysosome fusion. *J. Cell science* 126 (6), 1307–1316. doi: 10.1242/jcs.107805

Bollhöner, B., Prestele, J., and Tuominen, H. (2012). Xylem cell death: emerging understanding of regulation and function. *J. Exp. botany* 63 (3), 1081–1094. doi: 10.1093/jxb/err438

Bottanelli, F., Gershlick, D. C., and Denecke, J. (2012). Evidence for sequential action of rab 5 and rab 7 GTP ases in prevacuolar organelle partitioning. *Traffic.* 13 (2), 338–354. doi: 10.1111/j.1600-0854.2011.01303.x

Bozkurt, T. O., Belhaj, K., Dagdas, Y. F., Chaparro-Garcia, A., Wu, C., Cano, L. M., et al. (2015). Rerouting of plant late endocytic trafficking toward a pathogen interface. *Traffic.* 16 (2), 204–226. doi: 10.1111/tra.12245

Brillada, C., Zheng, J., Krüger, F., Rovira-Diaz, E., Askani, J. C., Schumacher, K., et al. (2018). Phosphoinositides control the localization of HOPS subunit VPS41, which together with VPS33 mediates vacuole fusion in plants. *Proc. Natl. Acad. Sci.* 115 (35), E8305–E8314. doi: 10.1073/pnas.1807763115

Coba de la Pena, T., Fedorova, E., Pueyo, J. J., and Lucas, M. M. (2018). The symbiosome: legume and rhizobia co-evolution toward a nitrogen-fixing organelle? *Front. Plant Sci.* 8, 2229. doi: 10.3389/fpls.2017.02229

Cui, Y., Zhao, Q., Gao, C., Ding, Y., Zeng, Y., Ueda, T., et al. (2014). Activation of the Rab7 GTPase by the MON1-CCZ1 complex is essential for PVC-to-vacuole trafficking and plant growth in Arabidopsis. *Plant Cell.* 26 (5), 2080–2097. doi: 10.1105/tpc.114.123141

Ebine, K., Inoue, T., Ito, J., Ito, E., Uemura, T., Goh, T., et al. (2014). Plant vacuolar trafficking occurs through distinctly regulated pathways. *Curr. Biol.* 24 (12), 1375–1382. doi: 10.1016/j.cub.2014.05.004

El-Esawi, M., and Alayafi, A. (2019). Overexpression of rice rab7 gene improves drought and heat tolerance and increases grain yield in rice (Oryza sativa L.). *Genes* 10 (1), 56. doi: 10.3390/genes10010056

Elias, M., Brighouse, A., Gabernet-Castello, C., Field, M. C., and Dacks, J. B. (2012). Sculpting the endomembrane system in deep time: high resolution phylogenetics of Rab GTPases. *J. Cell science* 125 (10), 2500–2508. doi: 10.1242/jcs.101378

Escamez, S., André, D., Zhang, B., Bollhöner, B., Pesquet, E., and Tuominen, H. (2016). METACASPASE9 modulates autophagy to confine cell death to the target cells during Arabidopsis vascular xylem differentiation. *Biol. Open* 5 (2), 122–129. doi: 10.1242/bio.015529

Fendrych, M., Van Hautegem, T., Van Durme, M., Olvera-Carrillo, Y., Huysmans, M., Karimi, M., et al. (2014). Programmed cell death controlled by ANAC033/SOMBRERO determines root cap organ size in Arabidopsis. *Curr. Biol.* 24 (9), 931–940. doi: 10.1016/j.cub.2014.03.025

Feng, Z., Inaba, J., and Nagy, P. D. (2021a). Tombusviruses target a major crossroad in the endocytic and recycling pathways *via* co-opting rab7 small GTPase. *J. Virology* 95 (21), e01076–e01021. doi: 10.1128/JVI.01076-21

Feng, Z., Inaba, J., and Nagy, P. D. (2021b). The retromer is co-opted to deliver lipid enzymes for the biogenesis of lipid-enriched tombusviral replication organelles. *Proc. Natl. Acad. Sci.* 118 (1), e2016066118. doi: 10.1073/pnas.2016066118

Gabe Lee, M., Mishra, A., and Lambright, D. G. (2009). Structural mechanisms for regulation of membrane traffic by rab GTPases. *Traffic.* 10 (10), 1377–1389. doi: 10.1111/j.1600-0854.2009.00942.x

Gavrin, A., Kaiser, B. N., Geiger, D., Tyerman, S. D., Wen, Z., Bisseling, T., et al. (2014). Adjustment of host cells for accommodation of symbiotic bacteria: vacuole defunctionalization, HOPS suppression, and TIP1g retargeting in Medicago. *Plant Cell.* 26 (9), 3809–3822. doi: 10.1105/tpc.114.128736

George, S., and Parida, A. (2011). Over-expression of a Rab family GTPase from phreatophyte Prosopis juliflora confers tolerance to salt stress on transgenic tobacco. *Mol. Biol. Rep.* 38, 1669–1674. doi: 10.1007/s11033-010-0278-9

Guerra, F., and Bucci, C. (2016). Multiple roles of the small GTPase Rab7. *Cells.* 5 (3), 34. doi: 10.3390/cells5030034

Han, S., Li, J., and Ting, A. Y. (2018). Proximity labeling: spatially resolved proteomic mapping for neurobiology. *Curr. Opin. Neurobiology* 50, 17–23. doi: 10.1016/j.conb.2017.10.015

Hao, L., Liu, J., Zhong, S., Gu, H., and Qu, L. J. (2016). AtVPS41-mediated endocytic pathway is essential for pollen tube–stigma interaction in Arabidopsis. *Proc. Natl. Acad. Sci.* 113 (22), 6307–6312. doi: 10.1073/pnas.1602757113

Hara-Nishimura, I., and Hatsugai, N. (2011). The role of vacuole in plant cell death. *Cell Death Differentiation* 18 (8), 1298–1304. doi: 10.1038/cdd.2011.70

Heucken, N., and Ivanov, R. (2018). The retromer, sorting nexins and the plant endomembrane protein trafficking. *J. Cell Sci.* 131 (2), jcs203695. doi: 10.1242/jcs.203695

Homma, Y., Hiragi, S., and Fukuda, M. (2021). Rab family of small GTPases: an updated view on their regulation and functions. *FEBS J.* 288 (1), 36–55. doi: 10.1111/febs.15453

Hu, S., Li, B., Wu, F., Zhu, D., Zouhar, J., Gao, C., et al. (2022). Plant ESCRT protein ALIX coordinates with retromer complex in regulating receptor-mediated sorting of soluble vacuolar proteins. *Proc. Natl. Acad. Sci.* 119 (20), e2200492119. doi: 10.1073/pnas.2200492119

Ivanov, S., Fedorova, E., and Bisseling, T. (2010). Intracellular plant microbe associations: secretory pathways and the formation of perimicrobial compartments. *Curr. Opin. Plant Biol.* 13 (4), 372–377. doi: 10.1016/j.pbi.2010.04.005

Ivanov, S., Fedorova, E. E., Limpens, E., De Mita, S., Genre, A., Bonfante, P., et al. (2012). Rhizobium–legume symbiosis shares an exocytotic pathway required for arbuscule formation. *Proc. Natl. Acad. Sci.* 109 (21), 8316–8321. doi: 10.1073/pnas.1200407109

Jha, S. G., Larson, E. R., Humble, J., Domozych, D. S., Barrington, D. S., and Tierney, M. L. (2018). Vacuolar Protein Sorting 26C encodes an evolutionarily conserved large retromer subunit in eukaryotes that is important for root hair growth in Arabidopsis thaliana. *Plant J.* 94 (4), 595–611. doi: 10.1111/tpj.13880

Jiang, D., He, Y., Zhou, X., Cao, Z., Pang, L., Zhong, S., et al. (2022). Arabidopsis HOPS subunit VPS41 carries out plant-specific roles in vacuolar transport and vegetative growth. *Plant Physiol.* 189 (3), 1416–1434. doi: 10.1093/plphys/kiac167

Kalde, M., Elliott, L., Ravikumar, R., Rybak, K., Altmann, M., Klaeger, S., et al. (2019). Interactions between Transport Protein Particle (TRAPP) complexes and Rab GTPases in Arabidopsis. *Plant J.* 100 (2), 279–297. doi: 10.1111/tpj.14442

Kim, T. W., Park, C. H., Hsu, C. C., Zhu, J. Y., Hsiao, Y., Branon, T., et al. (2019). Application of TurboID-mediated proximity labeling for mapping a GSK3 kinase signaling network in Arabidopsis. *bioRxiv* 35 (*3*), 975–993. doi: 10.1101/636324

Kwon, S. I., Cho, H. J., Jung, J. H., Yoshimoto, K., Shirasu, K., and Park, O. K. (2010). The Rab GTPase RabG3b functions in autophagy and contributes to tracheary element differentiation in Arabidopsis. *Plant J.* 64 (1), 151–164. doi: 10.1111/j.1365-313X.2010.04315.x

Kwon, S. I., Cho, H. J., Kim, S. R., and Park, O. K. (2013). The Rab GTPase RabG3b positively regulates autophagy and immunity-associated hypersensitive cell death in Arabidopsis. *Plant Physiol.* 161 (4), 1722–1736. doi: 10.1104/pp.112.208108

Kwon, S. I., Cho, HJ, LEE, JS, Jin, H, SHIN, SJ, Kwon, M., et al. (2011). Overexpression of constitutively active Arabidopsis RabG3b promotes xylem development in transgenic poplars. *Plant Cell environment* 34 (12), 2212–2224. doi: 10.1111/j.1365-3040.2011.02416.x

Lamark, T., and Johansen, T. (2012). Aggrephagy: selective disposal of protein aggregates by macroautophagy. *Int. J. Cell Biol.* 2012, 736905. doi: 10.1155/2012/736905

Liao, W., Nielsen, M. E., Pedersen, C., Xie, W., and Thordal-Christensen, H. (2023). Barley endosomal MONENSIN SENSITIVITY1 is a target of the powdery mildew effector CSEP0162 and plays a role in plant immunity. *J. Exp. Botany* 74 (1), 118–129. doi: 10.1093/jxb/erac403

Limpens, E., Ivanov, S., van Esse, W., Voets, G., Fedorova, E., and Bisseling, T. (2009). Medicago N2-fixing symbiosomes acquire the endocytic identity marker Rab7 but delay the acquisition of vacuolar identity. *Plant Cell.* 21 (9), 2811–2828. doi: 10.1105/tpc.108.064410

Lipka, V., Kwon, C., and Panstruga, R. (2007). SNARE-ware: the role of SNARE-domain proteins in plant biology. *Annu. Rev. Cell Dev. Biol.* 23, 147–174. doi: 10.1146/annurev.cellbio.23.090506.123529

Liu, F., Guo, J., Bai, P., Duan, Y., Wang, X., Cheng, Y., et al. (2012). Wheat TaRab7 GTPase is part of the signaling pathway in responses to stripe rust and abiotic stimuli. *PloS One* 7 (5), e37146. doi: 10.1371/journal.pone.0037146

Lürick, A., Gao, J., Kuhlee, A., Yavavli, E., Langemeyer, L., Perz, A., et al. (2017). Multivalent Rab interactions determine tether-mediated membrane fusion. *Mol. Biol. Cell.* 28 (2), 322–332. doi: 10.1091/mbc.e16-11-0764

Mazel, A., Leshem, Y., Tiwari, B. S., and Levine, A. (2004). Induction of salt and osmotic stress tolerance by overexpression of an intracellular vesicle trafficking protein atrab7 (AtRabG3e). *Plant Physiol.* 134 (1), 118–128. doi: 10.1104/pp.103.025379

Ménard, D., Escamez, S., Tuominen, H., and Pesquet, E. (2015). Life beyond death: the formation of xylem sap conduits. In: Gunawardena, A.N., and McCabe, P.F. (eds). *Plant Programmed Cell Death.* Springer, Cham. 55–76. doi: 10.1007/978-3-319-21033-9_3

Munch, D., Teh, O. K., Malinovsky, F. G., Liu, Q., Vetukuri, R. R., El Kasmi, F., et al. (2015). Retromer contributes to immunity-associated cell death in Arabidopsis. *Plant Cell.* 27 (2), 463–479. doi: 10.1105/tpc.114.132043

Nahm, M. Y., Kim, S. W., Yun, D., Lee, S. Y., Cho, M. J., and Bahk, J. D. (2003). Molecular and biochemical analyses of OsRab7, a rice Rab7 homolog. *Plant Cell Physiol.* 44 (12), 1341–1349. doi: 10.1093/pcp/pcg163

Noack, L. C., and Jaillais, Y. (2017). Precision targeting by phosphoinositides: how PIs direct endomembrane trafficking in plants. *Curr. Opin. Plant Biol.* 1, 40:22–40:33. doi: 10.1016/j.pbi.2017.06.017

Nodzyński, T., Feraru, M. I., Hirsch, S., De Rycke, R., Niculaes, C., Boerjan, W., et al. (2013). Retromer subunits VPS35A and VPS29 mediate prevacuolar compartment (PVC) function in Arabidopsis. *Mol. Plant* 6 (6), 1849–1862. doi: 10.1093/mp/sst044

Nordmann, M., Ungermann, C., and Cabrera, M. (2012). Role of rab7/ypt7 in organizing membrane trafficking at the late endosome. *Rab GTPases membrane trafficking* 132. doi: 10.2174/978160805365011201010132

Olvera-Carrillo, Y., Van Bel, M., Van Hautegem, T., Fendrych, M., Huysmans, M., Simaskova, M., et al. (2015). A conserved core of programmed cell death indicator genes discriminates developmentally and environmentally induced programmed cell death in plants. *Plant Physiol.* 169 (4), 2684–2699. doi: 10.1104/pp.15.00769

Ortmannová, J., Sekereš, J., Kulich, I., Šantrůček, J., Dobrev, P., Žárský, V., et al. (2022). Arabidopsis EXO70B2 exocyst subunit contributes to papillae and encasement formation in antifungal defence. *J. Exp. botany* 73 (3), 742–755. doi: 10.1093/jxb/erab457

Pan, T., Wang, Y., Jing, R., Wang, Y., Wei, Z., Zhang, B., et al. (2021). Post-Golgi trafficking of rice storage proteins requires the small GTPase Rab7 activation complex MON1–CCZ1. *Plant Physiol.* 187 (4), 2174–2191. doi: 10.1093/plphys/kiab175

Patel, S., and Dinesh-Kumar, S. P. (2008). Arabidopsis ATG6 is required to limit the pathogen-associated cell death response. *Autophagy.* 4 (1), 20–27. doi: 10.4161/auto.5056

Peng, X., Ding, X., Chang, T., Wang, Z., Liu, R., Zeng, X., et al. (2014). Overexpression of a vesicle trafficking gene, OsRab7, enhances salt tolerance in rice. *Sci. World J.* 2014, 483526. doi: 10.3390/genes10010056

Plackett, A. R., Thomas, S. G., Wilson, Z. A., and Hedden, P. (2011). Gibberellin control of stamen development: a fertile field. *Trends Plant science* 16 (10), 568–578. doi: 10.1016/j.tplants.2011.06.007

Robert, G., Yagyu, M., Koizumi, T., Naya, L., Masclaux-Daubresse, C., and Yoshimoto, K. (2021). Ammonium stress increases microautophagic activity while

impairing macroautophagic flux in Arabidopsis roots. *Plant J.* 105 (4), 1083–1097. doi: 10.1111/tpj.15091

Rodriguez-Furlan, C., Domozych, D., Qian, W., Enquist, P. A., Li, X., Zhang, C., et al. (2019). Interaction between VPS35 and RABG3f is necessary as a checkpoint to control fusion of late compartments with the vacuole. *Proc. Natl. Acad. Sci.* 116 (42), 21291–21301. doi: 10.1073/pnas.1905321116

Rosquete, M. R., Davis, D. J., and Drakakaki, G. (2018). The plant trans-Golgi network: not just a matter of distinction. *Plant Physiol.* 176 (1), 187–198. doi: 10.1104/pp.17.01239

Rutherford, S., and Moore, I. (2002). The Arabidopsis Rab GTPase family: another enigma variation. *Curr. Opin. Plant Biol.* 5 (6), 518–528. doi: 10.1016/S1369-5266(02)00307-2

Shi, W., Zeng, Q., Kunkel, B. N., and Running, M. P. (2016). Arabidopsis Rab geranylgeranyltransferases demonstrate redundancy and broad substrate specificity in vitro. *J. Biol. Chem.* 291 (3), 1398–1410. doi: 10.1074/jbc.M115.673491

Singh, M. K., Krüger, F., Beckmann, H., Brumm, S., Vermeer, J. E., Munnik, T., et al. (2014). Protein delivery to vacuole requires SAND protein-dependent Rab GTPase conversion for MVB-vacuole fusion. *Curr. Biol.* 24 (12), 1383–1389. doi: 10.1016/j.cub.2014.05.005

Takemoto, K., Ebine, K., Askani, J. C., Krüger, F., Gonzalez, Z. A., Ito, E., et al. (2018). Distinct sets of tethering complexes, SNARE complexes, and Rab GTPases mediate membrane fusion at the vacuole in Arabidopsis. *Proc. Natl. Acad. Sci.* 115 (10), E2457–E2466. doi: 10.1073/pnas.1717839115

Teh, O., and Moore, I. (2007). An ARF-GEF acting at the Golgi and in selective endocytosis in polarized plant cells. *Nature.* 448 (7152), 493–496. doi: 10.1038/nature06023

Thomas, H. (2013). Senescence, ageing and death of the whole plant. *New Phytologist* 197 (3), 696–711. doi: 10.1111/nph.12047

Touchot, N., Chardin, P., and Tavitian, A. (1987). Four additional members of the ras gene superfamily isolated by an oligonucleotide strategy: molecular cloning of YPT-related cDNAs from a rat brain library. *Proc. Natl. Acad. Sci.* 84 (23), 8210–8214. doi: 10.1073/pnas.84.23.8210

Tripathy, M. K., Deswal, R., and Sopory, S. K. (2021). Plant RABs: role in development and in abiotic and biotic stress responses. *Curr. Genomics* 22 (1), 26–40. doi: 10.2174/18755488MTEzxMzAuz

Tripathy, M. K., Tiwari, B. S., Reddy, M. K., Deswal, R., and Sopory, S. K. (2017). Ectopic expression of PgRab7 in rice plants (Oryza sativa L.) results in differential tolerance at the vegetative and seed setting stage during salinity and drought stress. *Protoplasma* 254 (1), 109–124. doi: 10.1007/s00709-015-0914-2

Ueda, T., Yoshizumi, T., Anai, T., Matsui, M., Uchimiya, H., and Nakano, A. (1998). AtGDI2, a novel Arabidopsis gene encoding a Rab GDP dissociation inhibitor. *Gene.* 206 (1), 137–143. doi: 10.1016/S0378-1119(97)00584-2

Uemura, T., and Ueda, T. (2014). Plant vacuolar trafficking driven by RAB and SNARE proteins. *Curr. Opin. Plant Biol.* 22, 116–121. doi: 10.1016/j.pbi.2014.10.002

Underwood, W., and Somerville, S. C. (2008). Focal accumulation of defences at sites of fungal pathogen attack. *J. Exp. botany* 59 (13), 3501–3508. doi: 10.1093/jxb/ern205

Van Doorn, W., Beers, E., Dangl, J., Franklin-Tong, V., Gallois, P., Hara-Nishimura, I., et al. (2011). Morphological classification of plant cell deaths. *Cell Death Differentiation* 18 (8), 1241–1246. doi: 10.1038/cdd.2011.36

Verchot, J. (2011). Wrapping membranes around plant virus infection. *Curr. Opin. Virology* 1 (5), 388–395. doi: 10.1016/j.coviro.2011.09.009

Vernoud, V., Horton, A. C., Yang, Z., and Nielsen, E. (2003). Analysis of the small GTPase gene superfamily of Arabidopsis. *Plant Physiol.* 131 (3), 1191–1208. doi: 10.1104/pp.013052

Vetter, I. R., and Wittinghofer, A. (2001). The guanine nucleotide-binding switch in three dimensions. *Science.* 294 (5545), 1299–1304. doi: 10.1126/science.1062023

Wang, Y., Li, J., Wang, J., Han, P., Miao, S., Zheng, X., et al. (2022). Plant UVRAG interacts with ATG14 to regulate autophagosome maturation and geminivirus infection. *New Phytologist* 236 (4), 1358–1374. doi: 10.1111/nph.18437

Yamazaki, M., Shimada, T., Takahashi, H., Tamura, K., Kondo, M., Nishimura, M., et al. (2008). Arabidopsis VPS35, a retromer component, is required for vacuolar protein sorting and involved in plant growth and leaf senescence. *Plant Cell Physiol.* 49 (2), 142–156. doi: 10.1093/pcp/pcn006

YIN, J., XIONG, J., XU, L., CHEN, X., and LI, W. (2022). Recent advances in plant immunity with cell death: A review. *J. Integr. Agriculture* 21 (3), 610–620. doi: 10.1016/S2095-3119(21)63728-0

Zárský, V., Cvrckova, F., BischofF, F., and Palme, K. (1997). At-GDI1 from Arabidopsis thaliana encodes a rab-specific GDP dissociation inhibitor that complements the sec19 mutation of Saccharomyces cerevisiae. *FEBS letters* 403 (3), 303–308. doi: 10.1016/S0014-5793(97)00072-0

Zelazny, E., Santambrogio, M., Pourcher, M., Chambrier, P., Berne-Dedieu, A., Fobis-Loisy, I., et al. (2013). Mechanisms governing the endosomal membrane recruitment of the core retromer in Arabidopsis. *J. Biol. Chem.* 288 (13), 8815–8825. doi: 10.1074/jbc.M112.440503

Frontiers in Plant Science

Cultivates the science of plant biology and its applications

The most cited plant science journal, which advances our understanding of plant biology for sustainable food security, functional ecosystems and human health.

Discover the latest Research Topics

See more →

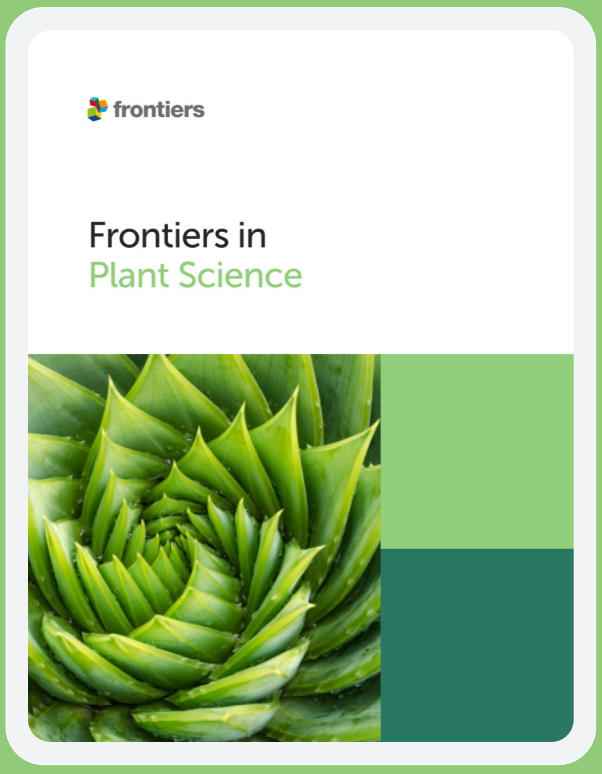

Frontiers

Avenue du Tribunal-Fédéral 34
1005 Lausanne, Switzerland
frontiersin.org

Contact us

+41 (0)21 510 17 00
frontiersin.org/about/contact